This electronic thesis or dissertation has been downloaded from the King's Research Portal at https://kclpure.kcl.ac.uk/portal/



Flow Contraction Matching In The Human Heart

Patterson, Tiffany

Awarding institution:
King's College London

The copyright of this thesis rests with the author and no quotation from it or information derived from it may be published without proper acknowledgement.

END USER LICENCE AGREEMENT



Unless another licence is stated on the immediately following page this work is licensed

under a Creative Commons Attribution-NonCommercial-NoDerivatives 4.0 International

licence. https://creativecommons.org/licenses/by-nc-nd/4.0/

You are free to copy, distribute and transmit the work

Under the following conditions:

- Attribution: You must attribute the work in the manner specified by the author (but not in any way that suggests that they endorse you or your use of the work).
- Non Commercial: You may not use this work for commercial purposes.
- No Derivative Works - You may not alter, transform, or build upon this work.

Any of these conditions can be waived if you receive permission from the author. Your fair dealings and other rights are in no way affected by the above.

Take down policy

If you believe that this document breaches copyright please contact librarypure@kcl.ac.uk providing details, and we will remove access to the work immediately and investigate your claim.

Download date: 08. Oct. 2023

Flow Contraction Matching In The Human Heart

Tiffany Patterson

MBBS BSc MRCP

A DISSERTATION SUBMITTED FOR THE DEGREE OF

Doctor of Philosophy

To the

University of London



Cardiovascular Division, Rayne Institute

British Heart Foundation Centre of Research Excellence

Faculty of Life Sciences and Medicine

ABSTRACT

Introduction

Induction of myocardial ischaemia results in a cascade of left ventricular haemodynamic effects, resulting in myocyte necrosis, scar formation and eventual heart failure, for which treatment is limited. Fundamental to enhancing our understanding of cardiovascular pathophysiology and therapeutics is the assessment of ventricular pump properties. The main aim of this work was to gain a greater understanding of the myocardial-coronary and ventricular-arterial interaction in humans in health and diseased states.

Methods

Simultaneous invasive left ventricular (LV) pressure-volume (PV) (by use of a conductance catheter) and intra-coronary haemodynamic assessment (dual-sensor pressure-flow wire) were performed in the catheterisation laboratory. A novel software system was developed to perform simultaneous analysis of PV loop and coronary haemodynamic data. *In-vitro* and *in-vivo* studies were performed for calibration; PV loop recordings from patients were used for validation.

Results

1) Using wave intensity analysis, the origin of the coronary wave energies were described, and their temporal relationship with the cardiac cycle was established. In the absence of autoregulation a direct relationship was found to exist between LV elastance and coronary flow velocity.

2) Assessment of coronary haemodynamics and LV PV measurements were performed during supine exercise to provoke ischaemia, with a control group comparator. Ischaemia led to a rightward shift in end-systolic and end-diastolic PV relations; VA interaction was adversely affected during ischaemia compared to control.
3) The effects of nitrates in patients with coronary artery disease were examined. Nitrates induced vasodilatation of the systemic vasculature and coronary circulation, decreasing myocardial oxygen consumption and inducing stenosis dilatation.
4) 3D speckle tracking echocardiography was performed in patients with preserved LV function and coronary artery disease followed by PV loop assessment. Parameters of strain correlated well with contractility indices *in-vivo*; thus has potential for use in prognostication and risk stratification.
5) The haemodynamic mechanisms of percutaneous ventricular restoration (PVR) therapy are not understood. Patients underwent PVR implantation and LV PV loops were recorded pre- and post-PVR and at 6-month follow up. PVR decreased dyssynchrony, LV volumes and induced reverse remodelling with improved contractility.

Conclusions

Development of software enabled understanding of the cardiac-coronary interaction: coronary wave energies were shown to be dependent on V-A interaction rather than myocardial-coronary interaction. Coronary systolic flow was directly related to LV elastance on abolition of autoregulation. Systemic response to demand ischaemia was described, as were the anti-anginal effects of nitrates; 3D deformation imaging was validated as a prognostic tool for subclinical heart disease and PVR was shown to induce reverse remodelling.

ACKNOWLEDGEMENTS

First and foremost, I would like to thank my supervisors Professor Simon Redwood and Professor Michael Marber. Their support, mentoring and inspiration were second to none. They provided me with an environment that nurtured creativity, drive and opened many doors. I would like to thank Professor Redwood for guiding me down the path of clinical research.

I would like to thank Dr Jack Lee, who treated me as if I was his own PhD student, and was always available for advice, support and feedback. A special thanks goes out to Dr Simone Rivolo, with whom I developed the SimpleWires software (Chapter 3). I would like to thank Professor Daniel Burkhoff for his constant enthusiasm, interest and support, his knowledge and input markedly raised the standard of the work we performed.

Professor Redwood, Dr Divaka Perera and Dr Brian Clapp were fundamental in catheter laboratory data collection for this thesis (Chapters 3,4 and 5), and Dr Kapetenakis very kindly performed 3D echocardiography and strain analysis (Chapter 6). Dr Jan Schreuder performed analysis for the Parachute PV Loop sub-study (Chapter 7). The catheter laboratory staff at St Thomas' were always on hand to help with these research studies.

I would like to thank the research fellows with whom I have worked alongside, who offered their support and encouragement. Finally a huge thanks goes out to my parents.

TABLE OF CONTENTS

ABSTRACT ..... **ii**

ACKNOWLEDGEMENTS ..... **iv**

TABLE OF CONTENTS ..... **v**

Publications ..... **xvii**

Abstracts ..... **xviii**

Collaborators ..... **xix**

Funding Bodies ..... **xx**

Awards, Prizes And Scholarships ..... **xx**

1 INTRODUCTION **1**

1.1 Cardiac Structure and Function **1**

1.1.1 Myocyte Architecture 1

1.1.2 Cardiac Excitation-Contraction Coupling 3

1.1.3 Force of Contraction 5

1.2 Assessment of Cardiac Function **7**

1.2.1 Cardiac Cycle and The Pressure-Volume Loop 7

1.2.2 Measuring Diastolic Properties and Relaxation 12

1.2.3 Markers of Contractility 14

1.2.4 Measures of Afterload 20

1.2.5 Deformation Imaging 22

1.3 Functional Arrangement of Coronary Circulation **26**

1.3.1 Autoregulatory Mechanisms 28

1.3.2 Pressure Gradient-Velocity Relationship 30

1.4 Invasive Measurements of Coronary Blood Flow **33**

1.4.1 Coronary Flow Reserve 34
1.4.2 Fractional Flow Reserve 35
1.5 Coronary Wave Intensity Analysis 38
1.5.1 Application of cWIA 40
1.6 Coordinated Cardiovascular Response to Exercise 46
1.6.1 Peripheral Vascular Responses 46
1.6.2 Cardiac Responses 48
1.7 Pathological Cardiovascular Responses 53
1.7.1 Impact of Ischaemic Heart Disease 53
1.7.2 Mechanism of Angina 54
1.7.3 Supply-Demand Mismatch 56
1.7.4 Regional Ischaemia and Pressure-Volume Loops 58
1.7.5 Nitrates in Ischaemic Heart Disease 61
1.7.6 Ischaemic Cardiomyopathy and Left Ventricle Partitioning 64
2 METHODS 68
2.1 Introduction 68
2.2 Measurements: Real-Time LV Haemodynamics 68
2.2.1 Conductance Catheter 68
2.2.2 Volume Calculation 70
2.2.3 Intra-Cardiac Analyser 73
2.2.4 Conduct NT Software 76
2.3 Measurements: Invasive Coronary Haemodynamics 78
2.3.1 ComboWire and ComboMap Console 78
2.3.2 Calibration and Data Acquisition 79
2.3.3 Data variables 81
2.4 Echocardiography Protocol 83

2.4.1 Echo Analysis 83

2.5 Instrumentation and Technical Considerations 84

2.5.1 Conductance Catheter Diameter 84

2.5.2 Equipment Alteration 86

2.6 Catheter Laboratory Protocol 88

2.6.1 Set-Up And Calibration 88

2.6.2 Procedural Techniques 92

2.6.3 Baseline Simultaneous Measurements 92

2.6.4 Vasodilator Administration: Isosorbide Dinitrate 93

2.6.5 Adenosine Induced Hyperaemia 93

2.6.6 Dynamic Exercise: Supine Cycle Ergometry 94

2.6.7 Left Ventricular Partitioning Device: PV Loop Sub-study 94

3 The Mechanical Determinants of Coronary Blood Flow: A Novel Analytical Software system 98

3.1 Introduction 100

3.2 Methods 103

3.2.1 Hardware configuration 103

3.2.2 Time-Phase Delay 105

3.2.3 SimpleWires Analysis software 110

3.3 Results 122

3.3.1 Simultaneous LV And Coronary Measurement In-Vivo 122

3.3.2 Software Validation 122

3.3.3 Mechanical Determinants Of Coronary Haemodynamics 126

3.3.4 Coronary Wave Energies And Events In The Cardiac Cycle 132

3.3.5 Correlations Between Timings Of Wave Generation And Mechanical Events 135

3.3.6 Mechanical Determinants Of Coronary Blood Flow 137

3.4 Discussion 139

3.5 Limitations 143

3.6 Conclusions 143

4 The Effects Of Dynamic Exercise On Myocardial Systolic And Diastolic Function: Exercise-Induced Ischaemia Versus Control Group Comparator 144

4.1 Introduction 146

4.2 Methods 148

4.2.1 Study Population 148

4.2.2 Catheter Laboratory Protocol and Instrumentation 148

4.2.3 Exercise Protocol 149

4.2.4 Data Acquisition and Analysis 151

4.2.5 Statistical Analysis 153

4.3 Results 154

4.3.1 Effect of Exercise On Haemodynamics At The Onset Of Ischaemia 157

4.3.2 The Ventricular-Arterial Interaction In The Presence Of Significant Coronary Artery Disease 162

4.3.3 Relationship Between Coronary Blood Flow Velocity And Diastolic Time Fraction In Ischaemia 164

4.3.4 Coronary Wave Intensity Analysis And Cardiac Mechanics 168

4.4 Discussion 172

4.5 Limitations 178

4.6 Conclusions 178

5 The Role Of Nitrates In Angina Pectoris Revisited 180

5.1 Introduction 182

5.2 Methods 184

5.2.1 Study Population 184

5.2.2 Catheter Laboratory Instrumentation and Protocol 184

5.2.3 Data Acquisition and Analysis 187

5.2.4 Statistical Analysis 191

5.3 Results 192

5.4 Discussion 205

5.5 Limitations 208

5.6 Conclusion 208

6 Three-Dimensional Myocardial Deformation Imaging: A Novel Non-Invasive Measure of Contractility 209

6.1 Introduction 211

6.2 Methods 213

6.2.1 Study Population 213

6.2.2 Haemodynamic Measurements 213

6.2.3 2D Echocardiography 215

6.2.4 3D Real-Time Transthoracic Echocardiography 215

6.2.5 Speckle-Tracking Echocardiography 217

6.2.6 Data Analysis 217

6.2.7 Statistical Analysis 218

6.3 Results 219

6.4 Discussion 225

6.5 Limitations 226

6.6 Conclusions 226

7 Percutaneous Ventricular Restoration Using The Parachute Device: The Parachute III Pressure-Volume Loop Sub-Study 227

7.1 Introduction 229

7.2 Methods 230

7.2.1 Study Design 230

7.2.2 Patient Selection 231

7.2.3 Study Device and Procedure 231

7.2.4 Instrumentation 233

7.2.5 Data Analysis 234

7.2.6 Statistical Analysis 235

7.3 Results 236

7.4 Discussion 247

7.5 Limitations 250

7.6 Conclusions 250

8 Synthesis 252

9 Bibliography 259

10 Appendix 275

List of Figures

FIGURE 1 CARDIAC MYOCYTE. 2

FIGURE 2 CALCIUM RELEASE. 3

FIGURE 3 SARCOMERE LENGTH AND FORCE GENERATION 5

FIGURE 4 THE CARDIAC CYCLE. 7

FIGURE 5 THE LEFT VENTRICULAR (LV) PRESSURE-VOLUME LOOP. 9

FIGURE 6 PHYSIOLOGICAL PARAMETERS DERIVED FROM THE PV LOOP. 11

FIGURE 7 END-DIASTOLIC PRESSURE VOLUME RELATIONS. 12

FIGURE 8 THE END-SYSTOLIC PRESSURE VOLUME RELATIONSHIP (ESPVR). 14

FIGURE 9 TIME VARYING ELASTANCE.. 16

FIGURE 10 TOTAL MECHANICAL ENERGY 18

FIGURE 11 ARTERIAL ELASTANCE (EA). 21

FIGURE 12 3D SPECKLE TRACKING ECHOCARDIOGRAPHY. 24

FIGURE 13 THE CORONARY CIRCULATION. 26

FIGURE 14 AUTOREGULATION OF CORONARY BLOOD FLOW. 28

FIGURE 15 EFFECT OF A CORONARY ARTERY STENOSIS ON CORONARY BLOOD FLOW. 30

FIGURE 16 PRESSURE DROP-VELOCITY RELATIONSHIPS. 32

FIGURE 17 CHANGES ON BLOOD FLOW WITH INCREASING DEGREE OF STENOSIS SEVERITY. 33

FIGURE 18 STENOSIS SEVERITY 35

FIGURE 19 FRACTIONAL FLOW RESERVE. 36

FIGURE 20 CORONARY WAVE INTENSITY ANALYSIS. 39

FIGURE 21 WAVE SEPARATION. 41

FIGURE 22 BLOOD FLOW AND EXERCISE. 47

FIGURE 23 MYOCARDIAL OXYGEN CONSUMPTION (VO2) AT THE ONSET OF EXERCISE. 48

FIGURE 24 DEATH FROM CARDIOVASCULAR DISEASE IN EUROPE 53

FIGURE 25 THE ISCHAEMIC CASCADE. 54

FIGURE 26 PATHOPHYSIOLOGICAL MECHANISMS OF MYOCARDIAL ISCHAEMIA. 55

FIGURE 27 THE CYCLE OF MYOCARDIAL ISCHAEMIA,. 56
FIGURE 28 METABOLISM OF ISOSORBIDE DINITRATE. 61
FIGURE 29 ISCHAEMIC CARDIOMYOPATHY. 65
FIGURE 30 PARACHUTE DEVICE ILLUSTRATION. 67
FIGURE 31 CONDUCTANCE CATHETER. 69
FIGURE 32 IMPEDANCE METHOD. 70
FIGURE 33 INTRA-CARDIAC ANALYSER (INCA®) 73
FIGURE 34 REAL-TIME DISPLAY. 74
FIGURE 35 ANIMATION OF COMBOWIRE. 78
FIGURE 36 COMBOMAP DISPLAY. 79
FIGURE 37 ASAHI SHEATHLESS GUIDE 86
FIGURE 38 PROXIMAL END OF THE ASG. 87
FIGURE 39 THE DISTAL END OF ASG. 87
FIGURE 40 FLUOROSCOPIC CONFIRMATION OF CONDUCTANCE CATHETER POSITION 92
FIGURE 41 BASELINE PATIENT EVALUATION. 95
FIGURE 42 PARACHUTE STUDY PROCEDURE. 97
FIGURE 43 ELECTRONIC ROUTING OF THE CORONARY SIGNAL INTO THE INCA. 105
FIGURE 44 TIME-PHASE DELAY. 106
FIGURE 45 PULSATILE FLOW PHANTOM. 107
FIGURE 46 TIME-PHASE MISALIGNMENT. 110
FIGURE 47 SIMPLEWIRES GRAPHICAL USER INTERFACE (GUI). 112
FIGURE 48 LEFT VENTRICULAR HAEMODYNAMICS. 113
FIGURE 49 CORONARY HAEMODYNAMIC SIGNALS. 114
FIGURE 50 BLAND-ALTMAN PLOTS. 125
FIGURE 51. SIMULTANEOUS ACQUISITION OF CORONARY AND LEFT VENTRICULAR HAEMODYNAMICS. 128
FIGURE 52. A REPRESENTATIVE EXAMPLE OF ENSEMBLE AVERAGED TRACINGS. 129
FIGURE 53 WAVE GENERATION DURING THE CARDIAC CYCLE. 131
FIGURE 54 CARDIAC CYCLE EVENTS AND WAVE ENERGIES DESCRIBED ON THE PV LOOP. 134
FIGURE 55. CORRELATIONS BETWEEN CARDIAC CYCLE EVENTS AND WAVE ENERGY. 136

FIGURE 57 CONDUCTANCE CATHETER AND COMBOWIRE POSITION (FLUOROSCOPY) 150
FIGURE 58 PATIENT FLOW DIAGRAM. 155
FIGURE 59 PERCENTAGE CHANGE IN HAEMODYNAMIC VARIABLES. 159
FIGURE 61 REPRESENTATIVE EXAMPLES OF CHANGES IN THE PRESSURE-VOLUME LOOP. 163
FIGURE 62 REPRESENTATIVE EXAMPLE OF HAEMODYNAMICS. 166
FIGURE 63 CHANGE IN CORONARY HAEMODYNAMICS. 166
FIGURE 64 CHANGE IN CORONARY WAVES 166
FIGURE 65 CORRELATION OF WAVES 166
FIGURE 66. INSTRUMENTATION DURING ISDN (FLUOROSCOPY). 186
FIGURE 67 SIMULTANEOUS SYSTEMIC AND INTRACORONARY RECORDING. 188
FIGURE 68 PATIENT FLOW DIAGRAM. 192
FIGURE 69 GRAPHICAL REPRESENTATION OF HAEMODYNAMIC CHANGE WITH ISDN 197
FIGURE 70. PERCENTAGE CHANGE FROM BASELINE FOLLOWING ISDN. 198
FIGURE 71 A REPRESENTATIVE EXAMPLE THE PRESSURE-VOLUME LOOP FOLLOWING ISDN. 199
FIGURE 72 TYPICAL HAEMODYNAMIC TRACINGS AND WAVE INTENSITY ANALYSIS. 202
FIGURE 73 CHANGES IN CORONARY HAEMODYNAMICS 203
FIGURE 74 CHANGES IN THE CORONARY WAVE ENERGIES. 204
FIGURE 75 FULL VOLUME ANALYSIS 216
FIGURE 76 CORRELATION OF GLOBAL CIRCUMFERENTIAL STRAIN (GCS) WITH CONTRACTILITY 223
FIGURE 78 PARACHUTE STUDY PROCEDURE. 232
FIGURE 79 DISPOSITION OF PATIENTS ENROLLED. 238
FIGURE 80 CLINICAL OUTCOMES. 239
FIGURE 81 END-DIASTOLIC VOLUME (EDV) AND END-SYSTOLIC VOLUME (ESV). 241
FIGURE 82 EJECTION FRACTION 241
FIGURE 83 DYSSYCHRONY INDEX. 242
FIGURE 84 PERCENTAGE CHANGE IN HAEMODYNAMIC VARIABLES. 242
FIGURE 85 PRESSURE VVOLUME LOOPS 244
FIGURE 86 PERCENTAGE CHANGE IN INDICES OF CONTRACTILITY. 245
FIGURE 87 RATIO OF EA:EES. 245

FIGURE 88 RATIO OF SW:PVA EXPRESSED AS A PERCENTAGE. 246

FIGURE 89 PERCENTAGE CHANGE IN MARKERS OF LV RELAXATION AND EFFICIENCY. 246

List of Tables

TABLE 1 SHEATH SIZES. INNER AND OUTER DIAMETERS OF ARTERIAL SHEATHS ARE SPECIFIED. 84

TABLE 2 THE DEFINITIONS AND FORMULAS OF LEFT VENTRICULAR (LV) HAEMODYNAMIC VARIABLES 116

TABLE 3 HAEMODYNAMIC VARIABLES DERIVED FROM THE TWO SOFTWARE SYSTEMS. 124

TABLE 4 TIMINGS OF WAVES AND CARDIAC CYCLE EVENTS. 130

TABLE 5. BASELINE DEMOGRAPHICS AND PROCEDURAL DETAILS OF STUDY PARTICIPANTS. 156

TABLE 6 HAEMODYNAMIC VARIABLES 159

TABLE 7 CORONARY HAEMODYNAMIC VARIABLES AND WAVE CHANGES 166

TABLE 8 BASELINE DEMOGRAPHICS AND PROCEDURAL DETAILS OF STUDY PARTICIPANTS. 193

TABLE 9 HEMODYNAMIC VARIABLES FOLLOWING ISDN. 196

TABLE 10 CORONARY HEMODYNAMICS AND WAVE ENERGIES 201

TABLE 11 BASELINE DEMOGRAPHICS. 220

TABLE 12 ECHOCARDIOGRAPHIC PARAMETERS AND LV PV LOOP ASSESSMENT. 221

TABLE 13 BASELINE CHARACTERISTICS 237

TABLE 14 HAEMODYNAMIC VARIABLES, ABBREVIATIONS SEE XVI 240

List of Equations

EQUATION 1 11

EQUATION 2 13

EQUATION 3 15

EQUATION 4 15

EQUATION 5 22

EQUATION 6 31

EQUATION 7 31

EQUATION 8 42

EQUATION 9 42

EQUATION 10 43

EQUATION 11 43

EQUATION 12 43

EQUATION 13 49

EQUATION 14 72

EQUATION 15 81

EQUATION 16 82

EQUATION 17 82

EQUATION 18 82

EQUATION 19 120

EQUATION 20 121

EQUATION 21 189

EQUATION 22 189

EQUATION 23 216

EQUATION 24 216

Abbreviations

A

Angiotensin Converting Enzyme Inhibitor (ACEI)
Arterial Elastance (Ea)

B

Backward Expansion Wave (BEW)
Backward Compression Wave (BCW)
Body Mass Index (BMI)

C

Cardiac Output (CO),
Coronary Flow Velocity Reserve (CFVR)
Coronary Wave Intensity Analysis (CWIA)
Circumflex Artery, 198

D

Diastolic Blood Pressure (DBP)
Diastolic Time Fraction (DTF)
Dyssynchrony Index 3 (DS3)
Dyssynchrony Index 3 (DS2)

E

End-Diastolic Pressure (EDP)
End-Diastolic Volume (EDV)
End-Diastolic Pressure-Volume Relationship (EDPVR),
End-Systolic Pressure (ESP)
End-Systolic Volume (ESV)
End-Systolic Pressure Volume Relationship (ESPVR)
End-Systolic Elastance (Ees)
External Stroke Work (EW Or SW)

F

Fractional Flow Reserve (FFR)
Forward Compression Wave (FCW)
Forward Expansion Wave (FEW)

H

Heart Rate (HR)

L

Left anterior descending artery (LAD)
Left Atrial Pressure (LAP)
Left Ventricle (LV)
Left Ventricular Pressure (LVP)

M

Myocardial Infarction (MI)
Microvascular resistance (MR)
Myocardial Oxygen Consumption (MVO2)

P

Percutaneous Coronary Intervention (PCI)
Distal coronary Pressure (Pd)
End-Systolic Pressure (Pes)
Potential Energy (PE)
PRSW Preload-Recruitable Stroke Work.
Pressure-Volume (PV)
Pressure Volume Area (PVA)

R

Right Coronary Artery (RCA)

S

Systolic Blood Pressure (SBP)
Starling Contractile Index (SCI)
Stenosis Resistance (SR)
Stroke Volume (SV)
Stroke Work (SW)
Systemic Vascular Resistance (SVR)

T

Time Varying Elastance (E(t))

U

Coronary Flow Velocity (U)

Δ

Pressure gradient (ΔP)

RELATED MATERIAL

PUBLICATIONS

1. Accurate And Standardised Coronary Wave Intensity Analysis, Rivolo S, **Patterson T**, Redwood SR, Lee J; IEEE Transactions On Biomedical Engineering, 2016
2. Percutaneous Ventricular Restoration Using The Parachute Device: The Parachute III Pressure-Volume Loop Sub-study. **Patterson T**, Schreuder J, Burkhoff D, Marc Vanderheyden M, Rajani R, Toth G, Redwood SR, Bartunek J (submitted Cath. Cardiovasc. Int. 2017)
3. Deployed But Not Irretrievable: A Novel Surgical Off-Pump Technique For Parachute Device Extraction. Lucchese G, Rajani R, **Patterson T**, Kapetanakis S, Redwood SR, Bapat V, International Journal Of Cardiology, 2015
4. Cardiac Myosin-Binding Protein C: A Potential Early Biomarker Of Myocardial Injury, Baker JO1, Tyther R, Liebetrau C, Clark J, Howarth R, **Patterson T**, Möllmann H, Nef H, Sicard P, Kailey B, Devaraj R, Redwood SR, Kunst G, Weber E, Marber MS; Basic Research Cardiology, 2015
5. The Effects Of Cold And Exercise On The Cardiovascular System, Manou-Stathopoulou V, Goodwin CD, **Patterson T**, Redwood SR, Marber MS, Williams RP; Heart BMJ, 2015
6. Intra-Aortic Balloon Pump For High-Risk Percutaneous Coronary Intervention, **Patterson T,** Perera D, Redwood SR; Circulation: Cardiovascular Interventions, 2014

7. Invasive Assessment Of Cardiac Mechanics And Coronary Flow: A Correlation With Three-Dimensional Left Ventricular Deformation Imaging, **European Heart Journal** 2016
8. Flow-Contraction Matching In The Human Heart: A Novel Invasive Study Of The Complex Cardiac-Coronary Interaction In Ischaemic Heart Disease, H**eart BMJ**, 2016
9. Novel Insights Into The Physiology Of Cardiac-Coronary Interaction: A First-In-Human Study Utilising Invasive Real-Time Simultaneous Measures Of Coronary And Left Ventricular Hemodynamics, **Journal Of The American College Of Cardiology**, 2016
10. The Mechanics Of Cardiac Contraction And Coronary Flow: Exercise, Ischaemia And Anti-Anginals, **Heart BMJ**, 2016
11. Unravelling The Mechanisms Of Exercise Induced Ischaemia, Its Optimal Assessment, And Alleviation With Nitroglycerine, **Heart BMJ**, 2014

COLLABORATORS

- Dr Simone Rivolo, King’s College London
- Dr Jack Lee, King's College London
- Dr Divaka Perera, King's College London
- Professor Daniel Burkhoff, Columbia University, USA
- Professor Jos Spaan, Amsterdam Medical Centre, Netherlands
- Dr Maria Siebes, Amsterdam Medical Centre, Netherlands
- Professor William C Little, University Of Mississippi, USA
- Professor Phil Chowienzcyk, King's College London
- Dr Jan Schreuder, CD Leycom, Zoetermeer, Netherlands
- Dr Jozef Bartunek, Onze-Lieve-Vrouwziekenhuis, Aalst, Belgium

FUNDING BODIES

- British Heart Foundation, UK (£217,476)
- Guys' And St Thomas' Charitable Foundation, UK (£65,000)
- Zoll Medical Corporation, Boston MA, USA (£20,000)
- Cardiovascular Directorate Commercial Funds, St Thomas' Hospital, UK (£32,000)

AWARDS, PRIZES AND SCHOLARSHIPS

NATIONAL

- British Cardiovascular Society Annual Conference Top Abstract 2016
- British Heart Foundation Clinical Research Training Fellowship
- British Cardiovascular Interventional Society Trainee Representative
- British Heart Foundation Travel Scholarship

INTERNATIONAL

- Interventional Scholarship Complex Catheter Cardiovascular Therapeutics 2016
- Interventional Scholarship Complex Catheter Cardiovascular Therapeutics 2015
- European Society Of Cardiology, Cardiologist Of Tomorrow Award

REPORT OVERVIEW

Aims

The main aim of this work was to gain a greater understanding of the myocardial-coronary and ventricular-arterial interaction in humans in health and diseased states.

Main Hypotheses Investigated

Examination of the interaction between the myocardium, coronary arteries and systemic vasculature will enable the following hypotheses to be investigated:

1) Coronary blood flow impediment is a function of left ventricular elastance

2) The diastolic dysfunction accompanying ischaemia is dependent on systolic function

3) The anti-anginal effects of nitrate is due to its action on vascular smooth muscle

4) The therapeutic effect of percutaneous ventricular restoration therapy results from a reduction in dyssynchrony

Chapter 1 provides a detailed literature review on the cellular mechanisms of contraction; the relationship between coronary blood flow and myocardial mechanics the assessment of systolic and diastolic properties on a macroscopic level, and the impact of ischaemic heart disease on contractile function.

Chapter 2 Assessment of myocardial pump properties and coronary blood flow was performed using invasive left ventricular pressure-volume assessment (by use of a conductance catheter) and intra-coronary haemodynamic assessment (dual-sensor pressure-flow wire) in human subjects in the cardiac catheterisation laboratory. This

chapter describes the current software and hardware tools used for invasive LV and coronary data acquisition and the catheter laboratory techniques used to perform this work. Techniques that incorporate invasive coronary and left ventricular haemodynamic assessment do not exist, previous work have examined these either in isolation or independently, the disadvantages are that these do not provide continuous assessment of the interaction between the two.

Chapter 3 Describes the results of how these methodological issues were addressed for the purposes of this body of work; novel techniques are described that include hardware configuration to enable real-time data acquisition in human subjects. This chapter also describes a novel software system that was developed as part of the work toward this doctoral thesis: matrix laboratory programming language was used, to employ automated algorithms that analyse left ventricular (LV) pressure-volume (PV) loop and coronary haemodynamic (pressure and velocity) data simultaneously in humans. The results of *in-vitro* (phantom flow model) and *in-vivo* (human) calibration are described, with validation using human subjects. This system was applied to investigate the origin of the coronary wave energies, and their temporal relationship with the cardiac cycle and the relationship between instantaneous LV properties and coronary blood flow velocity; the results of which are detailed.

Chapter 4: Describes the results of an investigation into left ventricular haemodynamics and coronary blood flow during dynamic exercise; exercise-induced ischaemia was examined with a control group comparator. At low impact, exercise demonstrated a beneficial effect in both groups, but adversely affected haemodynamic variables in

patients with significant coronary artery disease. The precise affects on end-diastolic and end-systolic pressure volume relations are reported.

Chapter 5: The anti-ischaemic mechanism of nitrates was examined with focus on the interaction between the myocardium, coronary arteries and systemic vasculature in patients with ischaemic heart disease, by use of invasive catheter laboratory techniques and the aforementioned software analysis programme.

Chapter 6: This details the results of a human validation (first-in-man) study of non-invasive strain parameters correlated with invasive assessment of contractile performance; the predictive value of 3D speckle tracking echocardiography was also examined.

Chapter 7: Percutaneous ventricular restoration (PVR) therapy is a novel treatment in patients with ischaemic cardiomyopathy; the precise cardiovascular effects are not understood. In this study, ten patients underwent PVR implantation in the cardiac catheter laboratory with invasive LV PV loop assessment. This chapter describes the haemodynamic outcomes associated with PVR.

1 INTRODUCTION

In this introductory chapter the basic concepts underlying cardiac contraction and relaxation are discussed stretching from a cellular level to a macroscopic description of cardiac function and assessment using the pressure-volume loop diagram; the application of wave intensity analysis in the coronary circulation with focus on the myocardial-coronary interaction is also described. There follows a brief literature review on the physiological changes associated with exercise, the underlying mechanisms of myocardial ischaemia and the action of organic nitrates as anti-anginal agents and the pathophysiology of end-stage ischaemic heart disease.

1.1 CARDIAC STRUCTURE AND FUNCTION

In this following section, the cellular mechanisms underlying cardiac contraction are described.

1.1.1 MYOCYTE ARCHITECTURE

The mechanisms underlying cardiac contraction are at the level of the myocytes and work under cellular control.[1] Cardiac myocytes are specialised muscle cells, 30 micrometers in diameter and 100 micrometers in length; these are composed of bundles of myofibrils that contain microfilaments, Figure 1. Myofibrils repeat in distinct anatomical units known as sarcomeres and it is these that form the base of the myocytes' contractile properties. The sarcomere, the region of myofilament structures between two Z lines, is approximately 2 micrometers in length and is composed of thick (myosin) and thin (actin) filaments.[1] Interaction between these enables the sarcomere to shorten,

with thin filaments sliding over the thick filaments. The thin filaments are composed of troponin (Tn), tropomyosin and actin which comprise the regulatory protein complex. The Tn complex is composed of TnT (attaches to tropomyosin), TnC (binding site for calcium) and TnI, which acts to inhibit the myosin binding site on actin. On calcium binding, a conformational change in the Tn complex moves TnI away from the myosin binding site on the actin making it accessible to the myosin head. When calcium is then removed from the complex, it resumes its inactive position, inhibiting myosin-actin binding. This mechanism underlies excitation-contraction coupling.[2,3]

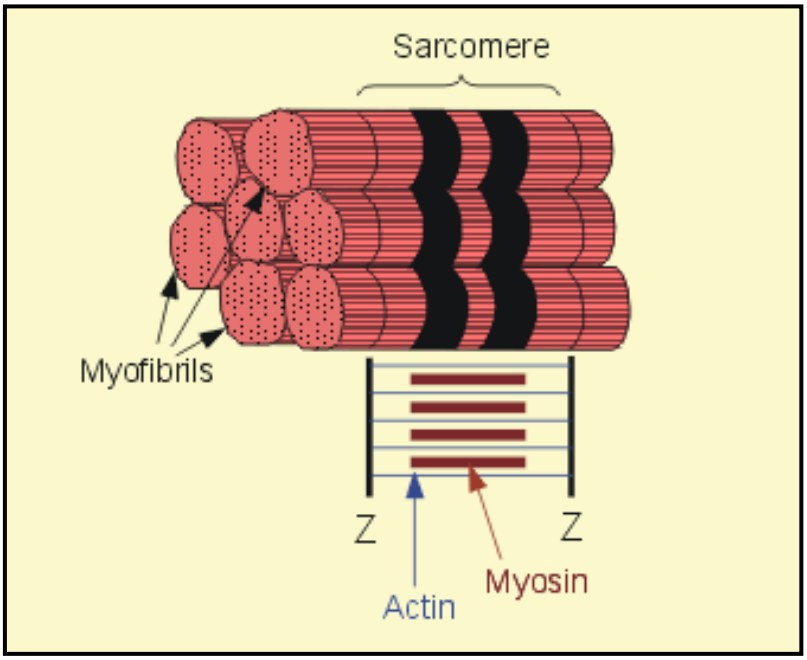


Figure 1 Cardiac myocyte.
These are composed of myofibril bundles, which are in turn comprised of myofilaments; the sarcomere is the region of the myofilament between two Z-lines and one M-line. Adapted from [4]

1.1.2 CARDIAC EXCITATION-CONTRACTION COUPLING

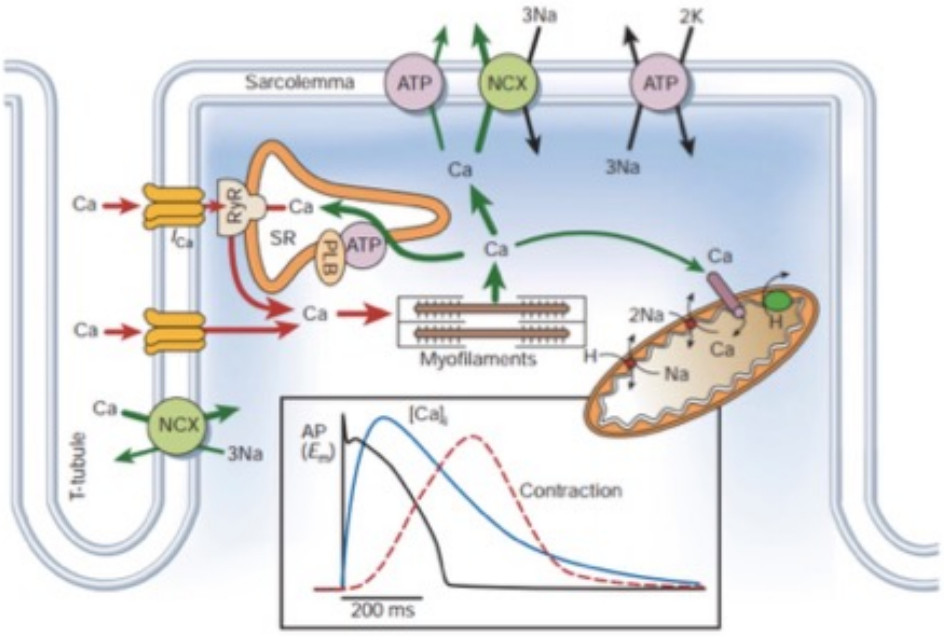


Figure 2 Calcium Release.
Entry of calcium into a myocyte triggers calcium release from the sarcoplasmic reticulum. Abbreviations: Ca Calcium, SR sarcoplasmic reticulum, Na Sodium, H hydrogen, K Potassium, ATP pumps, PLB phospholamban. Adapted from [5]

Excitation-contraction coupling is the process from electrical excitation of the heart to cardiac contraction. During the cardiac action potential, calcium (Ca) enters the cell: electrical depolarisation increases the probability of sarcolemmal calcium channel opening with calcium influx. A rise in calcium concentration follows in the sub-sarcolemmal space near the lateral cisternae of the sarcoplasmic reticulum (SR), this rise in local calcium concentration drives the release of an even larger pool of calcium from the SR (calcium-induced calcium-release), increasing the intra-cellular calcium concentration markedly, Figure 2. This intracellular Ca then binds to TnC inducing the aforementioned conformational change, thus exposing the actin molecule and enabling

it to bind the myosin ATPase on the myosin head; energy is supplied by hydrolysis to enable the conformational change and sliding of the filaments, thereby shortening the sarcomere. The Ca influx into the cell then slows, sequestered by the Ca ATP pumps within the sarcoplasmic reticulum; reduced calcium induces a conformational change in the troponin complex, and TnI once again inhibits the actin binding-site and ADP is displaced by an ATP molecule on the myosin head. Calcium is therefore fundamental to cardiac contraction, the more calcium made available to the cell increases the force of contraction. ATP production provides an energy source for the heart, this is derived from oxidative phosphorylation within the mitochondria, one third is used for excitation-contraction coupling and basal metabolism; the other two thirds are expended during mechanical contraction (discussed in section 1.2.3). [1-3,5-7 8]

1.1.3 FORCE OF CONTRACTION

The beta-adrenoceptor mechanism increases calcium availability to the myocytes, stimulation of which occurs when sympathetic drive is activated. This leads to an increase in cyclic adenosine monophosphate and therefore activation of protein kinase-facilitated Ca entry into the cell. This protein kinase activation also phosphorylates and releases phospholamban (an inhibitor of SR calcium uptake), therefore reuptake of calcium by the SR is more rapid; thus beta-adrenergic stimulation increases the force and velocity of contraction (positive inotropy) but also increases the rate of relaxation (lusitropy).[9,10] The increased contractile state increases oxygen consumption, driven almost entirely by the increased energy demand of excitation-contraction coupling (1.1.2).

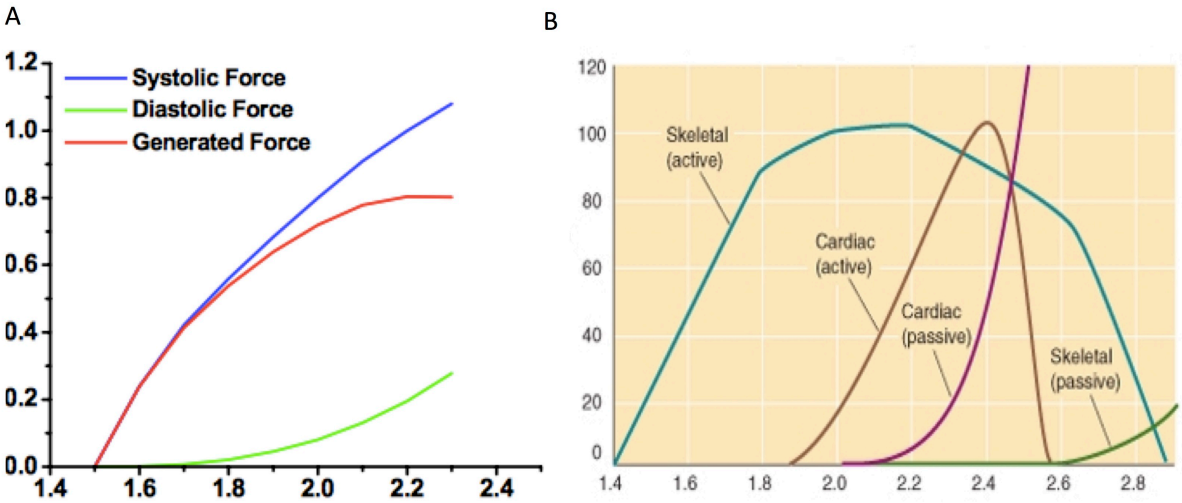


Figure 3 Sarcomere length and force generation.
Length versus the relative systolic and diastolic (μN) generated force exerted by muscle (**A**) sarcomere length (μm) related to the maximum tension (%) generated force (**B**). Adapted from [11]

Other mechanisms that influence contractility include force-length relations (Starling's law) calcium sensitivity.[12,13] Cardiac muscle length exerts a major influence on force production (strength of contraction); cardiac muscle length is directly proportional to sarcomere length. The optimal sarcomere length is 2.3 micrometers, this constitutes ideal overlap between the thick and thin filaments, and if this distance is shorter then less force is generated. Force-length relationships are conveniently used to characterise the systolic and diastolic contractile properties of cardiac muscle.[14,15] If a muscle is stretched from its slack length (the length at which no force is generated), both the resting (end-diastolic) tension and the peak (end-systolic) tension increase, Figure 3.

The end-diastolic force-length relationship is non-linear and exhibits a shallow slope at short lengths and a steeper slope at longer lengths, which is a reflection of the non-linear mechanical restraints imposed by the sarcolemma and extracellular matrix to prevent overstretch of the sarcomeres. End-systolic force increases with increasing muscle length to a much greater degree than end-diastolic force.[14] The difference in force at end-diastole as compared with end-systole increases as muscle length increases and indicates a greater amount of developed force as the muscle is stretched. Inotropic agents do not affect the end-diastolic force-length relationship, rather calcium availability and sensitivity, thus administration of inotropic agents drives an upward shift in the end-systolic force-length relationship, such that at any given length the muscle can generate more force. These force-length relationships can be described on a larger scale; at the level of the ventricle, these pressure-volume relations are the macroscopic counterpart of cellular markers of contractility; therefore are fundamental to assessing ventricular systolic and diastolic properties.

1.2 ASSESSMENT OF CARDIAC FUNCTION

In the following section, the physiological measurements derived from the pressure-volume loop diagram are described. This includes measures of both preload and afterload, the interaction between the heart and the great vessels (ventriculo-arterial coupling) manifesting in ventricular efficiency, and gold standard measures of contractility and diastolic properties. In addition to these invasive measurements of cardiac function, the potential for non-invasive assessment in the form of 3D echocardiographic strain imaging is discussed.

1.2.1 CARDIAC CYCLE AND THE PRESSURE-VOLUME LOOP

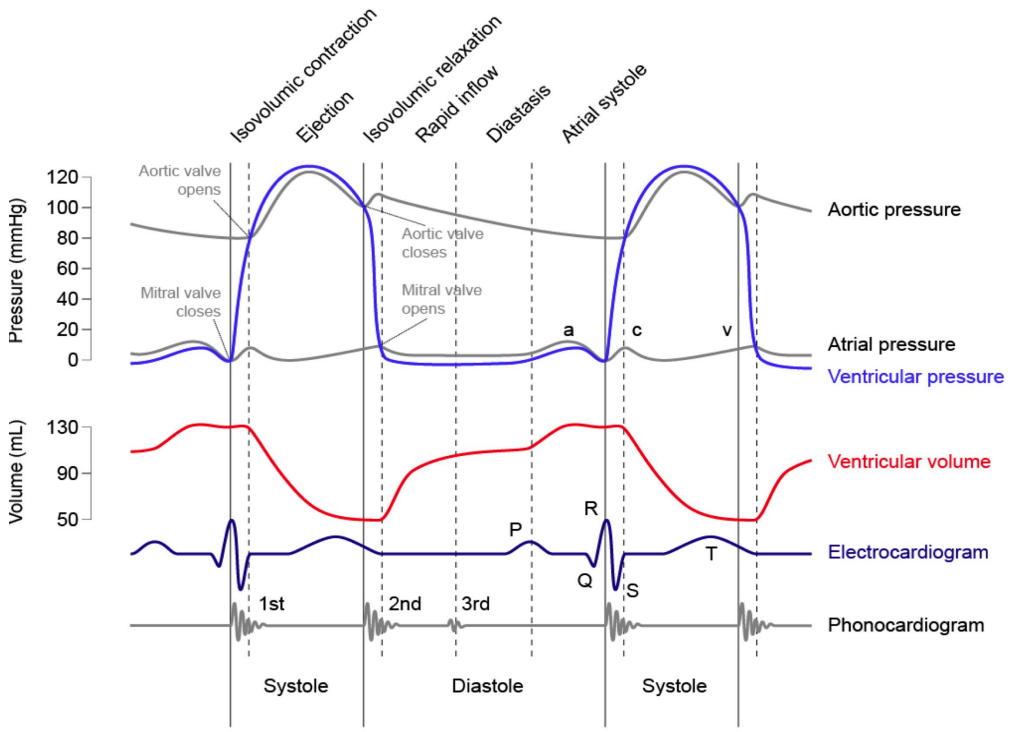
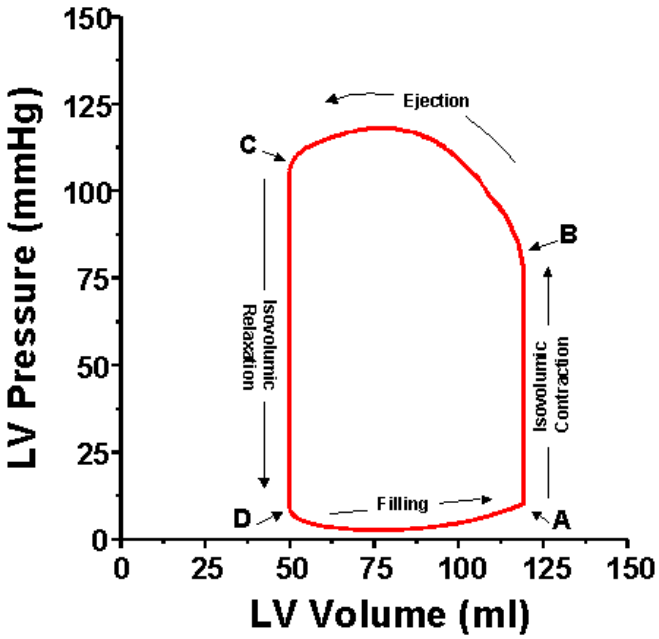


Figure 4 The cardiac cycle.
This is depicted over two cardiac cycles (heart beats); aortic pressure (black), ventricular pressure (blue), left atrial pressure (grey) and left ventricular volume (red) plotted as a function of time, adapted from [4].

The cardiac cycle is divided into systole and diastole. In systole, myocardial transformation in the form of cell membrane depolarisation enables calcium entry and cross-bridge formation to the point of maximal mechanical activation. During diastole, muscle relaxation and cross-bridge uncoupling restores the myocardium to its resting state. Systole comprises isovolumic contraction and ejection; diastole comprises isovolumic relaxation and filling. The cardiac cycle is commonly represented by plotting changes in left ventricular pressure and volume over time, Figure 4. At the start of the cardiac cycle, passive filling of the left ventricle (LV) is followed by atrial depolarisation and kick; electrical activation of the ventricle leads to depolarisation and contraction triggering mitral valve closure as left ventricular pressure (LVP) exceeds left atrial pressure (LAP); there follows rising LV pressure in the face of constant LV volume (isovolumic contraction) until the point at which LVP exceeds aortic valve pressure and the aortic valve opens. At this point LVP and aortic pressure remain relatively similar and the LV volume reduces as blood is ejected from the LV into the aorta. The duration of systole is predominantly governed by aortic stiffness. As myocardial contractility reaches it maximal state of contraction, ejection slows, LVP starts to fall and the myocardium begins to relax. The aortic valve closes once LVP drops below aortic pressure and the ventricle is at end-systole, with minimal volume. The myocardium continues to relax as denoted by the further drop in LVP, with no change in volume (isovolumic relaxation). Once LVP drops below LAP, the mitral valve opens and passive filling takes.

Assessing the changes in contractility within a patient and furthermore between groups of patients is a challenge. However, as alluded to earlier, force-length relations are a good indicator of contractility; these force-length relationships can be described on a larger scale; at the level of the ventricle, thus pressure-volume relations are the macroscopic counterpart of these cellular measures of contractility; thus to perform measurements of contractility in humans, it is necessary to generate data in the form of a ventricular pressure-volume loop. Plotting ventricular pressure against volume in the form of a pressure-volume loop produces a powerful and accurate approach to determining both contractile function and diastolic properties of the heart.

Figure 5 The left ventricular (LV) pressure-volume loop.



The cardiac cycle is depicted by describing pressure as a function of volume, mitral valve closure (A), aortic valve opening (B), aortic valve closure (C), mitral valve opening (D). Adapted from [11]

In Figure 5, the corresponding stages of the cardiac cycle (initially seen in Figure 4) have been marked on the PV loop demonstrating the sequence of events that take place in the left ventricle (LV) over one cardiac cycle; each cycle is represented by a single

loop travelling in an anticlockwise direction. At the point of mitral valve closure, filling is complete, electrical depolarisation triggers ventricular contraction; a period of isovolumic contraction takes place in the presence of aortic and mitral valve closure until aortic pressure is exceeded and the aortic valve opens with ejection. A reduction in LV volume follows as ejection takes place, with continued contraction, until the point of maximal contraction (elastance) is reached; LVP falls as the rate of contraction slows until LVP drops below aortic pressure and the aortic valve closes. With both valves closed, a period of isovolumic relaxation follows until LVP falls below left atrial pressure (LAP) and the mitral valve opens and passive LV filling takes place; the ventricle continues to relax thus pressure continues to drop despite an increase in volume. Volume in the LV increases to the point of maximal volume at end-diastole and the cycle repeats. Depiction of the cardiac cycle as a pressure-volume loop enables measurement of haemodynamic parameters.

1.2.1.1 PRESSURE AND VOLUME INDICES

A number of physiological measurements, markers of contractility and relaxation as well as the total mechanical energy generated by the heart can be derived from the PV loop. In its simplest application, indices of volume and pressure can be derived. In Figure 6 (A) the maximum LV volume is achieved at end-diastole, at this point, end-diastolic volume (EDV) can be measured. The importance of deriving end-diastolic volume is that it represents sarcomeric stretch, therefore is a direct indicator of preload; the end-diastolic pressure (EDP) Figure 6(B), measured at the end-diastolic point, is the pressure required to generate this preload volume.

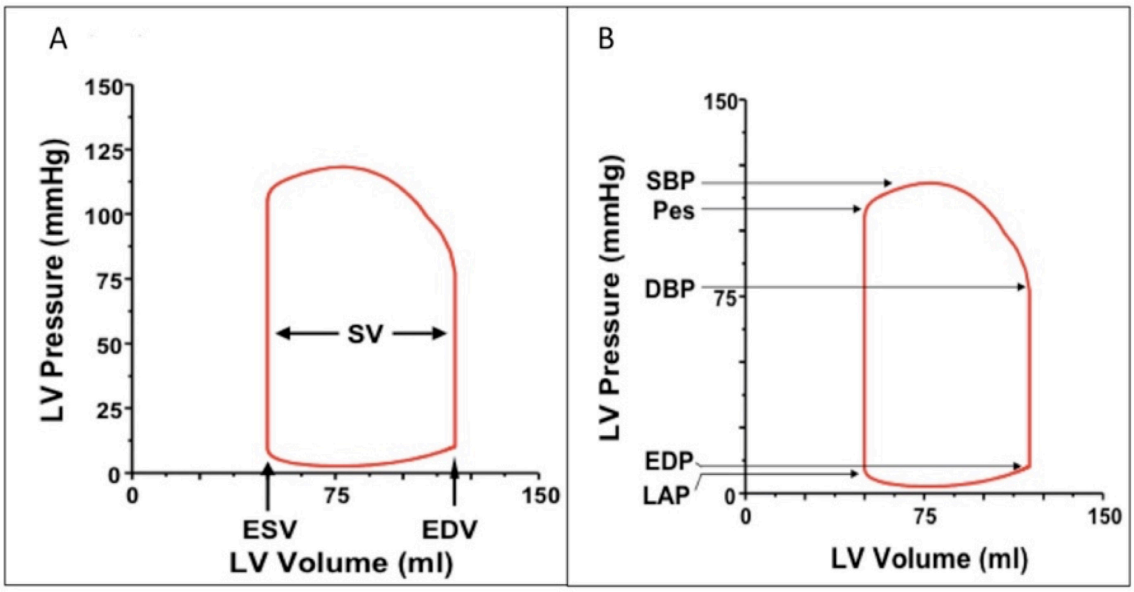


Figure 6 Physiological parameters derived from the PV loop.
Left: volume indices, right: pressure indices. Abbreviations: LV left ventricle, ESV end-systolic volume, EDV end-diastolic volume, SV stroke volume, SBP systolic blood pressure, Pes end-systolic pressure, DBP diastolic blood pressure, EDP end-diastolic pressure, LAP left atrial pressure.

The minimum volume in the ventricle is at end-systole, which is the end-systolic volume (ESV), thus stroke volume (SV) can be derived from EDV and ESV. Furthermore, by incorporating heart rate, the cardiac output (CO) can be calculated, Equation 1.

Equation 1

$$\boldsymbol{CO = HR\ X\ SV}$$

In Figure 6(B) the maximum pressure in the ventricle at any point in the absence of aortic valve disease equals systolic blood pressure (SBP); the point of aortic valve opening is equal to diastolic blood pressure (DBP); end-systolic pressure (Pes) can be derived at end-systole and LAP at the point of mitral valve opening.

On the PV loop we see that through one cardiac cycle, the ventricle moves from a state of maximal contraction at end-systole to a relaxed state at end-diastole. At this point, the myocardium is in a state of maximal relaxation and it is possible to describe the diastolic properties of the heart.

1.2.2 MEASURING DIASTOLIC PROPERTIES AND RELAXATION

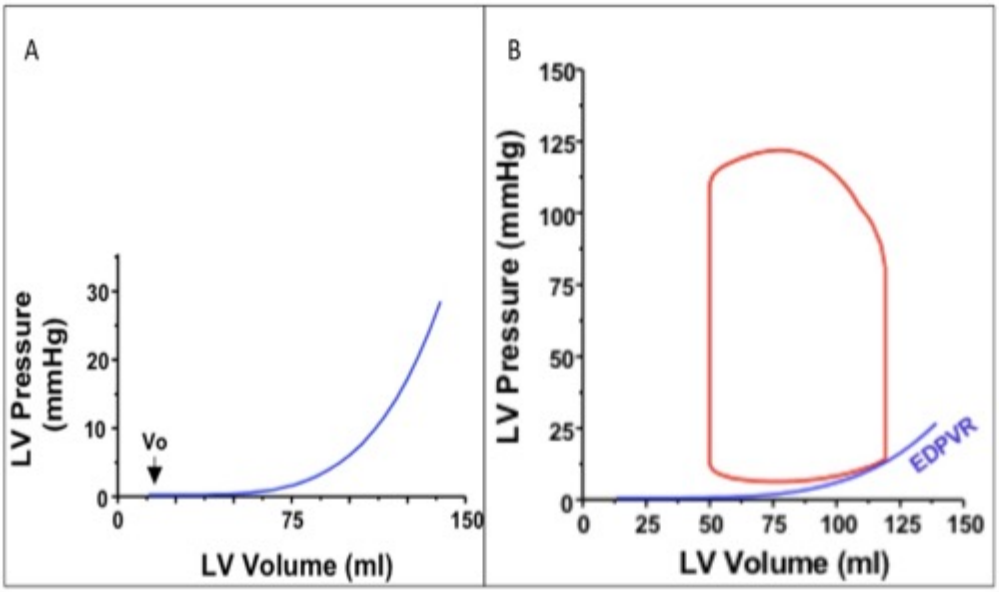


Figure 7 End-diastolic pressure volume relations. EDPVR intersects the x-axis at V0 when extrapolated backward (**A**); it forms the lower boundary on the PV loop, intersecting the loop at the end-diastolic pressure-volume point (**B**), adapted from [11].

At the end of diastole, the heart is in a state of maximal relaxation. The relationship between pressure and volume at end-diastole is described in

Equation 2 where EDP is the end-diastolic pressure, V is the volume inside the ventricle, Po is the pressure asymptote at low volumes (generally close to 0 mmHg), and α and β are constants, which specify the curvature of the line, which is in turn determined by the mechanical properties of the muscle and structural features of the ventricle.[16]

Equation 2

$$\boldsymbol{EDP = Po + \beta V \alpha}$$

The curve is called the "end-diastolic pressure-volume relationship" (EDPVR),

Figure 7. LV EDPVR is the most important means of characterising passive ventricular properties; it is the global, integrated expression of chamber geometry, wall thickness, and all aspects of passive material properties of the myocardial wall.[17,18] This relationship is non-linear (compliance falls as volume increases); however, at pressures of less than 2-5 mm Hg the pressure-volume relationship is linear (with α approaching zero).[16] The EDPVR curve, generated by preload reduction, can be extrapolated back to the horizontal axis, intersecting at the point V_0; this represents the minimum volume required to cause a change in LV pressure and is known as the unstressed volume. By definition, the EDPVR indicates the amount of diastolic filling that will occur for a specified filling pressure and is therefore a key physiological determinant of preload. Furthermore diastolic filling is a well-known determinant of LV function.[19,20] The α constant is unaffected by changes in initial volume and directly altered only by changes in wall stiffness, it can therefore be used as a quantitative index of wall stiffness; the β constant, although directly related to wall stiffness, is inversely related to the initial volume of the ventricular chamber (V_0).[16] Changes in this relationship occur in health and disease and can result from cardiomyopathy, myocardial infarction and scar.[16,19]

At end-systole, the myocardium is in a state of maximal activation. At this end-systolic point, we can similarly describe the contractile properties of the ventricle.

1.2.3 MARKERS OF CONTRACTILITY

1.2.3.1 END-SYSTOLIC PRESSURE VOLUME RELATIONS

During systole, the extent of myofilament activation achieved in one beat is dependent not only on the amount of calcium available to the myofilaments but also on the length of the muscle. As mentioned previously (1.1.3) the shape of the end-systolic tension length relation (ESTLR) varies with contractile state.[21] This is likely related to either 1) muscle fibre affinity to calcium or 2) calcium release dependent on muscle length.[22,23] The shape of the ventricular end-systolic pressure-volume relationship (ESPVR; the ventricular level counterpart of ESTLR) is linear within physiological ranges of preload and afterload, independent of contractile state. The ESPVR slope reflects the contractile state and describes the myocardium at end-systole during maximum activation, Figure 8.[24,25]

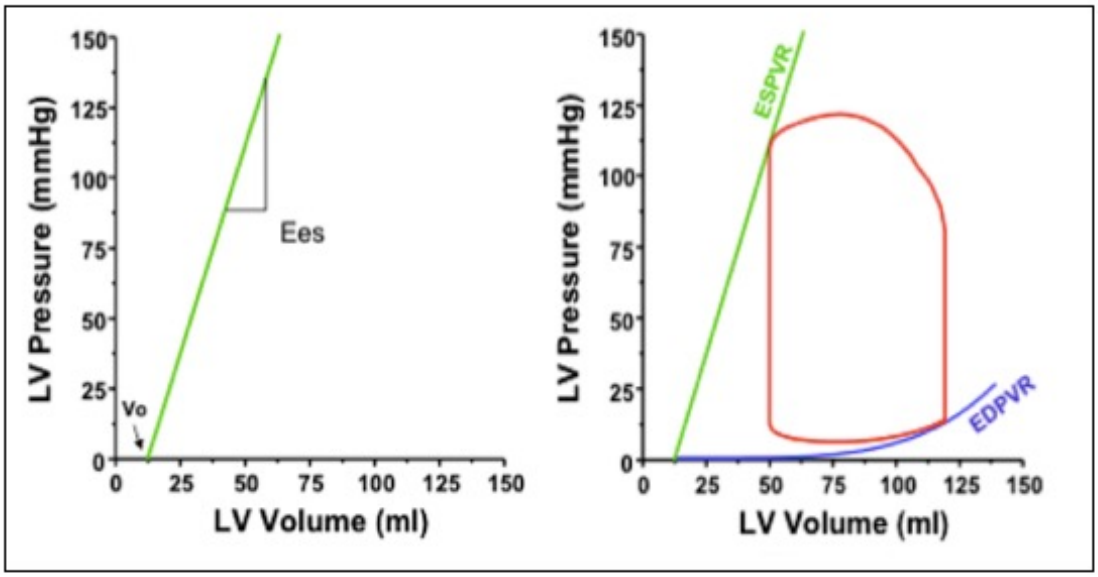


Figure 8 The end-systolic pressure volume relationship (ESPVR).
The slope Ees can be extrapolated to V_0 on the x-axis and forms the upper boundary of the pressure-volume loop, intersecting the loop at the ESPVR point, adapted from [11]

The advantage of ESPVR as a measure of contractility is that it has been shown in many studies to separate poorly contracting ventricles from normal ones more accurately than ejection fraction or end-systolic volume.[26] The slope of the end-systolic pressure-volume relationship line is designated Ees.[25] The ESPVR line intersects the x-axis at a positive finite value V_0, this can be calculated as shown in Equation 3, where Pes is the end-systolic pressure, V is the volume of interest and Ees is the slope of the linear relation based on experimental observations.[25] V_0 varies over time from end-diastole (the unstressed volume) to end-systole, however varies very little at end-systole, thus for calculations V_0 can be viewed as a constant.[26]

Equation 3

$$\boldsymbol{Pes} = \boldsymbol{Ees}\,(\boldsymbol{V} - \boldsymbol{V_0})$$

Whilst describing the myocardium during contraction, instantaneous pressure and volume are the two most fundamental variables; during contraction and relaxation the instantaneous pressure and volume can be related in a simple manner as seen in Equation 4, where E(t) is the slope of the curve over time and follows the same basic (linear) shape, Figure 9[27] This instantaneous pressure-volume relationship over time is known as the time varying elastance E(t) and the peak is E_{max}.

Equation 4

$$\boldsymbol{E(t)} = \boldsymbol{P(t)/[V\,(t) - V_0]}$$

The time-varying elastic diagram can be used to relate the instantaneous pressure to volume at any point throughout the cardiac cycle. Thus if the E(t) function and the time course of volume change is known, it can be possible to predict pressure changes

throughout the cardiac cycle. The function E(t) is unaffected by end-diastolic volume or arterial pressure, however it is affected by changes in inotropic state. Furthermore on increasing contractile state, both peak E(t) increases and time to peak E(t) shortens.[25]

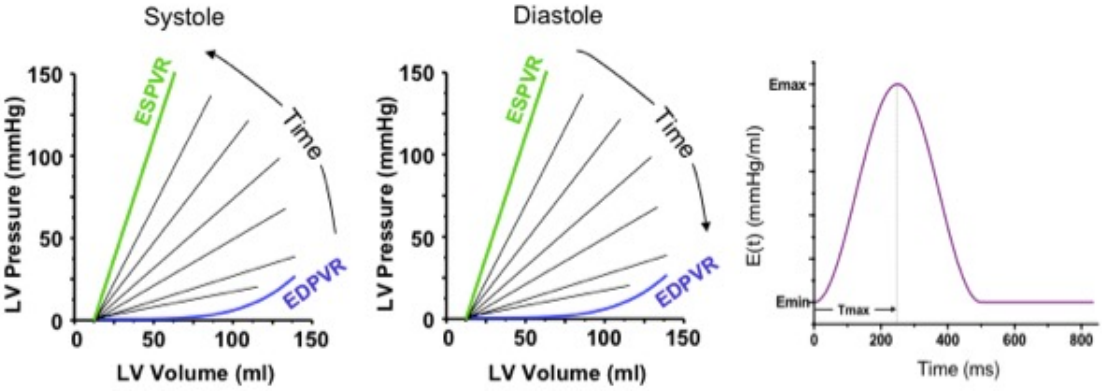


Figure 9 Time varying elastance. E(t) (right) generated from the instantaneous pressure volume relationship at various stages in time (hypothetical straight lines) during contraction (left) and relaxation (middle), adapted from [11].

Due to the fact that end-systole and end-ejection are not the same (coincidentally in the left ventricle, ejection normally finishes shortly after end-systole), end-systole can be difficult to determine; thus by using the time varying elastance, end-systole can be designated at the point of E_{max} when the ventricle is in its maximal contractile state.[26] The slope of the ESPVR line (Ees), can therefore be calculated based on estimations of E_{max} generated from time-varying elastance curves. These calculations provide increased accuracy because the slope of the instantaneous pressure-volume relation, known as E(t), increases with time until it reaches a point E_{max}. The true ESPVR slope (Ees) is generated from connecting points on the left uppermost corner of the PV loop, thus is similar but not identical to E_{max}; for the purposes of simplicity and single beat estimation of ESPVR (section 3.2.3.4), the two are presumed to be the same.

The energy consequences of time-varying elastance provide the theoretical basis for understanding cardiac energetics. An increase in the time-varying elastance and the counterclockwise transition of the systolic PV relation enables us to total mechanical energy.

1.2.3.2 CARDIAC ENERGETICS

The subject of myocardial energetics has been much debated in the past.[28-30] The most dominant line of investigation into myocardial energetics is the measure of total mechanical energy generation of the ventricle. Invasive measurement using pressure-volume loops is the current gold standard measurement of total mechanical energy. PV loop measurement has enabled direct determination of contractile efficiency and the quantification of total mechanical energy, thus the use of the PV loop diagram extends beyond haemodynamic parameters, entering into cardiac energetics and mechano-energetic coupling and is the best way to quantify cardiac efficiency.[8]

Time-Varying Elastance and Mechanical Energy

The total area bounded by the systolic component (isovolumic contraction through ejection) of the PV loop and the EDPVR and ESPVR lines, generates two smaller areas: the area of the PV loop or external stroke work (EW or SW) and the potential energy (PE). Thus pressure-volume area (total mechanical energy expenditure) is therefore equal to SW+PE, Figure 10.[8]

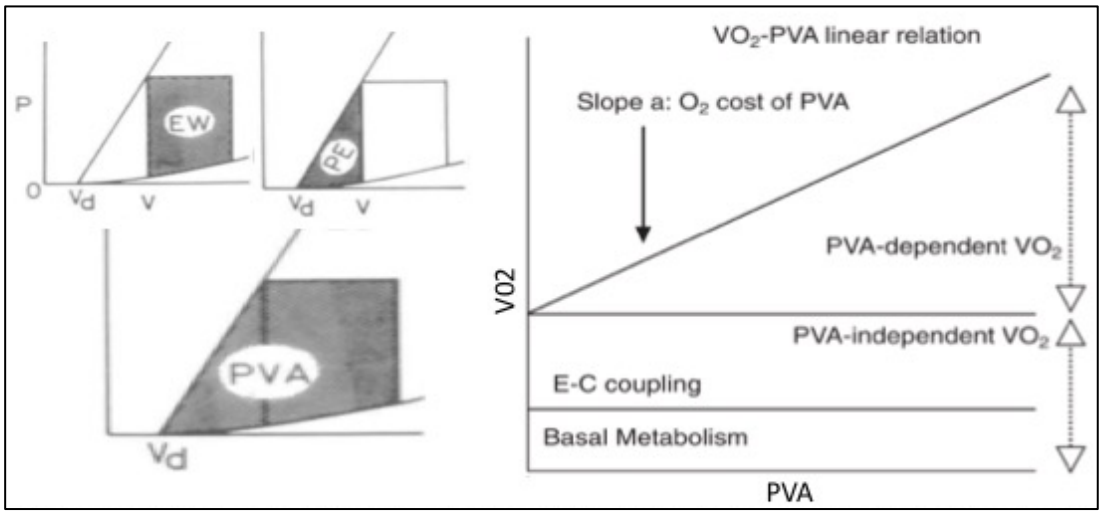


Figure 10 Total mechanical energy.
This is also known as PVA or pressure volume area, and is comprised of EW: external work (the area of the PV loop) and PE: potential energy, the PVA is bound by the ESPVR and EDPVR lines (left). PVA is linearly related to myocardial oxygen consumption VO2 (right), adapted from [8]

The potential energy comprises the energy used for basal metabolism and excitation-contraction coupling, but the majority is seen as heat. SW is the actual produced work of contraction and is seen as useful energy. The importance of this model of total mechanical energy is that it correlates with myocardial oxygen consumption (VO2) in excised, cross-circulating canine hearts under varying loading, heart rate and inotropic conditions. There is a linear relationship between PVA and VO2. The relationship consists of a baseline "unloaded VO2" primarily for basal metabolism and excitation-contraction coupling and the "excess VO2-PVA" relationship, Figure 10. Thus by measuring PVA, we can accurately estimate myocardial oxygen consumption. This energy output by the heart is essentially the force multiplied by displacement and is measured in Joules, thus PV loop area (expressed in mmHg.mL) must be converted into Joules: 1mmHg.ml = 1.33×10^{-4} Joules.[29] With variations in contractility either during exercise or with dobutamine, the upward shift in the PVA-VO2 relationship is consistently seen, i.e. for a higher contractility (with inotropic intervention), there is a

higher oxygen cost of PVA, as explained earlier, this is due to the increase energy consumption of excitation-contraction coupling, because the slope of the PVA-VO2 relation remains unchanged. [31-33]

Ventricular Efficiency

Efficiency of the heart is the conversion of oxygen to useful work, in other words, the work performed by the ventricle in relation to myocardial oxygen consumption, and can been defined in a number of ways. Clinically the only work seen by the vascular system is the stroke work; therefore the most appropriate definition of efficiency is believed to be the SW to VO2 ratio.[31,32] This is the product of two stages, firstly the conversion of myocardial oxygen consumption to total mechanical energy; and secondly the efficiency of energy transfer of PVA to SW. Put more simply, SW/PVA is the efficiency of conversion of total mechanical energy to external stroke work, and SW/VO2 is the efficiency of conversion of metabolic energy to stroke work. Under normal conditions efficiency of VO2 to SW conversion is in the region of 25%, with the rest lost as heat.[8]

For the purposes of this study, we examine the efficiency of energy transfer of PVA to SW. In the absence of arterio-venous sampling, VO2 cannot be directly measured, thus the SW: PVA ratio is used as a surrogate marker of ventricular efficiency. Importantly loading conditions can influence pressure-volume area and ventricular efficiency. Usefully, these can also be measured by way of the PV loop.

1.2.4 MEASURES OF AFTERLOAD

The left uppermost point on the PV loop is where we measure Pes; the importance of Pes is that it corresponds to mean arterial blood pressure, therefore can be utilised in estimation of systemic vascular resistance. Systemic vascular resistance (SVR) is calculated as the ratio of mean aortic pressure (minus right atrial pressure) to cardiac output. This is an accurate measure of peripheral vasomotor tone.[34] SVR is a frequently used index to estimate left ventricular afterload; however, this measures only one component of LV afterload, the non-pulsatile component of peripheral tone, and does not incorporate left ventricular internal fibre load, i.e. factors internal to the myocardium.[35,36] LV systolic performance is inversely related to the force opposing LV fibre shortening (afterload), therefore utilisation of the pressure-volume diagram can generate a simplified measure of arterial load known as arterial elastance or Ea, Figure 11. Ea is the ratio of end-systolic pressure to stroke volume. This incorporates the principal elements of vascular load including peripheral resistance, vascular compliance, impedance and systolic and diastolic time intervals, and closely approximates arterial load obtained from aortic impedance and arterial compliance data, although this model does not account for reflected waves, the net effects of these are functionally accounted for in the PV loop.[34,37] The arterial elastance can be extended to examine ventricular-arterial coupling: the arterial elastance to end-systolic elastance ratio (Ea:Ees). This is an important parameter that measures the interaction between the left ventricle and the arterial system; it is a determinant of net ventricular performance and cardiac energetics.[37,38] Ea: Ees falls between a range of 0.7 to 1.2, where the heart and great vessels are working optimally to provide the greatest work, power and efficiency.[39,40] Previous modeling by Burkhoff et al. have demonstrated that stroke work

(effective external work performed by the heart) is at its maximum when Ea is equal to Ees.[31] Therefore, measurements of afterload can greatly enhance our understanding of the ventricular-arterial interaction. Measures of afterload used in this thesis are: 1) end-systolic pressure (Pes) 2) systemic vascular resistance (SVR) 3) arterial elastance (Ea) and 4) ventricular-arterial coupling (Ea:Ees ratio).

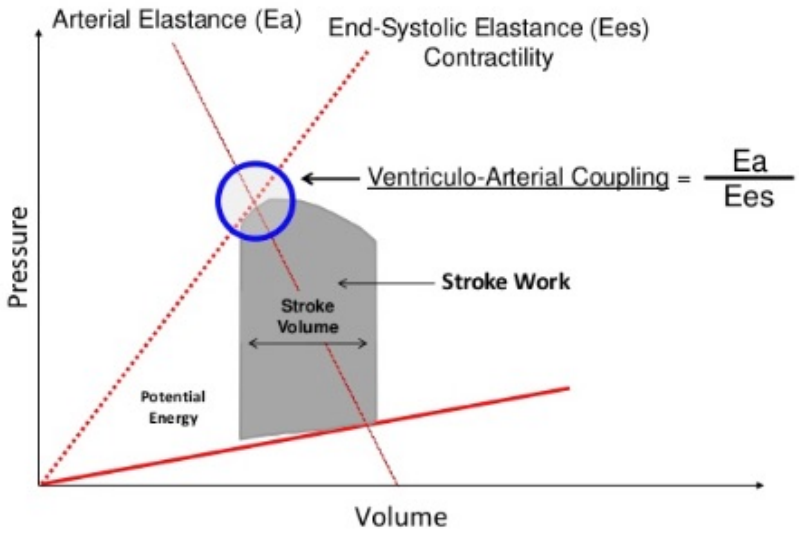


Figure 11 Arterial elastance (Ea).
This is calculated as the ratio of end-systolic pressure to stroke volume, and can be used in assessment of ventriculo-arterial coupling.

1.2.5 DEFORMATION IMAGING

Until this point, we have described invasive measurements of cardiac contraction, in the following section, we describe the potential of echocardiographic deformation imaging as a tool for the non-invasive assessment of left ventricular function.

Assessing the impact of coronary artery disease on cardiac function is a key task in clinical assessment and remains difficult to quantify non-invasively. Echocardiography in the assessment of regional myocardial function is advantageous over other modes of assessment such as computed tomography and cardiac magnetic resonance imaging due to its widespread availability, safety and high temporal resolution.[41] Tissue Doppler imaging during echocardiography can be used to quantify regional myocardial function; by measuring changes in phase shift of the returning ultrasound signals from the myocardium, tissue velocities can be determined; [42]however, tissue velocities represent the net effect of the contractile and elastic properties of the area in question. Thus myocardial strain or deformation is thought to be more representative of local myocardial function.[43,44] Strain is a dimensionless index and represents deformation, in other words fractional change from the original dimensions, produced by the application of stress. This can be described as positive strain (lengthening or expansion) or negative strain (shortening or contraction). [44,45] The ideal would to be to measure Langranian strain defined in Equation 5.

Equation 5

$$\boldsymbol{LS} = \frac{(\boldsymbol{L}-\boldsymbol{L0})}{\boldsymbol{L}}$$

Where L_0 is the length corresponding to zero strain and L is the instantaneous length; however this is often replaced by initial muscle length or end-diastolic length. Strain

rate, the temporal derivative of strain is the rate of deformation measured as units per second, which also correlates with the shortening velocity per fibre length.[44]

Tissue velocities are a function of the local rate of deformation, therefore it could be argued that velocities and strain rate provide the same information, however in regional wall motion abnormalities following dobutamine administration in coronary artery disease, tissue velocities were also seen to decline in the non-ischaemic segments, whereas regional strain remained unchanged, suggesting that tissue velocities (as a measure of cardiac function) are influenced by the ischaemic regions due to the tethering of myocardium, whereas strain is not.[46] The principles types of myocardial strain described are longitudinal, radial, circumferential and rotational. Although these strain measures are assessed individually, the reality is that these strain vectors occur in a 3D integrative manner due to myocardial fibre orientation.

1.2.5.1 SPECKLE TRACKING AND INDICES OF CONTRACTILITY

The most recent approach to myocardial strain is echo-derived speckle tracking, Figure 12. This is a post-processing computer algorithm of grey-scale images applied to a user-defined region of interest that automatically defines regions into blocks of pixels tracking stable patterns of speckles. Subsequent frames are analysed locating these speckles. Spatial and temporal data from the location shift is used to calculate the velocity vectors and temporal alterations in these stable speckle patterns are identified as moving further apart or closer together thus creating regional strain vectors; these are not reliant on the Doppler angle of incidence like tissue Doppler imaging strain thus enhancing the robustness of analysis.[46,47]

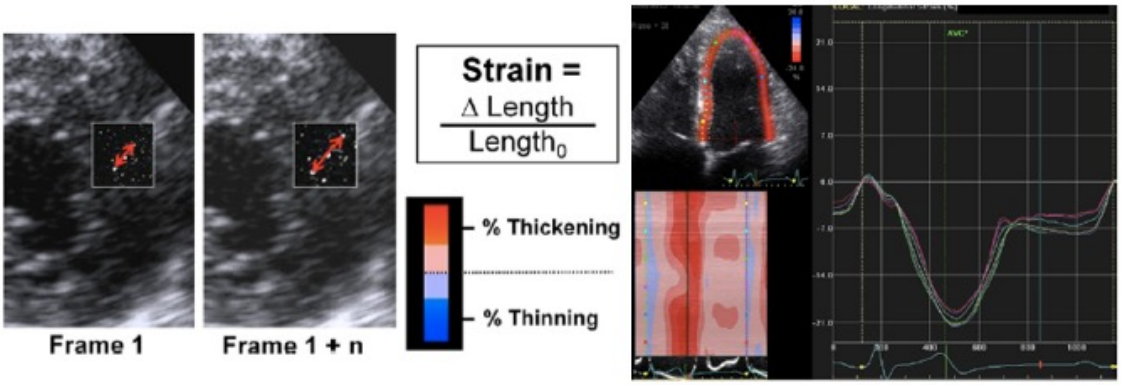


Figure 12 3D speckle tracking echocardiography.
Left: diagram of speckle tracking, information about strain is generated by changes in speckles from frame to frame. Right: an example of speckle tracking longitudinal strain using a four chamber apical view, adapted from [41].

Significant insights from the addition of strain imaging has refined the ability of echocardiography to detect patterns of ischaemia and infarction, through its ability to differentiate passive motion from active contraction; strain has been shown to improve on restoration of flow during coronary angioplasty or acute infarction, which has been validated in animal models.[48,49] There is also a role for strain imaging during dobutamine stress echo, improving the sensitivity and specificity when compared to visual assessment alone.[50-52] Interestingly, a study examining rat hearts found further advantages to strain assessment, specifically they found longitudinal and circumferential strain to correlate with invasive markers of contractility derived from LV pressure-volume assessment; the potential for this type of application is vast: strain could provide accurate non-invasive information regarding contractility indices, far superior to our currently used methods.[53] This has not yet validated been in humans, and isthe main focus of strain application in this thesis. Assessment of myocardial function in the presence of preserved LV function can provide valuable information with respect to outcome, particularly in the patient with ischaemic heart disease. It is believed that in

subjects with preserved left ventricular function at rest, that 3D speckle tracking echocardiography is able to detect underlying coronary artery disease through detection of subclinical LV systolic dysfunction, thus enabling a more accurate assessment for both risk stratification and further ongoing treatment.

Accurate assessment of contractile function is fundamental to our understanding of cardiovascular pathophysiology; however, to fully understand pump properties, it is important to assess the components of the system. The myocardium and coronary vasculature are in close proximity such that an interaction between the two occurs. This is due to the functional arrangement of the coronary circulation within the myocardium.

1.3 FUNCTIONAL ARRANGEMENT OF CORONARY CIRCULATION

The coronary circulation is a complex system of branching vessels comprising the epicardial vessels, intramural vessels and veins,

Figure 13.[54,55] The myocardium and coronary vasculature are in close proximity such that a two-way interaction known as cross talk occurs. This predominates between the myocardium and the intra-myocardial vessels, which can be further separated into intramural vessels and the microcirculation. The microcirculation is composed of more than 10^{10} arterioles and capillaries. Intramural vessels ranging from 20-300 micrometers in diameter penetrate the myocardium from the subepicardium to the subendocardium.[56]

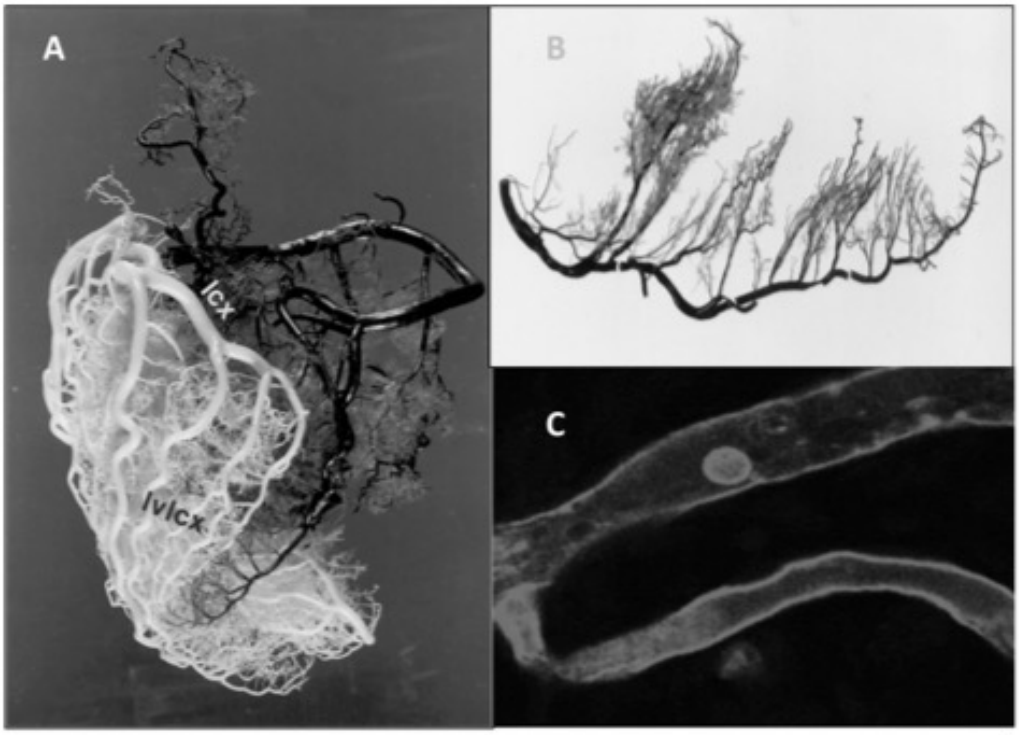


Figure 13 The coronary circulation.
A, a cast of the coronary circulation depicting the epicardial vessels branching and subdividing; **B** The left anterior descending artery and its intramural; branches visualised; **C** Brightfield electron microscopy identifying a post-capillary, adapted from [57].

The microcirculatory bed is the major site of resistance in the coronary circulation, impeding the blood flow during myocardial contraction. Pressure measurements in differently sized arteries and arterioles have indicated that under normal conditions, 45-50% of total coronary vascular resistance resides in vessels larger than 100 μm.[58,59] The number of resistance vessels in the subendocardium is higher than that in the subepicardium, the result being that during diastole, flow is approximately 10% greater. However, there is a preferential decrease in subendocardial flow during systole as a result of intramural compressive forces. Despite the differences in structure of the vascular bed to compensate for these compressive forces, the subendocardium is more vulnerable to ischaemia than the subepicardium due to perfusion heterogeneity; the greater impedance in flow on the subendocardial layers during contraction is only somewhat compensated for by the increased vascularity.[60-62] Intramural systolic compressive forces render subendocardial flow entirely dependent on the relative duration of diastole, or the diastolic time fraction (DTF), which is the ratio between the time the heart is in diastole and the duration of a complete heart cycle.[63] The DTF decreases with increasing heart rate, although the two are not uniquely related, and at a fixed perfusion pressure, subendocardial perfusion is dependent on DTF.[64,65] It follows on that at lower perfusion pressures (in the presence of a coronary stenosis) at the ischaemic threshold, subendocardial perfusion decreases more than proportionally with DTF than perfusion pressure. Under normal conditions however, oxygen supply is well matched to oxygen demand due to autoregulatory processes.

1.3.1 AUTOREGULATORY MECHANISMS

The relationship between coronary pressure and blood flow is strongly determined by autoregulation. This is the capacity of an organ to regulate blood flow in the face of changing perfusion pressures. As coronary perfusion is essential to cardiac function, under normal conditions oxygen supply is matched very well to demand. As myocardial oxygen extraction is near maximal under resting conditions, coronary perfusion is the major determinant of oxygen supply.[66]

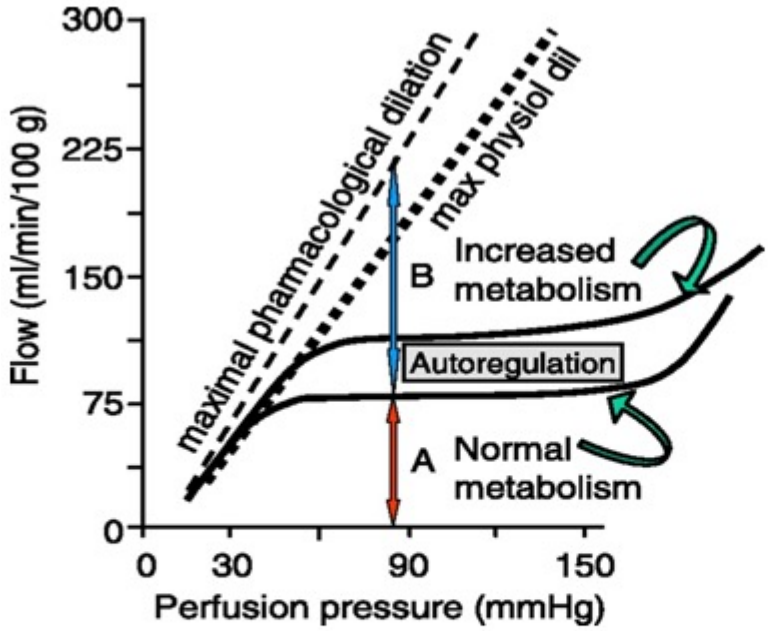


Figure 14 Autoregulation of coronary blood flow.
This maintains a stable plateau when perfusion pressure is within the normal range. The level of the plateau is related to the metabolic state of the heart. The dashed line indicates maximal pharmacological vasodilatation. The dotted line shows the maximal physiological dilatation, which is smaller than can be reached pharmacologically. The flow reserve is given by the ratio (B+A)/A, adapted from [67].

This is regulated in a number of ways, broadly divided into extrinsic (humoral-nervous) and intrinsic regulation (autoregulation).[68-70] Autoregulatory mechanisms are an integrated, coordinated interaction of 3 main control mechanisms that enable

modulation of the mechanistic properties of the vasculature, such that in the face of changing perfusion pressures the organ can create an autoregulatory "plateau", Figure 14, whereby flow is relatively independent of perfusion pressure:

- Myogenic control: this is the response of vascular smooth muscle to changes in intra-luminal pressure. In the presence of rising pressure, there is a resulting constriction of arterioles; in response to a drop in perfusion, dilatation occurs.[67,71,72]
- Metabolic adaptation: cardiac muscle plays an important role in coronary autoregulation. The level of the plateau is dependent on cardiac muscle metabolism, such that as metabolism increases, e.g. during exercise, the plateau increases thus coronary flow increases, Figure 14. This metabolic adaptation enables increased supply in the face of increasing metabolic demand.
- Endothelial based control: shear stress on the endothelium resulting from an increase in flow, triggers a response in the form of release of endothelial-derived factors including nitric oxide (and its derivatives), a known relaxant of underlying vascular smooth muscle, leading to vasodilatation.[73,74]

Thus autoregulatory processes influence the mechanistic properties of the coronary vasculature, and it is these dimensional changes that regulate blood flow to the artery. However, in the presence of a coronary stenosis although blood flow can remain stable at baseline, the greater the pressure drop, the more marked the reduction in flow; this can be explained using the principles of fluid mechanics.

1.3.2 PRESSURE GRADIENT-VELOCITY RELATIONSHIP

The principles of pressure loss across a coronary artery stenosis are based on theories of fluid dynamics in rigid tubes, Figure 15.[75,76] The two main anatomical characteristics that influence the pressure drop are 1) the narrowing of the arterial lumen and 2) its abrupt expansion when returning to the normal artery size.

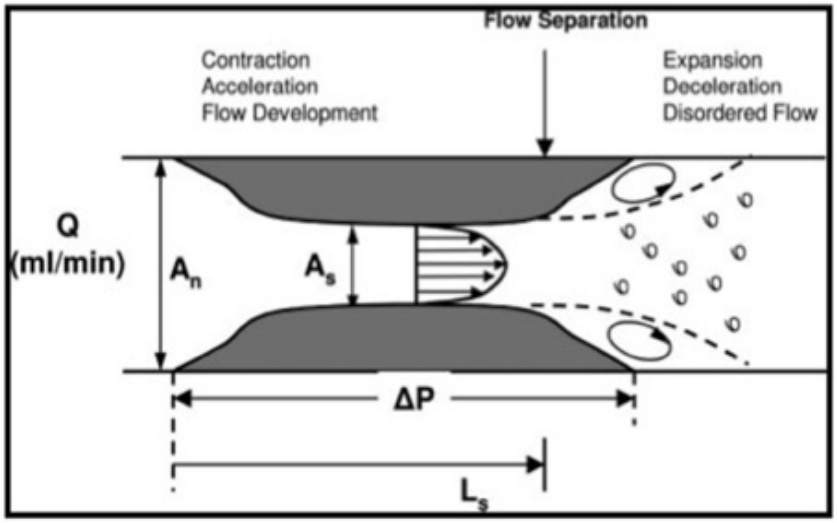


Figure 15 Effect of a coronary artery stenosis on coronary blood flow. The two principle sources of pressure loss across a stenosis are 1) frictional losses at the entrance and throat of stenosis (related to flow, Q) and 2) exit losses which describe inertial loss due to flow separation which occurs following the sudden expansion at the exit of the stenosis (increase with square of the flow). Abbreviations: A_n normal vessel diameter, A_s stenosis diameter, ΔP -pressure drop across the stenosis, Q flow in the reference vessel, L_s length of stenosis. Adapted from [77]

Viscous friction losses occur when the flow of blood slides against itself and against the endothelium of the artery, this happens in normal and diseased arteries; however, it is more marked in a narrow lumen because vascular resistance to flow is inversely related to the fourth power of the lumen diameter, Equation 6, where R is resistance to flow and D is the diameter of the artery.

Equation 6

$$R = \frac{1}{D^4}$$

This pressure loss is also related to the length of the stenosis, the viscosity of the blood and coronary blood flow velocity. Exit losses due to rapid expansion of the artery are dependent on flow just before exit, which is inversely related to the square of the stenotic area when expressed in terms of volumetric flow rate.[78] Pulsatility of coronary flow has little influence on such losses thus the instantaneous pressure is solely determined by the friction and exit losses. Thus the pressure drop (ΔP) across a stenosis can be described as the quadratic equation, Equation 7, where v is the volumetric flow, A is the constant of pressure loss due to friction and B is the constant of pressure loss due to exit losses.[79]

Equation 7

$$\mathbf{\Delta P = Av + Bv^2}$$

This quadratic pressure gradient-flow relationship can be plotted and has been validated in vivo. With increasing flow, adenosine-induced hyperaemia for example, the change in pressure increases in a non-linear upward fashion, since the pressure gradient is raised to the second power of flow. At low or normal flow rates, the pressure drop is influenced by pressure loss due to friction but at higher flow rates, this becomes influenced by exit losses as this is raised to the function of the second power of velocity.[80] Figure 16 describes how for an increase in coronary blood flow velocity, the pressure gradient changes more markedly in coronary stenosis.

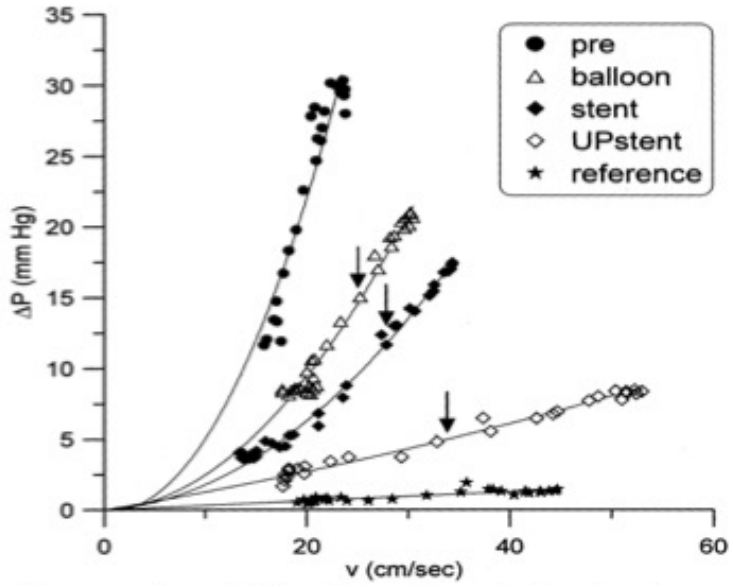


Figure 16 Pressure drop-velocity relationships.
Obtained at different stages of treatment by a dual-sensor guide wire in patients; obtained before (pre) and after successive treatment of the stenosis; note that the relations are curvilinear and become less steep at subsequent stages of vessel treatment. (UPstent indicates upsized stent; arrows indicate maximum flow achievable if microvascular resistance had remained at pretreatment level). The main observation of the solid spots taken from a vessel with stenosis is that as the coronary flow velocity increases, there is a more marked drop in pressure across the stenosis that increases in a curve-linear manner. Adapted from [80]

At baseline, in the presence of a stenosis, flow can remain relatively stable, with compensatory vasodilatation of the resistance vessels preserving basal coronary blood flow; the vasodilatory capacity is however exhausted as stenosis resistance (SR) increases, such that on induction of hyperaemia, the maximal flow rates that can be achieved markedly decrease and the perfusion pressure decreases with square of the flow Figure 17.[81,82] Thus either an increase in demand or increase in stenosis resistance can lead to insufficient oxygen supply, myocardial ischaemia and angina pectoris.[67]

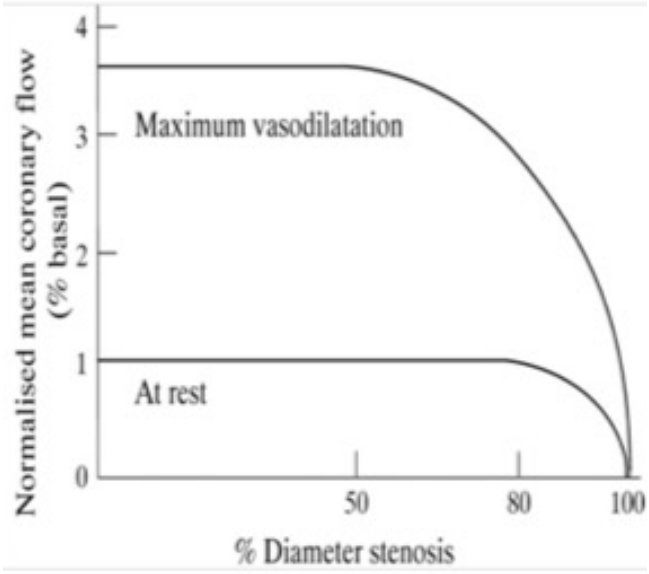


Figure 17 Changes on blood flow with increasing degree of stenosis severity. Adapted from [83].

Importantly, we can measure pressure and velocity distal to a stenosis at rest or during hyperaemia, enabling us to further understand the complex interaction of stenosis with coronary blood flow during resting and ischaemic states. Intra-coronary derived physiological parameters are used to measure functional stenosis severity. This is most commonly in the form of Fractional Flow reserve (FFR) derived from intra-coronary pressure measurements or coronary flow velocity reserve (CFVR) derived from intra-coronary Doppler indices.

1.4 INVASIVE MEASUREMENTS OF CORONARY BLOOD FLOW

As coronary angiographic data are not sufficient to assess the functional significance of a coronary artery lesion particularly in intermediate lesions, increasingly intra-coronary physiological measurements are being used in clinical practice: coronary flow velocity reserve (CFVR) and fractional flow reserve (FFR).

1.4.1 CORONARY FLOW RESERVE

CFR is based on the concept that under normal conditions, coronary flow increases with increased myocardial oxygen demand, as is the case with exercise or pharmacological stimuli.[78,79,84] CFR is the ratio of maximal flow to flow at rest at the same perfusion pressure.[79] In the absence of coronary stenosis, in epicardial artery subtending normal myocardium, coronary blood flow can increase by more than 3 fold. However, in the presence of a flow limiting stenosis, at rest, compensatory vasodilatation of the resistance beds occurs to account for the pressure drop and maintain coronary flow in the face of a drop in perfusion pressure distally. Therefore the capacity of the microcirculation to vasodilate further decreases, thus a stenosis results in a reduction in CFR, of epicardial coronary disease.

Figure 18.[85] Coronary flow velocity reserve (CFVR) is a surrogate for CFR; this uses Doppler-derived velocity measurements. In adults with completely normal epicardial arteries and normal myocardium a CFVR in the range of 3.5-5.0 would be expected.[86,87] However, in patients with unobstructed epicardial coronary arteries but with risk factors for ischaemic heart disease, the normal range is closer to 2.7 (likely due to microcirculatory disease) with the cut off for ischaemia at <2.0.[85] CFVR however, is the summed response of both epicardial and microvascular flow to hyperaemia, and can vary with physiological changes in basal and hyperaemic flow (heart rate, contractility, age, gender).[88] This variability leads clinicians to use this less in the assessment of stenosis severity and more in the determination of microvascular disease in the absence of epicardial coronary disease.

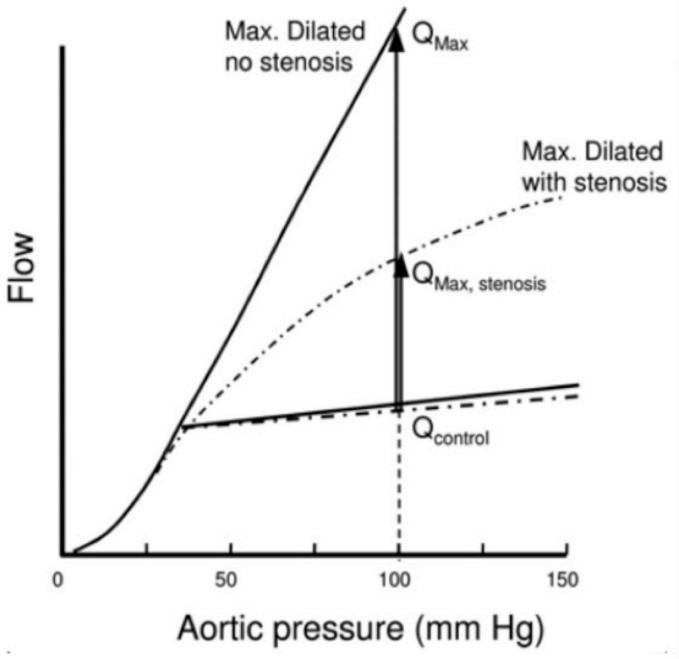


Figure 18 Stenosis severity (A) Effect of a stenosis on CFR: Solid lines represent the coronary pressure-flow relationship at baseline and maximal vasodilation (maximally dilated) without a stenosis. Changes in baseline and hyperemic flow affect coronary vasodilatory reserve (vertical arrows). CFR is represented by the ratio of flow at maximal dilation (Q_{Max}) to flow at baseline ($Q_{control}$). A stenosis progressively decreases the maximal flow (dashed lines) because the resistance of the stenosis is added to the resistance of the microcirculation. Flow reserve with a stenosis (the ratio of $Q_{Max, stenosis}$, to $Q_{control}$) is therefore markedly diminished. [83]

1.4.2 FRACTIONAL FLOW RESERVE

Under normal circumstances, in the absence of appreciable coronary or microcirculatory disease, the perfusion pressure transmitted to the myocardial bed in the distal coronary vasculature is equal to the aortic pressure minus left ventricular end-diastolic pressure (or central venous pressure). As a concept initially born in 1977, Gould and colleagues devised an intra-coronary physiological measurement based on the theory that a pressure drop across a stenosis (pressure gradient) would be proportional to a drop in coronary flow. It follows that in the context of hyperaemia, or maximal coronary flow, the ratio of distal perfusion pressure to the aortic pressure would give a ratio or a

fraction of normal flow: Fractional Flow Reserve (FFR).[89] Pijls et al demonstrated that FFR can give functional indication of stenosis severity, measuring the ischaemic potential of a stenotic lesion.[90] This model assumes that at hyperaemia, resistance is minimal in the myocardium and is uniform across the myocardial beds, such that blood flow is directly proportional to perfusion pressure. The FFR calculation is simplified to hyperaemic Pd/Pa because venous pressure is commonly considered negligible in comparison to Pa, Figure 19. A normal FFR value is 1.0; this makes interpretation of FFR easier for the clinician and makes FFR a favourable physiological index over other indices. Interestingly, although there may have been an initial indication in animal studies, human studies have shown no variability in "normal" FFR with age, heart rate, blood pressure or contractility.[91] Furthermore FFR has been validated in large experimental and clinical studies as a functional indicator of stenosis severity and predictor of ischaemic capability of coronary lesions. [91,92]

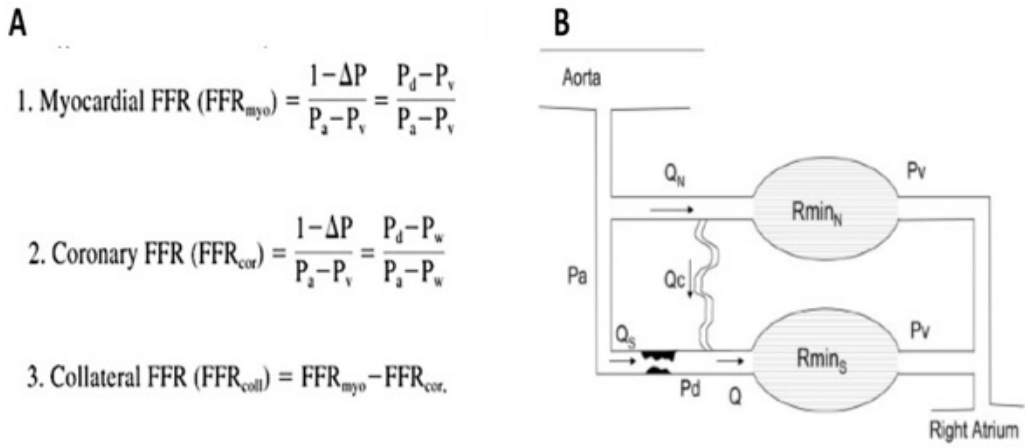


Figure 19 Fractional Flow Reserve.
(A) The calculation simplified (B) Model of the coronary circulation: top and bottom circuits represent equivalent myocardial mass, without a stenosis in the bottom, $Rmin_N$ = $Rmin_S$, Q_c (collateral flow)=0, Q_s=Q_N where Q is volumetric flow and Pd = Pa. Q_s indicates hyperaemic flow with stenosis, Q_N =hyperaemic flow without stenosis, adapted from [89].

FFR has a few limitations based on the assumptions made: 1) it presumes pressure is directly proportional to flow, however we see above that this is a non-linear relationship particular marked at higher velocities; also neglecting the effect of cardiac contraction on hyperaemic blood flow and 2) it assumes homogeneity of microvascular resistance, and that microvascular resistance is minimal. Interestingly FFR and CFVR contradict in approximately 30% of cases, in instances of high microvascular resistance, CFVR reduces and FFR increases (as flow is reduced but distal pressure is high, and vice versa. [93,94]

As there are limitations to derived indices of coronary flow or coronary pressure in isolation,[77] there is benefit to measuring both, not only to determine true flow and pressure drop across a stenosis but also to identify the driving factors of coronary blood flow. Real-time measurements of coronary blood flow velocity and pressure can be performed using a dual sensor tipped wire; not only does this enable us to accurately assess coronary haemodynamics but also increases our understanding of pressure-flow wave propagation, which is responsible for these measured profiles. This wave intensity analysis has the potential to increase our knowledge of the complex interactions between the coronary circulation and cardiac contraction.

1.5 CORONARY WAVE INTENSITY ANALYSIS

The basis of modern arterial haemodynamics is that the heart acts as a pump generating pulsatile pressure and flow waves through a series of elastic tubes (arterial system). These waves can be broken down into smaller waves (or wavelets) from which the summation makes a larger wave. One method of interpreting these waveforms is by analysing them in the time domain as successive wave fronts. This enables coronary wave intensity analysis (cWIA) to be performed; this can be used to describe the coronary pressure and flow waves at a certain time point (or sampling period).

Wave intensity analysis was developed just over two decades ago as a new approach to analysing waves.[95] It is understood that within the coronary circulation, wave intensity analysis (cWIA) generates forward and backward travelling waves. The following description refers to previously published descriptions of cWIA.[96,97] The forward waves are believed to arise upstream, although as a result of left ventricular ejection and relaxation, these waves are believed to be transmitted from the aorta to the coronary artery, thus are forward travelling. Backward travelling waves identified within the coronary artery are thought to originate directly from the myocardium, and are generated from the transmission of downstream events in a retrograde manner through the coronary artery. Waves that cause a pressure increase are referred to as compression waves; waves causing a decrease in pressure are referred to as suction or expansion waves. The effect on coronary blood velocity can then be determined by both the origin (forward or backward) and the change in pressure (compression or expansion); for example an increase in coronary blood velocity can be generated either by a forward travelling compression wave (increase in pressure) or a backward travelling expansion

wave, a decrease in coronary blood velocity can be caused by a forward expansion wave or a backward travelling compression wave, .

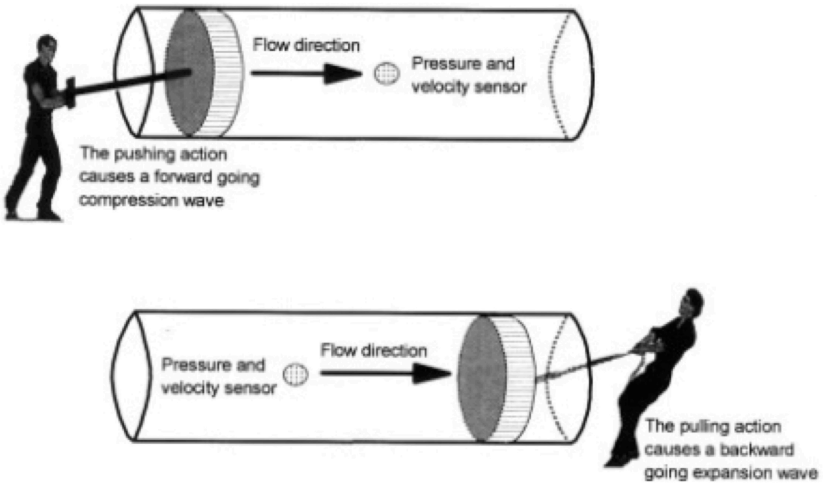


Figure 20 Coronary wave intensity analysis.
A description of flow propagating waves, the forward travelling compression wave (arising proximally during systole), and the backward travelling expansion wave (arising distally during diastole), adapted from [98].

Therefore in the coronary circulation, wave intensity (cWIA) can differentiate between forward waves arriving via the aorta and backward waves originating in the microcirculation.[96] Hence, wave intensity is a powerful tool to investigate cardiac-coronary interaction and it is increasingly being used to interpret clinical data. The relevance of wave intensity analysis when investigating coronary blood flow is that it may be extended in the future to diagnosing epicardial coronary or microvascular disease.[96,99]

1.5.1 APPLICATION OF CWIA

The theoretical explanation for the timings of each of these waves has been previously described.[96,99] cWIA enables us to separate the events in the cardiac cycle into forward and backward waves, the theoretical background to the waves is as follows: during systole, 1) an early systolic backward compression wave (BCW) is generated by isovolumic contraction, as a result of the increase in intra-myocardial wall tension compressing the intramural vessels, this drives an increase in pressure but a decrease coronary blood velocity; 2) following isovolumic contraction, aortic valve opening and LV ejection results in a forward compression wave (FCW), this increases pressure and increases coronary blood flow velocity (the myocardium has reached its maximum contractile state, thus further compression of the coronary vessels is prevented); 3) at the onset of diastole, the decay in aortic pressure leads to a suction effect arising proximally thus generating a (3) forward expansion wave (FEW) which reduces coronary pressure and reduces blood velocity; ventricular relaxation during diastole also has a direct effect on the myocardium, as tension is released a 4) backward expansion wave (BEW) is generated that is a result of a decrease in distal pressure, this drives an increase in coronary blood velocity. Aortic valve closure at end-ejection generates a small (4) late forward compression wave, Figure 21. The reality is the events are not completely separated in time and there is overlap; moreover, there is continued interest in the clinical utility of these tracings. Corresponding intra-ventricular changes with changes in coronary pressure and flow have not been measured in humans, but to date this is the best descriptive predictor of how cardiac contraction influences coronary pressure and flow waveforms. The cardiac-coronary interaction remains complex, and

there is still much to be understood of the mechanical events in the cardiac cycle driving coronary flow.[96,100,101]

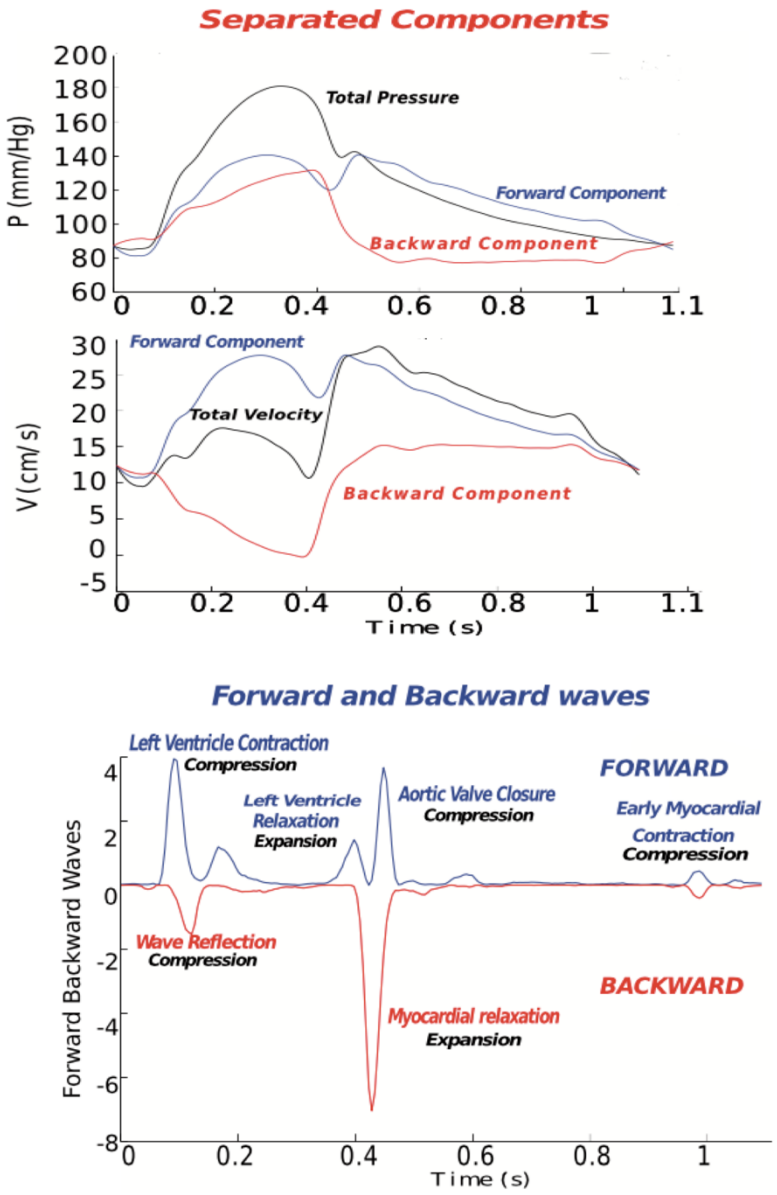


Figure 21 Wave separation.
Coronary pressure and coronary flow plotted against time with the average pressure and flow (black) and the separated forward (blue) and backward (red) components (top). The physiological events in the cardiac cycle driving individual waves driving changes in pressure and flow (bottom).

1.5.1.1 WAVE SPEED

The speed of wave travel (pulse wave velocity, c) is a fundamental parameter for separating net wave intensity into the forward and backward components, and is dependent on the density and stiffness of blood and the cross-sectional area of the artery.[102] This can be simplified using the Moens-Korteweg equation (Equation 8), which relates pulse wave velocity to the stiffness of the arterial wall.

Equation 8

$$c = \sqrt{\frac{h.Einc}{D.\rho}}$$

In other words, pulse wave velocity (*c*) is proportional to the square root of the incremental elastic modulus (*Einc*) of the vessel wall given constant ratio of wall thickness to vessel radius (*D*), under the assumption that wall thickness (*h*) and vessel radius do not significantly change. Separation into forward and backward travelling components requires knowledge of pulse wave velocity at the point of measurement, which ideally should be calculated by assessing the transit time between pressure waveforms that are set a known distance apart.[103] This is known as the foot-to-foot method but cannot be accurately performed in the coronary arteries. Thus another method has been developed known as the single point technique (SPc), which uses a single point estimate of the local coronary wave speed, obtained using the sum of squares method[96]:

Equation 9

$$SPc = \frac{1}{\rho}\sqrt{\frac{\varepsilon dP^2}{\varepsilon dU^2}}$$

Local wave speed was shown to correlate well with the foot-to-foot technique in the systemic circulation. Furthermore, Rolandi et al demonstrated that at baseline, single point calculated wave speed was equal to direct measurement of coronary wave speed in normal coronary arteries.[104] This has been validated against measured waves speeds in the human coronary artery, and although the accuracy in diseased vessels is not known, it is within limits for calculating wave separation in cWIA.

1.5.1.2 MEASUREMENT OF CWIA

Net wave intensity (dI) can be defined at any point as the energy flux per unit area (J/m2) and is the product of change in pressure and change in velocity:

Equation 10

$$dI = dP.dU$$

The net wave intensity affected by the sampling time, it is normalised to time:

Equation 11

$$dI = \frac{dP}{dt}.\frac{dU}{dt}$$

Mathematical equations have been used to separate net wave intensity into it's forward and backward component. A positive value for wave intensity suggests the changes in pressure and velocity caused by the forward wave is greater than those caused by the backward wave and a negative value suggests the opposite,[97] when the forward (+) and backward (-) components are separated.[99]

Equation 12

$$dI\pm = \pm\frac{1}{4\rho c}\left(\frac{dP}{dt} \pm \rho c\frac{dU}{dt}\right)^2$$

1.5.1.3 MYOCARDIAL-CORONARY INTERACTION

Although the major determinant of coronary blood flow is the aortic pressure gradient, it is clear that coronary pressure and flow are not merely a function of aortic pressure. The myocardium and coronary vasculature are within close proximity of each other and a two-way interaction known as cross-talk exists. Coronary blood flow velocity is determined by both upstream and downstream events. The coronary circulation is unique in that its driving force and impedance to flow are dynamic functions of myocardial contraction, thus cardiac muscle affects the coronary vasculature.[105,106] Contraction of the left ventricle not only increases coronary perfusion pressure but also immediately prior to this at end-diastole increases compression of the microcirculation. Conversely, relaxation of the left ventricle decreases perfusion pressure but also reduces compression of the microcirculation. As cardiac contraction impedes coronary flow in systole, coronary flow predominates in diastole thus coronary flow is dependent on the length of diastole relative to the cardiac cycle. This unique property of the coronary circulation is due to its functional arrangement in the myocardium. A number of studies have elucidated, at least in part, this complex interplay; the ground-breaking work by Davies et al applied wave intensity analysis to enhance our understanding of the cardiac-coronary interaction. Lockie et al examined the underlying mechanism behind warm up angina, they hypothesised that a reduction in microvascular resistance lead to an increase in the BEW seen in second relative to first exercise.[101] However Rolandi et al suggest that coronary waves represent left ventricular mechanical change, contrary to initial understanding: a marked drop in dP/dT and was associated with a similar reduction in the wave energies.[100] This followed on from work by Sun et al, who examined the effects of contractility (Emax) and coronary resistance on systolic flow

impediment, they found at the greatest contractility and least resistance that coronary systolic flow was markedly impaired, and the backward compression wave was at its greatest at this point. They concluded that coronary systolic flow impediment driven by increased contractility and decreased resistance, worked by modulating the BCW.[107]

1.6 COORDINATED CARDIOVASCULAR RESPONSE TO EXERCISE

Thus far cardiac contraction and coronary blood flow have been described in isolation; however it is the combination of these mechanisms and the heart's interaction with the rest of the cardiovascular system that is of particular clinical importance in both normal and diseased states. There follows a description below of the cardiovascular response to exercise.

From an evolutionary and survival-of-the-fittest point of view, the ability of the body to adapt to exercise by markedly increasing delivery of oxygen and nutrients to the peripheries is one of the most important circulatory adjustments the body has to make.[108-114] The cardiovascular responses to exercise necessitated by the increased metabolic requirements of skeletal muscle are driven by the autonomic nervous system.[115-118] A reduction in cardiac parasympathetic activity and an increase in sympathetic activity to the cardiac, renal and splanchnic regions together increase heart rate, stroke volume and therefore cardiac output and facilitate the redistribution of blood flow to the active skeletal muscles, Figure 22.

1.6.1 PERIPHERAL VASCULAR RESPONSES

From resting state to maximal exercise, blood flow to the skeletal muscle groups can increase by up to forty times. Blood flow increases linearly with increasing metabolic rate in exercising skeletal muscle, myocardium and exocrine glands.[109,114] This is known as metabolic hyperemia and is caused by an increase in vasodilatation through the direct action of vasodilator substances adenosine and its derivatives, and potassium and hydrogen ions on vascular smooth muscle cells to stimulate endothelium derived

relaxing factor (EDRF) production. Dilatation of the main artery is then accompanied by dilatation of resistance vessels due to flow induced EDRF production.[73]

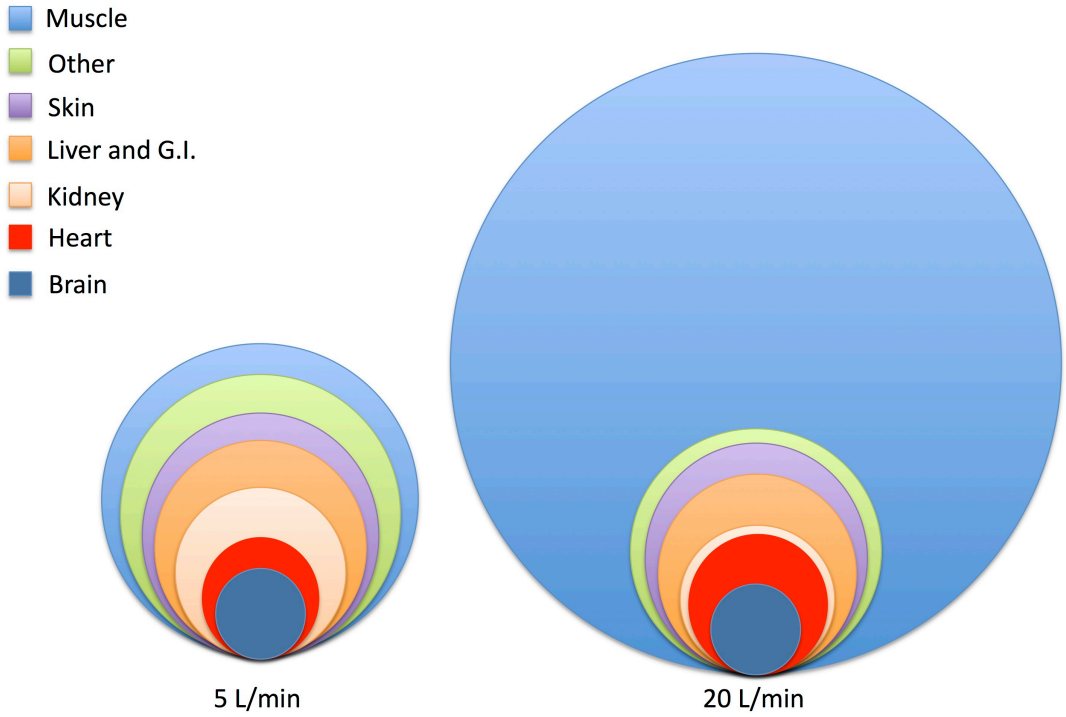


Figure 22 Blood flow and exercise.
The redistribution of blood flow from rest (left) and during maximal exercise (right), adapted from [119].

Due to the marked oscillation of blood flow during muscle contraction-relaxation, the majority of this hyperaemia occurs during resting phases. Hyperaemia continues for two to three minutes after exercise to repay the oxygen debt in both skeletal and cardiac muscle. Dynamic exercise differs from static exercise in that mean pressure rises very little, by 20mmHg or less, systolic pressure and pulse pressure do increase to a greater extent but there is little increase in diastolic pressure. Muscle vasodilatation causes a drop in systemic vascular resistance (SVR), creating a vital permissive effect in light of the increased cardiac output. A drop in SVR is compensated for by vasoconstriction of

the splanchnic circulation, this vasoconstrictor response supports the arterial pressure. Therefore, maintenance of central venous pressure is possible through the action of sympathetic vasomotor nerves driving splanchnic vasoconstriction and skeletal muscle pump compression, which result in central venous pooling.[109,110]

1.6.2 CARDIAC RESPONSES

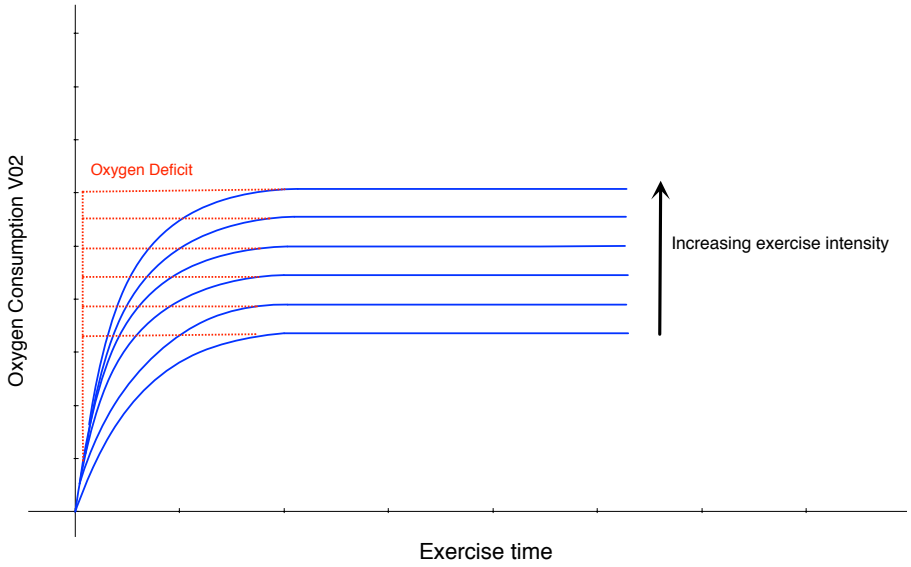


Figure 23 Myocardial oxygen consumption (VO2) at the onset of exercise.
An early increase in heart rate and cardiac output drives an increase in VO2 (animation).

Even in an untrained adult, the maximum cardiac output can reach approximately 20 litres per minute, a roughly four-fold increase from rest. For every additional litre of oxygen consumed, cardiac output increases by approximately 6 litres per minute. Thus dynamic exercise is associated with an increase in myocardial oxygen consumption. This is particularly the case during the first minute of sustained exercise, where there is a very rapid increase in heart rate and cardiac output and a more gradual increase in mean blood pressure.[111,120] During this first minute of exercise, the oxygen consumption

of the heart increases rapidly to match the intensity of exercise, plateauing when supply meets demand. If exercise intensity increases, a point is reached whereby myocardial oxygen consumption plateaus, i.e. the maximum oxygen consumption achievable by the heart, Figure 23. Thus, despite an increase in workload there is no further increase in consumption. The increase in myocardial oxygen consumption in the face of increasing whole-body demand, can be summarised using the Fick equation (Equation 13) where $VO2$ = oxygen consumption, CO = cardiac output and $CaO2$ and $CvO2$ are arterial and mixed venous oxygen saturations respectively.[110]

Equation 13

$$\boldsymbol{VO2 = CO(CaO2 - CvO2)}$$

Heart rate (HR) has a direct, almost linear relationship with oxygen consumption; during intense exercise, HR can reach a maximum of 180-200 beats per minute. This tachycardic response is due to both sympathetic stimulation and removal of vagal inhibition.[109,114]

1.6.2.1 CORONARY BLOOD FLOW

There is distinct lag of three to four seconds before coronary vasodilatation occurs in exercise, there then follows a sharp rise in coronary blood flow. Increased heart rate has been shown to increase coronary blood flow as has flow-mediated dilatation, which relies on an intact endothelium. The endothelium acts as a mechano-transducer that senses changes in shear stress (resultant increased flow and widening of the central pulse pressure) and subsequently modifies the output of dilating factors including prostaglandins, adenosine triphosphate and nitric oxide. Flow mediated dilatation dilates

vascular smooth muscle and maintains a constant concentration of nitric oxide on the luminal surface of vascular endothelium.[121-123]

1.6.2.2 STROKE VOLUME AND CARDIAC OUTPUT

Cardiac output has a similar relationship to oxygen consumption and is the product of heart rate and stroke volume, Equation 1. Posture during exercise influences the overarching driving factor to the increase in cardiac output. In a supine position, the increase in cardiac output is almost entirely driven by heart rate, with stroke volume only increasing by 10-20%. In the upright position however, stroke volume can increase by 50 to 100%. The increase in end-diastolic volume is driven by central venous pooling as described above, the increased filling pressure and increase in myocardial contractility as a result of increased sympathetic drive together drive a reduction in end-systolic volume.[124] External cardiac work or stroke work (SW) increases the volume, pressure and velocity of blood in the circulation, the work involved in displacing this pressurised volume of blood is the product of SV and mean pressure rise, which is the area of the ventricular pressure-volume loop. Mechanical efficiency is equal to the stroke work relative to total energy expended. In resting states this is only around 5-10%; this includes energy expended during isovolumic contraction, generation of this tension requires energy but generates no external work. Importantly during dynamic exercise in healthy subjects, SV increases more than arterial pressure, and efficiency increases to 15%.[32] This can be understood better in terms of ventricle-arterial coupling, which is described in section1.6.2.3.

The importance of the coordinated cardiovascular response is reflected in studies whereby only one stimulus is changed. If the heart rate is increased in isolation in a

paced heart, the cardiac output does not change because stroke volume falls: an increase in heart rate transfers the whole-body blood volume to the systemic circulation, thus increasing afterload and offloading the right heart resulting in reduced filling pressure (or end-diastolic pressure). An increase in artificial pacing favours the shortening of diastole, thus reducing filling time. The result is a marked decrease in cardiac output at high pacing rates, rather than simulation of the physiological adaptation to exercise.[121,125,126]

1.6.2.3 VENTRICULO-ARTERIAL COUPLING

Due to the complex interplay between the heart and the peripheral vascular system during exercise, exercise provides a powerful tool to examine the response of the cardiovascular system to stress. Few studies have examined this interaction closely. Arterial elastance (Ea) is the global characterisation of arterial load. (4) End-systolic elasatance (Ees, the slope of ESPVR) is the gold standard index of left ventricular contractility; thus the Ea:Ees ratio is the measure of the interaction between the left ventricle and the arterial system; importantly they are measured in the same units thus derivation of this ratio gives a non-dimensionless measurement of net cardiac performance, expressed as a fraction (optimal 0.7-1.2).[37,38] During exercise, arterial stiffness has a greater impact on Ea than on systemic vascular resistance. Thus with exercise, Ea increases but SVR falls. The importance of the Ea:Ees ratio, is that appropriate matching results in optimal stroke work and efficiency. During exercise this ratio drops, both Ea and Ees increase, however Ees increases to a greater extent in healthy subjects thus reducing this ratio by up to 65% in some cases.[32,127,128] Ventricular-arterial coupling has not been examined in patients with ischaemic heart disease with effort angina; however in systolic heart failure, patients have a high resting

Ea:Ees ratio due to high Ea (increased arterial stiffness) and low Ees (poor contractility).[129] Therefore it is predicted than on induction of ischaemia during exercise in coronary artery disease, that the Ea:Ees ratio will increase in patients suggesting a decrease in efficiency.

1.7 PATHOLOGICAL CARDIOVASCULAR RESPONSES

In this section, there follows a description of ischaemic heart disease, its prevalence and the pathophysiological response to exercise and the manifestation of end-stage disease resulting in ischaemia cardiomyopathy.

1.7.1 IMPACT OF ISCHAEMIC HEART DISEASE

All causes	Men	4 519 403
	Women	4 336 346
All circulatory	Men	1 963 644
	Women	2 307 945
CHD	Men	967 258
	Women	983 229
Stroke	Men	504 307
	Women	775 571
Other	Men	492 079
	Women	637 405

Figure 24 Death from cardiovascular disease in Europe.
Adapted from [130]

Cardiovascular disease (CVD) is a huge public health burden. CVD was a direct cause of more than 4 million deaths in Europe in the year 2000 increasing to more than 4.3 million in 2005, Figure 24.[130] Furthermore, CVD is responsible for just under 2 million premature deaths a year in Europe in the under-75 age group. The cost of CVD to the European Union in 2006 exceeded 190 billion Euros, more than 110 billion of this was on healthcare costs, and of this, more than half was spent on inpatient hospital care. The majority of deaths from CVD are preventable, an increased understanding of which may

aid the development of therapeutic interventions.[131,132] Of all CVD, ischaemic heart disease is the most prevalent, the clinical manifestation of which, is angina pectoris.

1.7.2 MECHANISM OF ANGINA

Angina pectoris, classically described as a retrosternal crushing or burning, is the clinical manifestation of myocardial ischaemia; it occurs late in the ischaemic cascade and is a result of myocardial oxygen supply-demand mismatch, Figure 25.[133,134]

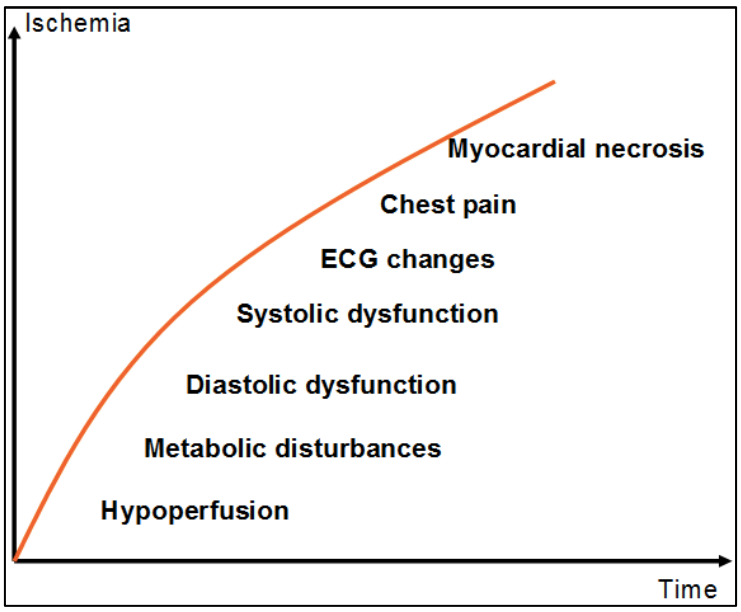


Figure 25 The ischaemic cascade.
Angina pectoris presents late following a cascade of haemodynamic events, adapted from.

Supply-demand mismatch can occur at rest as a result of atheroma expansion, endothelial erosion and plaque rupture with platelet aggregation. Supply-demand mismatch during stress (exercise) will manifest when severe obstructive lesions prevent the necessary increase in coronary blood flow during exercise, thus 1) myocardial oxygen supply is reduced and 2) myocardial oxygen demand is increased (the physiological response to exercise) from an increase in heart rate (HR), blood pressure

(BP) and contractility, Figure 26.[121,135] A critical duration and severity of ischaemia is required for a subject to experience pain, although it is important to note that the cause of ischaemia does not influence the features of angina. For example, the character of pain may be similar in a patient with chronic stable angina episodes who experiences unstable angina or myocardial infarction.[136]

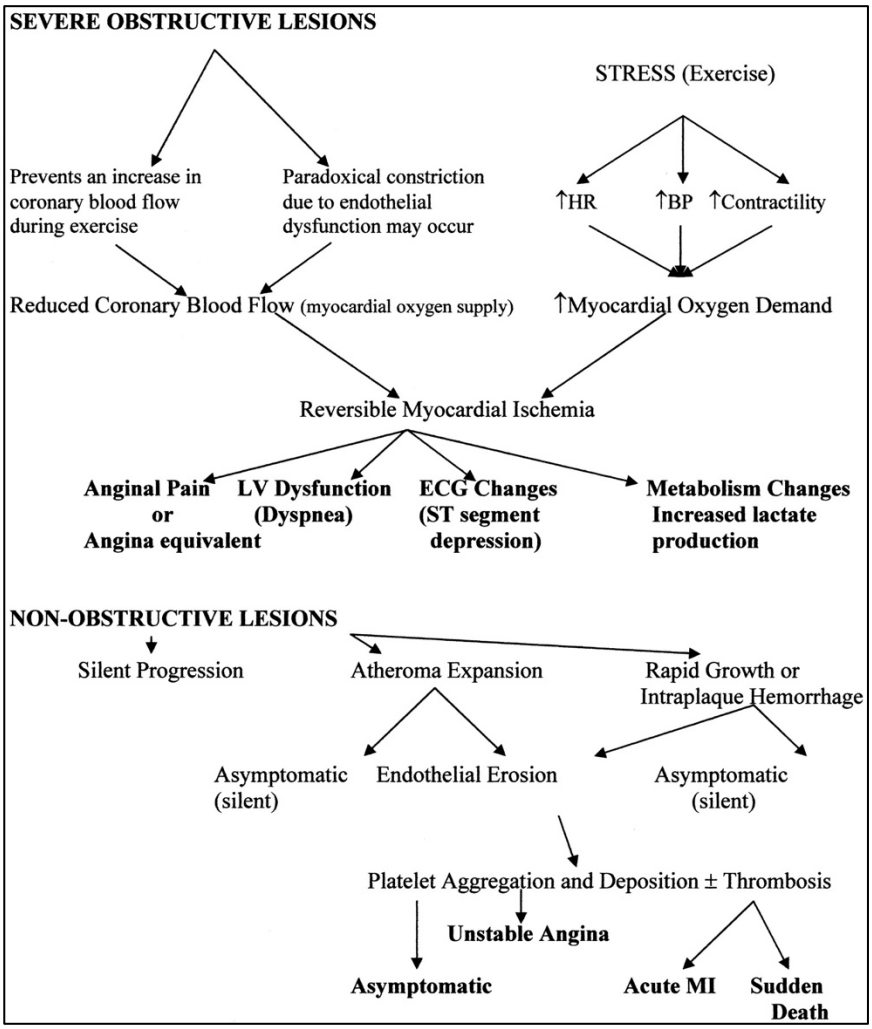


Figure 26 Pathophysiological mechanisms of myocardial ischaemia.
These result in adverse outcomes in stable angina, adapted from [133].

At the turn of the century it was proposed that ischaemic pain was as a result of distension of the left ventricle: the mechanical hypothesis.[137] However, just over three decades later, it was suggested that ischaemic pain was elicited by the release of

substances during ischaemia that cause pain: the chemical hypothesis.[138,139] In the 1990s, studies carried out further supported the chemical hypothesis, consistently demonstrating adenosine to be the mediator of cardiac pain: adenosine-induced pain is through stimulation of A_1 receptors and is potentiated by substance P.[140] This nervous activity is fed back to the cortex via the cardiac, mediastinal and thoracic ganglia where it is modulated and interpreted as a painful sensation.[141,142] The negligible contribution of left ventricular (LV) dilatation to ischaemic sensation of pain has been shown on ergonovine-induced ischaemic episodes, whereby the rate and degree of mechanical dilatation was similar in painless and painful sensations.[143] This is further substantiated by the recognition that episodes of acute left ventricular failure resulting in LV dilatation are painless. Although peri-arterial mechanoreceptor stimulation on stretching the epicardial coronary arteries during angioplasty has been shown to contribute the pain of myocardial ischaemia, its role in angina episodes has not been completely examined.[142,144]

1.7.3 SUPPLY-DEMAND MISMATCH

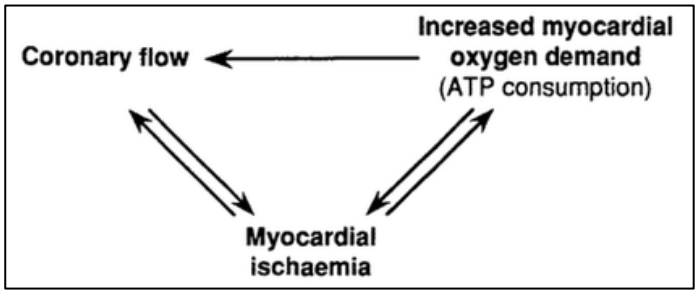


Figure 27 The cycle of myocardial ischaemia, adapted from [133].

The initial trigger of myocardial ischaemia can be either increased myocardial oxygen demand or a reduction in coronary blood flow. What follows is a vicious cycle or cascade of events amounting to what we know to be an ischaemic episode; this results

in a further increase in myocardial oxygen demand and decrease in blood flow, Figure 27. Increase myocardial oxygen demand leads to an increased heart rate, left ventricular dilatation and increased left ventricular end-diastolic pressure and catecholamine release, which in the setting of coronary disease can lead to myocardial ischaemia.[145,146] Catecholamine release drives a further increase in heart rate, systolic and diastolic blood pressure, which further increases myocardial oxygen demand. Increased heart rate reduces the diastolic time fraction, the fraction of the cardiac cycle that the heart is in diastole where coronary flow predominates; this coupled with increased end-diastolic pressure results in a reduction of coronary blood flow.[133] This complex interplay of the myocardium and coronary blood flow is intuitive as the coronary circulation and the myocardium are in such close proximity, interaction undoubtedly occur.

1.7.4 REGIONAL ISCHAEMIA AND PRESSURE-VOLUME LOOPS

In an animal model, the effects of regional ischaemia on contractility in the isolated canine heart have demonstrated a parallel rightward shift in the ESPVR without significant change of the slope Ees. This resultant shift changes the V_0 intercept on the X-axis, with the degree of rightward shift related to the degree of ischaemia as studied by microspheres. Curvi-linearity of the Ees slope was also observed in regional ischaemia. This is in contrast to global ischaemia in which a change in the Ees slope occurs without an observed change in the V_0 intercept.[147,148] Following this animal work, Kass et al. performed balloon occlusion during coronary angioplasty in humans with pressure volume analysis of the left ventricle. They found a combination of the findings above: a rightward shift of the ESPVR line (representing the LV working at higher volumes) and a downward shift in the slope of the line. As contractility is measured by the gradient of the slope, a rightward shift alone would not suggest a change in contractility. However, a downward shift would be consistent with this. Associated with this, an increase in end-diastolic and end-systolic volumes (ESV) were seen, measured by left ventriculography, with a marked decrease in dP/dt.[149] Although only performed in 10 patients, these changes were seen consistently and the greater the starting ESPVR, the greater the decrease observed in Ees slope. Diastolic changes were manifest initially as higher filling pressures then followed impairment of diastolic function as shown by an upward shift of the EDPVR slope.[149] A similar study by Remmelink et al, 20 years on, showing balloon occlusion during angioplasty found similar changes: a decrease in diastolic function as demonstrated by prolonged time constant of relaxation (Tau, i.e. the time required for dP/dtmin to reduce by half), an increase in end-diastolic pressures (EDP) and end-diastolic volumes (EDV). Reduced

systolic function was demonstrated by a rightward shift in the ESPVR slope, decreased dP/dT, decreased ejection fraction, and increased ESV. [150] A study by the same group examining reperfusion post acute myocardial infarction in humans demonstrated the greatest effect of reperfusion was on diastolic indices. A reduction in EDP/EDPVR and end-diastolic wall strain was shown and thus an improvement in the passive diastolic properties on reperfusion, but no change in active diastolic properties (filling/tau).[151]

With regard to demand ischaemia, Dawson et al performed pacing-induced ischaemia in humans using ventriculography and an LV micromanometer to construct PV loops. They demonstrated a prolongation of Tau (relaxation time constant), increase in EDP and an upward shift of the EDPVR curve.[152] Pacing-induced ischaemia and balloon coronary occlusion appear to have opposing effects in the ischaemic myocardium of dogs. Early studies comparing the two demonstrated an upward shift in the pressure-segment length relation with pacing compared to an outward bulge and rightward shift with balloon coronary occlusion. Suggesting that decreased diastolic distensibility with a minor reduction in systolic shortening characterised ischaemic myocardium during pacing, whereas increased distensibility and replacement of systolic shortening with passive outward bulging was the hallmark of ischaemia secondary to occlusion.[125,153] Further studies comparing the two changes in man showed there was an upward shift both in the end-diastolic pressure volume curve and pressure-length relations in both cases, with a greater upward shift (reduction in diastolic distensibility noted) on pacing induced ischaemia.[154] Persistent systolic shortening (i.e. preserved systolic function) of ischaemic myocardium was demonstrated to be a prerequisite for a decrease in diastolic distensibility of the ischaemic segment. With a correlation between the degree of

diastolic dysfunction and the persistence of systolic shortening.[154,155] Consistent with these latter findings, a retrospective analysis examining the changes incurred by pacing-induced ischaemia compared to balloon coronary occlusion in fact found that the mode of ischaemia was less relevant than the effect on contractility; the more contractility is affected, the farther rightward and downward the EDPVR shifts. [155]

In a canine model of control versus induced coronary stenosis, Steendijk et al assessed the effects of a critical stenosis on global systolic function, demonstrating that regional ischaemia induces global LV changes. At baseline, the canines with induced stenoses already experienced a substantial increase in resting end-systolic volume.[156] With low-dose dobutamine, systolic function improved in this group; however, this declined on higher doses (with a rightward shift of the ESPVR), suggesting a biphasic response, whereas the control group showed a continued improvement in systolic function as expected with increased ESPVR slope thus increased global systolic function and contractility.[156]

There is continued debate with regard to the effects of a critical stenosis on systolic function. A combination of factors could produce the observed effects. This includes the duration and extent of ischaemia, the technique used to provoke ischaemia, and the affect on contractility. The majority of anginal episodes are triggered by exercise, thus the aim of the investigation into demand ischaemia was to examine the changes incurred with exercise-induced angina to delineate the changes. Furthermore, an understanding of the changes incurred by ischaemia, would enable us to examine and better understand the anti-anginal effects of nitrates.

1.7.5 NITRATES IN ISCHAEMIC HEART DISEASE

Organic nitrates are the most commonly used anti-anginals worldwide. They are available in multiple formulations including glyceryl-trintrate, isosorbide mononitrate and isosorbide dinitrate. First noted in 1879, the administration of long acting nitrates relieved angina and was found to prevent subsequent anginal episodes.[134,157] Nitrates are now frequently used worldwide as a treatment for angina including chronic stable angina, unstable angina and even in heart failure.[135,157] Their safety profile makes them an attractive choice for initial anti-anginal therapy. The main limitation of nitrates is the development of tolerance, although detailed work has been performed in this area, this is not within the scope of this investigation.

1.7.5.1 PHARMACOLOGY AND MECHANISMS OF ACTION

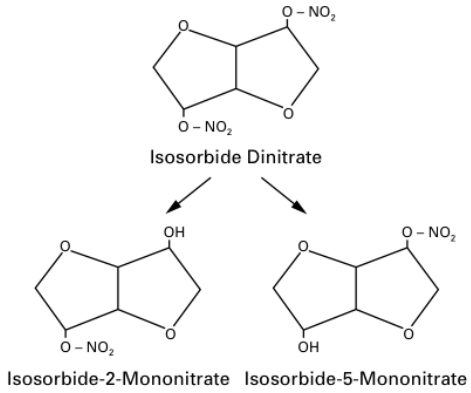


Figure 28 Metabolism of isosorbide dinitrate.
The major metabolites are isosorbide-2-mononitrate and isosorbide-5-mononitrate, adapted from [157].

Isosorbide dinitrate (ISDN) when given orally experiences first past metabolism through the liver, Figure 28. Although initially thought to render it inactive, later studies have shown that despite this, its haemodynamic and anti-anginal effects remain marked.

ISDN is rapidly metabolised with a half-life of 20 to 40 minutes.[158-160] Orally administered nitrates are pro-drugs, which need to be metabolised to have therapeutic effects. This biological transformation includes denitration of the nitrate with liberation of nitric oxide, this stimulates the enzyme gunaylyl cyclase to convert guanosine triphosphate to cyclic guanosine monophosphate, which in turn is responsible for vasodilatation.[157,158,160] Interestingly, nitric oxide also known as endothelial derived relaxing factor, exerts vasodilatory effects, but in addition to this reduces platelet adhesion and aggregation; controls endothelial function and is also thought to have a positive effect on myocardial contractility. In the presence of endothelial dysfunction, nitric oxide production is reduced, thus administration of exogenous nitrates, may replete these and thus have a beneficial effect.[74,161]

It is believed that the haemodynamic actions of nitrates work through the dilatation of the capacitance vessels and conductive arteries, thus reducing ventricular volume and preload, thus lowering myocardial oxygen requirements and improving sub-endocardial flow.[162,163] Dilatation of the systemic arteries, in combination with reduction in preload then acts to reduce afterload and is thought to reduce myocardial oxygen consumption through a decrease in systolic wall tension; the reduction in diastolic filling may improve the transmural distribution of blood flow by reducing extrinsic diastolic compression of the sub-endocardial vessels.[164-166] It is hypothesised that the anti-anginal action of nitrates is through dilatation of epicardial coronary vessels leading to stenosis dilatation and increased collateral supply. Thus increasing blood flow to areas of coronary ischaemia, particularly sub-endocardial flow. It is most likely however that the "nitrate-effect" is a combination of systemic and coronary changes.[161,167-171]

Early invasive studies of pressure-volume (PV) relations repeatedly demonstrated a leftward, downward shift of the PV loop with nitrates. These studies supported a predominant preload and afterload reduction on the ventricle rather than a change in myocardial diastolic compliance. Later studies found conflicting results with a change in the time constant of LV pressure decay (tau) suggestive of direct diastolic effect, which does not seem to be a feature of other anti-anginals.[166,172] One study suggested that the dominant effect of nitrates varies according to patients' baseline characteristics: afterload reduction predominated in those with marked hypertension compared to a preload reduction in those with normal ventriculo-vascular coupling.[164] Thus the complexities of this drug are much debated; with novel technology and software, however, delineation of this complex anti-anginal mechanism is certainly achievable and is one of the major aims of the following body of work.

1.7.6 ISCHAEMIC CARDIOMYOPATHY AND LEFT VENTRICLE PARTITIONING

1.7.6.1 EPIDEMIOLOGY AND PATHOPHYSIOLOGY

Coronary artery disease is the commonest cause of heart failure worldwide. Chronic heart failure remains a huge unsolved problem and is one of the most prevalent causes of death. Up to half of patients develop severe left ventricular (LV) impairment following acute myocardial infarction (MI). Left ventricular dilatation and remodelling following acute myocardial infarction (AMI) is most commonly associated with anterior AMI and has been well documented in both experimental and clinical investigations, Figure 29.[173-175] One third of patients enrolled in the GISSI-3 trial (n=13,679) demonstrated evidence of this progressive LV dilatation and remodelling following AMI.[176] Treatment advances have led to increased survival from AMI. However, this may have led to a larger population at risk of congestive heart failure (CHF). [177] Despite huge advances in pharmacological and device therapies, the onset of CHF is associated with a 32% 1-year mortality.[178] LV remodelling following AMI leads to scar formation, distorted geometry, increased wall stress and eventual dilatation. Thus LV volume assessment in CHF can be used as an independent predictor of clinical outcomes.[178] An important measure of therapeutic efficacy is the demonstrable improvement in LV volume and geometry.

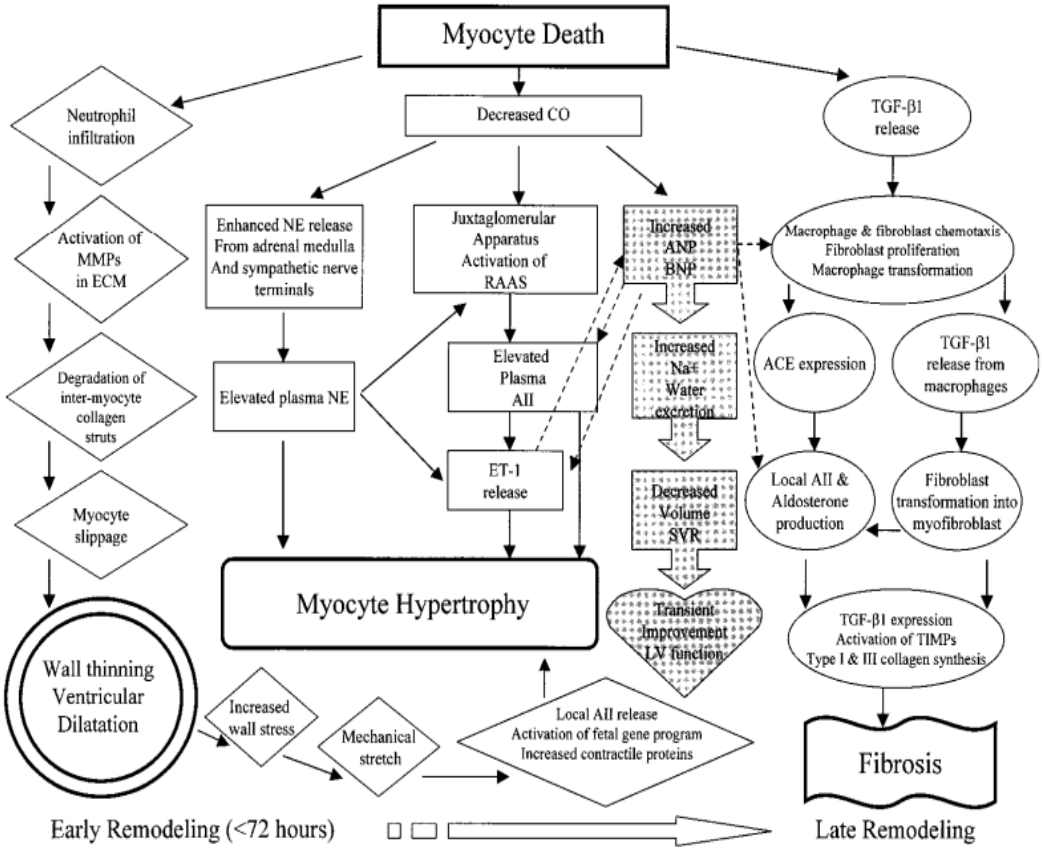


Figure 29 Ischaemic cardiomyopathy.
A diagrammatic representation of the multi-factorial components of ventricular remodelling; abbreviations: ECM extra-cellular matrix, RAAS renin-angiotensin-aldosterone system, CO cardiac output, SVR systemic vascular resistance, LV left ventricle, AII angiotensin II, TGF β transforming growth factor beta. [179]

1.7.6.2 LEFT VENTRICULAR PARTITIONING DEVICE

The aim of percutaneous ventricular restoration (PVR) therapy in this cohort of CHF patients is to reduce LV volumes and thus reduce wall stress; remodelling of the LV thus increasing synchronicity can lead to a more effective ejection without the increased morbidity and mortality associated with surgery. [180,181] PVR is a catheter-based approach to delivery of a compliant partitioning (PARACHUTE) device to the LV apex, thus partitioning the akinetic myocardium; the conical nitinol frame with ePTFE membrane enables device compression and therefore percutaneous implantation, Figure

30. The Parachute system includes the Parachute device, the pre-shaped delivery catheter and dilator, and the balloon delivery system that facilitates expansion of the device Figure 30.The Parachute device is composed of a self-expanding nitinol frame (16 struts; radio-opaque), an ePTFE impermeable membrane, and an atraumatic polymer foot available in 4 sizes (65, 75, 85 and 95mm) with two different “foot” heights. The tips of the struts anchor the device on the myocardium and the atraumatic foot provides contact between the LV apex and the device, orientating it toward the LV outflow tract.

However data on the haemodynamic consequences are lacking, perticularly, the effect of the device on preload, afterload and dyssynchrony. Accurate assessment of cardiac performance is critical in CHF to gauge prognosis and assess therapeutic response. Although ejection fraction is the most commonly used measure of cardiac function, the gold standard for assessing cardiac performance and its interaction with the arterial system is pressure-volume (PV) analysis. In CHF ventricular-arterial uncoupling occurs, this can accurately be measured by PV analysis as the ratio of Ea:Ees where Ea is a measure of net arterial load and Ees is a load-independent measure of LV contractility, which is one of the aims of this work.

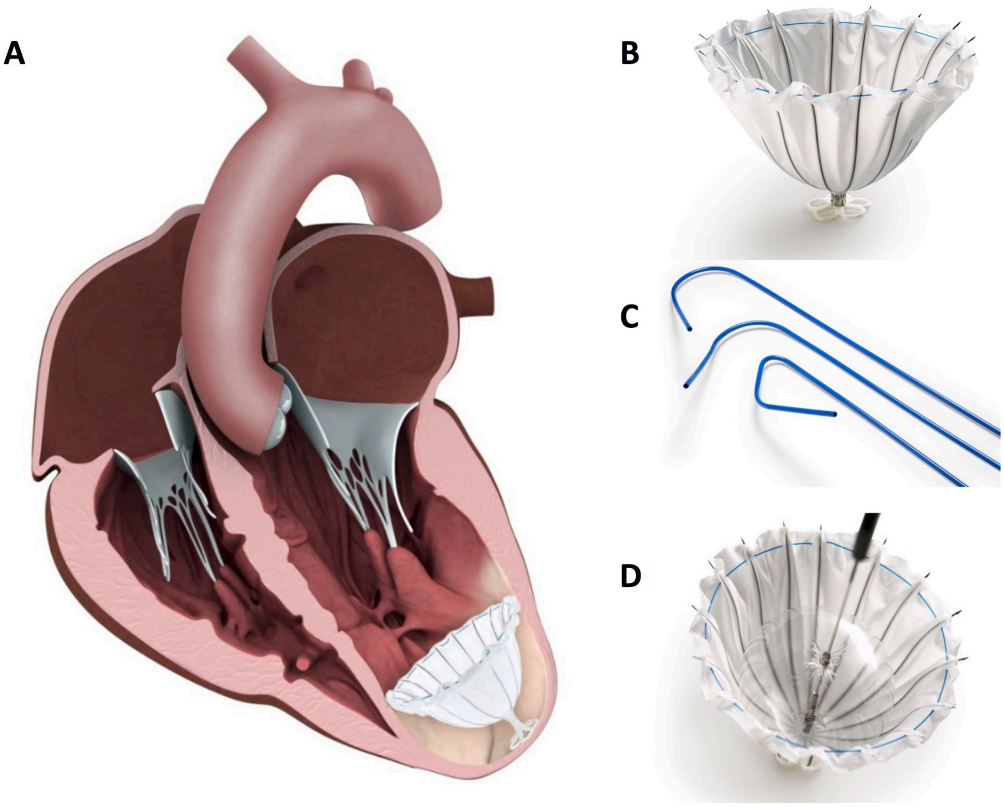


Figure 30 Parachute Device Illustration. The left panel demonstrates an illustration of the Parachute device implanted in a dilated left ventricle (A); the right panels demonstrate an open Parachute device (**B**), various shapes of the delivery catheters (**C**), and the 20cc balloon delivery system (**D**), adapted from[182].

2 METHODS

2.1 INTRODUCTION

In the following chapter the methodology used to undertake this research including the invasive measurement of pressure-volume loops, invasive measurement of coronary blood flow and 3-dimensional echocardiographic techniques are described. The detail included is such that accurate reproducibility is possible. The methods describe commercially available tools and their respective software for data acquisition and protocol specific techniques.

2.2 MEASUREMENTS: REAL-TIME LV HAEMODYNAMICS

In this section there follows a detailed discussion with regard to the acquisition of left ventricular haemodynamic measurements.

2.2.1 CONDUCTANCE CATHETER

Simultaneous LV pressure and volume measurements were performed using a conductance catheter (CD Leycom, Zoetermeer, Netherlands), Figure 31. This equipment is capable of real-time acquisition and analysis of left ventricular pressure and volume data via the Intra-Cardiac Analyser console (INCA) (CD Leycom, Zoetermeer, Netherlands). The conductance catheters are commercially available; CE marked for research techniques. The two available sizes are: 4Fr (no lumen) and 7Fr (lumen, over the wire) with a choice of electrode spacing. These catheters are flexible and have a pigtail shaped end to aid placement in the left ventricle. The catheters are

equipped with solid-state high fidelity pressure sensor (to prevent drift of tracing) that sits in the mid-LV cavity and twelve electrodes spaced at regular intervals to enable acquisition of volume data. The 4Fr CC was used for radial or simultaneous data acquisition; the 7Fr CC was used in study protocol five, section 7 (PVR).

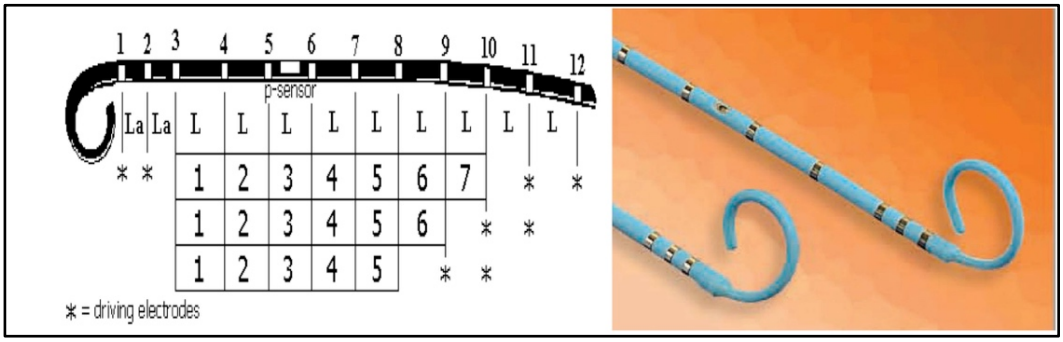


Figure 31 Conductance catheter.
The driving electrodes are on either end with multiple segmental electrodes and a solid-state pressure sensor between electrodes 5 and 6 (left); the pigtail end facilitates positioning of the catheter in the left ventricle, images courtesy of CD Leycom, Zoetermeer, Netherlands.

2.2.1.1 CONDUCTANCE CATHETER POSITION

The correct position of the conductance catheter is verified fluoroscopically, and on inspection of the segmental conductance signals and assessment of the total pressure-volume loop generated. Optimal pressure-volume recordings are highly dependent on catheter size selection (based on LV dimensions) and appropriate and stable positioning of the catheter: coaxial with the ventricular long axis with the pigtail tip sitting in the apex.

2.2.2 VOLUME CALCULATION

2.2.2.1 THE IMPEDANCE METHOD

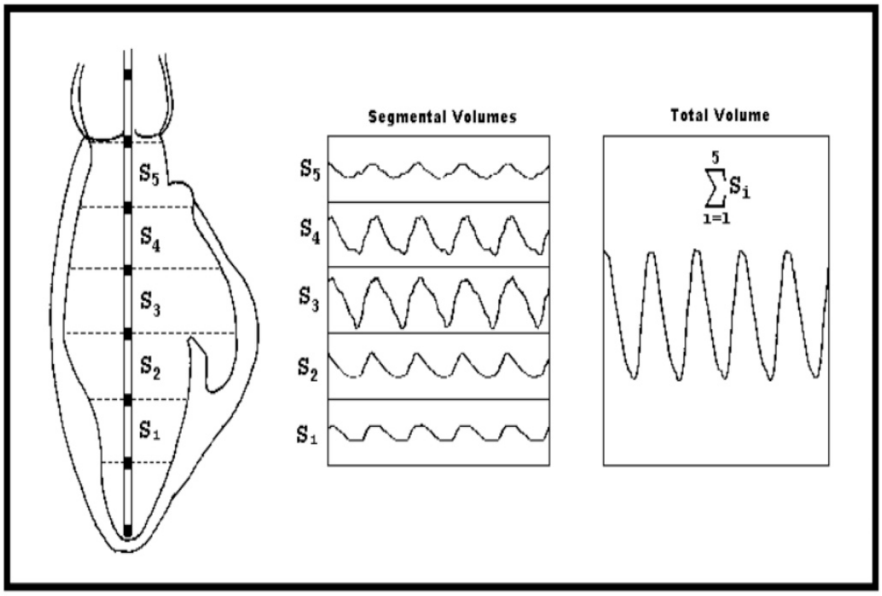


Figure 32 Impedance method.
The conductance catheter is in a vertical position in the left ventricle (left); segmental calculated volumes are shown (middle) and the total volume as a sum of these segments (right), adapted from [183].

Essential information for the assessment of cardiovascular performance can be obtained by measuring intra-cardiac pressure and volume. As intra-cardiac volume is primarily a dynamic variable, real-time accurate measurements are extremely valuable; the conductance method calculates continuous left ventricular (LV) volume tracings by measuring parallel electric conductance between adjacent electrodes. The benefit of the conductance catheter method in enabling measurement of simultaneous LV volumes and pressures is that it provides invasive measures of cardiac mechanics and haemodynamics. Generation of pressure volume loops therefore: (1) provides a characterisation of pump performance that allows loading factors to be reasonably separated from ventricular properties; (2) identifies both diastolic and systolic properties

in common terms and therefore helps clarify their interrelationship; (3) provides a description of coupling between ventricle and vasculature, which enables predictions of stroke volume and stroke work response to various loading interventions. The technique of using electrical conductance, or impedance measurement of intravascular volume was first developed for pump function assessment in humans in the early 1980s.[183] Validation of this technique has been performed against cine computed tomography and electro-conductive balloons in animals; thus the conductance catheter is capable of reproducing accurate global LV volumes and estimates of stroke volume as well as segmental volume calculation.[184,185] The conductance catheter method used today enables online beat-to-beat assessment of left ventricular volume. The time-varying electrical conductance of separated segments of blood in the left ventricle is proportional to the intra-ventricular volume (Ohm's law), therefore an alternating current (0.4mA) is applied establishing an electrical field in the LV cavity (proximal and distal electrodes); five segmental volumes (time-varying segmental conductance) defined by the 10 remaining electrodes (S1 to S5) are measured, and the sum is the total LV volume, Figure 32.

2.2.2.2 SLOPE FACTOR AND PARALLEL CONDUCTANCE

The conical apex is excluded from the segmental calculation, normally corrected for by the addition of 1/3 of the 1st segmental volume. This can also be calculated using a slope factor (value between 0.5-1.0), determined by Equation 14. The reference stroke volume is calculated by thermo-dilution techniques (2.2.3.4).

Equation 14

$$\alpha = \frac{conductance\ stroke\ volume}{reference\ stroke\ volume}$$

Parallel conductance of the myocardium, which can lead to overestimation of LV volume, is corrected for using the correction volume, determined by hypertonic saline administration. This drives a transient change in blood conductivity, performed by injecting 5% (10% under general anaesthesia) hypertonic saline into the pulmonary artery via a pulmonary artery catheter, to extrapolate the effects.[183] This is only necessary when the intervention is driving acute volume changes. Therefore this correction method is only relevant for Chapter 7. Importantly, the correct volume can also be determined by non-invasive imaging.

2.2.3 INTRA-CARDIAC ANALYSER

2.2.3.1 HARDWARE

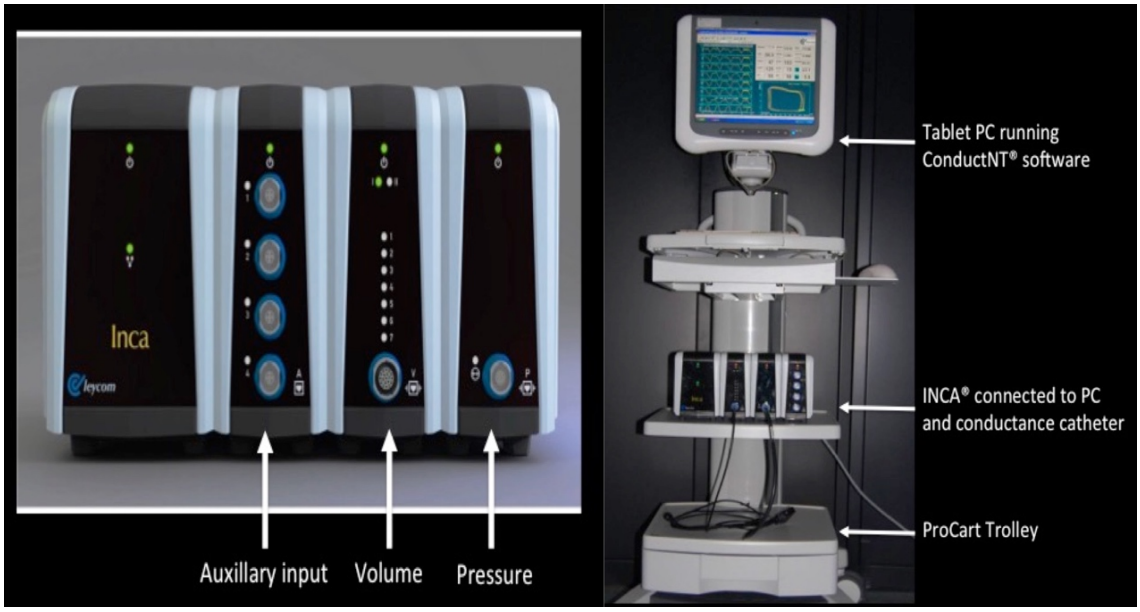


Figure 33 INtra-Cardiac Analyser (INCA®)
INCA (left); the Pro-Cart trolley setup: INCA on shelf and PC tablet monitor with Conduct NT software running real-time data acquisition (right).

The INCA® is an integrated, stand-alone system for the acquisition, display and analysis of intra-ventricular pressure and volume (by conductance) data in humans to which the conductance catheter is connected, Figure 34. The data analysed by the INCA is displayed on a tablet PC (windows 32-bit operating system) and runs with Conduct NT© (version 3.18.1) software, (CD Leycom, Zoetermeer, Netherlands); the tablet and INCA are connected via an ethernet cable. The conductance catheter has two external connecting cables feeding into the INCA. The pressure cable is connected to the corresponding port on the INCA, which detects and automatically calibrates the pressure. The volume cable is connected to the corresponding port on the INCA. In

Figure 34 a live recording is demonstrated. The tablet PC can display measured LV haemodynamic indices (top right), real-time PV loops (bottom right), and haemodynamic tracings (left). This enables both optimisation of recorded signals and an immediate appreciation of the underlying physiology.

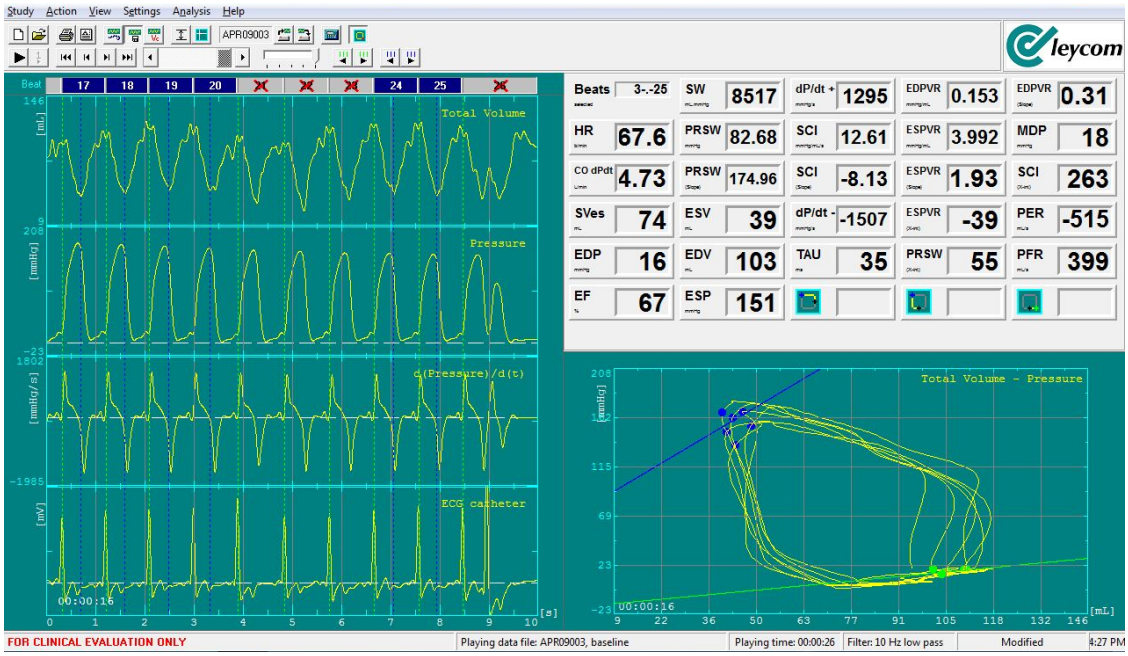


Figure 34 Real-time display.
A zoomed-in view of the tablet PC seen in Figure 33; total LV volume (top left panel); LV pressure (second panel); dP/dT (third panel) and the intra-cardiac ECG (bottom left); PV loop generated (bottom right hand corner) from the real-time pressure and volume data; calculated and measured haemodynamic indices (top right of display).

2.2.3.2 INCA SETUP AND CALIBRATION

Equipment setup and device calibration is performed prior to conductance catheter (CC) insertion. Two cable leads arise from the distal end of the CC, one for pressure connection and one for volume. The sterile proximal (pigtail) end with electrodes and pressure sensor is fully submerged in normal saline for 10 seconds (operator 1); the pressure cable (arising distally, not sterile) is connected to the INCA (operator 2). On connection, the PC software performs pressure calibration. For additional accuracy,

following measurements, the CC is externalised and the pressure tracing is recorded to document the zero offset and applied offline to selected data sets as necessary. For volume calibration, an extension cable is attached to the CC volume cable (operator 1), which is connected to the INCA (operator 2) The CC is inserted into the participant via arterial access and placed into the left ventricle. Volume is calibrated in the LV using invasive calibration methods (section 2.2.3.3) or with volumetric data obtained by either 3D echocardiographic or cardiac magnetic resonance imaging (section 2.2.3.4).

2.2.3.3 NON-INVASIVE VOLUMETRIC DATASET

3-Dimensional transthoracic echocardiography performed, ideally immediately prior to the procedure, is used to acquire the volume datasets necessary for calibration. This volumetric data collection enables volume calibration using the ConductNT software. The software allows input of direct values of end-diastolic and end-systolic volumes obtained from the 3D echo measurements, this can be used to calibrate all data files recorded in the same patient. 3D volume dataset acquisition is described in section 2.4.

2.2.3.4 INVASIVE CALIBRATION

Invasive calibration is more accurate but requires more instrumentation. 7Fr Right femoral venous access enables insertion of a 7Fr pulmonary artery catheter (PAC) into the right pulmonary artery via the right ventricle. Standard thermo-dilution techniques involve injection of 10 mL bolus of cold saline via the proximal port of the PAC, repeated three times. This calculates the reference volume, to incorporate the slope factor alpha, accounting for the conical shape of the left ventricular apex. Hypertonic saline (5% for sedated; 10% for general anaesthesia due to respiratory irritation) is injected in 3x10mL boluses into the pulmonary artery. This calculates the correction

factor to account for parallel conductance of the myocardium. During injection, the dataset is recorded and inputted into the stroke volume calculator function available on the software in real-time.

2.2.4 CONDUCT NT SOFTWARE

2.2.4.1 DATA ACQUISITION

Data capture was performed using the dedicated data acquisition and analysis software (Conduct NT, version 3.18.1, CD Leycom, Zoetermeer, Netherlands). At least three baseline datasets were recorded; each dataset is recorded separately and in sequence because signal optimisation cannot be performed during the recording. These data files are stored according to participant ID and date in numerical order for later export and analysis. Conduct NT acquires all necessary LV chamber haemodynamics; however, for the purposes of this study, a number of additional calculated LV indices and coronary haemodynamic measurements were necessary, which negated the use of this software in isolation. This includes measurements of cardiac energetics, single beat estimation of EDPVR and ESPVR slopes and time-varying elastance. The development of an analytical software system for this purpose is described in the results chapter, section 3.

2.2.4.2 DATA VARIABLES

The collection of raw variables during live acquisition is essential prior to the calculation of derived parameters. These are as follows:

- Intra-cardiac ECG: an ECG sensor is present on the CC mid-LV cavity; this enables accurate timing of events, and determination of end-diastole and end-systole.

- Instantaneous LV volume: segmental volumes directly measured via the electrodes, are summed and calibrated to provide total LV volume (LVV), from which end-diastolic (EDV), end-systolic (ESV) are therefore stroke volumes (SV) are derived.
- Instantaneous LV pressure: measured directly from the solid-state high-fidelity pressure sensor in the mid-LV cavity, from which end-diastolic (EDP) and end-systolic pressure (ESP) are derived.
- Pressure-volume loop: generated from instantaneous LV pressure and LV volume, from which stroke work (SW) (area of the PV-loop) can be derived. The PV loop enables determination of the end-systolic pressure-volume (ESPVR) and end-diastolic pressure-volume points (EDPVR).
- Rate of LV pressure change: directly measured by the pressure sensor over time to derive the maximum rate of pressure rise (dP/dTmax) and decay (dP/dTmin)

Derived parameters:

- Contractility: Cardiac output: (HR x SV) and ejection fraction (SV/EDV x100).
- Load-independent markers of contractility: starling contractile index (SCI) (dP/dT max to EDV ratio); preload recruitable stroke work (PRSW) (SW to EDV ratio)
- Load independent markers of relaxation: EDPVR, and the time constant of relaxation: Tau, defined as the time required for the cavity pressure at dP/dT_{min} to be reduced by 1/e, expressed in milliseconds.[186]

2.3 MEASUREMENTS: INVASIVE CORONARY HAEMODYNAMICS

In this section there follows a detailed discussion with regard to the acquisition of coronary haemodynamic measurements.

2.3.1 COMBOWIRE AND COMBOMAP CONSOLE

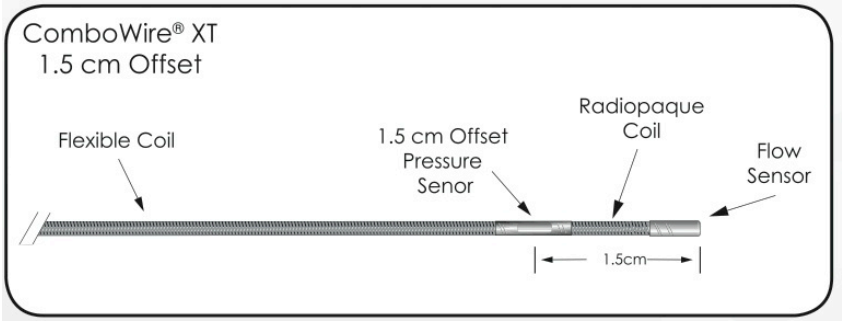


Figure 35 Animation of Combowire.
The pressure and flow transducers are located at the distal end, images courtesy of Volcano Corp, USA.

For the purposes of complete assessment of coronary haemodynamics, intravascular blood pressure and blood flow velocity in the coronary artery were measured using the ComboWire® (Volcano Therapeutics, USA). This dual sensor pressure and flow (Doppler) wire is manufactured commercially to standard guidewire specifications (0.014" diameter; 185cm), Figure 35. The flow sensor (Doppler crystal) is located at the distal most tip, with the high-fidelity, solid state pressure sensor offset by 1.5cm. This is the only available guidewire capable of simultaneous measurement (via the ComboMap 6800 system) of coronary pressure and blood flow velocity in the coronary artery for interventional and research procedures; and is the most accurate means of coronary data acquisition. The distal pressure transducer receives pressure signals, which are sent to the Combomap Console, which processes and displays these in waveforms and numerical values. The flow transducer transmits and receives ultrasound signals, which are processed by the Combomap, which calculates the coronary blood flow velocity

based on the Doppler shift, thus displaying a spectral waveform as well as measured and calculated parameters.

2.3.2 CALIBRATION AND DATA ACQUISITION

To perform accurate measurements, adequate device setup and calibration is necessary. The sterile ComboWire® comprises the guidewire (inserted into participant) and two connecting ports, one for pressure and one for velocity, these are connected to the ComboMap console via the patient interface module (PIM) prior to insertion. This ComboMap console is a PC monitor on a trolley that runs the ComboMap software on Windows XP (together these comprise the ComboMap system). The PC has a Touch Screen monitor for input of participant details, and for later optimisation of flow and pressure signals and display, Figure 36**.**

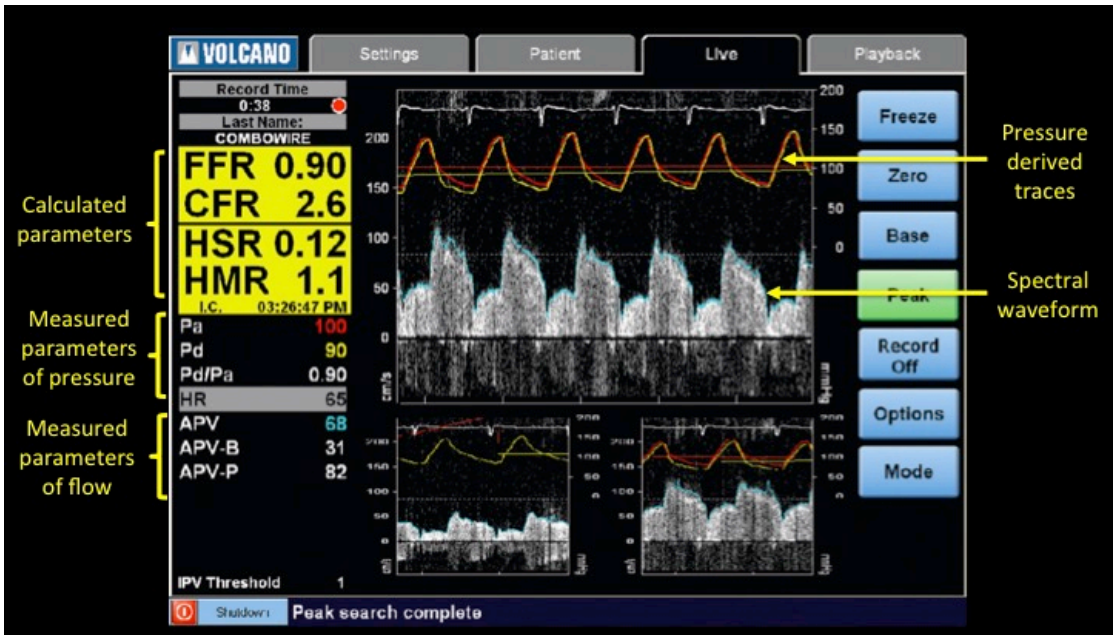


Figure 36 ComboMap Display.
Haemodynamic parameters displayed numerically and as pressure and spectral (Doppler) waveforms, the latter has a blue envelope from which the IPV is derived. Calculated parameters top left hand corner.

Prior to the start of the case, the distal pressure filters are enabled to reduce noise, which implements a delay between coronary pressure and velocity that is corrected for on post-hoc analysis. For intra-coronary measurements a wall filter is set and fixed at 200Hz. The monitor is set on live mode and the catheter lab operator connects the pressure plug via an Ethernet connection on the patient interface module (PIM), once the pressure is calibrated, the flow plug is connected to the PIM and the wire is ready for insertion. In the aortic root, the distal (combowire) and proximal pressure (aortic pressure from physio monitor) signals are normalised (Pd/Pa equals 1.0). ComboWire calibration triggers the recording until it is manually stopped. The ComboWire is advanced down the target vessel beyond the lesion into a steady position, and the position of the wire tip (anterograde or retrograde) determines the flow settings on the ComboMap system. The flow signal is then optimised by fluoroscopic positioning of the wire and by assessment of flow velocity traces by varying the instantaneous peak velocity (IPV) upper and lower thresholds and by adjusting the display scales. The importance of this step is that during analysis, coronary flow velocity tracings measured equate to the spectral Doppler envelope, the true spectral Doppler waveform cannot be measured offline due to current software limitations.

2.3.3 DATA VARIABLES

Simultaneous measurement of intracoronary pressure and blood flow velocities allows for the generation of multiple indices of haemodynamic assessment.

Direct Measurements:

- Distal coronary pressure (Pd) is measured directly via the pressure sensor, proximal aortic (Pa) pressure (low fidelity; measured by fluid filled manometry) and the continuous ECG tracing are transduced via the Physiology Monitoring System in the cardiac catheter lab provided as a low level input.
- The coronary flow velocity is displayed in real-time as a Doppler signal and can be viewed on the PC monitor during recording (live and on playback settings).

Derived Measurements:

- Pd/Pa, the ratio of distal coronary pressure to proximal aortic pressure
- Instantaneous peak velocity (IPV) is sampled in real time, every 5 ms (200Hz), from the most recent cardiac cycles.
- Mean coronary blood flow (U) is calculated from 3 cardiac cycles and is the IPV averaged over the number of cardiac cycles where x is the number of cycles +1 (Equation 15); mechanical systole and diastole are estimated from the ECG.

Equation 15

$$U\ (cm/sec) = \frac{\sum_{n=R1}^{Rx-1} IPV\ (n)}{Rx - R1}$$

- Velocity time integral (VTI) is the integral under the IPV curve, this is calculated as the sum of the IPV sample magnitude multiplied by the value over the number of cardiac cycles divided by the number of cycles (shown for 2 cardiac cycles, Equation 16):

Equation 16

$$VTI\ (cm/cycle) = \frac{0.01}{2} \sum_{n=S1}^{S3-1} IPV\ (n)$$

- Fractional Flow Reserve (FFR) is the minimum value of the normalised pressure ratio during hyperaemia (maximal vasodilatation), which equates to the ratio of distal coronary pressure minus venous pressure to proximal aortic pressure minus venous pressure.
- Hyperaemic Stenosis Resistance (HSR) is an indicator of stenosis resistance, which may be compromised by a flow-limiting lesion or microvascular disease. It is the ratio of the proximal distal pressure mean gradient (Pa - Pd) to the peak U (U-P). The data is captured at the peak APV sample (Equation 17):

Equation 17

$$HSR = [hPa - hPd)]/hU$$

- Hyperaemic Microvascular Resistance (HMR) is an indicator of microvascular resistance, which may be compromised by microvascular disease. It is the ratio of the distal pressure (Pd) to the peak U (U-P). The data is captured at the peak APV sample (Equation 18):

Equation 18

$$HMR = hPd/hU$$

2.4 ECHOCARDIOGRAPHY PROTOCOL

Echocardiography was performed either immediately before or after the cardiac catheter lab procedure. Echocardiographic examinations were performed with Philips or Vivid, GE ultrasonic system. All patients were examined in the left supine position, using the parasternal short axis view at the level of the papillary muscle, and both 2, and 4-chamber apical views of the LV and parasternal long access view of the LV, with emphasis on high quality recordings of all LV walls. Three consecutive cardiac cycles were stored during breath-hold. Images were stored digitally. All grey-scale images were obtained with a minimum frame rate of 50 frames/sec.

2.4.1 ECHO ANALYSIS

Left Ventricular Ejection Fraction by echocardiography was assessed by the modified biplane Simpson's method from the apical 2 and 4-chamber grey-scale recordings. End-diastole was defined as the frame closest to the R-wave and end-systole was defined as the minimal cavity area just before mitral valve opening. Strain measurements were performed using TomTec 4D analysis software. The strain software identifies the endocardial border, and myocardial motion is automatically tracked in each grey-scale imaging view. Segmental longitudinal and circumferential strain curves reflect the average strain value of all the acoustic markers within each segment. Segments with poor tracking were readjusted by the observer. Results are reported as the peak systolic strain and strain rate during the whole cardiac cycle. Furthermore, measurements from the individual LV apical and parasternal segments were averaged and reported as LV global longitudinal or circumferential strain and strain rate. Global strain was calculated

as an average of strain measurements from 16 LV segments. In addition, time to peak strain was measured from the aortic valve opening to peak negative strain.

2.5 INSTRUMENTATION AND TECHNICAL CONSIDERATIONS

This subsection deals with the technical considerations and equipment selection for certain aspects of the data collection protocol. The importance of this study centres around simultaneous acquisition; however, both the INCA and ComboMap console were designed to be used in isolation, thus their design hinders their use in combination in-vivo. Overcoming this initial challenge required adjustments to be made to the equipment used to acquire the data.

2.5.1 CONDUCTANCE CATHETER DIAMETER

The 4Fr CC (no inner lumen), is a pigtail shaped catheter with an outer diameter of 1.4mm, a guide catheter is required to deliver this to the left ventricle. The outer diameter necessitates delivery with a minimum of a 6Fr guide catheter, the inner diameter of which 1.7mm.

Sheath Size (Fr)	Inner Diameter	Outer Diameter
5	1.7mm/0.066”	7-8Fr
6	2.0mm/0.079”	8-9Fr
7	2.3mm/0.092”	9-10Fr
8	2.7mm/0.105”	10-11Fr
9	3.0mm/0.118”	11-12Fr
10	3.3mm/0.131”	12-13Fr

Table 1 Sheath sizes. Inner and outer diameters of arterial sheaths are specified.

To perform simultaneous measurement from a single access site, both the ComboWire and the CC are introduced via the same guide catheter. The combined outer diameter of both is 1.8mm; thus for measurements via the femoral artery an 8Fr guide catheter was used. Radial access site was used for Protocol 2 (supine cycle ergometry), for which the maximum deliverable sheath size is 6Fr (outer diameter of 2.7mm, inner diameter 2mm), Table 1. Using standard equipment this would need to be performed via femoral access thus precluding bicycle exercise. The solution is to deliver a guide with an equivalent inner diameter of an 8Fr standard guide catheter, without the need for an arterial sheath (8Fr arterial sheath OD 3.3mm). The commercially available 7.5Fr Asahi Sheathless Guide™ (Vascular Perspectives, UK), has an outer diameter just smaller than a 6Fr sheath and an inner diameter equivalent to that of an 8Fr standard guide catheter, thus enabling single site radial access with simultaneous introduction of conductance catheter and ComboWire, Figure 37.

The 7Fr conductance catheter is a pigtail shaped catheter with an inner lumen. This catheter can be delivered over the wire via femoral access into the left ventricle. The inner lumen requires a 0.25" super stiff guide wire (Terumo). In the absence of simultaneous measurements in Protocol 5 (left ventricular partitioning device) the 7Fr CC was used in isolation; the 7Fr is more stable in dilated left ventricles. The outer diameter of the 7Fr CC is 2.3mm, necessitating a minimum 8Fr femoral sheath, Table 1. To deliver the ComboWire and 4Fr CC together an 8Fr guide catheter was required.

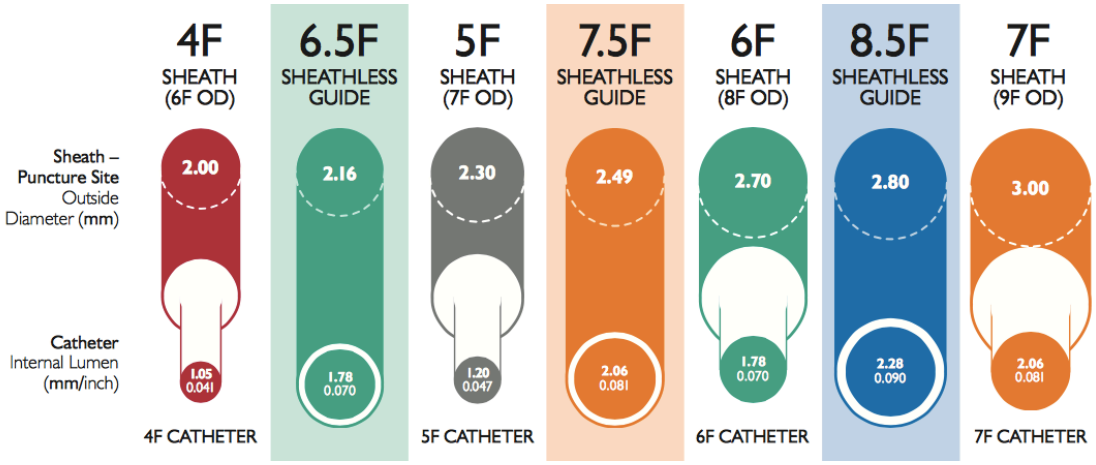


Figure 37 Asahi Sheathless Guide.
The outer (OD) and inner diameters (ID) are compared to those of standard arterial sheaths, images courtesy of Vascular Perspectives, UK.

2.5.2 EQUIPMENT ALTERATION

The conductance catheters were designed as a diagnostic tool, to be delivered via femoral access. Their length therefore precludes delivery through a standard guide catheter (100cm). For electrode measurements in the left ventricle, the distal end of the conductance catheter needs to be exposed. Therefore commercially available, 80cm 8Fr guide catheters were used for research procedures performed via femoral access.

Data acquisition performed via radial access raised two issues:

- The distance from the radial puncture site to the coronary ostia is greater than via the femoral route; further catheter length loss is incurred by tortuosity of the arterial tree in this region; thus conductance catheter measurements could not be performed via the artery in patients over 175cm. This limited the exercise cohort in Protocol 2. Diagnostic catheterisation was therefore performed in the first instance in all patients (100cm catheters), to measure this distance prior to enrollment.
- Asahi Sheathless Guides are commercially available in only one size (100cm). Guide catheters had to therefore be manually shortened under sterile conditions by the operator, on a case-by-case basis. Sterile 7" angled scissors were used to cut a

10cm segment out of the proximal end of the 7.5Fr guide. A 1.5cm section of the lumen of a 6Fr sheath (pre-dilated with an 8Fr dilator) was used to reattach the severed ends, to create a temporary seal. The proximal end can be seen in Figure 38 and the distal end with the CC electrodes exposed can be seen in Figure 39.

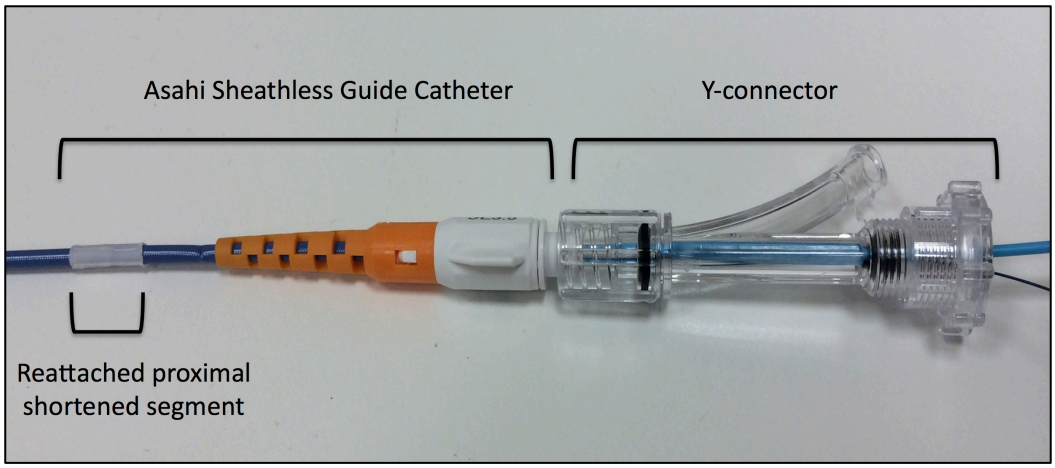


Figure 38 Proximal end of the ASG.
Reattachment of two severed ends of guide catheter can be seen. The ASG is connected to the Y-connector.

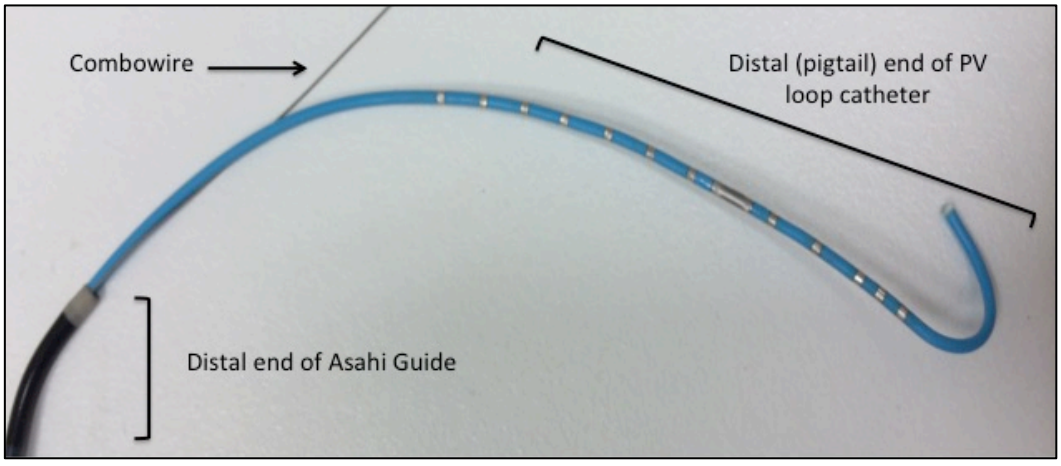


Figure 39 The distal end of ASG.

Combowire and pigtail end conductance catheter exposed to facilitate placement in the left ventricle.

2.6 CATHETER LABORATORY PROTOCOL

The following protocols describe the catheter lab set-up and methodology necessary for data acquisition. Further detail is provided in the specific results chapters. All research interventions were approved by the UK National Research Ethics Committee. The patient information sheet with quoted risk and the protocol submitted for all catheter laboratory based procedures is in the Appendix.

2.6.1 Set-Up And Calibration

2.6.1.1 RADIAL ACCESS:

Diagnostic Procedure:

- 5Fr radial access
- 5000 IU heparin injected into aortic root.
- Diagnostic angiography using 5Fr JL3.5 and JR4.
- Residual catheter distance measurement.
- Identification of target vessel lesion.

Research Protocol:

- 7.5Fr ASG guide shortened proximally (10cm) with 7"angled scissors.
- 1.5cm section of 6Fr femoral sheath lumen to reattach ASG.
- Introducer inserted into ASG.
- Setup of angioplasty kit as per routine clinical protocol.
- 5Fr radial sheath exchange for 7.5Fr ASG over 300cm diagnostic J-wire.
- Introducer removed in the ascending aorta.
- ASG intubation of target vessel coronary ostium.

- Further intra-arterial Heparin to achieve 70IU/kg and the target vessel with guide catheter.

2.6.1.2 FEMORAL ACCESS:

Diagnostic Procedure:

- 8Fr femoral access
- Diagnostic angiography using 6Fr JL4 and JR4
- Residual catheter distance measurement
- Identification of target vessel lesion

Research Protocol:

- 8Fr 80cm Medtronic Launcher Guide Catheter
- Intubation of target vessel coronary ostium
- IA Heparin to achieve 70IU/kg

2.6.1.3 COMBOWIRE INSERTION:

Calibration and Insertion:

- Research participant details recorded
- Appropriate pressure and flow settings selected
- Auxiliary cables connected to INCA
- ECG lead connected to Physio Monitor
- ComboWire connected to patient interface module and calibrated
- ComboWire inserted into guide catheter
- Signal normalised in aortic root or coronary ostium - triggers continuous recording
- ComboWire advanced to distal target vessel beyond lesion
- Optimisation of flow signal
- Guide catheter disengaged

2.6.1.4 CONDUCTANCE CATHETER INSERTION:

Calibration:

- Research Participant details recorded on panel PC
- Catheter number selected
- Submergence of Conductance Catheter (CC) in normal saline -10 seconds
- CC Pressure cable connected to corresponding INCA port
- Pressure calibration confirmation
- Volume cable placed in sterile bag with porthole and connected to CC volume cable on one end and corresponding INCA port at the other end.

Insertion:

- CC pigtail angled away from Y-arm on introduction into the guide catheter.
- CC advanced to aortic root and across aortic valve into LV apex.
- Stable position confirmed by stability of PV loop trace and fluoroscopic confirmation.
- Exclusion of electrodes outside of LV (for accurate volume calculation)
- Volume calibration performed with baseline dataset recording using invasive calibration or predetermined non-invasive volumes (EDV and ESV).
- Serial recordings and data collection followed

2.6.2 PROCEDURAL TECHNIQUES

The following section focuses on the details of the specific interventions performed in each study cohort following ComboWire and conductance catheter insertion.

2.6.3 BASELINE SIMULTANEOUS MEASUREMENTS

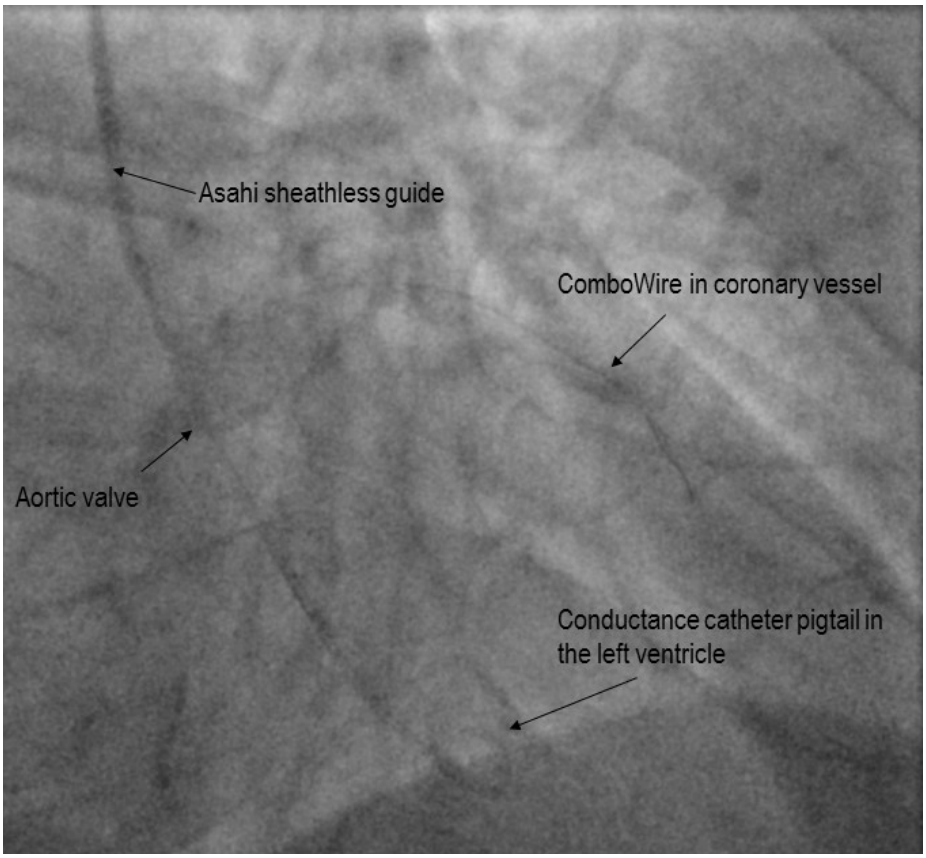


Figure 40 Fluoroscopic confirmation of conductance catheter position

Baseline measurements were taken with the patient in a resting supine position. Signals were optimised and recorded for 30 seconds to 1minute. Measurements are repeated three times to account for any variability or loss of signal, Figure 40.

2.6.4 VASODILATOR ADMINISTRATION: ISOSORBIDE DINITRATE

2mL of sterile 0.1% ISDN solution was diluted 1:5 in 10ml 0.9% Saline. The resulting approximate drug concentration was 2mg/10mL. On manual injection outside the patient through the manifold, 1-2mg ISDN was delivered via the guide catheter into the patients' aortic root. Injection was mandated over 5 seconds; however due to intra-and inter-operator variability, aortic root size and proximity to the coronary ostia, the rate of injection and coronary infiltration could not be controlled for. Dataset recording was commenced at the onset of manual injection and continued for 2 minutes, this captured the immediate changes induced in the coronary artery, left ventricle and peripheral vasculature. Further recordings were performed on return to baseline. ISDN administration was performed twice.

2.6.5 ADENOSINE INDUCED HYPERAEMIA

Prior to the start of the procedure, the research participant underwent sterile peripheral venous cannulation, either in the left (preferable) or right ante-cubital fossa. This provided venous access for the purposes of administration of adenosine infusion. The adenosine infusion was attached via an intravenous giving set to the peripheral cannula and the adenosine administered using a syringe driver at a rate of 140mcg/kg/min (calculations based on the patient weight and height determined the rate of infusion). Dataset recording was commenced at the onset of the infusion. The adenosine was administered for a minimum of 90 seconds, until a steady state was achieved. Dataset recording continued for the duration of adenosine and continued for a further 1 minute after the infusion had ceased. A further baseline recording was taken after adenosine administration.

2.6.6 DYNAMIC EXERCISE: SUPINE CYCLE ERGOMETRY

Dynamic exercise was performed solely in the cardiac catheter laboratory. This was performed prior to the angioplasty procedure. The supine cycle ergometer (Ergosana®, Schiller, Germany) is a specialist device, placed on the catheter laboratory table and secured to underlying structures. The patient performed a trial, 15-20 second attempt at supine cycle ergometry to ensure feasibility. Dataset recording on the INCA, of both coronary and LV measurements was recorded from the start and for the duration of exercise, and 1 minute into recovery. Supine cycle ergometer exercise was started at 60 rpm, at 30 Watts for the 1st minute. This increased incrementally by 20 Watts per minute maintaining a cadence of 60rpm where possible on a pre-specified ergometer protocol. Continuous intra-cardiac ECG monitoring was provided by the CC. This was continued for 5 minutes or until the research participant experienced any of the following: 1) chest pain 2) fatigue 3) >3mm ST depression on intra-cardiac ECG 4) arrhythmia 5) maximal age-related heart rate.

2.6.7 LEFT VENTRICULAR PARTITIONING DEVICE: PV LOOP SUB-STUDY

Prior to insertion of the device all patients underwent baseline evaluation with: 3D echocardiography, Cardiac CT for device sizing and placement, Cardiac MRI and coronary angiography (Figure 41). Suitability for Parachute device implantation was discussed for all patients in multi-disciplinary team meeting. Based on further core lab assessment, the optimal parachute device was selected.

Via the left femoral artery (LFA) a 6Fr sheath (non-interventional access site) was introduced and remained in-situ. Intra-arterial Heparin was administered to maintain an activated clotting time of greater than 250, via left venous access a 7Fr sheath was

introduced and remained in situ, through this a pulmonary artery catheter (PAC) was floated in the pulmonary artery. This enabled administration of hypertonic saline (5-10%) and thermodilution techniques to calibrate the INCA. Via the LFA, a 7Fr conductance catheter was introduced into the ventricle over a 0.025" super stiff 240cm wire. Once the conductance catheter (CC) was in position, thermodilution and hypertonic saline administration was performed three times and LV haemodynamic recordings were taken pre-device implantation. The CC was then removed in preparation for device implantation; the pulmonary artery catheter remained in situ.

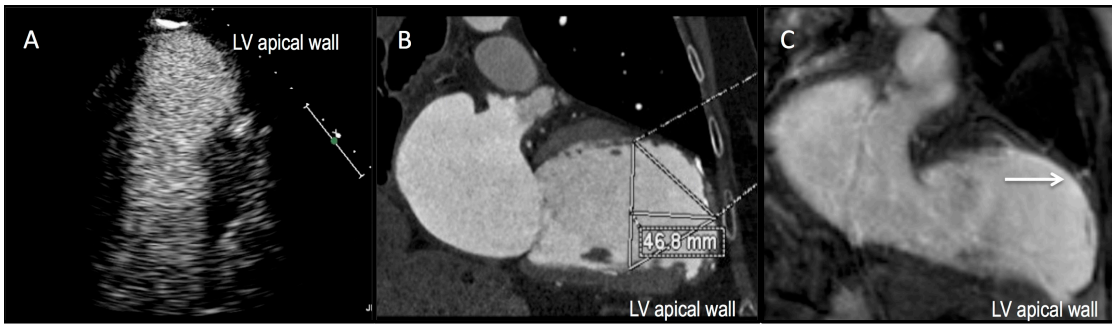


Figure 41 Baseline Patient Evaluation.
Anatomical assessment is performed using echocardiography with contrast to demonstrate aneurysmal apical wall and exclude thrombus (A). Device selection was based on multi-slice computed tomography, which also allowed for identification of pseudochordae or severe calcification, precluding safe deployment (B). Cardiac magnetic resonance imaging with late gadolinium enhancement confirms scarring of the LV apical wall secondary to myocardial infarction, white arrow (C).

A 5Fr 125cm (long) diagnostic pigtail catheter was then introduced via the LFA and used to cross the aortic valve into the left ventricle. A left ventriculogram was performed to visualise apical hypokinesia, and the optimal view device positioning. This was then retracted into the aortic root. Right femoral arterial access was then obtained using an 8Fr sheath, (the device access site) through which the Parachute device was delivered, the access site was pre-prepared with two closure devices

(Perclose Proglide, Abbott Vascular). A 2nd 125cm (long) pigtail was introduced through the sheath in the right femoral artery, this again crosses the aortic valve and was placed in the left ventricle using a soft j-tipped wire, which was then exchanged for a preshaped Safari wire™ (Boston Scientific); the pigtail was retracted and the safari wire remained in the left ventricle. A superstiff Safari wire provided enough support for exchange of the 8Fr with a 16Fr Vascular Sheath (Edwards, US). The Parachute delivery catheter was then introduced using pigtail into left ventricle across aortic valve, during which time the PARACHUTE® device was prepared. The Guide Catheter and Delivery Catheter were advanced together so that the PARACHUTE® Implant Foot is in contact with the apex. The delivery catheter position was maintained while the pigtail catheter was retracted, leaving a clear attachment zone. Parachute deployment Figure 42: the position of the PARACHUTE implant foot is maintained in the LV apex, whilst holding this in place, the guide catheter is withdrawn to completely expose the PARACHUTE® implant; 20cc. of 50:50 contrast-saline mixture is then injected into the delivery catheter balloon and inflation maintained for 1-2 minutes. The delivery catheter balloon was then deflated and guide catheter advanced over the deflated delivery system, the entire system was removed and LAO and RAO views confirm positioning of the device. The 7Fr CC was then reinserted, thermodilution and hypertonic saline calibration was repeated, and haemodynamic measurements taken.

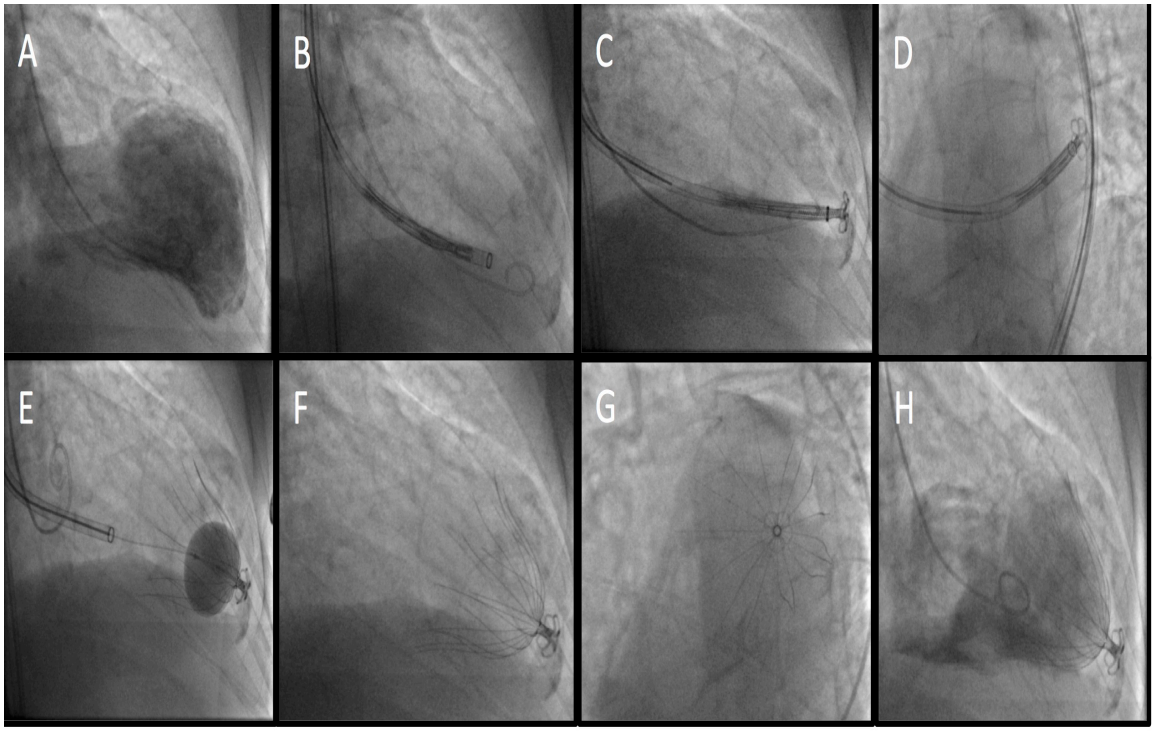


Figure 42 Parachute Study Procedure.
The sequence of parachute implantation in the LV: LV angiography is performed with a pigtail catheter in the LV (A) followed by pre-procedure PV measurements, the delivery catheter is position in the apex (B), the Parachute foot is then exposed and contact is made with the antero-apical wall, confirmed in LAO (C) and RAO (D) views. Device delivery is facilitated by 20cc balloon expansion (E), retraction of the delivery system, followed by fluoroscopic confirmation of position in LAO (F) and RAO (G) views. LV angiogram confirms partitioning of akinetic myocardium (H) and immediate post-procedure LV PV measurements are performed.

3 THE MECHANICAL DETERMINANTS OF CORONARY BLOOD FLOW: A NOVEL ANALYTICAL SOFTWARE SYSTEM

ABSTRACT

Coronary blood flow is phasic in nature, increasing in diastole and markedly decreasing in systole. Several hypotheses have been used to describe systolic flow impediment however data are conflicting. Recently, coronary wave intensity analysis (WIA), a time domain method for investigating incremental changes in coronary pressure and velocity described in terms of successive wave fronts, has been used to describe the impact of myocardial contraction on coronary blood flow morphology, making it a potentially powerful research tool. Previous work in this area have measured coronary and LV haemodynamics independently, reassembling to provide beat-to-beat averages, the disadvantages are that these do not provide continuous assessment of the interaction between the two. This study describes a novel software system that employs automated algorithms to perform simultaneous analysis of left ventricular (LV) pressure-volume (PV) loop and coronary haemodynamic data.

METHODS

The software was written using matrix laboratory programming language written by by Simon Rivolo with my input; integration of myocardial energetics and single beat estimations of pressure-volume relations make this a superior analytical tool to those currently available. Software calibration (temporal alignment of LV and coronary data) was performed using *in-vitro* (phantom flow model) and *in-vivo* experimentation. Subsequently real-time LV pressure-volume loop recordings from 15 patients in the

catheter laboratory setting were used to compare haemodynamic outputs from the new software with the gold standard CE marked software; furthermore, coronary wave energies were aligned with instantaneous LV pressure-volume changes and the impact of LV elastance on coronary blood flow velocity was examined.

RESULTS

Validation demonstrated statistical and clinical agreement between the novel and gold standard LV PV loop software; wave energies were aligned to the LV pressure volume loop: forward and backward travelling wave energies generated in the coronary artery were found to be strongly dependent on the ventriculo-arterial interaction, forward waves were delimited by diastolic blood pressure and backward waves by aortic valve opening; in the absence of autoregulation, coronary blood flow velocity was found to be closely related to LV elastance, suggesting that coronary blood flow velocity morphology is dependent on myocardial contractile properties and microvascular resistance during resting conditions.

CONCLUSIONS

The unique ability of this novel technology to describe the ventriculo-arterial and coronary interaction in terms of continuous real-time assessment enables an in depth examination of the relationship between coronary and LV haemodynamics; furthermore this tool was developed to facilitate future work in this area with a view to enhancing our understanding of pathophysiological mechanism of disease states and therapeutic interventions.

3.1 INTRODUCTION

There has been a long-standing interest in the interaction of cardiac contraction with coronary perfusion.[72,187] Coronary blood flow is phasic in nature, increasing in diastole and markedly decreasing in systole. Several hypotheses have been used to describe systolic flow impediment including the time-varying elastance theory of Suga et al, whereby the myocardium conducts elastance directly to the coronary arteries, however data are conflicting.[107,188-190] More recently, coronary wave intensity analysis (WIA) has been used to describe the impact of myocardial contraction on coronary blood flow morphology.[96,107] Coronary WIA is a time domain method for investigating incremental changes in coronary pressure and velocity, described in terms of successive wave fronts.[97] It has been proposed that wave energies measured by wave intensity analysis may be related to contractile properties of the ventricle, making it a potentially powerful clinical research tool.[100,191] To perform wave intensity analysis, invasive assessment of coronary haemodynamics with simultaneous measurement of both coronary pressure and blood flow velocity by means of spectral Doppler is necessary. However, WIA has several limitations, both in terms of signal calculation and invasive validation. Differencing of the WIA inputs generates noise and relies on operator smoothing of the signals to derive wave energies thus inducing variability in derived measurements; furthermore application of the single point technique to derive WIA in the coronary arteries limits its application during hyperaemic states.[104,192] In an attempt to describe cWIA in terms of changes in left ventricular haemodynamics, measurements of left ventricular pressure and wave energies have been measured independently and reassembled to provide beat-to-beat averages; the disadvantages are these methods do

not provide continuous assessment of the cardiac-coronary interaction and are unable to accurately measure contractile force independent of loading conditions.

Left ventricular pressure and volume measurements and their relationship has been the mainstay in describing myocardial properties since their early description a few decades ago; recently, advances in technology have enabled application of the conductance catheter method to enhance our understanding of myocardial disease states and the assessment of therapeutic interventions.[193-195] This method accurately measures left ventricular volume by way of an insulated catheter placed in the left ventricle. In summary, several evenly spaced electrodes measure intervening voltages from the current applied from the base of the ventricle to the apex; the solid-state pressure sensor derives high fidelity LV pressure measurements, thus enabling simultaneous assessment of left ventricular volumes and pressure.[183] The instantaneous LV pressure-volume relationship allows for determination of contractile and diastolic properties independent of the impact of loading conditions on the heart.

To address these issues, it was considered necessary to create a tool for the simultaneous continuous assessment of both left ventricular myocardial function and coronary blood flow velocity that would be comparable to each of these gold standards in terms of accuracy and reproducibility. We present a novel software analysis system that supports assessment of simultaneous coronary pressure and velocity measurements and left ventricular pressure-volume relations. The aim of this work was to create a clinical research tool that enabled analysis of LV PV loop data and coronary blood flow measurements (with wave intensity analysis) that were acquired simultaneously, and to

create a software programme that was accessible for future work in this area. This system was validated using ConductNT software (CD Leycom, Zoetermeer, Netherlands) as the "gold standard" measure of LV pressure-volume loop assessment. Incorporation of an adaptive filter (Savitsky-Golay) that uses automated algorithms for smoothing was used to remove inter- and intra-observer variability; application of baseline pulse wave velocity to the measurement of cWIA during hyperaemic states was used to decrease error.[192,196,197] Subsequently, real-time recordings utilising the conductance catheter hardware system (INCA, CD Leycom, Zoetermeer, Netherlands) with electronic routing of ComboWire (Volcano corp, Philips, USA) haemodynamic data were performed in human subjects; the software system was used to temporally align coronary and LV changes over one cardiac cycle to 1) the LV mechanical determinants of coronary wave energies; 2) accurately determine the relationship between instantaneous LV properties and coronary blood flow at rest and on abolition of microvascular resistance.[198,199]

3.2 METHODS

The hardware and software components of the coronary-PV analysis system (SimpleWires) are described. This is includes temporal alignment of the LV and coronary signals by *in-vitro* and *in-vivo* experimentation methods. This is followed by validation against the gold standard and delineation of the relation between LV myocardial properties, coronary blood flow and wave intensity analysis.

3.2.1 HARDWARE CONFIGURATION

Coronary pressure and flow velocity and LV pressure-volume were simultaneously acquired using a ComboWire (Volcano Corp) and conductance catheter (CC) respectively. Data acquisition was performed using the commercially available hardware consoles. The conductance catheter signal provides real-time beat-to-beat measurement of LV pressure-volume assessment; the hardware consists of the cardiac function laboratory (CFL-M) known as the INCA device (CD Leycom, Zoetermeer, Netherlands), connected to a panel PC with hard-disk running 32-bit Windows 7 operating system. The INCA is accessed using the built-in Conduct NT software (CD Leycom, Zoetermeer, Netherlands), which performs as a data acquisition and analysis tool. The conductance catheter is pressure calibrated in normal saline prior to placement in the left ventricle, following this; volume calibration is performed against baseline dataset recordings using volumetric data obtained from three-dimensional echocardiographic assessment of left ventricular volume.

The Combowire is calibrated outside the patient following connection to the ComboMap 6800 system via a patient interface module; in the aortic root, the coronary

pressure sensor is normalised to aortic pressure readings from the catheter laboratory physiology monitor prior to delivery down the target coronary vessel. Coronary pressure and flow velocity signals are acquired and interpreted by the ComboMap 6800 system, filters implemented during data acquisition (smoothing of haemodynamic pressure trace) apply a 55ms delay between coronary pressure and flow velocity, signals are digitally archived at 200Hz. Traditionally, following data acquisition on the ComboMap console, coronary data is digitally stored for later offline analysis using Study Manager Software (Amsterdam Medical Centre, Netherlands) to display files (.sdy) as haemodynamic tracings over time. This programme facilitates identification and extraction of relevant and optimal cardiac cycles for further analysis, data are then exported as snapshots (.txt) and uploaded (in our institution) to Cardiac Waves (in-house custom made programme for coronary haemodynamic analysis (KCL, London); this software generates numerical data and is capable of performing wave intensity analysis.

However, for the purposes of simultaneous acquisition and real-time display of coronary and LV haemodynamic data, we performed electronic routing of the ComboMap signals to the INCA device via the auxillary input ports (Figure 43). The INCA console runs on Conduct NT software (CD Leycom, Netherlands), this acquires LV PV loop data and can also be used to visualise data in real-time and analyse data offline. ConductNT enables auxiliary inputs to be viewed alongside haemodynamic variables (Figure 43). Coronary tracings on the ConductNT software were displayed as voltages: coronary pressure (1V/100mmHg) and velocity (1V/50 cm/s). Following electronic routing of the coronary data, the INCA introduced a time-delay between the coronary and LV signals; this was determined by in-vitro and in-vivo experimentation.

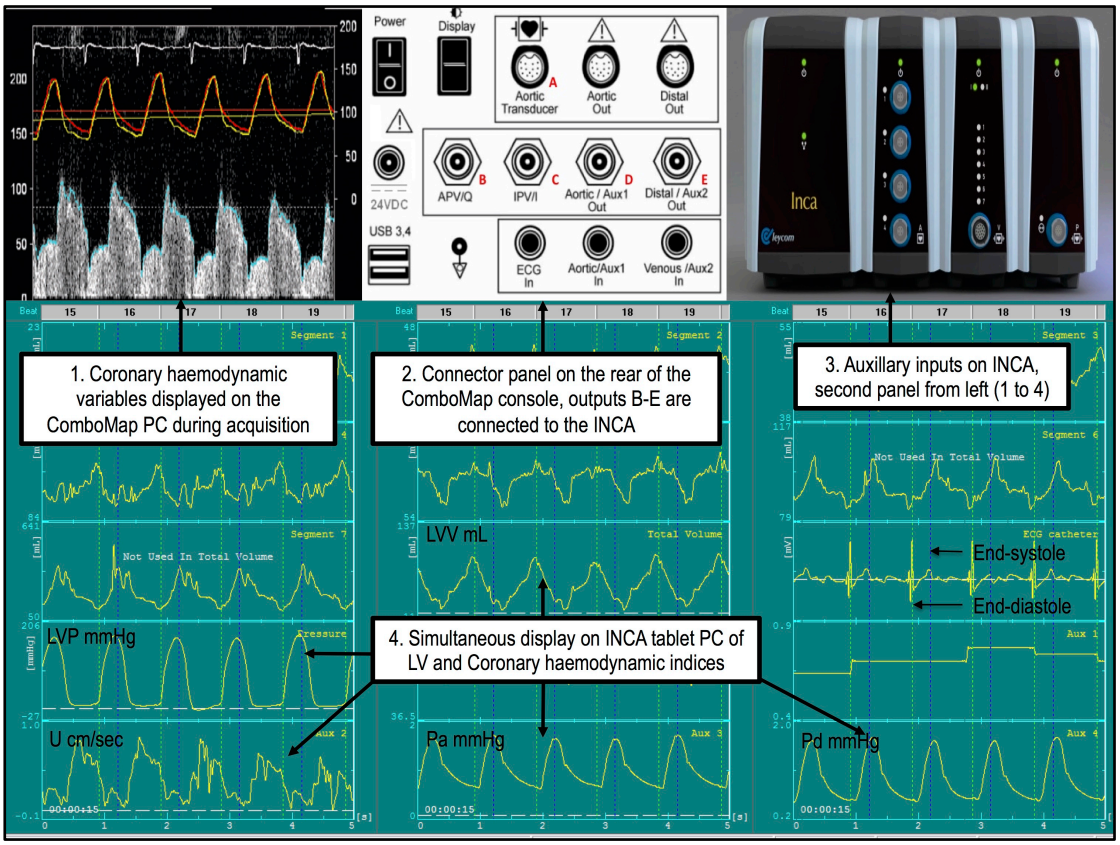


Figure 43 Electronic routing of the coronary signal into the INCA.
Displayed on the tablet PC (INCA). Abbreviations: LVP left ventricular pressure, LVV left ventricular volume, U mean coronary flow velocity, Pa aortic pressure (provided by fluid filled manometer in guide catheter)), Pd distal coronary pressure.

3.2.2 TIME-PHASE DELAY

In the early phase of software development, a time phase misalignment at end-diastole was noted between the left ventricular pressure signals (acquired by the INCA and ECG gated) and the signals routed from the ComboMap (coronary and aortic haemodynamic traces). The ECG gating of end-diastole on the LV pressure trace did not coincide with end-diastole on the aortic pressure trace. This can be visually appreciated in Figure 44, which demonstrates the real-time recording on the ConductNT software and offline analysis. Initially, the origin of this delay was not clear; however, during real-time

acquisition, it was established to have arisen from post-processing by the INCA and was not a physiological delay between LV and aortic pressure. In order to perform accurate simultaneous analysis, the post-processing delay was determined in two phases 1) in-vitro experimentation using a phantom aortic flow model followed by 2) in-vivo confirmation in the aortic root.

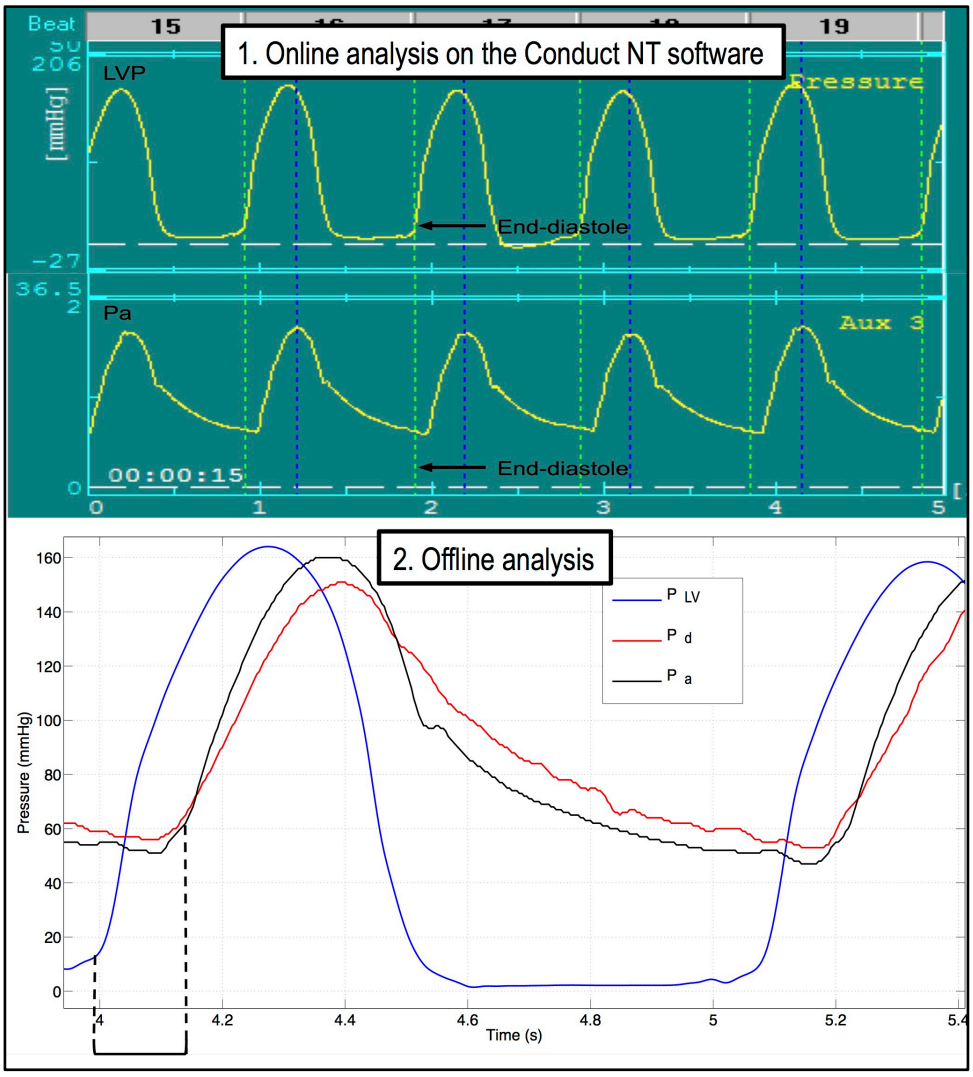


Figure 44 Time-phase delay.
The ECG gating of end-diastole for LVP (left ventricular pressure) occurs earlier than that of the aortic pressure transduced from the ComboMap.

3.2.2.1 IN-VITRO EXPERIMENTATION:

The pulsatile aortic flow phantom was built to simulate a working ventricle with simplified pulmonary and systemic vessels. Its aortic equivalent is a silicon tube, 1.2mm in thickness and 1200mm in length. A diagrammatic representation and the different parts forming the experimental rig are shown in Figure 45.

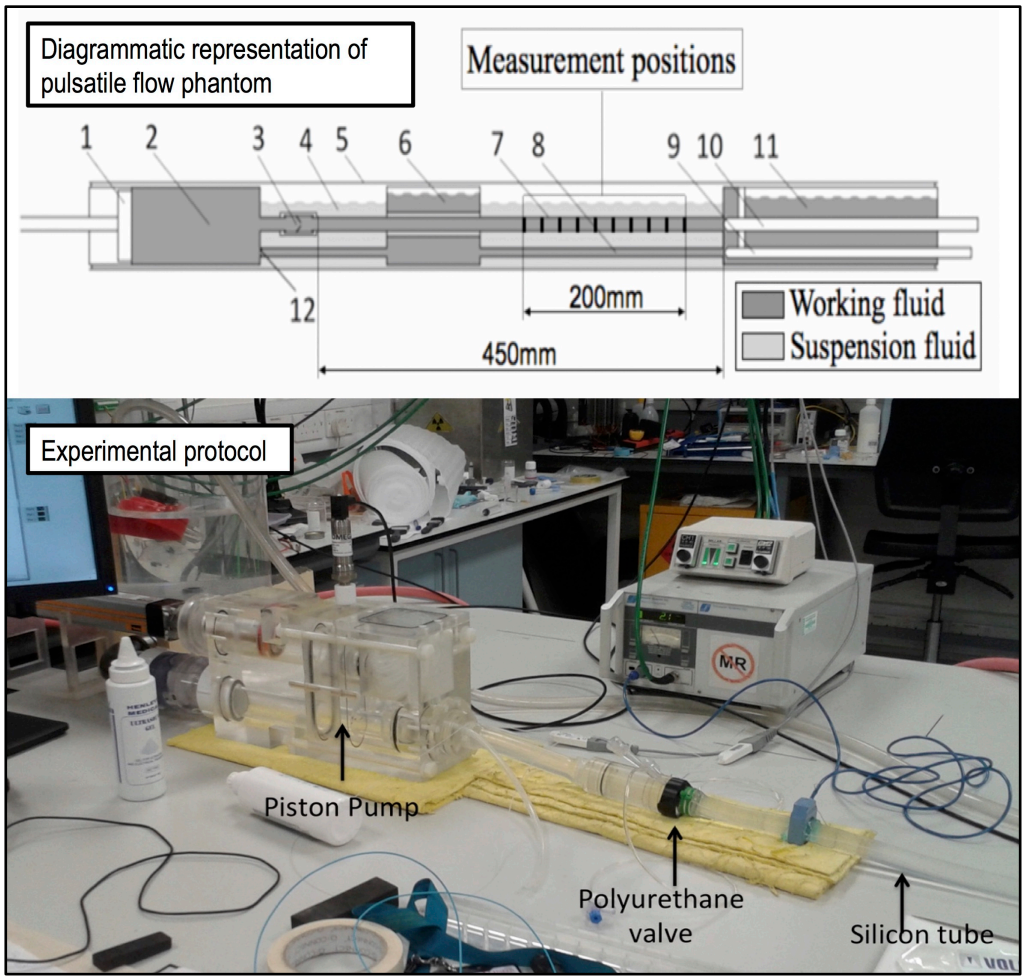


Figure 45 Pulsatile Flow Phantom.
Above: diagrammatic representation of the pulsatile flow phantom: 1) Ventricle piston; 2) Ventricle and working fluid; 3) Arterial valve; 4) Suspension fluid; 5) Outer cylindrical case; 6) Venous reservoir; 7) Silicone vessel; 8) Venous channel; 9) Venous resistance screw; 10) Arterial resistance screw and catheter access; 11) Arterial compliance chamber; 12) Venous valve. Reproduced from[200]. Below: experimental set-up for in-vitro determination of time-delay.

This device is used in computational fluid dynamics to closely mimic the physiological system. The piston-pump ejects the fluid contained in a cylindrical chamber through a

tri-leaflet polyurethane valve into a straight silicone tube. At the opposite end, a Windkessel system consisting of an adjustable resistance screw and a compliance chamber provide the desired afterload if required. At the proximal end is a generator used to create pulsatile flow of up to 20L/minute. The in vitro set-up provides a range of physiological systolic pressures without adding confounding factors typical of the patient context, such as beat-to-beat variability and localised changes in wall stiffness. This allows close control of the fluid-dynamic conditions, which can be accurately modelled using computer simulations to provide a physical interpretation of the observed discrepancies. This has previously been validated as a model and further detail on the flow phantom is available and was performed with the help the aforementioned collaborators.[200]

EXPERIMENTAL PROTOCOL

The conductance catheter and ComboWire were aligned such that both pressure transducers were in the same location in the phantom aorta, the experimental set-up is shown in Figure 45. Pulses were generated initially by the piston pump; however due to the silicon nature of the tube, the distance between the input generator and receiver was shortened (1cm) to minimise wave reflection. A repetitive impulse, generated by tapping the aorta just proximal to the pressure transducers was performed and repeated three times, with varying degrees of pressure change. Simultaneous recordings were performed on the ComboMap and INCA console; electronic routing of the ComboMap recordings into the INCA enabled display of both tracings (conductance catheter and ComboWire) on the INCA tablet PC. Data were recorded and exported from the INCA.

3.2.2.2 *IN-VIVO* EXPERIMENTATION

To determine if the signal misalignment persisted in-vivo and was not further influenced by patient factors (anatomy of aortic root, heart rate, temperature), the experiment was conducted in 3 healthy adult volunteers. 8Fr femoral access site was used to introduce an 8Fr 80cm guide catheter in three patients who had consented to the study protocol. A 4Fr PV loop conductance catheter (CC) and 0.014" ComboWire were aligned in the aortic root. The pressure sensors were aligned temporally and spatially. The pressure sensor on the CC has a radio-opaque marker; the pressure sensor on the ComboWire is immediately proximal to the radio-opaque region, thus enabling fluoroscopic alignment of the two. Simultaneous recordings were performed on the ComboMap and INCA console, with electronic routing of ComboWire signal into the INCA as described previously. Recordings were performed for one minute; this represented the average duration of recording performed in the clinical research setting.

3.2.2.3 RESULTS

The *in-vitro* and *in-vivo* measurements are depicted graphically in Figure 46. To increase accuracy, measurements were performed trough to trough in both the *in-vitro* and *in-vivo* experiments. The delay was found to be 88ms (4ms sampling time) in both. An adjustment feature was therefore incorporated into the SimpleWires software, enabling automatic alignment between the left ventricular signals and the coronary signals (auxiliary inputs) on data upload for analysis.

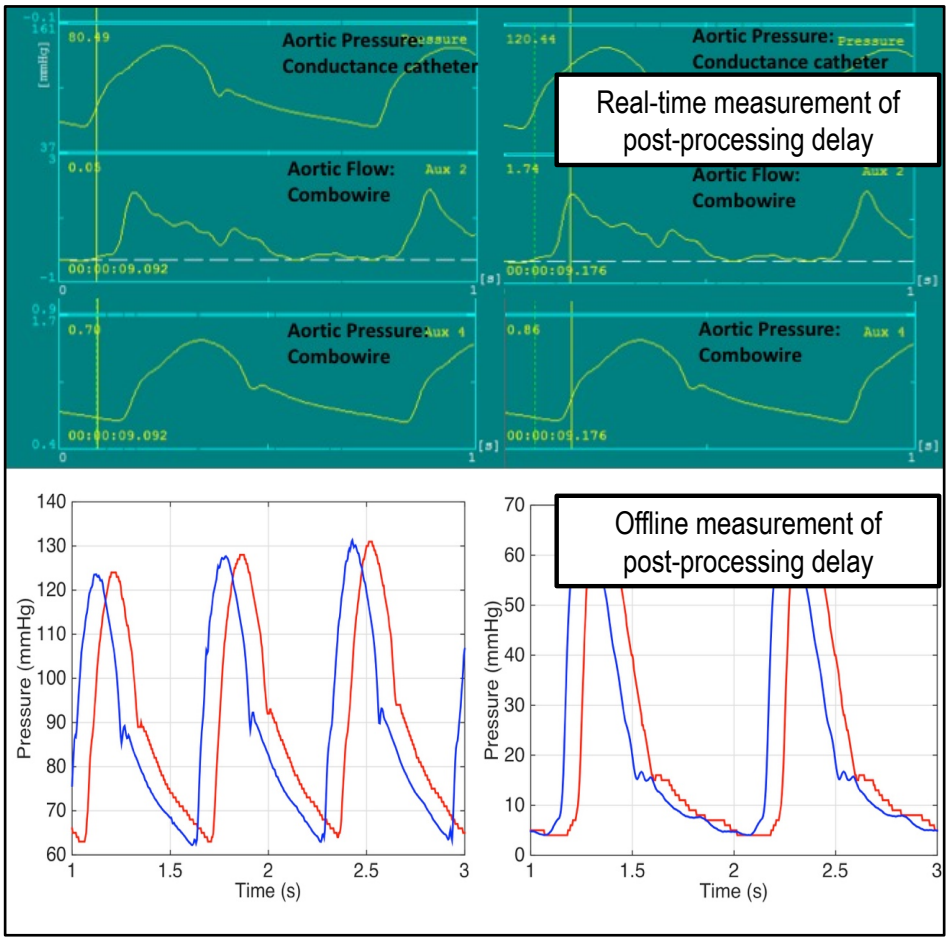


Figure 46 Time-phase misalignment.
The pressure transduced from the INCA is seen in blue and from the combowire in red; impulse generation in-vivo is seen on the left and from the phantom aortic model on the right. The delay was measured from trough to trough.

3.2.3 SIMPLEWIRES ANALYSIS SOFTWARE

All data were recorded on and exported from Conduct NT software (CD Leycom). For analysis using the novel SimpleWires software, end-diastolic markers were ECG-gated (peak R-wave) and end-systolic markers were aligned to the maximum ratio of total LV volume to pressure prior to export and a low pass filter 25Hz was instituted. Combined coronary and LV data were exported from the INCA as comma separated value (csv) files onto a portable memory stick. Each dataset is exported as a separate file. Data were uploaded to the SimpleWires software analysis system, analysis at 10Hz for LV data

and 25Hz for coronary data were performed using the matrix laboratory graphical programming language (Mat lab).

3.2.3.1 DATA ANALYSIS

On opening the SimpleWires programme, a graphical user interface (GUI) appears, Figure 47. To perform the analysis, the operator uploads the dataset of interest to the GUI from the csv files exported from Conduct NT (CD Leycom). The consecutive cardiac cycles of interest (beats) from the haemodynamic signals can then be accessed from the uploaded data file. The "beats" function enables the operator to select consecutive cycles from one of a range of parameters including left ventricular pressure (LVP), left ventricular volume (LVV), beat number (range of 1 to x where 1 is the first recorded cardiac cycle within that dataset and x is the last), ECG, coronary pressure, coronary flow velocity, aortic pressure, time (seconds). To select beats of interest, data are visualised as their respective recorded waveforms.

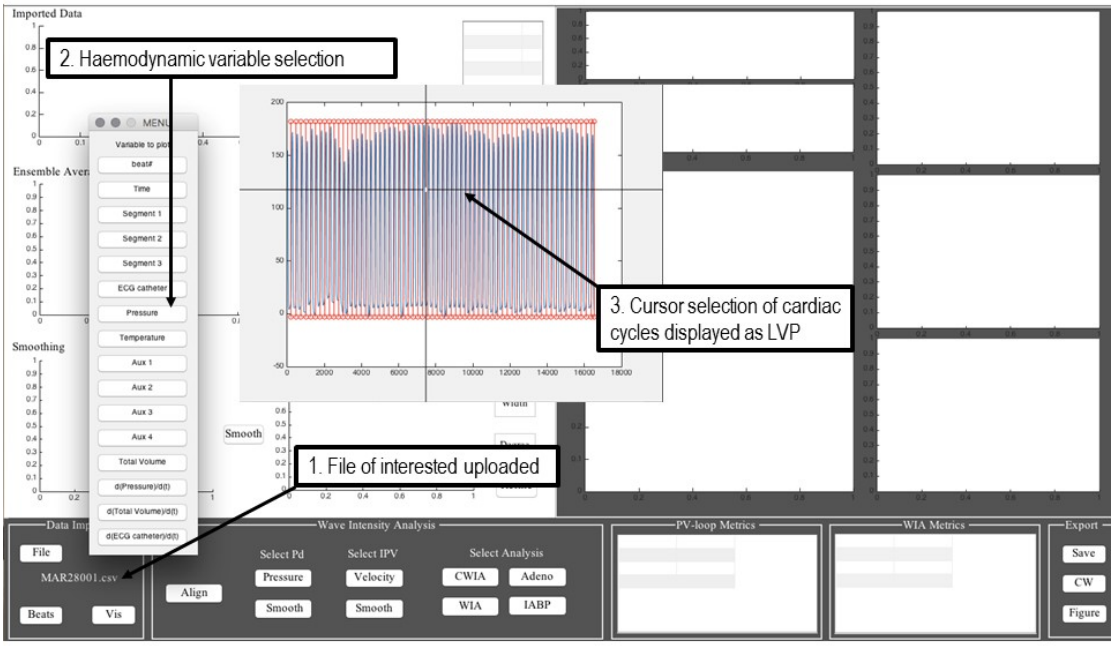


Figure 47 SimpleWires graphical user interface (GUI).
The dataset of interest is selected and consecutive cardiac cycles are selected. Abbreviations: LVP left ventricular pressure.

The software then plots the LV haemodynamic tracings over time (left ventricular pressure, LVP and volume, LVV); calculates and displays an ensemble average of LVP and LVV plotted over one cardiac cycle; and displays LVP as a function of LVV (pressure-volume loop) for each cardiac cycle and as an average of the selected cycles. The end-systolic pressure-volume relationship (ESPVR) and end-diastolic pressure volume relationship (EPDVR) relationship slope are calculated (based previously published and validated methodology, described in section 3.2.3.4) and depicted on the ensemble averaged PV loop as black lines intersecting the end-systolic and end-diastolic points on the loop respectively. The numerical values that accompany the left ventricular haemodynamic tracings are displayed at the bottom of the screen, Figure 48.

The software performs temporal alignment of the acquired coronary and LV data by removal of the post-processing delay (determined from in-vitro and in-vivo

experimentation, section 3.2.2) implemented by the INCA, allowing the observer to view LV and coronary haemodynamic variables over one cardiac cycle. Coronary pressure and flow velocity measurements are ensemble averaged over 5 beats and displayed graphically over one cardiac cycle. SimpleWires software is capable of converting the ConductNT voltages displayed for coronary pressure and velocity and therefore exported, to mmHg and cm/sec respectively.

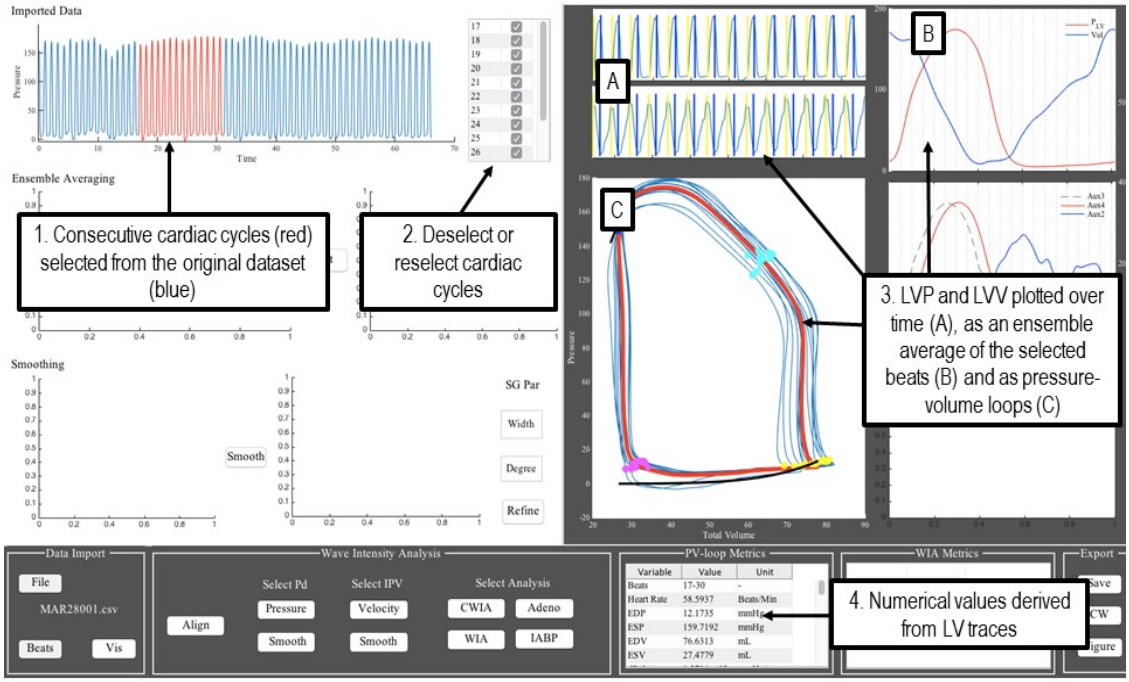


Figure 48 Left ventricular haemodynamics.
The recorded measurements are displayed graphically in a number of formats and as numerical values. Abbreviations: LVP left ventricular pressure, LVV left ventricular volume, LV left ventricle.

The observer can select coronary pressure or velocity signals displayed as a function of time to aid optimal selection of cardiac cycles prior to wave intensity analysis. The "align" function can be used to correct the 55ms delay implemented by the ComboMap pressure filters (previously established). The software enables visualisation of coronary

blood flow velocity or coronary pressure traces after smoothing with the option of Savitsky-Golay (S-G) filters or adaptive S-G filter, which can then be implemented to perform wave intensity analysis, Figure 49.

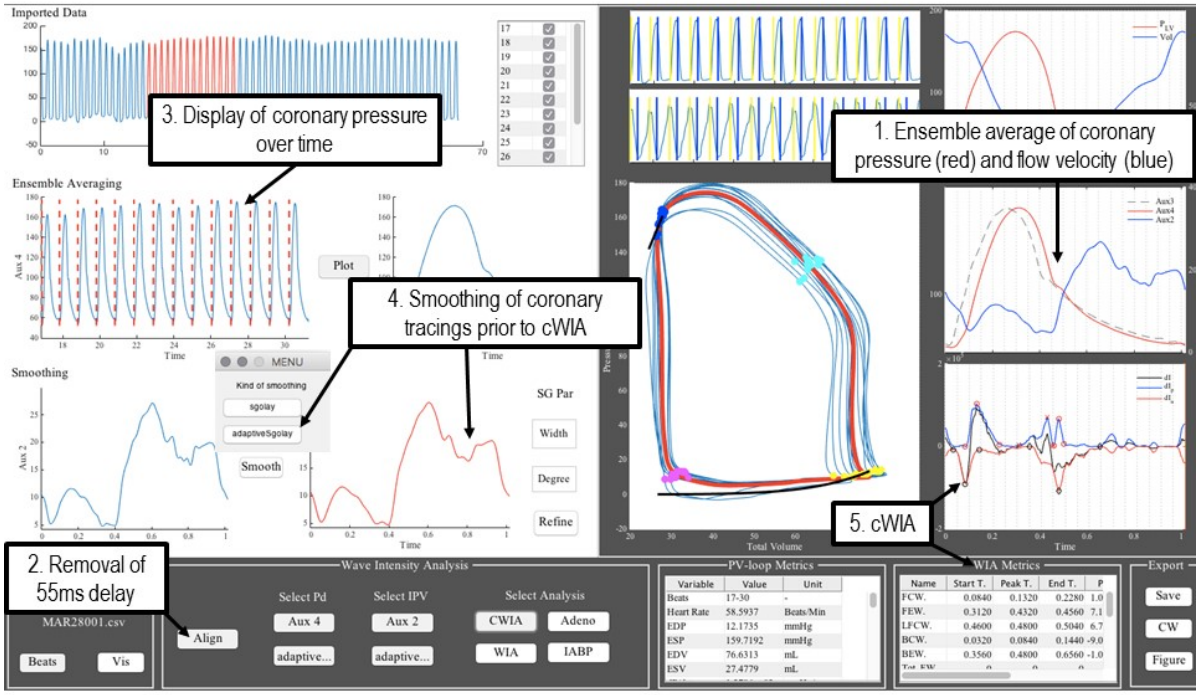


Figure 49 Coronary haemodynamic signals.
The observer can align the pressure and velocity signals, smooth the data and perform wave intensity analysis.

3.2.3.2 STANDARDISED PV LOOP VARIABLES

The left ventricular (LV) haemodynamic variables that are derived from the recorded LV haemodynamic traces are defined Table 2. In addition to instantaneous left ventricular pressure and volume, load-independent measures of ventricular function can be determined.

Contractility and cardiac work: The end-systolic PV relationship (ESPVR) represents the ratio of LV pressure to volume at the end of ventricular systole (left uppermost corner of the loop) and the slope (Ees) is calculated from single-beat estimation methods described below. The Starling contractile index (SCI) was calculated as the maximal rate of pressure change over time during isovolumic contraction (dP/dTmax) normalised to end-diastolic volume (EDV). The (external) stroke work (SW) was calculated as the area within the PV loop. Preload-recruitable stroke work (PRSW) was calculated as SW normalised to EDV.

Diastolic Function: In addition to measured dP/dtmin, load-independent markers of relaxation were derived. Tau is a measure of active relaxation, and is the time in milliseconds (ms) for dP/dt min to be reduced by 1/e. The end-diastolic PV relationship (EDPVR) represents the ratio of LV pressure to volume at the end of ventricular diastole, measured at the peak of the R wave on the electrocardiogram. The slope of this curve, represents the passive diastolic properties of the myocardium.

Haemodynamic Indices	**Definition**
EDP, mmHg	ECG-gated end-diastolic pressure
ESP, mmHg	Measured at left uppermost point of PV loop
EDV, mL	ECG gated end-diastolic volume
ESV, mL	Measured at left uppermost point of PV loop
dP/dtmax, mmHg/sec	Slope of peak maximum derivative of pressure change over time
dP/dtmin, mmHg/sec	Slope of peak minimum derivative of pressure change over time
EDPVR, mmHg/mL	ECG gated pressure to volume ratio
ESPVR, mmHg/mL	Left uppermost point of PV loop, pressure to volume ratio
SV, mL	EDV - ESV
CO, L/min	SV x HR
EF, %	SV/ESV x 100
SW, mmHg.mL	Area of PV loop
PRSW, mmHg	SW/EDV
PVA, Joules	$PVA = SW+(0.5\ xESP^2/\ ESPVR)$
SCI, mmHg/sec/mL	$dP/dT_{max}/EDV$
Tau, ms	Time for dP/dt min to be reduced by 1/e
Ea, mmHg/mL	Ea = ESP/SV = (Heart Rate) Resistance = (HR) R.
DTF, %	Diastolic time/total time of cardiac cycle
EDPVR beta	Beta coefficient of EDPVR slope
EDPVR alpha	Alpha coefficient of EDPVR slope
Ees	Slope of the ESPVR line

Table 2 The definitions and formulas of left ventricular (LV) haemodynamic variables
Abbreviations: EDP End-Diastolic Pressure, ESP End-Systolic Pressure, EDV End-Diastolic Volume, ESV End-Systolic Volume, EDPVR End-Diastolic Pressure-Volume Relationship, ESPVR End-Systolic Pressure Volume Relationship, SV Stroke Volume, CO Cardiac Output, EF Ejection Fraction, SW Stroke Work, PRSW Preload-Recruitable Stroke Work, PVA Pressure Volume Area, SCI Starling Contractile Index, Ea Arterial Elastance, DTF Diastolic Time Fraction.

3.2.3.3 STANDARDISED CORONARY VARIABLES

Coronary indices measured by SimpleWires: Simultaneous measurement of intracoronary pressure and blood flow velocities allows for the generation of multiple indices of haemodynamic assessment. Direct Measurements: Distal coronary pressure (Pd), proximal aortic (Pa) pressure, instantaneous peak velocity (IPV), mean coronary flow and the continuous ECG tracing are provided as direct inputs.

Net coronary wave intensity (dI) and total wave intensity (dI+ and dI-) generation were also incorporated into SimpleWires software, the benefit of additional net wave intensity, defined as the product of incremental changes in local pressure and flow velocity, is that this is thought to more accurately reflect the impact of cardiac contraction and relaxation on coronary haemodynamics. The wave intensity analysis feature on SimpleWires, enables the observer to generate data on the six main coronary wave energies previously identified during the cardiac cycle.[96] Calculation of wave energies has been previously described, in brief, the software provides the observer with wave areas, peaks and percentage.

3.2.3.4 NOVEL SOFTWARE FEATURES

A number of additional features not currently available to clinical researchers have been incorporated into the SimpleWires analysis software. These are broadly divided below into coronary wave intensity analysis and LV haemodynamic analysis tools.

CWIA INCORPORATED FEATURES

Pulse Wave Speed:

This is a fundamental factor in cWIA determination as is calculated using the sum of squares method (SPc), which has been previously validated.[97,201] However, this method has limitations in the context of hyperaemic intervention: the SPc underestimates wave speed under these conditions, thus overestimating magnitudes of the forward travelling compression wave and backward compression wave energies that arise during systole, potentially invalidating results.[104] Cardiac therapeutic interventions frequently involve induction of vasodilatation and hyperaemia, thus require accurate estimation of pulse wave speed.[101,202] The novel capability of this software is that it enables the wave speed value calculated at baseline to be applied to derivation of cWIA during hyperaemia, which is acceptable given that wave speed is not influenced by vasodilatation.

Adaptive Savitzky-Golay Filter:

Differencing data results in noise in the signal, as cWIA is the product of two differences, this greatly increases signal noise; therefore the use of a Savitzky-Golay (S-G) filter is crucial to cWIA.[203] The acquired pressure and velocity signals are ensemble-averaged over a few cardiac cycles and then smoothed using the Savitzky-Golay (S-G) filter to remove the acquisition noise and estimate the pressure and velocity time derivatives prior to WIA.[97,204] S-G is a digital filter that can smooth datasets by increasing the signal-to-noise ratio without distorting the signal. The S-G filter calculates the least squares fit to a polynomial of order **N** to the data of frame-size **F** centered on a particular sample time **t**.[203] Operator selection of such filters (a feature of all currently available cWIA analysis programmes) introduces marked inter- and intra-observer variability. Recently, Rivolo et al. showed, using *in-vivo* human and animal

data that the pressure and velocity time derivatives are strongly sensitive to the S-G parameters chosen, which in turn markedly effects the areas and peaks of the main waves generated. The main reason for the variability observed in wave generation is the incapability of the S-G filter to deal with the different timescale features present in the velocity waveform, spanning from the relatively flat systolic plateau to the sharp early-diastolic rise. An adaptive S-G filter algorithm automatically selects the optimal S-G filter parameters, smoothing the acquired pressure and velocity waveforms; the percentage error in the cWIA derived metrics post ensemble-averaging using the adaptive filter was found to be ≤ 10% for all levels of noise tested within physiological range. On validation in human and animal datasets, this technique improved robustness by a 60% reduction in variability in outcome in wave peak and area.[196,197] Thus the adaptive S-G algorithm was integrated into the SimpleWires software as it removes operator bias, providing an accurate and standardised method to perform coronary WIA.

LV PV INCORPORATED FEATURES

In addition to instantaneous LV pressure and volume measurements, novel analytical tools were incorporated in the software to calculate additional parameters that do not currently feature on the CE marked software system that is commercially available.

Single beat estimations of ESPVR and EDPVR curves:

It is not easy to change loading conditions without provoking reflex changes in contractility of the heart in human subjects, therefore estimating contractility from a single beat is of prime importance.[26] The novel software system incorporates single beat assessment of the end-diastolic pressure volume relationship (EDPVR) and end-systolic pressure volume relationship (ESPVR) curves (load independent measures of contractile function and passive diastolic properties), without the need for inferior vena cava

occlusion. Single beat estimation of the ESPVR slope (Ees) has been shown to be very accurate when compared to actual measured Ees in human and animal studies.[205-207] The model applied in this software is that described by Shishido et al.[206] The advantages of this model over others is that the time-varying elastance is approximated linearly using two functions, one for isovolumic contraction and one for the ejection phase; quantitatively correlating with contractility and loading conditions (r=0.9); generating an accurate estimation of Ees.[206,207]

The end-diastolic pressure-volume relationship (EDPVR) can also be estimated from a single end-diastolic Pressure and Volume point. This method is based on the premise that overall EDPVRs share a common underlying shape; when a wide range of EDPVR slopes were normalised with scaling of LV volumes, all EDPVR slopes were identical and described by a common non-linear analytical expression with coefficient values that were reasonably well linked with the size of the heart such that:

Equation 19

$$\boldsymbol{EDP = An \cdot EDVBn}$$

Where A_n = 282 mmHg and B_n = 2.79.[208,209] This model was found to be applicable to normal and diseased hearts in humans; furthermore, the predicted error measured over a range 0-40mmHg EDP was <3mmHg.[208]

Single beat estimation was performed from an ensemble average cardiac cycle (5 beats).

Myocardial energetics: The time varying elastance was calculated as the instantaneous pressure-volume relationship through one cardiac cycle. The measurement of pressure

volume area (PVA) or total mechanical energy facilitates an understanding of the left ventricle in terms of myocardial energetics and efficiency. Pressure-Volume Area (PVA), the measure of total mechanical energy generated by ventricular contraction, was calculated as the sum of SW and elastic potential energy according to the following equation:[193]

Equation 20

$$\boldsymbol{PVA = SW + (0.5 \times \frac{ESP^2}{ESPVR})}$$

The incorporation of arterial elastance (Ea) to this analysis software enables the observer to appreciate the ventricular-arterial interaction. This is calculated as the ratio of ESP to stroke volume.

3.3 RESULTS

3.3.1 SIMULTANEOUS LV AND CORONARY MEASUREMENT IN-VIVO

Subjects:

Fifteen volunteers were selected to undergo baseline, simultaneous resting measurements. The measurements were performed in the cardiac catheter laboratory. Patients were included in the study if there were on the waiting list for outpatient coronary angiography. Subjects were excluded if they had LV impairment; significant comorbidities; arrhythmia; valvular heart disease; unstable angina or recent myocardial infarction. Patients provided written and informed consent for the study, which had local ethical approval.

Protocol:

8Fr femoral access site was used to introduce an 8Fr 80cm guide catheter to the aortic root, followed by intra-arterial heparin (70IU/kg). The hardware was set-up as described above and calibrated. The ComboWire was placed in the coronary artery and the pressure-volume loop catheter was placed in the left ventricle; recordings were performed for one minute at rest and on administration of intravenous adenosine (140mcg/kg/min) on commencement of infusion, for at least 90 seconds.

3.3.2 SOFTWARE VALIDATION

To assess the accuracy and reproducibility of the quantitative data generated by SimpleWire software analysis system it was compared against the commercially available CE marked software system ConductNT that was used as the gold standard.

Datasets:

Data were acquired as per the above in-vivo protocol, on ConductNT software using the INCA. All fifteen datasets were analysed on both ConductNT and SimpleWires software analysis system (as described above). Datasets were considered acceptable if they: 1) had a steady baseline recording 2) more than 5 consecutive cardiac cycles were recorded at baseline with no ventricular ectopic beats identified. The exact same cardiac cycles were used for analysis of LV haemodynamic indices on both software programmes. PV loop variables were generated from the ensemble average of the five consecutive cardiac cycles.

Statistical Analysis:

Statistical analysis was performed using GraphPad Prism v7.0 (GraphPad Software Inc., CA). Quantitative data are expressed as mean±SD; data were assessed for normality of (Gaussian) distribution both graphically and by use of the Shapiro Wilk's test. Paired t-tests were used to establish the level of significance of differences between the two analytical software. The Bland Altman test was used as a measure of statistical agreement between the matched data generated by the software analysis programmes; the difference of the paired measurements was compared against the mean of the measurements; $P < 0.05$ was considered statistically significant.

Results:

Table 3 summarises all the haemodynamic output variables from fifteen patients generated, the bias and 95% level of agreement. There was clinically acceptable agreement between the two software programmes; no statistically significant difference was demonstrated. Figure 50 demonstrates the Bland-Altman plots generated, there

were no relationships identified between the differences and magnitudes of the measurement, nor was there evidence of proportional or systematic error.

Indices	**SimpleWires**	**ConductNT**	**P Value**	**Bias**	**95% Limit of Agreement**
HR, bpm	67.5±14.3	67.3±14.1	0.7	0.2	-0.6 to 0.9
EDP, mmHg	14.9±5.7	15.7±6.1	0.4	-0.8	-8.2 to 6.6
ESP, mmHg	131.3±24.4	133.7±24.3	0.3	-2.4	-17.6 to 12
EDV, mL	105.8±20.5	106.4±20.0	0.9	-0.6	-23.6 to 22.4
ESV, mL	48.0±17.5	47.8±16.8	0.4	0.2	-3.4 to3.8
dP/dtmax, mmHg/s	1307±272	1351±278	0.7	-44	-71 to -17
dP/dtmin mmHg/s	-1391±277	-1426±286	0.8	34.9	13.6 to 56.1
EDPVR, mmHg/mL	0.155±0.08	0.143±0.081	0.5	0.01	-0.03 to 0.05
ESPVR, mmHg/mL	3.2±1.3	3.2±1.3	0.6	-0.08	-0.025 to 0.8
SV, mL	60.1±13.5	58.8±15.6	0.5	1.2	-21.3 to 23.7
EF, %	61±12.5	64±9.4	0.4	-3.7	-24.0 to 16.5
SW, mmHg.mL	7212±1931	7193±2191	0.5	18.8	-955 to 952
SCI, mmHg/sec/mL	13.0±4.5	13.5±4.6	0.8	-0.5	-3.0 to 2.0
PRSW, mmHg	69.2±21.2	69.2±20.4	0.5	-0.02	-7.0 to 7.0

Table 3 Haemodynamic variables derived from the two software systems.
Abbreviations: EDP End-Diastolic Pressure, ESP End-Systolic Pressure, EDV End-Diastolic Volume, ESV End-Systolic Volume, EDPVR End-Diastolic Pressure-Volume Relationship, ESPVR End-Systolic Pressure Volume Relationship, SV Stroke Volume, EF Ejection Fraction, SW (External) Stroke Work, SCI Starling Contractile Index, PRSW Preload-Recruitable Stroke Work.

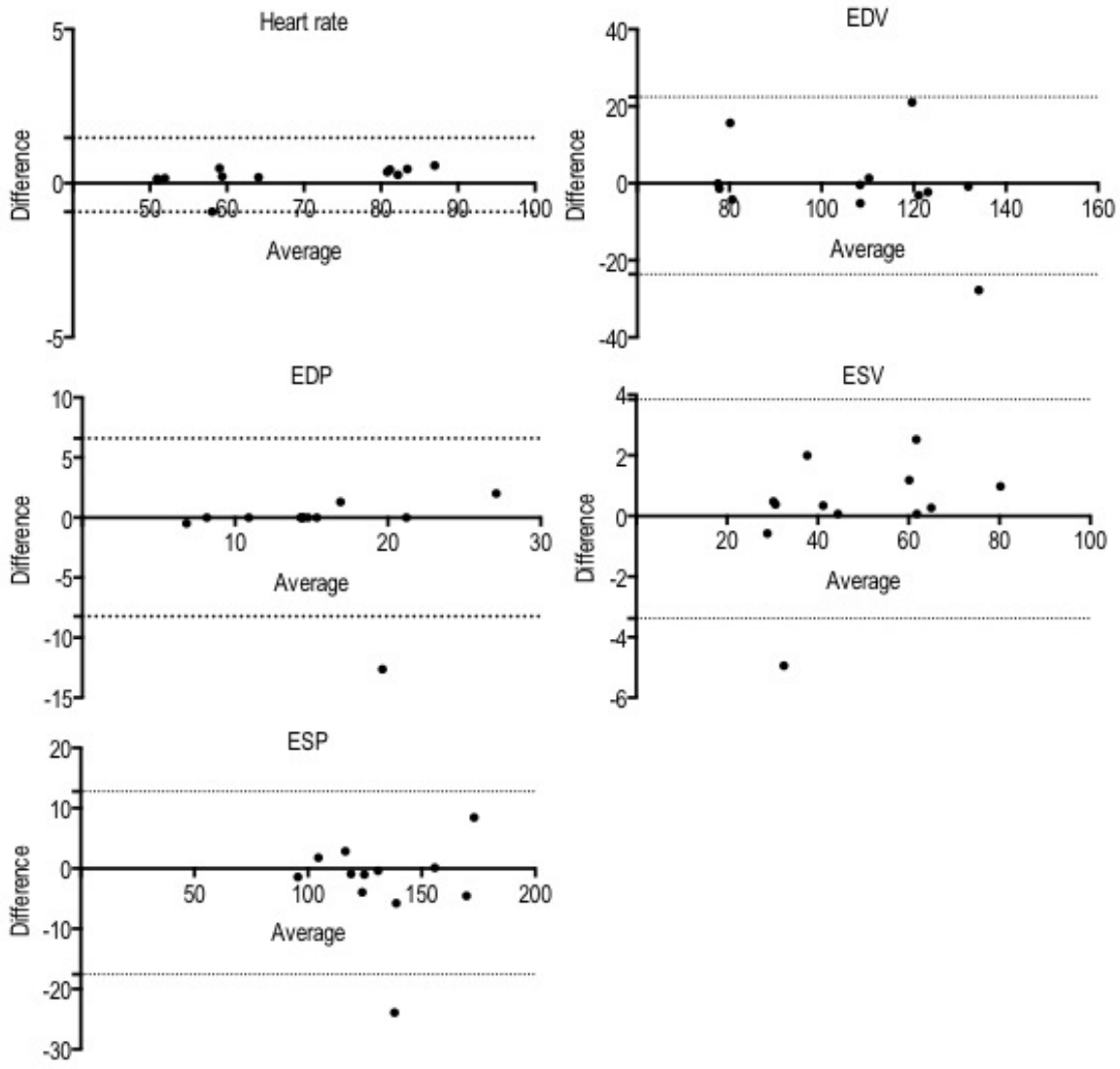


Figure 50 Bland-Altman plots.
Difference from the mean of major haemodynamic variables.

3.3.3 MECHANICAL DETERMINANTS OF CORONARY HAEMODYNAMICS

This was an exploratory study examining the impact of myocardial properties on coronary haemodynamics. As wave intensity analysis has the ability to discriminate between forward and backward travelling waves in the coronary circulation, thus those arising proximally or distally respectively, the aim was firstly to determine the timings of coronary wave energies and ascertain their origin by investigating the temporal relationship between coronary wave energies and LV mechanical change through one cardiac cycle; furthermore as waves arising distally are believed to originate from change in myocardial properties, the second aim was to delineate the myocardial contribution to changes in coronary blood flow morphology. Following work by Krams et al, myocardial properties have been suggested as a mechanism behind the phasic nature of coronary blood flow and coronary systolic flow impediment. The theory behind this is that left ventricle can be seen as a continuum with LV elastance being transferred to the microvasculature.[188] Thus increasing elastance would decrease systolic flow. Time varying elastance, Equation 4, first described by Suga et al, is discussed in detail in section 1.2.3.1 and used to describe the contractile properties of the ventricle by relating instantaneous LV pressure to volume through one cardiac cycle. [8] Although coronary blood flow has been examined as a function of E(t) in open chested dogs, this has never before been examined in humans. [190] Simultaneous coronary and instantaneous LV pressure and volume measurements allow this mechanism to be revisited and examined in more detail.

Datasets:

Data were acquired as per the above in-vivo protocol, datasets were considered acceptable if they were 1) simultaneous 2) high quality LV and coronary

haemodynamic tracings 3) absence of ectopic beats and 4) steady state recordings. Coronary wave energies and PV loop variables were generated from an ensemble average of 5 consecutive cardiac cycles.

Statistical analysis:

Due to heart rate variability between subjects, timings were non-dimensionalised. Statistical analysis was performed using GraphPad Prism v7.0 (GraphPad Software Inc., CA). Quantitative data are expressed as mean±SD; statistical comparison of quantitative data were performed using Student's t-test. Simple linear regression analysis was used to evaluate the association between coronary wave energy timings with LV cardiac cycle events times; the results from different measurements were correlated using Pearson's correlation coefficient.

Results:

A representative example of a 1-minute recording of simultaneous LV and intracoronary haemodynamic data at baseline is displayed in Figure 51. A typical example of the visual display of systemic and intra-coronary haemodynamic waveforms, mechanical events during one cardiac cycle defined as: end-diastole, dP/dtmax, end-systole, dP/dtmin and the accompanying coronary wave intensity analysis including net wave intensity, generated from the ensemble averaging of 5 consecutive cardiac cycles, is shown in Figure 52. The timing of the cardiac cycle events and the initiation, peak and end of the four main coronary wave energies are shown in Table 4, and depicted graphically in Figure 53; end-diastole was defined as Time 0.

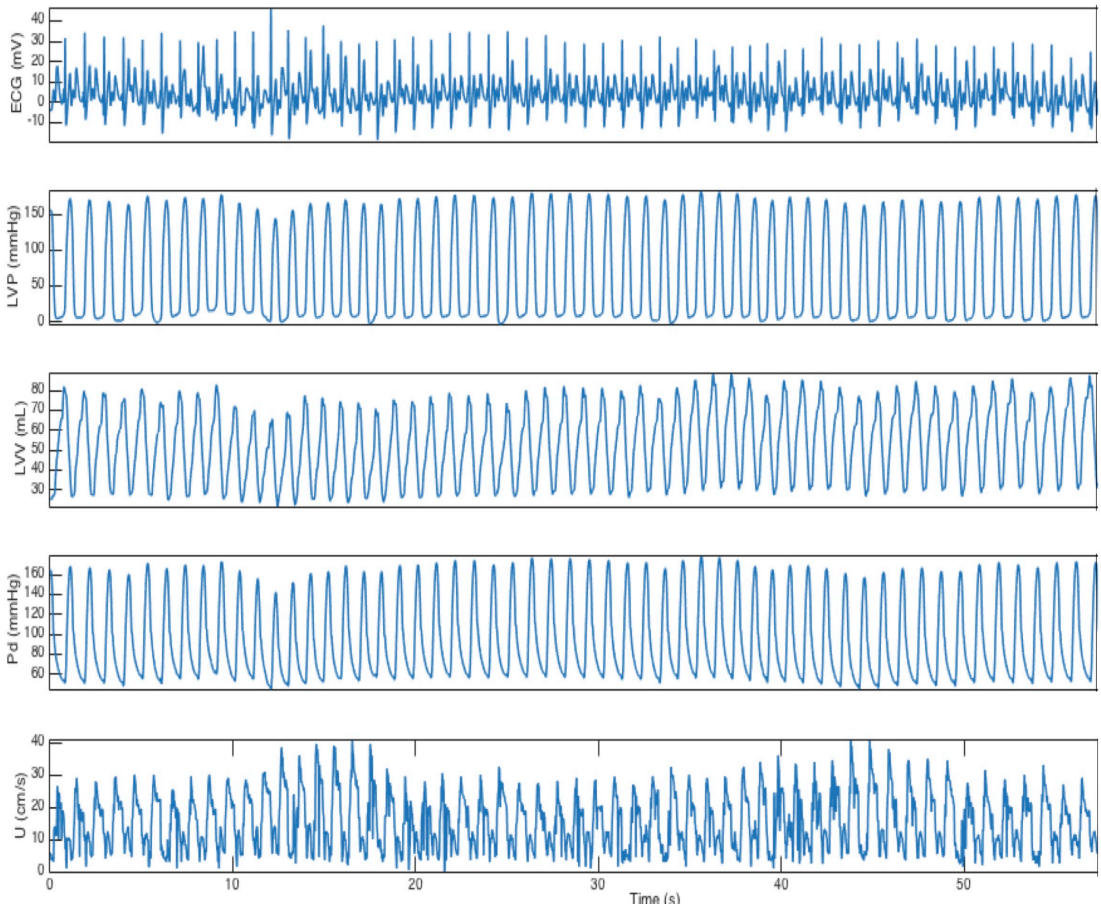


Figure 51. Simultaneous acquisition of coronary and left ventricular haemodynamics. This is a representative dataset; tracings show continuous ECG recordings, left ventricular pressure (LVP), left ventricular volume (LVV), distal coronary pressure (Pd), and mean coronary flow velocity (U) measured by the conductance catheter and ComboWire.

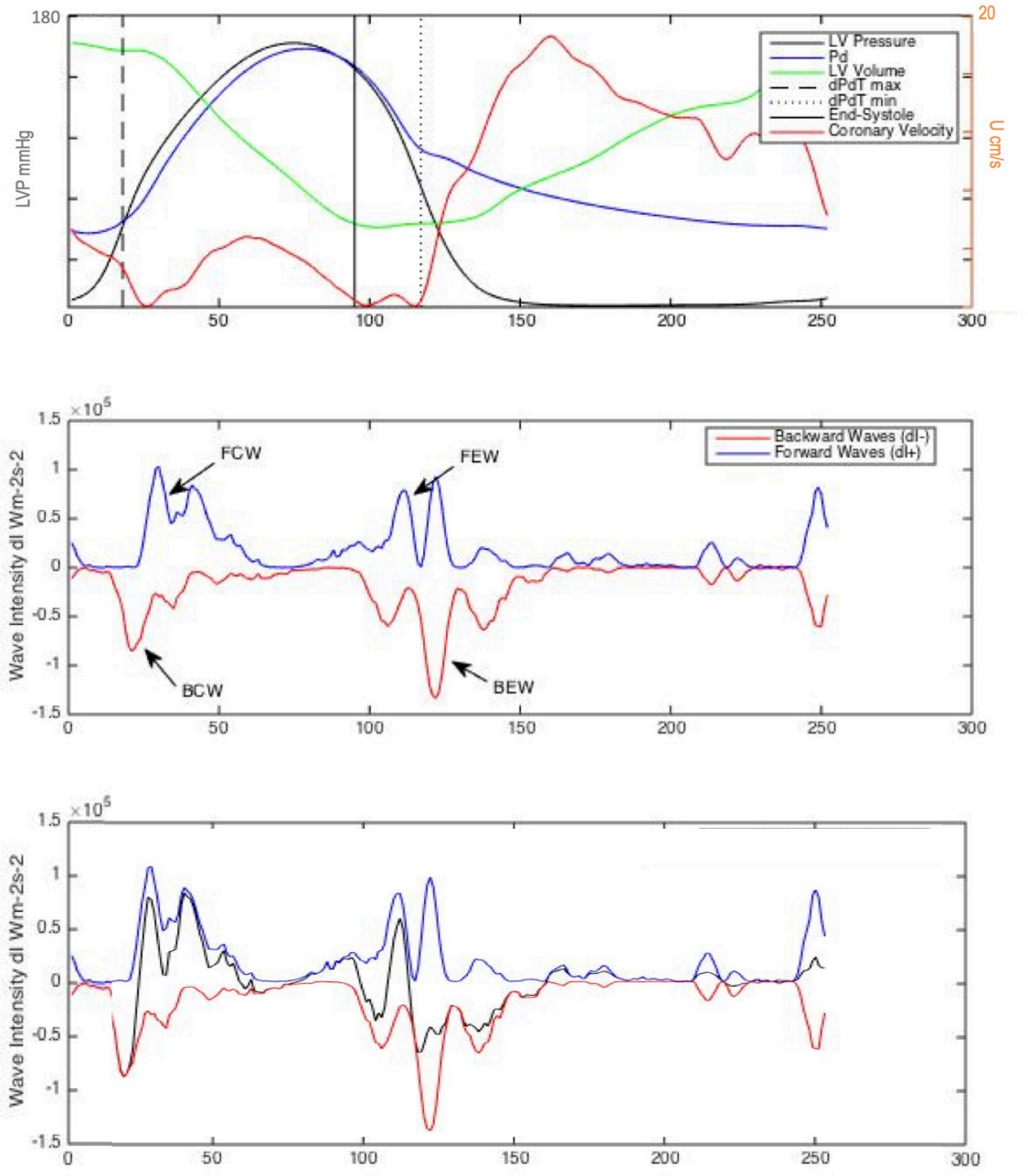


Figure 52. A representative example of ensemble averaged tracings.
In the top panel, left ventricular (LV) pressure and volume in addition to distal coronary pressure and flow velocity are described over one cardiac cycle; time 0 is end-diastole, the first broken line denotes dP/dtmax, the solid line denotes end-systole and the second broken line is dP/dtmin. The middle panel shows the main backward and forward wave energies generate from the above coronary tracings. The bottom panel depicts net wave intensity (black).

Cardiac Cycle Event	**Time (ms)**
End-Diastole	6±8
dP/dt max	76±26
Start BCW	36±25
Peak BCW	105±43
End BCW	202±53
Start FCW	69±29
Peak FCW	117±34
End FCW	158±41
End-Systole	382±54
dP/dt min	448±60
Start BEW	376±61
Peak BEW	464±113
End BEW	581±71
Start FEW	337±60
Peak FEW	409±63
End FEW	442±62

Table 4 Timings of waves and cardiac cycle events.
Abbreviations: BCW backward compression wave, FCW, forward compression wave, BEW backward expansion wave, FEW forward expansion wave, ms milliseconds.

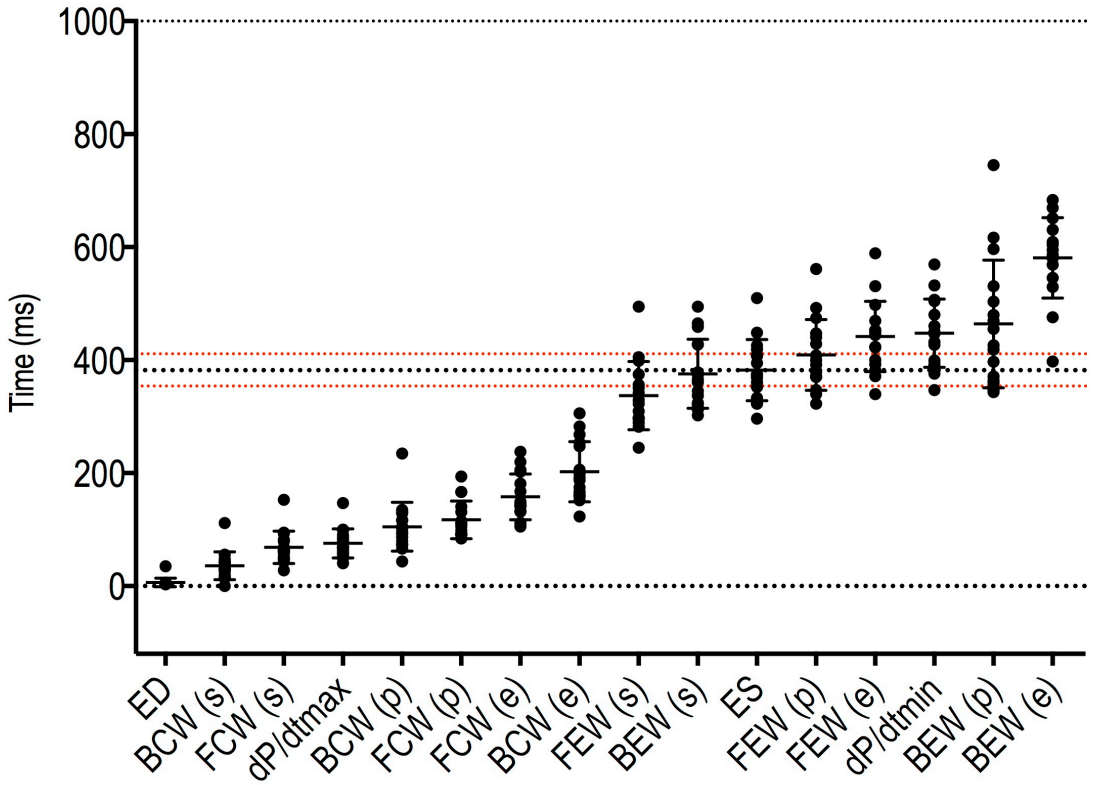


Figure 53 Wave generation during the cardiac cycle.
The black broken line represents end-systole, with standard deviation (red broken line) Abbreviations: Abbreviations: ED end-diastole, BCW backward compression wave, FCW, forward compression wave, BEW backward expansion wave, ES end-systole, FEW forward expansion wave, ms milliseconds, (s) start, (p) peak, (e) end.

3.3.4 CORONARY WAVE ENERGIES AND EVENTS IN THE CARDIAC CYCLE

Compression waves were seen to occur in what is traditionally known as systole and the expansion waves seen to occur in diastole. The backward travelling compression or pushing wave (BCW) drives an increase in coronary pressure but a decrease in coronary flow velocity, arising distally. This is the first wave seen and is initiated soon after end-diastole (while the aortic valve is still closed) during the start of cardiac contraction; the BCW overlaps with dP/dtmax and reaches its peak immediately after dP/dtmax, the BCW ends soon after the aortic valve opens and LV ejection commences. The maximum rate of pressure increase in the ventricle (dP/dtmax) coincides with aortic valve opening, at the onset of aortic pressure rise the forward travelling compression wave (FCW) commences. The FCW is a forward travelling wave that increases pressure and velocity, arising proximally in the coronary artery; this peaks at mid-systole, ending at end-systole. The forward expansion wave, or suction wave, reduces pressure and reduces velocity in the coronary artery arising proximally. The onset of the FEW occurs just before end-systole, after peak LV and aortic pressure; although the myocardium is still contracting, the FEW coincides with the drop in aortic pressure; the FEW peaks then troughs following aortic valve closure. Interestingly the forward travelling waves, believed to originate from the aorta only start once LV pressure has exceeded diastolic pressure (FCW) and end once LVP falls below diastolic aortic pressure (FEW), even though the aortic valve has closed, this is clearly seen in Figure 54 where the wave durations are described relative to the PV loop, the forward waves start and stop at exactly the same LV pressure. The backward travelling expansion wave (BEW), arising distally, reduces pressure but increases coronary velocity; the initiation of the BEW coincides with end-systole, the point of maximal LV activation, following which, cross-

bridge uncoupling occurs and LV relaxation commences. The BEW continues beyond the FEW reaching a peak at the maximum rate of pressure decay in the LV (dP/dtmin). The BEW tends to follow LV pressure drop, and terminates when LV pressure is at equipoise, this occurs after mitral valve opening, because although the ventricle is filling, the LV pressure continues to drop. Interestingly, the backward waves appear to be delimited by aortic valve opening and closure. Interestingly, we note for the first time that forward travelling waves are delimited by diastolic blood pressure and the backward travelling waves are delimited by the aortic valve; overall, the wave energies closely follow the mechanical events described in the cardiac cycle. This is depicted graphically in Figure 53 through one cardiac cycle and in Figure 54 as a pressure volume loop.

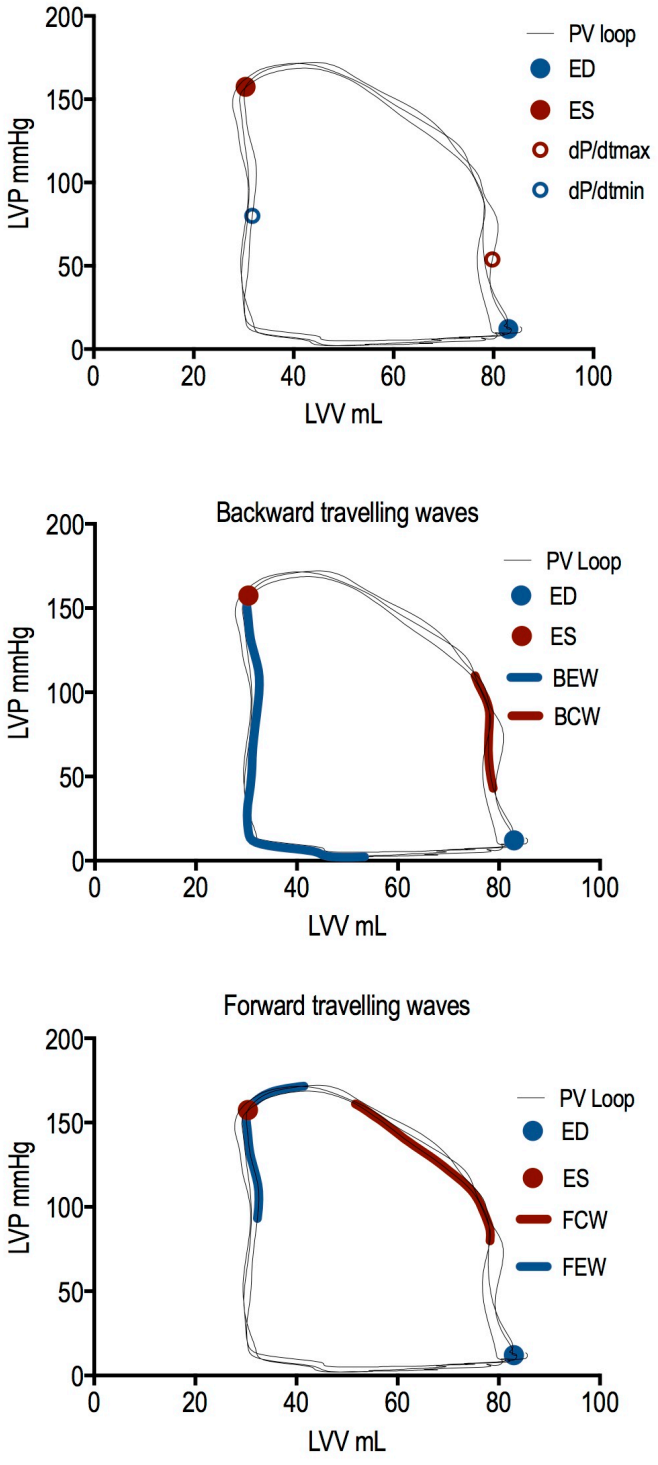


Figure 54 Cardiac cycle events and wave energies described on the PV loop.
Abbreviations: LVP left ventricular pressure, LVV left ventricular volume, ED end-diastole, ES end-systole, BCW backward compression wave, FCW, forward compression wave, BEW backward expansion wave, FEW forward expansion wave.

3.3.5 CORRELATIONS BETWEEN TIMINGS OF WAVE GENERATION AND MECHANICAL EVENTS

Data from the fifteen patients were analysed. Cardiac cycles were normalised to adjust for heart rate variability between patients such that the duration of each cycle became one second (cardiac cycle duration multiplied by 60, divided by the heart rate). The timing of the initiation of the FCW correlated with dP/dtmax time (69±29 versus 76±26 milliseconds; $r = 0.8$, $P < 0.001$). The timing of the initiation of the BEW correlated with end-systolic time (382±54 versus 376±61 milliseconds; $r = 0.9$; $P < 0.001$). The time of peak BEW correlated with dP/dtmin (464±113 versus 448±60 milliseconds; $r = 0.8$, $P < 0.001$), Figure 55.

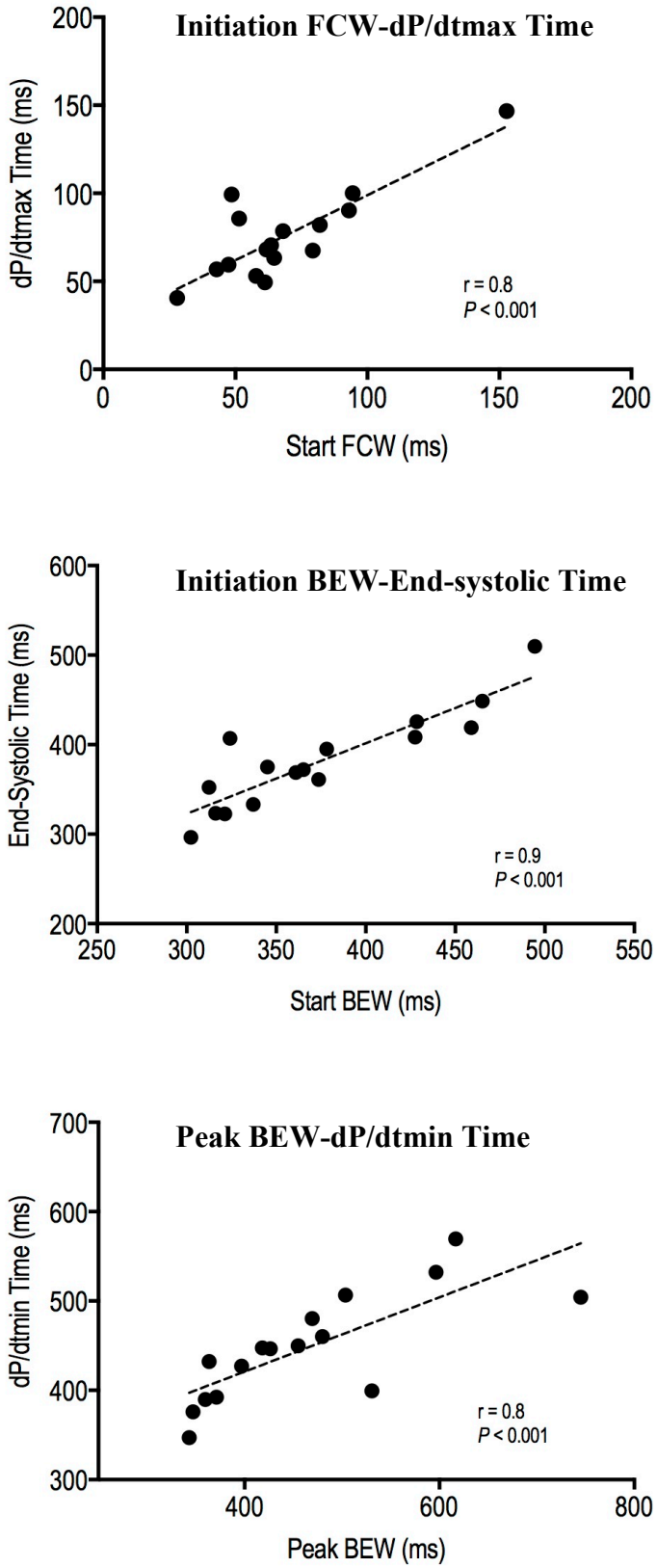


Figure 55. Correlations between cardiac cycle events and wave energy.
Abbreviations: FCW, forward compression wave, BEW backward expansion wave.

3.3.6 MECHANICAL DETERMINANTS OF CORONARY BLOOD FLOW

In Figure 56, a representative example of the time-varying elastance curve is demonstrated; and the relationship between coronary pressure and coronary blood flow velocity and instantaneous elastance both at rest and during steady-state hyperaemia. As expected time varying elastance rises and falls and reaches a peak E(max); graphical evaluation of mean coronary blood flow velocity plotted against LV elastance demonstrate maximum systolic flow impediment at two points during systole, the first is just prior to aortic valve opening, and the second is at peak LV elastance; when elastance is at its maximum and minimum, coronary blood flow velocity appears uniquely related to elastance. Graphical evaluation of mean coronary pressure plotted against elastance demonstrates an inverse relationship to that of coronary blood flow velocity. On abolition of microvascular resistance, on administration of adenosine, further graphical evaluation was performed during hyperaemia. The time varying elastance curve peaks at the same point, but the E(max) is greater; mean coronary blood flow velocity plotted against LV elastance demonstrates that the course of coronary blood flow in systole is almost identical to that in diastole in the absence of autoregulatory processes, suggesting in the absence of autoregulation, the myocardium acts as a continuum, with the coronary microvasculature vulnerable to transmission of myocardial contractile properties; as expected, peak coronary blood flow velocity increases. Mean coronary pressure plotted against elastance, demonstrates a similar relationship to that at rest; however, as expected peak and trough pressures are lower than at baseline.

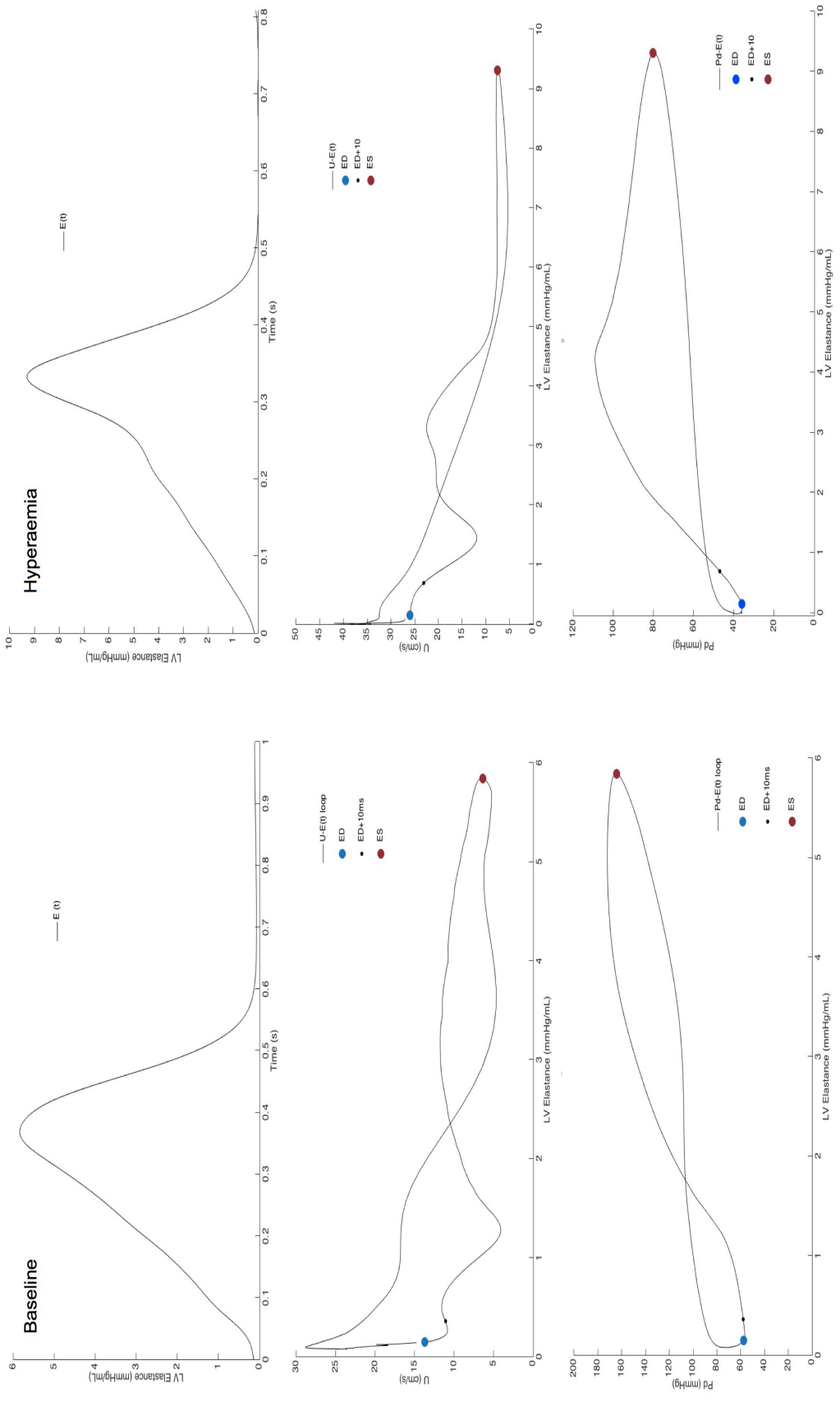


Figure 56 Coronary haemodynamics as a function of LV elastance, during baseline and hyperaemia. Top panel: LV elastance as a function of time or E(t); middle panel: coronary blood flow velocity (U) as a function of E(t); bottom panel: distal coronary pressure (Pd) as a function of E(t).

3.4 DISCUSSION

This study utilises novel analytical software to assess simultaneous coronary and haemodynamic waveforms in human subjects. This is the first time that simultaneous LV pressure-volume data and coronary haemodynamic signals have been acquired in-vivo, in human subjects, and analysed to this degree of accuracy. This study demonstrates that it is possible to measure simultaneous LV and coronary haemodynamics at high resolution in the cardiac catheter laboratory setting. The main findings of this study can be summarised as follows: 1) Forward travelling coronary wave energies arise only when LV pressure exceeds aortic diastolic pressure; 2) backward travelling coronary wave energies are generated in the presence of aortic valve closure; 3) the maximum rate of change in intra-cavity pressure only occurs during the isovolumic phases of the cardiac cycle 4) the timing of wave energies closely follow cardiac cycle events; 5) LV elastance is related to coronary blood flow velocity when LV elastance is at its maximum and minimum 6) in the absence of autoregulation, coronary blood flow velocity is directly, inversely related to LV elastance.

One of the major aims of this study was to describe the temporal relationship between coronary wave energy timings (derived from wave intensity analysis) and the mechanical events that occur throughout one cardiac cycle from end-diastole to end-systole. Previous studies have attempted to describe cWIA in term of LV mechanical changes; the measurement of instantaneous LV pressure and volume however are fundamental parameters when describing myocardial properties, the absence of which, limits conclusions that may be drawn from the cardiac-coronary interaction. The unique ability of this work to simultaneous measure myocardial properties and coronary

haemodynamics has enabled demonstration of the relationship between the two, building on prior work performed in this area.

The relationship between coronary wave energies and the cardiac cycle

Performing simultaneous measurements not only allows temporal alignment of coronary with LV haemodynamics, but also enables visualisation of coronary wave energies as part of the pressure-volume loop, from which a number of physiological derivations can be made. Conceptually forward travelling waves are believed to arise from the aorta, proximal to the coronary artery. This study demonstrates that the origin of these waves is likely to be far more complex; they are a result of the interaction between the left ventricle and the aorta, our study shows that a minimum ventricular pressure is required to generate the forward travelling compression wave; this is a flow-accelerating wave, generated on aortic valve opening, the start of which coincides with and has shown to correlate with dP/dtmax, it continues until aortic and LV pressure reach a peak in systole, this coincides with the ejection phase and aortic valve opening. We've shown this to initiate when LV pressure is equal to and exceeds diastolic aortic pressure. Following ejection, LV and aortic pressure decline, there follows a period of isovolumic relaxation accompanied by a forward travelling expansion (suction wave), this wave decelerates flow, arising immediately after peak LV and aortic pressure, continues beyond aortic valve closure until the minimum cut-off of diastolic pressure is reached, which is just prior to dP/dtmin. Diastolic aortic pressure represents the limit at which the LV can induce changes in aortic blood flow and therefore drive transmission of forward travelling wave energies.

The backward travelling waves have been shown in this study to be delimited by aortic valve closure; suggesting the generation of these waves are also as a result of LV-aortic interaction, not purely distal microcirculatory events. The backward travelling waves follow the pattern of LV pressure rise and fall, and are absent in the presence of zero LV pressure. The backward compression wave (BCW) arises soon after LV depolarisation, the generation of which overlaps with dP/dtmax, however, this wave terminates on aortic valve opening. The initiation of the backward expansion wave (BEW) coincides with end-systole, unlike the forward expansion wave, which occurs once LV and aortic pressure has peaked, the BEW occurs at the point of maximal LV activation, following which, cross-bridge uncoupling and LV relaxation occurs, suggesting that backward expansion wave is more related to transmission of myocardial properties than intra-cavity LV or aortic pressure alone. The BEW peak coincides with dP/dtmin, then continues through diastole, beyond mitral valve opening, although the ventricle is filling, the myocardium is continuing to relax and the LV pressure continues to drop; the BEW continues until the LV is in equipoise, and LVP is at a minimum.

This study is in agreement with investigations previously performed in humans by Davies et al, they examined the origin of coronary wave energies and their relationship to LV mechanical events, furthermore, the findings in relationship to temporal alignment of events is consistent with animal work in this area.[96,107] The addition of simultaneous LV PV loop measurements places this study in a unique position, PV loop measurements enable accurate determination of cardiac cycle events: end-systole, end-diastole, dP/dtmax and dP/dtmin, enabling validation of hypotheses and an increased understanding of the origin of coronary wave energies, building on work performed by

Rolandi et al.[100] The current knowledge is based on the premise that backward waves originate from the distal microcirculation and forward waves originate from the aorta;[96,100,101] this study demonstrates for the first time, that although coronary wave energies have proximal and distal origins, their generation is dependent on the ventricular-arterial interaction, suggesting the mechanisms behind wave generation may be far more complex than initially understood.

LV elastance describes myocardial properties through one cardiac cycle, coronary pressure increases as LV elastance increases; conversely, coronary blood flow velocity decreases as LV elastance decreases. We demonstrate that at rest coronary blood flow velocity is not solely dependent on LV elastance, consistent with previous animal work performed in open chested dogs;[190] however peak LV elastance coincides with maximal systolic flow impediment, this is the basis behind work performed by Sun et al., they related systolic flow impediment to the contractile properties of the ventricle.[107] The unique relationship between the two is maintained during hyperaemic states; the benefit of this technology means that we have demonstrated for the first time, that in the absence of autoregulation, coronary blood flow is closely dependent on LV elastance; the pattern of systolic flow and diastolic flow through one cardiac cycle become similar suggesting that on abolition of microvascular resistance, the myocardium acts as a continuum thus transmitting forces to the microvasculature; this is consistent with previous work performed by Krams et al.[188]

3.5 LIMITATIONS

The data were analysed offline and acquired using PV loop analytical software, the major limitations of this method of acquiring coronary data is the absence of direct recording, with electronic routing of coronary haemodynamics into the INCA; this imposed a post-processing delay on the data, however, this was calculated and adjusted for. The next step in this software development involve developing SimpleWires into an online tool, capable of real-time acquisition; the aims are to integrate the software into the INCA, although currently limited by the hardware, which requires further development. LV elastance was calculated on the premise that V0 was zero, in the absence of changes in LV contractility and relaxation however, this was inconsequential. This was an exploratory physiological to enhance our understanding of the myocardial-coronary interaction.

3.6 CONCLUSIONS

Novel analytical software was developed to enhance understanding of the interaction between coronary haemodynamics and mechanical changes during the cardiac cycle. The technology used enabled temporal alignment of coronary wave energies with cardiac cycle events and facilitated an understanding of the impact of instantaneous elastance on coronary blood flow velocity.

4 THE EFFECTS OF DYNAMIC EXERCISE ON MYOCARDIAL SYSTOLIC AND DIASTOLIC FUNCTION: EXERCISE-INDUCED ISCHAEMIA VERSUS CONTROL GROUP COMPARATOR

INTRODUCTION

Stable angina, often referred to as angina of effort, has been recognised for over two centuries. Induction of ischaemia leads to a cascade of left ventricular haemodynamic effects; these however depend on the technique used to provoke it. The effect of exercise-induced ischaemia on left ventricular haemodynamics has not been extensively studied. As most episodes of ischaemia in patients with coronary artery disease are provoked by exercise, the aim of this work was to identify the precise haemodynamic changes incurred by exercise-induced ischaemia by studying the interaction between the myocardium, coronary arteries and systemic vasculature and comparing these to patients without ischaemia.

METHODS

Sixteen patients (6 control, 10 ischaemia) underwent invasive cardiac catheterisation with left ventricular pressure volume loop and invasive coronary assessment using dual-sensor pressure-flow wire. Patients exercised using a supine cycle ergometer.

RESULTS

At low impact, exercise demonstrated a beneficial effect in both groups, but adversely affected haemodynamic variables in patients with coronary artery disease at the onset of ischaemia: end-diastolic (90±28 versus 109±31 mL; $P<0.05$) and end-systolic volumes (39±14 versus 71±31 mL; $P<0.001$) significantly increased, with overall decrease in ejection fraction (57±19 versus 36±15%; $P<0.001$) and cardiac output compared to control group (7±2.3 versus 4.5±1.9; $P<0.05$). Demand ischaemia led to a rightward shift in end-systolic and end-diastolic pressure volume relations. The ventricular-arterial interaction was adversely affected with an increase in systemic vascular resistance seen in patients with ischaemia compared to control (44±18 versus 24±17 mmHg.min/L; $P<0.05$).

CONCLUSIONS

This study delineates the changes that occur with demand ischaemia during dynamic exercise in humans. A biphasic response to exercise was seen in patients with significant coronary artery disease: low impact exercise exhibiting a beneficial effect on acute haemodynamics, whereas ischaemia was detrimental.

4.1 INTRODUCTION

Stable angina, often referred to as angina of effort, has been recognised for over two centuries. [134] The principal cause of which is luminal narrowing of the epicardial coronary arteries. During effort angina, adaptations in coronary microvascular resistance are exhausted in the presence of a coronary stenosis, limiting the necessary increase in coronary blood flow in the face of increased oxygen consumption.[121,210] Induction of ischaemia leads to a cascade of left ventricular haemodynamic effects; this complex cardiac-coronary interaction is poorly understood.[211] Diastolic pressures frequently increase dramatically during ischaemia and have attracted much attention.[145,149,155,212] Changes in left ventricular diastolic function have been shown to be of clinical importance; experimental studies have demonstrated that ischaemia induced diastolic abnormalities often precede the development of systolic abnormalities and resolve more slowly on resolution of the ischaemia.[213,214] Late and early diastolic changes suggest a number of factors are in operation, including changes in compliance reflective of the late diastolic phase, and early diastolic pressure change reflecting pressure decay from preceding systole. The left ventricular diastolic pressure-volume relationship changes when the heart is made ischaemic; the particular response of the left ventricular diastolic pressure volume relation has been thought to depend on how ischaemia is induced. When induced by rapid pacing in the presence of critical coronary stenosis (demand ischaemia), the diastolic pressure-volume relationship shifts upwards.[125,155,215] When ischaemia is induced by coronary occlusion, (supply ischaemia), the relationship shifts rightwards or downward.[125,153] However, recent studies in humans and earlier preclinical work have shown that an upward shift can also occur with coronary occlusion.[149,150] Furthermore, a rightward shift has also been

demonstrated with demand ischaemia, although the direction of the shift may be more dependent on left ventricular contractility than the mechanism of ischaemia.[155] However the haemodynamic accompaniments of ischaemia are variable, and depend on the technique used to provoke it; as most episodes of ischaemia in patients with coronary artery disease are provoked by exercise, they may be accompanied by different haemodynamic changes to those provoked by pacing. The effect of exercise-induced ischaemia on left ventricular haemodynamics has not been extensively studied. The limitation of previous work examining left ventricular pump properties and the coronary vasculature is the inability to convey the interaction between the components of the system. To identify the precise haemodynamic changes incurred by exercise-induced ischaemia, we applied left ventricular pressure-volume loop assessment with invasive measurement of distal coronary pressure and flow velocity in patients with ischaemic heart disease causing angina and in a group of patients without ischaemia; the aim was to explain the pathophysiological response of ischaemia by way of the interaction between the myocardium, coronary arteries and systemic vasculature.

4.2 METHODS

4.2.1 STUDY POPULATION

We included consecutive patients scheduled for routine coronary angiography ± proceed to angioplasty at St Thomas' Hospital, London, United Kingdom. Patients were selected for the study if they had symptoms of exertional angina; angiographic criteria for inclusion was one or more epicardial coronary artery with > 50% diameter stenosis. Exclusion criteria were unstable symptoms, previous myocardial infarction, coronary artery bypass graft surgery, impaired left ventricular function, severe co-morbidities, valvular heart disease, atrial fibrillation, or the inability to undertake exercise. Patients with a left main stem stenosis, severe multi-vessel coronary disease or chronic total occlusions were not included. Oral nitrate preparations, calcium channel blockers and beta-blockers were stopped at least 48 hours before the procedure. All patients underwent written, informed consent prior to partaking in the study. This study received approval from the National Research Ethics Committee (09/H0802/39).

4.2.2 CATHETER LABORATORY PROTOCOL AND INSTRUMENTATION

A specially adapted supine cycle ergometer (Ergosana, Germany) was attached to the catheter laboratory table. Cardiac catheterisation was performed via the right radial artery using a standard 5Fr arterial sheath. Weight adjusted heparin was administered (70IU/kg) intra-arterially. Right and left coronary angiograms were then taken using standard diagnostic catheters. Intracoronary nitrates were not used. The 5Fr arterial sheath was exchanged over a long wire for a 7.5Fr shortened sheathless guide (Asahi, Vascular Perspectives), which was introduced into the aortic root; see section 2.6.1.1 for

details on guide catheter alteration. A dual-sensor pressure velocity 0.014" coronary guide wire (Combowire, Volcano Corp, San Diego, CA) was then connected to the Combomap console (Volcano Corp) and was delivered through the sheathless guide; auxillary inputs were electronically routed to the Inca (CD Leycom) to enable for simultaneous acquisition. The Combowire pressure signal was normalised against the fluid filled catheter signal at the tip of the guide.[80,101] The guide catheter was then inserted into the coronary ostium and the Combowire advanced distal to the stenosis in the target coronary artery (Figure 57), full details regarding ComboWire calibration are in section 2.3.2. The guide catheter was then disengaged and left ventricular pressure and volume measurements were assessed with a 4Fr conductance catheter (CC) system (CD Leycom, The Netherlands). This flexible pigtail catheter has a solid-state pressure sensor and electrodes situated at regular intervals; continuous left ventricular volumes are calculated by measuring time-varying elastance; this technique has been previously validated and applied in the study of cardiac disease states.[184,185,193,194] The CC is connected to a signal processor (Inca, CD Leycom, The Netherlands) and delivered to the ventricular cavity across the aortic valve via the sheathless guide. Correct positioning was confirmed by fluoroscopy and conductance signals. Volume calibration was performed by left ventricular (LV) volume measurements obtained from transthoracic three-dimensional echocardiography.[193] Full details regarding calibration can be found in section 2.2.3.2. Optimisation of the coronary Doppler velocity traces and LV pressure-volume measurements was performed.

4.2.3 EXERCISE PROTOCOL

Baseline measurements were taken before the patients underwent one period of exercise. This protocol was a standardised incremental programme, starting at 30 W and

increasing incrementally by 20 W per minute at a cadence of 60 revolutions per minute. Exercise was continued until any of the following occurred: 1) ST segment depression >3mm; (2) maximal age-related heart rate; (3) severe chest pain; (4) physical exhaustion and (5) arrhythmia. Continuous surface ECG recordings, left ventricular haemodynamic tracings, and coronary pressure and flow velocity signals were recorded throughout the intervention. After the exercise protocol, the patients underwent physiological assessment of the coronary stenosis with intravenous adenosine and underwent angioplasty where necessary.[216]

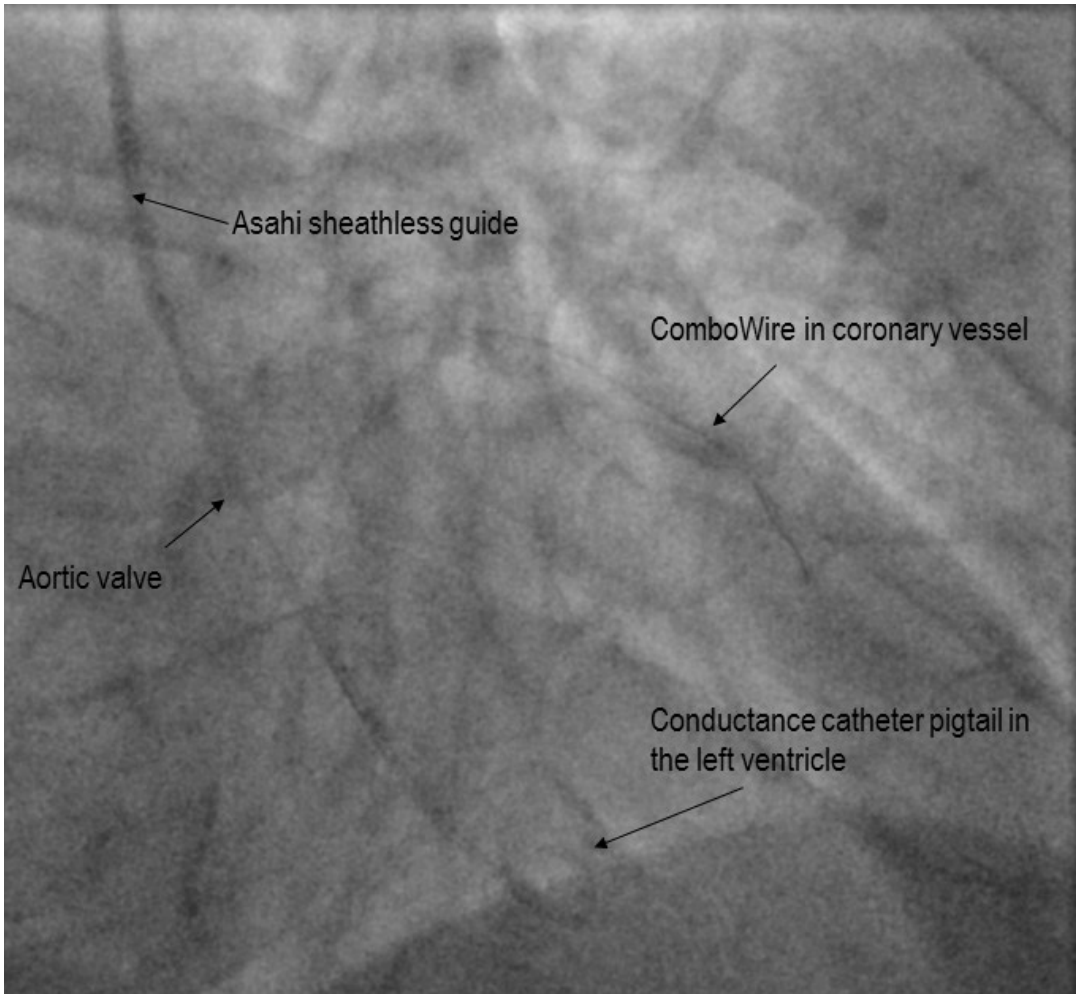


Figure 57 Conductance catheter and ComboWire position (fluoroscopy)

4.2.4 DATA ACQUISITION AND ANALYSIS

Coronary pressure and flow velocity signals were sampled at 200Hz and acquired online on the Combomap system (Volcano Corp); the coronary signals were electronically routed to the Inca (CD Leycom) to facilitate real-time simultaneous acquisition and visualisation of all haemodynamic variables.[198,199] CC measurements were acquired online using the dedicated data acquisition and analysis software (Conduct NT, version 3.18.1 CD Leycom); recording was continuous throughout the exercise protocol. Coronary and LV data were imported into the custom made SimpleWires programme (King's College London, United Kingdom) for offline analysis. Ten consecutive cardiac cycles were selected from baseline and each minute of exercise and into recovery. Peak exercise was determined by maximal power output; ischaemia was identified by ST segment depression. Ensemble averages of the cardiac cycles were used in further analysis and presented as baseline, 50% peak and peak.

Mean coronary blood flow velocity (U) and distal coronary pressure (Pd) were determined from the Doppler signal and high-fidelity pressure signal respectively, distal to the coronary stenosis. Wave intensity analysis (WIA) explains phasic flow in terms of a series of wave fronts that underlie the changes in coronary pressure and flow velocity in the coronary arteries.[97] WIA enables separation of the local net waveform in the coronary artery into forward (arising proximally) and backward (arising distally) travelling components; thus WIA is a powerful tool for investigating cardiac-coronary interactions and has been used previously to interpret clinical data.[96,101,202] Adjustment for the non-physiological time-delay between the digitally archived signals (coronary pressure and velocity, 55ms; coronary and left ventricular pressure; 88ms) was

performed, see section for 3.2.2 details.[101,198] Time derivatives were obtained after smoothing the raw signals using an adaptive Savitzky-Golay filter; the adaptive filter algorithm has been shown to improve WIA robustness, thus providing an accurate standardised approach to coronary WIA.[192,196] Net wave intensity was performed and normalised to the sampling rate and separation into forward and backward components was performed using the single–point technique.[97,201] Because coronary blood flow was being examined during exercise hyperaemia, baseline pulse wave velocity was implemented for WIA determination during exercise to account for limitations in the single-point technique during hyperaemia.[104]

CC measurement allows for acquisition of instantaneous LV volumes and pressure. Left ventricular conductance volumes (EDV, ESV) were calculated at the maximum rate of LV pressure rise (dP/dT_{max}) and pressure decay (dP/dT_{min}); stroke volume was calculated as the difference in these volumes. In addition to instantaneous LV volumes and pressure, the software calculates load-independent parameters of LV contractility.[217] The end-systolic PV relationship (ESPVR) represents the ratio of LV pressure to LV volume at the end of ventricular systole (uppermost left corner of the PV loop). The Starling contractile index (SCI) is calculated as the maximal rate of pressure change over time during isovolumetric contraction (dP/dT_{max}) normalised to end-diastolic volume (EDV). LV stroke work (SW) was calculated as the area of the PV loop; preload-recruitable stroke work (PRSW) was calculated by normalising the SW to EDV. LV stroke work was calculated as the product of peak LV peak systolic pressure and stroke volume.[193,218] Pressure volume are (PVA) a measure of total mechanical energy generated by ventricular contraction, was calculated as the sum of stroke work

and elastic potential energy see Equation 20. Systemic vascular resistance was calculated as the ratio between the pressure drop across the vascular bed and the cardiac output and decribed as Wood units (mmHg.min/L). End-diastolic pressure volume relations (EDPVR) were performed from single-beat estimations, previously validated in humans.[208] The slope of ESPVR was calculated using the single beat method (Ees), shown to accurately reflect acute inotropic change, with minimal influence from loading conditions.[205] Arterial elastance (Ea) was calculated as the ratio of end-systolic pressure (ESP) to stroke volume (SV) to assess the impact of arterial load on the ventricle. [37] The ventricular-arterial interaction was described as the ratio of Ea: Ees where Ea is a measure of net arterial load and Ees is a load-independent measure of LV contractility, ESPVR was used as a surrogate for Ees. Optimal efficiency is achieved when the ratio of Ea: Ees=1, in failing hearts this has been shown to be elevated.[37,40,128]

4.2.5 STATISTICAL ANALYSIS

Statistical analysis was performed using GraphPad Prism v7.0 (GraphPad Software Inc., CA). Quantitative data are expressed as mean ± SD; categorical variables are described as proportions and percentages. Data were assessed for normality of (Gaussian) distribution both graphically and by use of the Shapiro-Wilk normality test. Baseline characteristics were compared using unpaired t-test for normally distributed data and Mann-Whitney U for those without normal distribution; categorical data (two nominal variables) were compared by use of the Fisher exact test. Statistical comparison of serial haemodynamic measurements (quantitative data) of normal distribution were performed using a repeated measures two-way ANOVA with comparison to baseline and the previous step, adjustment for multiple comparisons were performed using the Bonferroni correction to generate adjusted P values. A P value < 0.05 was considered

statistically significant for all tests. Results from different measurements of normal distribution were correlated using the Pearson correlation coefficient.[219]

4.3 RESULTS

Between April 2014 and May 2016, thirty patients were screened and twenty-nine consented into the study. Figure 58 demonstrates the flow of patients in the study. Sixteen patients successfully completed the study protocol. Reasons for exclusion were as follows: no significant coronary disease (4), three-vessel coronary disease requiring coronary artery bypass graft surgery (2) inability to deliver the conductance catheter into the LV (4); technical inability to perform pressure-volume measurements (1); guide catheter-related complication prior to taking research measurements (1); access site crossover to right femoral approach (1). Full background demographics and procedural details in patients with and without exercise-induced ischaemia are shown in Table 5. There were no significant differences in baseline characteristics between the two groups. Invasive pressure-volume loop acquisition was performed in all patients; coronary physiology measurements were performed in thirteen patients and wave intensity analysis was performed in twelve patients; of the thirteen patients, simultaneous data were obtained in eight, and sequential coronary and LV physiological measurements were obtained in five, Figure 58.

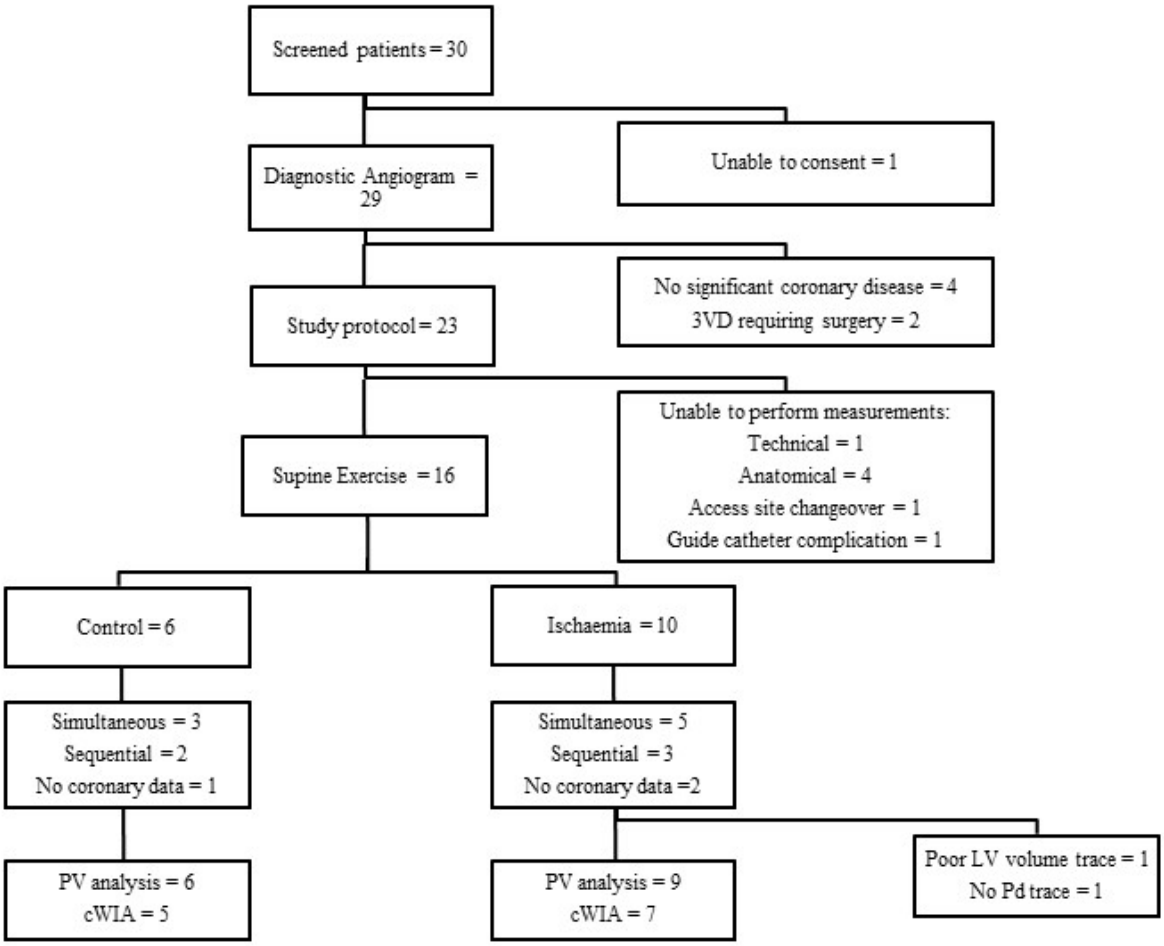


Figure 58 Patient flow diagram.
Abbreviations: 3VD three-vessel disease, LV left ventricle, Pd distal coronary pressure, PV pressure-volume loop, cWIA coronary wave intensity analysis.

Patient Demographics	**Total (16)**	**Control (6)**	**Ischaemia (10)**	**P**
Male sex	13/16 (81%)	6/6 (100%)	7/10 (70%)	0.25
Age, years	66.9±10.6	65.5±9.2	67.7±11.7	0.70
Height, cm	167.9±8.5	168.5±3.9	167.6±10.4	0.84
BMI kg/m^2	29.1±4.4	31.6±4.6	27.5±3.7	0.07
Previous PCI	8/16 (50%)	4/6 (67%)	4/10 (40%)	0.61
Previous MI	3/16 (19%)	1/6 (33%)	2/10 (20%)	>0.99
LVEF, %	57±8	58±6	56±9	0.64
Diabetes mellitus	9/16 (56%)	4/6 (67%)	5/10 (50%)	0.63
Hypertension	13/16 (81%)	5/6 (83%)	8/10 (80%)	>0.99
Dyslipidemia	14/16 (88%)	6/6 (100%)	8/10 (80%)	0.50
Family History	10/16 (63%)	4/6 (67%)	6/10 (60%)	>0.99
Smoking history	11/16 (69%)	4/6 (67%)	7/10 (70%)	>0.99
Current Medications				
Beta-blockers	10/16 (63%)	4/6 (67%)	6/10 (70%)	>0.99
Nitrates	4/16 (25%)	2/6 (33%)	2/10 (20%)	0.60
Statins	13/16 (81%)	6/6 (100%)	7/10 (70%)	0.25
ACEi	10/16 (63%)	3/6 (50%)	7/10 (70%)	0.61
Aspirin	14/16 (88%)	5/6 (83%)	9/10 (90%)	>0.99
Clopidogrel	11/16 (69%)	4/6 (67%)	7/10 (70%)	>0.99
Procedural details				
Diseased vessels	2 (1 to 2)	1 (1 to 1)	2 (2 to 3)	<0.01
Hyperaemic Pd/Pa	0.77 (0.62 to 0.88)	0.92 (0.87 to 0.97)	0.62 (0.6 to 0.75)	<0.01
LAD/Cx/RCA*	8/2/6	3/1/2	5/1/4	-
Duration (mins)	97 (84 to 111)	97 (88 to 102)	97.5 (84 to 117)	0.72

Table 5. Baseline demographics and procedural details of study participants.
Categorical data are expressed as counts and percentages (n/N). Quantitative data that is normally distributed is described as mean +/- standard deviation; quantitative data that is not normally distributed is described as median and interquartile range (IQR). Abbreviations see xvi.

4.3.1 EFFECT OF EXERCISE ON HAEMODYNAMICS AT THE ONSET OF ISCHAEMIA

The haemodynamic effects of exercise in patients with preserved left ventricular function with and without functionally significant coronary artery disease are shown in Table 6. Functional significance of coronary artery disease was determined at the end of the study protocol following adenosine administration with an FFR<0.8; coronary artery disease with a resting Pd/Pa measurement of <0.8 and angiographically >70% stenosis was considered functionally significant and intravenous adenosine was not administered.[216] At low impact, exercise demonstrated a beneficial effect in both groups, but adversely affected haemodynamic variables in patients with coronary artery disease at the onset of ischaemia. In both groups, exercise significantly increased heart rate, end-diastolic and end-systolic pressure, dP/dtmax and dP/dtmin (Figure 59). Compared with baseline values, end-diastolic (90±28 versus 109±31 mL; *P*<0.05) and end-systolic volumes (39±14 versus 71±31 mL; *P*<0.001) were significantly increased in the group with ischaemia at peak exercise, this resulted in a decrease in ejection fraction (57±19 versus 36±15%; P<0.001); this did not occur group without ischaemia. Furthermore, at peak exercise, cardiac output dropped in the ischaemia group but continued to increase and was significantly higher in the control group (7±2.3 versus 4.5±1.9; *P*<0.05), Figure 60.

	No ischaemia (Control n=6)			P value (within group)			Ischaemia (n=9)			P value (within group)			P value between group		
	Baseline	**50%**	**Peak**	**Bvs50%**	**BvsP**	**50%vsP**	**Baseline**	**50%**	**Peak**	**Bvs50%**	**BvsP**	**50%vsP**	**Baseline**	**50%**	**Peak**
HR bpm	77±10	90±11	101±8	<0.05*	<0.001*	0.13	72±12	90±19	103±20	<0.001*	<0.001*	<0.05*	>0.99	>0.99	>0.99
EDP mmHg	15±6	23±5	29±5	<0.05*	<0.001*	0.11	13±3	29±5	29±6	<0.001*	<0.001*	>0.99	0.99	0.12	>0.99
ESP mmHg	125±23	146±23	152±16	<0.05*	<0.001*	>0.99	134±15	152±23	165±23	<0.05*	<0.001*	0.10	>0.99	>0.99	0.69
EDV mL	106±21	110±23	113±31	>0.99	0.91	>0.99	90±28	89±25	109±31	>0.99	<0.05*	<0.05*	0.75	0.49	>0.99
ESV mL	48±14	43±15	42±15	>0.99	>0.99	>0.99	39±14	39±23	71±31	>0.99	<0.001*	<0.001*	>0.99	>0.99	<0.05*
EF %	55±8	61±10	63±12	0.75	0.46	>0.99	57±8	57±19	36±15	>0.99	<0.001*	<0.001*	>0.99	>0.99	<0.05*
SV† mL	65±25	67±25	70±25	>0.99	0.81	>0.99	51±23	52±19	44±17	>0.99	0.23	0.10	0.70	0.59	0.10
CO† L/min	4.9±1.8	6±1.9	7±2.3	0.07	<0.001*	0.09	3.6±1.6	4.6±1.8	4.5±1.9	<0.05*	0.07	>0.99	0.53	0.52	<0.05*
dP/dt_{max}	1459±150	1678±351	1899±299	0.23	<0.05*	0.22	1365±212	1676±487	1862±430	<0.05*	<0.001*	0.19	>0.99	>0.99	>0.99
dP/dt_{min}	-1376±235	-1730±345	-1864±286	<0.05*	<0.001*	0.55	-1386±220	-1673±309	-1764±337	<0.05*	<0.001*	0.79	>0.99	>0.99	>0.99
Load-independent markers of contractility															
SCI mmHg/mL/s	14±3	16±4	18±5	>0.99	0.14	0.74	16±5	20±7	19±7	0.07	0.51	0.99	>0.99	0.51	>0.99
ESPVR mmHg/mL	2.9±1.2	3.8±1.3	4.1±1.8	0.33	0.08	>0.99	3.8±1.2	4.9±2	2.7±1	0.06	<0.05*	<0.001*	0.69	0.46	0.21
PRSW mmHg	70±20	82±20	89±21	0.26	<0.05*	0.87	68±15	83±23	59±24	<0.05*	0.37	<0.001*	>0.99	>0.99	<0.05*
Load independent markers of relaxation															
Tau ms	34±5	32±3	30±4	>0.99	>0.99	>0.99	36±5	34±7	32±6	0.58	0.88	>0.99	>0.99	0.83	0.90
EDPVR Beta	5.9±0.3	5.5±0.5	5.1±0.2	0.17	<0.01*	<0.05*	5.9±0.1	5.1±0.2	5.1±0.4	<0.001*	<0.001*	>0.99	>0.99	<0.05*	>0.99
EDPVR mmHg/mL	0.15±0.07	0.23±0.08	0.28±0.1	<0.05*	<0.05*	0.29	0.15±0.06	0.34±0.08	0.29±0.1	<0.001*	<0.001*	0.24	>0.99	<0.05*	>0.99
LV myocardial energetics															
Watts	1.8±0.5	2.4±0.8	3.0±0.8	<0.05*	<0.01*	0.14	1.4±0.4	2.1±0.7	2.7±0.8	<0.05*	<0.001*	<0.05*	0.84	0.88	>0.99
SW mmHg.mL	7453±2794	9074±3294	10024±3378	0.07	<0.05*	0.53	6256±2603	7351±2767	6289±2800	0.19	>0.99	0.21	>0.99	0.80	0.06
PVA (Joules)	1.4±0.4	1.6±0.5	1.8±0.5	0.12	<0.05*	0.60	1.2±0.4	1.4±0.4	1.6±0.5	0.07	<0.001*	<0.05*	>0.99	0.95	>0.99
SW: PVA %	71±9	74±10	75±10	>0.99	0.98	>0.99	70±8	71±15	51±16	>0.99	<0.001*	<0.001*	>0.99	>0.99	<0.05
Ventricular-arterial interaction															
SVR mmHg.min/L	28±10	26±7	24±7	>0.99	0.95	>0.99	44±18	37±13	44±18	0.21	>0.99	0.28	0.12	0.46	<0.05*
Ea mmHg/mL	2.2±0.5	2.3±0.5	2.3±0.7	>0.99	>0.99	>0.99	2.9±1.0	3.7±2.0	5.5±2.9	0.65	<0.001*	<0.05*	>0.99	0.38	<0.05*
Ea: Ees	0.8±0.3	0.7±0.4	0.7±0.4	>0.99	>0.99	>0.99	0.8±0.3	1.1±1.4	2.6±0.8	>0.99	<0.05*	<0.05*	>0.99	>0.99	<0.05*

Table 6 Hemodynamic variables at baseline, at 50% peak exercise and at peak.
exercise for both the control and ischaemia groups. Data are expressed as mean±SD.

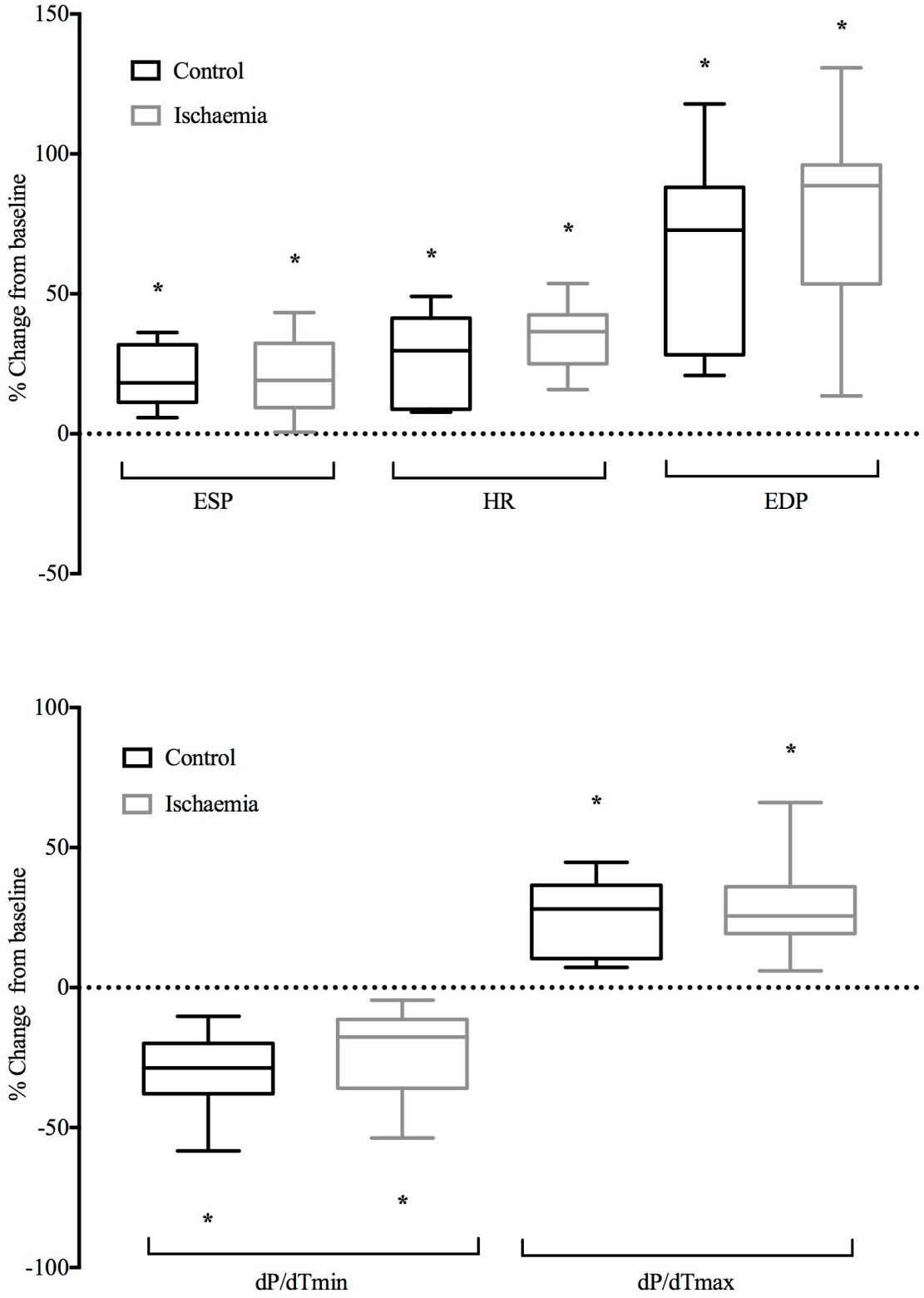


Figure 59 Percentage change in haemodynamic variables.
In the control and ischaemia groups at peak exertion compared to baseline; *P< 0.05 compared to baseline.

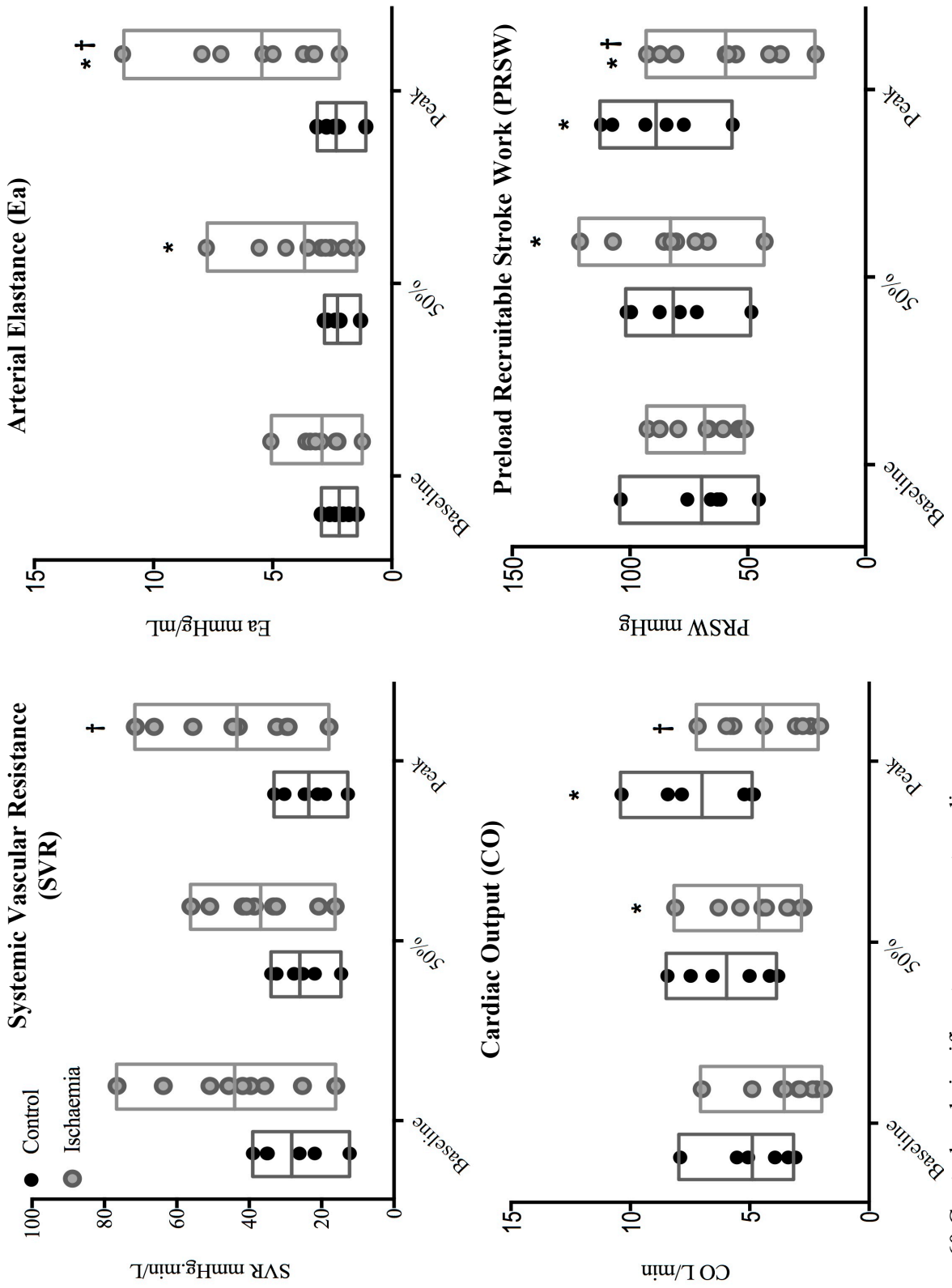


Figure 60 Control and significant coronary artery disease.
Preload recruitable stroke work (PRSW), arterial elastance (Ea), cardiac output (CO) and systemic vascular resistance (SVR) in the control and ischaemia groups; * $P<0.05$ compared to baseline $^{\dagger}P<0.05$ compared to control.

The maximum cardiac power output, measured in watts, increased in both groups, and did not significantly differ between the groups. Compared to baseline, stroke work (the external work performed by the heart) significantly increased in the control group (7453±2794 versus 9074±3294 mmHg.mL; $P<0.05$) but not in the ischaemia group. Compared to baseline, pressure volume area (the sum of external stroke work and potential energy) significantly increased in both the control group (1.4±0.4 versus 1.6±0.5 Joules; $P<0.05$) and the ischaemia group (1.2±0.4 versus 1.4±0.4 Joules; $P<0.001$). The ratio of stroke work to pressure volume area (a marker of ventricular efficiency) remained unchanged in the control group but significantly decreased at the onset of ischaemia in the group with significant coronary artery disease (71±15 versus 51±16%; P<0.001) and at peak exercise was significantly lower than the control group (51±16% versus 75±10%; P<0.05).

At 50% maximal workload, contractility (PRSW) increased in both groups compared to baseline (control group 82±20 versus 70±20 mmHg, P<0.05; ischaemia group 83±23 versus 68±15 mmHg, P<0.05), Figure 60; but at maximal workload, contractility decreased in the group with significant coronary artery disease at the onset of ischaemia (59±24 versus 83±23 mmHg; $P<0.001$). At 50% maximal workload, passive diastolic function (beta coefficient of end-diastolic pressure volume relationship), improved in both groups (control: 5.9±0.3 versus 5.5±0.5, $P<0.001$; ischaemia: 5.9±0.1 versus 5.1±0.2, $P<0.001$) compared to baseline, this continued to improve in the control group at peak exercise (5.5±0.5 versus 5.1±0.2; $P<0.05$) but not in the ischaemia group. Active diastolic relaxation, measured by Tau, showed a numerical reduction in both groups but this did not reach significance.

During exercise in the control group of patients, without functionally significant coronary artery disease and preserved left ventricular function, a rightward shift was of the PV loop was seen, accompanied by an upward shift in the end-systolic pressure volume relation (ESPVR), Figure 61. In patients with significant coronary artery disease, on initiation of exercise, an upward shift of the EDPVR was demonstrated with a leftward shift of the ESPVR. On continued exercise, at the onset of ischaemia, a profound rightward shift was demonstrated of both the EDPVR and ESPVR (relative to both initial exercise and baseline), accompanied by a reduction in the area of the pressure-volume loop (Figure 61).

4.3.2 THE VENTRICULAR-ARTERIAL INTERACTION IN THE PRESENCE OF SIGNIFICANT CORONARY ARTERY DISEASE

An increase in vascular stiffness was demonstrated at peak exercise in the cohort of patients with ischaemia compared to the control group. Arterial elastance (Ea), which is a component of lumped mean and pulsatile load to the left ventricle increased at peak exercise compared to baseline in the ischaemia group (2.9±1.0 versus 5.5±2.9 mmHg/mL; $P<0.001$), driven by the increase in end-systolic pressure and a reduction in stroke volume in the former, Figure 60. Systemic vascular resistance (SVR) was significantly higher at peak exercise in the ischaemia group compared to the control group (44±18 versus 24±17 mmHg.min/L; $P<0.05$). These changes in the ischaemia group adversely affected the ventricular-arterial interaction; the ratio of Ea to end-systolic elastance increased in the ischaemia group (0.8±0.3 versus 2.6±0.8; $P<0.05$) and was significantly higher than the control group at peak exercise (2.6±0.8 versus 0.7±0.4; $P<0.05$).

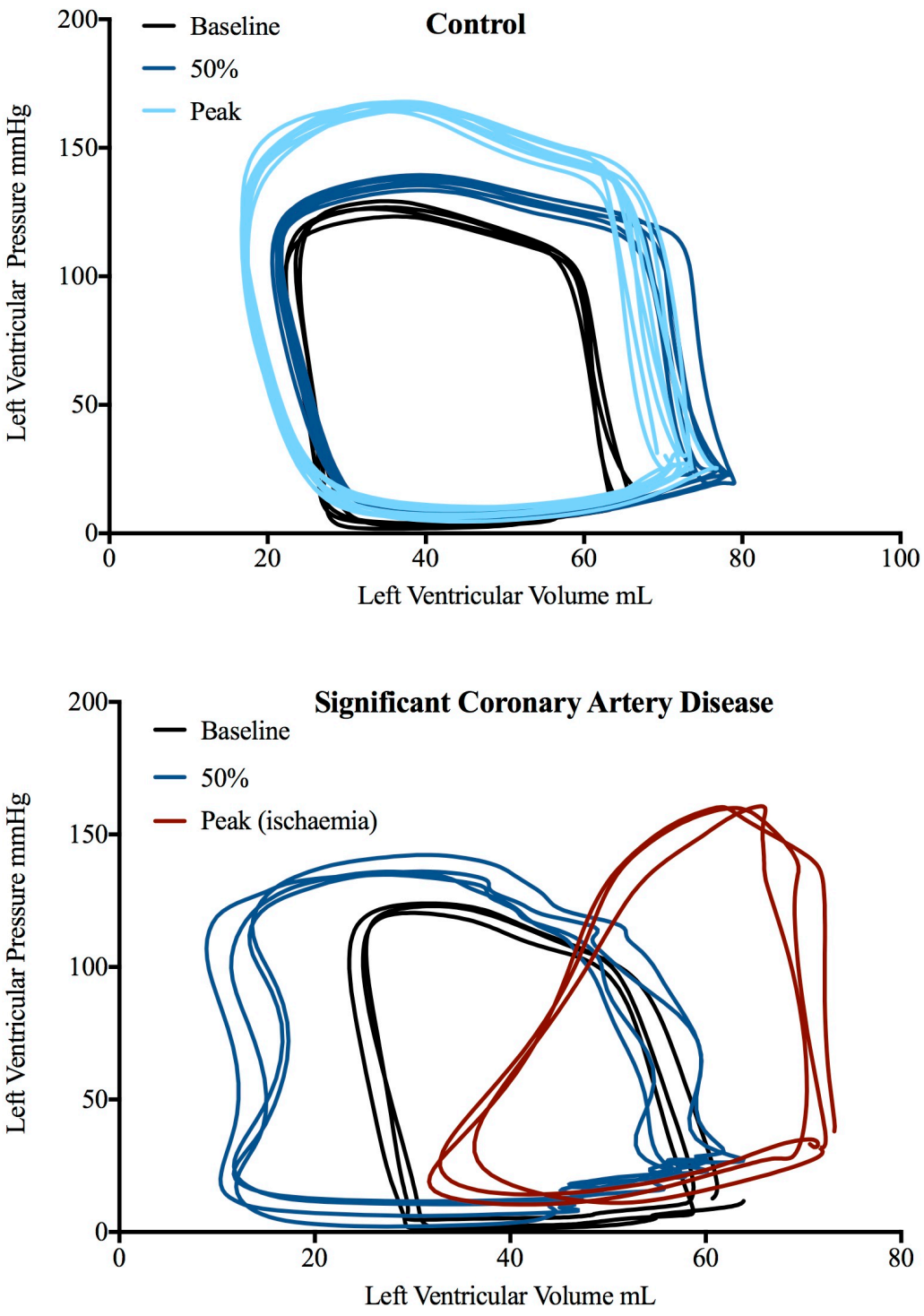


Figure 61 Representative examples of changes in the pressure-volume loop.
At the onset of exercise in patients with and without significant coronary artery disease.

4.3.3 RELATIONSHIP BETWEEN CORONARY BLOOD FLOW VELOCITY AND DIASTOLIC TIME FRACTION IN ISCHAEMIA

Coronary haemodynamic changes are summarised in Table 7. Representative examples of haemodynamic signals and associated wave intensity are depicted in Figure 62. In the overall cohort of patients, compared to baseline values, coronary blood flow velocity significantly increased at peak exercise (12.3±5.4 versus 17.6±7.8; $P<0.005$); this was driven by a significant increase in coronary blood flow velocity in the control group (10.8±3.0 versus 17.1±6.4; $P<0.05$), and a trend toward an increase in coronary blood flow velocity in the ischaemia group (13.3±6.7 versus 17.8±9.2; $P= 0.06$). A trend toward a decrease in microvascular resistance was observed overall at peak exercise compared to baseline but this did not reach significance. Compared to baseline values, distal coronary pressure significantly increased in the control group (103±15 versus 119±12; $P<0.05$) but not in the ischaemia group, driven by the increase in mean aortic pressure (Figure 63). The pressure gradient across the stenosis could not be calculated in patients with simultaneous pressure-volume loop measurements and ComboWire measurements through a single guide catheter, due to the impact of the equipment on the fluid filled manometer pressure tracing. In patients with sequential coronary haemodynamic measurements, compared to baseline, the pressure gradient significantly increased at peak exercise (ischaemia) in patients with significant coronary artery disease (15±10 versus 24±17; $P<0.05$) but not in those without significant coronary artery disease. Diastolic time fraction significantly decreased in the control group on peak exercise compared to baseline values (53±4 versus 61±5; $P<0.05$) but did not decrease in the group with significant coronary artery disease despite a significant increase in heart rate (Figure 63).

	All exercise (n=12)			Control (n=5)			Ischemia (n=7)		
	Baseline	**50%**	**Peak**	**Baseline**	**50%**	**Peak**	**Baseline**	**50%**	**Peak**
U cm/sec	12.3±5.4	15.1±6.5	17.6±7.8*	10.8±3.0	12.8±2.1	17.1±6.4*	13.3±6.7	16.8±8.4	17.8±9.2
Pd mmHg	98±13	107±18*	108±20*	103±15	118±15*	119±12*	95±11	101±19	101±21
MR mmHg/cm/sec	9.0±2.9	8.4±4.0	6.1±2.9	9.9±2.8	9.5±2.4	7.5±2.1	8.4±3.0	7.7±4.9	5.0±3.0
ΔP mmHg[†]	11±11	16±15	20±16*	1±2	5±5	7±7	15±10	21±15	24±17*
DTF	60±5	55±8	55±6	61±5	54±4*	53±4*	59±5	56±10	56±8
Wave Intensity $J/m^2/sec^2x10^3$[‡]									
FCW	4.0±2.1	5.6±2.6	7.6±5.1*	3.1±1.1	5.9±3.1	8.9±7.2	4.8±2.6	5.3±2.5	6.6±2.8
FEW	3.6±1.8	6.9±3.6	7.8±5.1**	3.1±1.7	6.1±3.8	10.8±6.0**	3.6±1.3	4.5±2.6	6.8±2.4*
BCW	-5.1±3.1	-6.7±4	-9.2±5.2**	-4.5±3.5	-4.7±1.9	-8.6±3.8*	-5.1±3.1	-6.8±4.5	-11±4.6**
BEW	-4.0±1.4	-6.8±1.5*	-9.4±3.7**	-3.0±1.4	-6.3±1.6*	-10±3.7**	-4.7±0.9	-7.9±10*	-11±2.8**

Table 7 Coronary hemodynamics and wave energies

Overall and in the control and ischaemia groups; * $P<0.05$ compared to baseline. **P<0.05 compared to 50% and baseline. Abbreviations: U mean coronary blood flow velocity, Pd mean distal coronary pressure MR microvascular resistance. [†] Total number of patients 7(2 in control group, 5 in ischemia group). [‡] Total number of patients 11 (5 in control group, 6 in ischemia group).

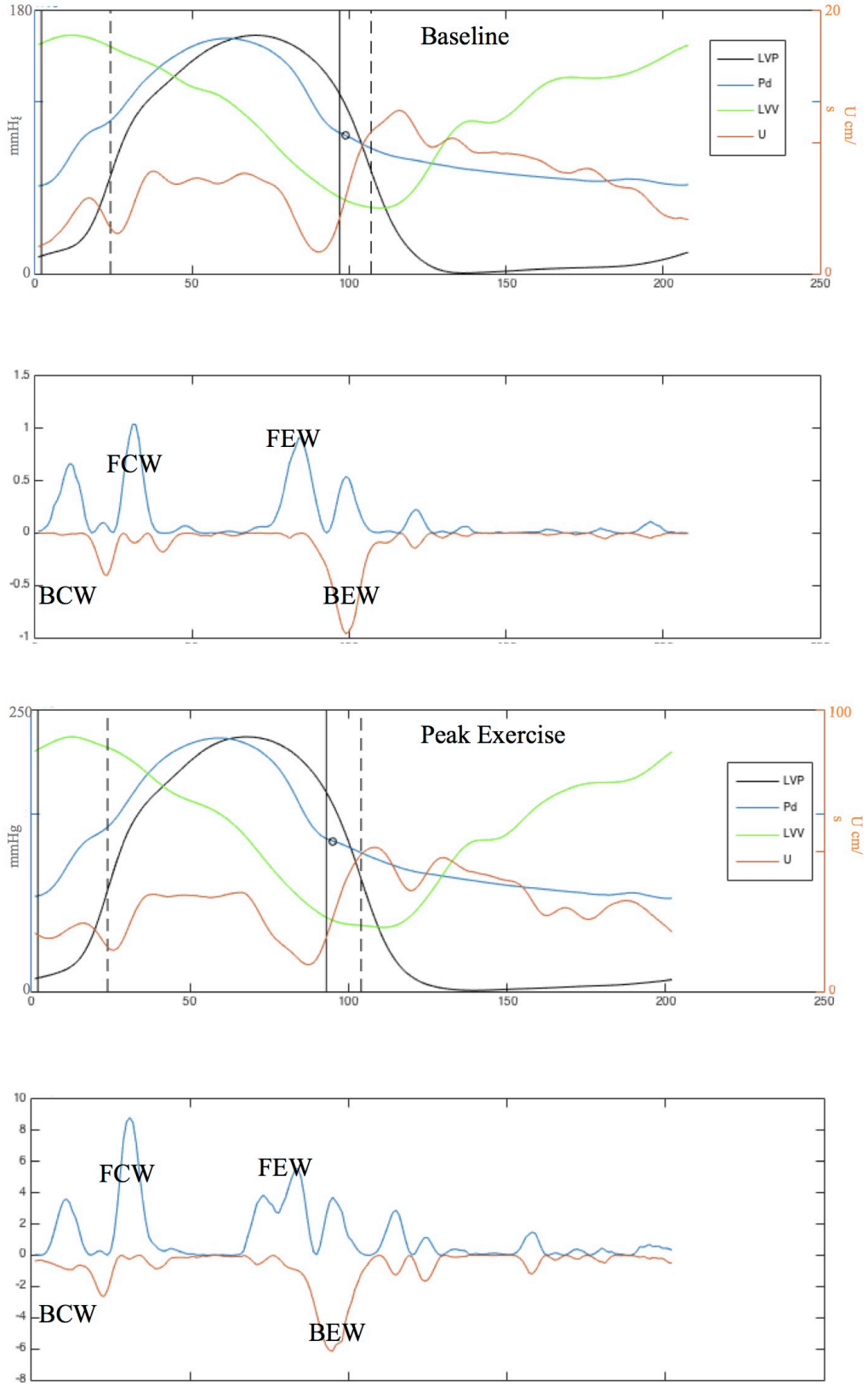


Figure 62 Representative example of haemodynamics: baseline versus peak exercise. Haemodynamic tracings (above) and wave intensity ($Jm^{-2}s^{-2}x10^5$) (below).

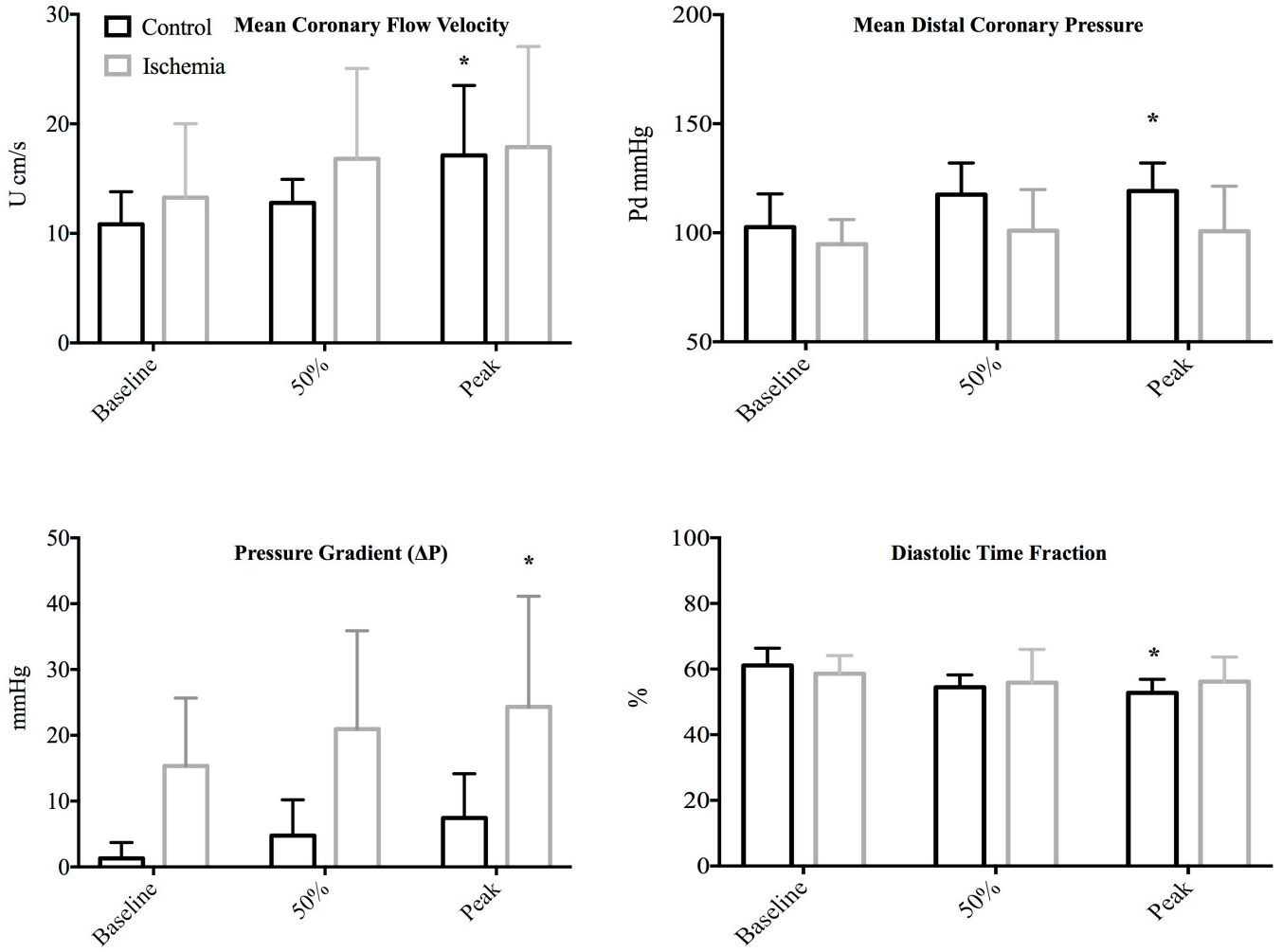


Figure 63 Changes in coronary haemodynamics.
Mean coronary blood flow velocity (U; top left); distal coronary pressure (Pd; top right); pressure gradient across the stenosis (ΔP; bottom left) and diastolic time fraction (DTF, %; bottom right) in the control and ischaemia groups; *P<0.05 compared to baseline.

4.3.4 CORONARY WAVE INTENSITY ANALYSIS AND CARDIAC MECHANICS

In reference to the coronary wave energies arising distally, coronary wave intensity analysis demonstrated a significant increase in the net energy of the backward travelling suction wave (during diastole), this increased compared to baseline in both the control group (-10±3.7 versus -3.0±1.4x10^3 J/m^2/sec^2; P<0.001) and the ischaemia group (-11±2.8 versus -4.7±0.9 x10^3 J/m^2/sec^2; P<0.001). There was also an increase in the net energy of the backward travelling compression or pushing wave (during early systole) in both the control group (-8.6±3.8 versus -4.5±3.5 x10^3 J/m^2/sec^2; P<0.05) and ischaemia group (-11±4.6 versus -5.1±3.1 x10^3 J/m^2/sec^2; P<0.001) at peak exercise compared to baseline values. In reference to the wave energies arriving proximally in the aorta, there was no significant increase in the net energy of forward travelling compression wave; however, the peak of the forward compression wave (arising in systole) was significantly increased at peak exercise compared to baseline values in the control group (12.5±8.3x10^4 versus 22±15x10^4 J/m/sec^2; P<0.05) but not in the ischaemia group. The forward travelling suction wave (arising in early diastole) increased significantly on exercise compared to baseline in the both the control group (10.8±6.0 versus 3.1±1.7 x10^3 J/m^2/sec^2; P<0.001) and the ischaemia group (6.8±2.4 versus 3.6±1.3 x10^3 J/m^2/sec^2; P<0.05) (Figure 64).

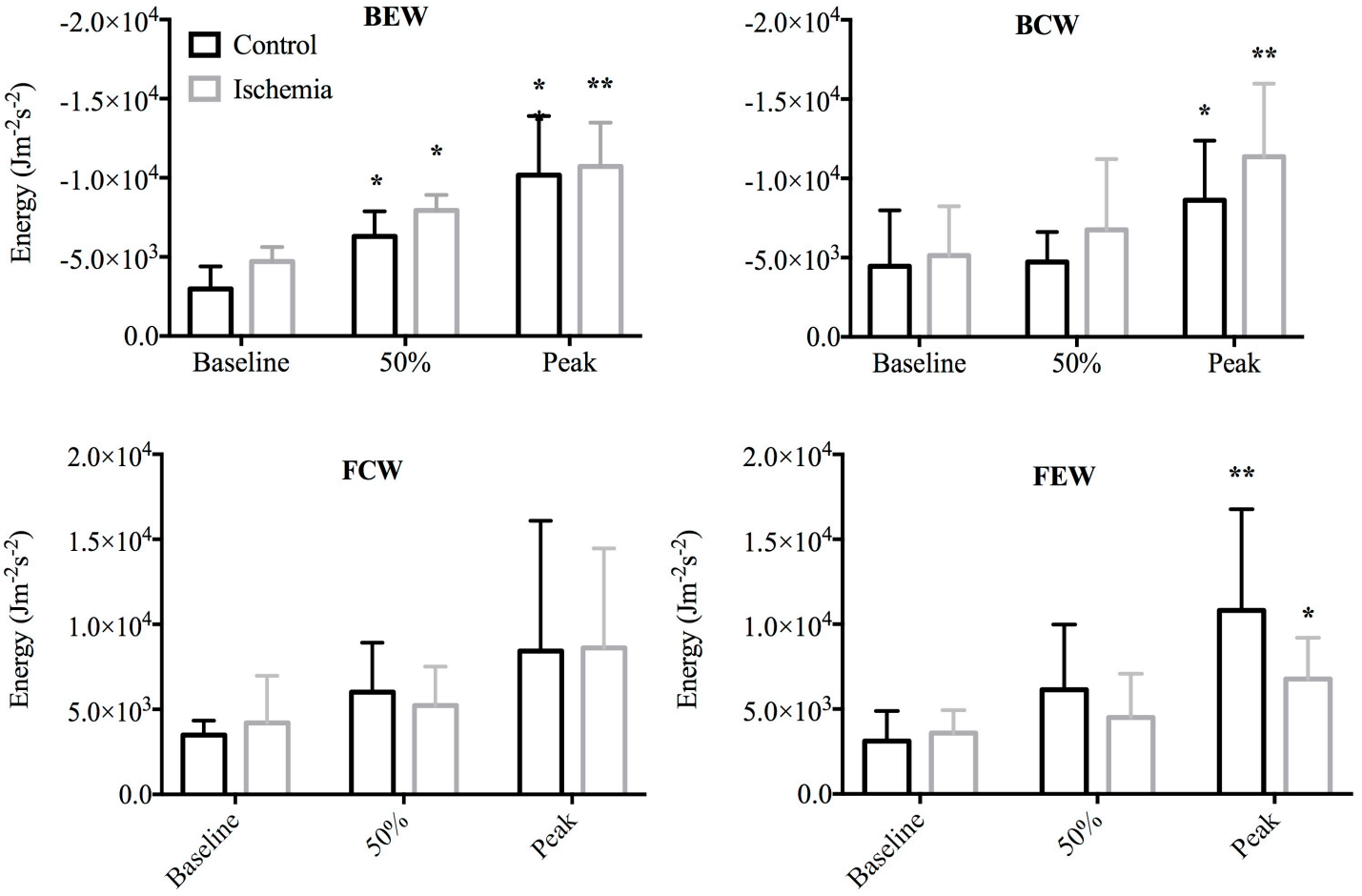


Figure 64 Changes in the coronary wave energies of the four main waves
Backward expansion wave (top left), backward compression wave (top right); forward compression wave (bottom left) and forward expansion wave (bottom right) in the control and ischaemia groups; *P<0.05 compared to baseline; **P<0.05 compared to baseline and 50%.

Analysis of seven patients with simultaneous coronary and LV haemodynamic measurements revealed a correlation with the coronary wave energies and cardiac mechanics during exercise both in the presence and absence of significant coronary artery disease. The peak of the forward travelling compression wave (arising in systole) correlated with dP/dtmax ($r = 0.5$; $P<0.001$); the net wave energy of the backward travelling compression wave (arising in early systole) also correlated with dP/dtmax ($r = -0.6$; $P<0.0001$); the net wave energy of the backward travelling suction wave (arising in diastole) correlated with dP/dtmin ($r = 0.6$; $P<0.0001$) (Figure 65).

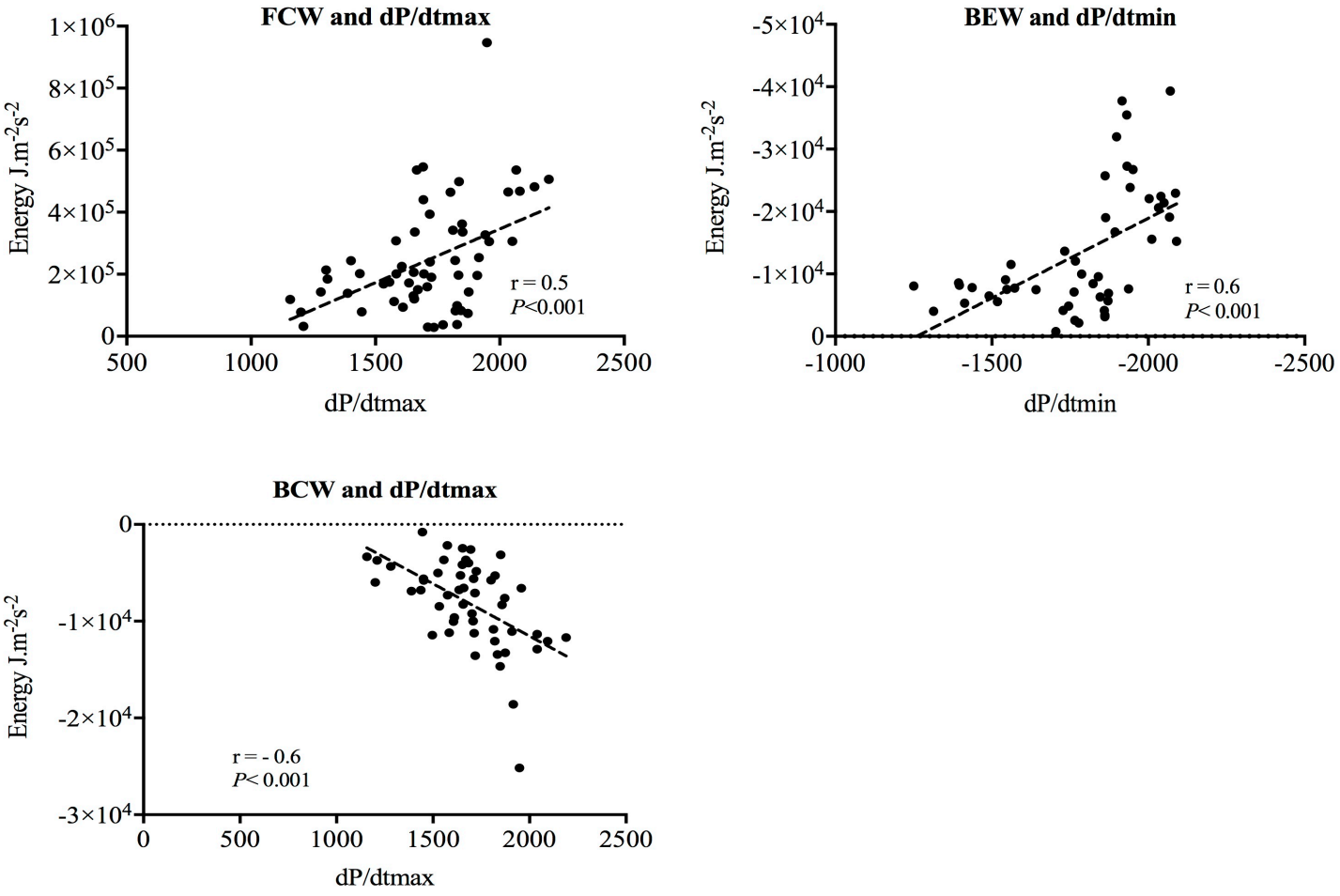


Figure 65 Correlation of major wave energies with cardiac mechanics

Peak forward compression wave versus left ventricle (LV) dP/dt max (top left); energy of the backward expansion wave versus LV dP/dt min (top right); backward compression wave versus LV dP/dt max (bottom left).

4.4 DISCUSSION

This is the first time to our knowledge, coronary and left ventricular haemodynamics have been measured simultaneously in humans, both at rest and during exercise and to this degree of accuracy. The main findings of this study can be summarised as follows: 1) At low impact, exercise exhibits a beneficial haemodynamic effect on the cardiovascular system, but adversely affects stroke volume and cardiac output at the onset of ischaemia; 2) demand ischaemia initially drives the PV loop upward followed by a rightward shift after a specific duration and intensity of ischaemia, with a reduction of the external (useful) work performed by the heart; 3) in the presence of significant coronary artery disease, the ventricular-arterial interaction is impaired on peak exercise; 4) coronary blood flow velocity is maintained through preservation of the diastolic time fraction in the presence of significant coronary artery disease when autoregulatory mechanisms are exhausted; 5) coronary wave intensity analysis is a surrogate for cardiac mechanics.

Control group

In the absence of significant coronary artery disease, dynamic exercise improves haemodynamic variables. An increase in heart rate and stroke volume drives an increase in cardiac output. Stroke work and total mechanical energy expenditure increases with an increase in ventricular efficiency. Contractility increases, as demonstrated by an increase in the ESPVR slope; these findings are consistent with pre-clinical work performed by Nozawa et al in this area, they demonstrated an increase in the area of the pressure-volume loop (stroke work) accompanied by an increase in the ESPVR slope in

conscious dogs.[32] As contractility increases, basal energy consumption of the myocardium increases, thus shifting the pressure-volume area-myocardial oxygen consumption ratio upward; in the absence direct measurement of MVO2 in the study, we were unable to demonstrate an increase in mechanical efficiency as was performed in the instrumented dogs.[8,32]

The systemic response to exercise in this cohort was manifest as a decrease in systemic vascular resistance and a decrease in arterial elastance, which represents lumped mean and pulsatile load to the left ventricle. Changes in systemic vascular resistance enhance stroke volume, thus facilitating the increased cardiac output necessary for sustained exercise. This theory was supported by the improvement seen in ventricular-arterial coupling (Ea:Ees ratio) during exercise.

The increased in total mechanical energy was accompanied by a significant increase in coronary blood flow velocity and an increase in distal coronary pressure, which followed the rise in mean aortic pressure. The increase in coronary blood flow velocity, (and therefore increased oxygen supply) has been previously studied and is a recognised consequence of increase myocardial oxygen demand (consumption).[110,121] Similarly distal coronary pressure rise has been shown to follow a rise in mean aortic pressure.[101] During peak exercise, there was no increase in the pressure gradient across the coronary lesion; exercise represents true physiological hyperaemia, this is less than can be achieved pharmacologically, thus would be consistent with a negative fractional flow reserve measurement in this patient cohort.[67,92]

Significant coronary artery disease:

This is the first time that end-systolic and end-diastolic pressure volume relations have been studied simultaneously in humans with angina pectoris. The advantage of this is that the sequence of events during the onset of ischaemia with regard to systolic and diastolic function can be described. Importantly, this study benefitted from direct measurement of coronary pressure and flow velocity to demonstrate functional significance of coronary artery disease, which has not been previously performed. We hypothesised that diastolic properties are a function of systolic properties and that changes are not manifest in isolation.

Myocardial work and Contractility

In patients with significant coronary artery disease, on initiation of dynamic exercise, there was an initial improvement in haemodynamic variables: the initial increase in stroke volume and therefore cardiac output enabled the body to sustain physical activity; this was accompanied by an initial increase in contractility, the slope of the ESPVR curve became steeper, with an increase in the area of the pressure volume (PV) loop, the latter representing an increase in external stroke work. However, continued exercise, lead to a decrease in cardiac output, with a rightward shift of the ESPVR slope. The striking rightward shift of the PV loop is representative of decreased contractility and acute LV dilatation, with higher end-diastolic and end-systolic volumes. These findings are consistent with pre-clinical work performed by Steendijk et al in canines; they delivered increasing doses of dobutamine after inducing coronary stenosis, an initial increase in cardiac output and increase in the gradient of the ESPVR slope was seen; however, at the highest doses of dobutamine, a drop in cardiac output

occurred, followed by a rightward downward shift of the ESPVR curve.[156] During ischaemia, a rightward shift and reduction in the area of the pressure-volume loop corresponds to an increased in total mechanical energy expenditure but a decrease external stroke work, and therefore a decrease in ventricular efficiency (conversion of metabolic energy to external work). These findings were also demonstrated by Steendijk et al.[156] Importantly, we found in the presence of single vessel coronary disease: left anterior descending (5), dominant right coronary artery (4), dominant left circumflex (1), inducing regional ischaemia effect the total PV loop.

Diastolic function

In patients with significant coronary artery disease, the early stages of exercise were accompanied by the physiological response expected in healthy individuals: an increase in contractility, stroke work and cardiac output. However, on observation of the pressure volume loop, an upward shift of the end-diastolic pressure-volume relationship can be seen early on, prior to the clinical manifestation of ischaemia (ECG changes and chest pain). This upward shift demonstrated on exercise is consistent with the previously recognised increase in diastolic pressure relative to volume with demand ischaemia in patients with coronary artery disease.[145,149,212] Previous studies of pacing induced ischaemia have shown similar findings.[125] Importantly we demonstrated an upward then rightward shift of both the ESPVR and EDPVR relations; these latter changes have been shown to occur with coronary occlusion in humans but not with demand ischaemia. Paulus et al induced two different types of ischaemia in in dogs (pacing and coronary occlusion): pacing induced an upward shift and occlusion drove a rightward shift of the EDPVR. As both changes were seen in this patient cohort, the

theory that the technique used to provoke ischaemia dictates the direction of the EDPVR is brought into question. The findings of this study clearly demonstrated that systolic and diastolic function are closely linked, initially, contractility is preserved or improved, thus driving the end-diastolic pressure-volume relationship upward; there then follows impairment of contractile function, that occurs after continued supply-demand mismatch that may be related to a specific duration or intensity of ischaemia; impaired systolic function is then accompanied by a rightward shift of the EDPVR relation; these findings reflect work by Takano et al: they found that on inducing ischaemia by pacing in dogs that the EDPVR response was dictated by the change in left ventricular contractility; as pacing is not true physiological ischaemia, there were not able to demonstrate the continuum shown in this study.[155] We have therefore shown that systolic and diastolic function are closely related, with ischaemic changes acting as a continuum, of which the end-stage is a rightward shift of the EDPVR.

Ventricular-Arterial Interaction

The dynamic interaction between the heart and the systemic vasculature is fundamental to the heart providing adequate cardiac output and the arterial pressures necessary for distal organ perfusion; in the case of exercise, the increased perfusion necessitated by skeletal muscle.[109,114] We showed this normal physiological response of the peripheral vasculature to be adversely affected in the presence of significant coronary artery disease. In this study, an initial decrease in systemic vascular resistance was seen, followed by a steep rise. Arterial elastance significantly increased on exercise in the presence of significant coronary artery disease; arterial elastance is inversely related to compliance. Ventriculo-arterial coupling (Ea:Ees ratio) correlates inversely to pump

efficiency such that the heart is optimally efficient at a ratio of 0.7 and an Ea:Ees>1.0 is seen in failing hearts.[37,40,128] In this cohort of patients with preserved left ventricular function, the Ea:Ees ratio was within normal limits at rest; however, on exercise this increased dramatically, driven by initially by the increase in Ea, followed by a reduction in contractile function (Ees). This acute increase in afterload is likely to play a key role in LV dysfunction during ischaemia, and is likely to contribute to the acute LV dilatation and global systolic impairment that was observed. Thus cardiac efficiency becomes impaired and VA uncoupling occurs. The VA uncoupling seen in exercise-induced ischaemia is similar to those in acute heart failure.[38] Therefore demonstrating the systemic effects of ischaemia.

Coronary haemodynamics

In the presence of significant coronary artery disease, the pressure gradient across the coronary stenosis increased on exercise; thus the increase in myocardial demand in patients with ischaemic heart disease could not be sustained by an increase in coronary flow velocity. This is due to the exhaustion of autoregulatory mechanisms in the presence of a flow limiting stenosis.[67,220] Despite the increase in heart rate, diastolic time fraction was seen to be preserved in this cohort of patients, which has previously been suggested as a mechanism for maintaining coronary perfusion in the presence of coronary artery disease.[65]

Interestingly, coronary wave energies increased in both groups on exercise; simultaneous LV and coronary measurements demonstrated that these wave energies follow dP/dTmax and dP/dtmin. These findings would suggest that cWIA could be used

as a potential surrogate for cardiac mechanical changes; these support findings of previous preclinical and human work.[100,107] The importance of this is the potential application of cWIA in assessment of LV haemodynamics, when LV invasive measurements may not be practical.

4.5 LIMITATIONS

This was a small single centre observational study; however, this is the first time to our knowledge, coronary and left ventricular haemodynamics have been measured simultaneously in humans, both at rest and during exercise and to this degree of accuracy. Pressure-volume loop and coronary wave intensity analysis during exercise introduces noise despite the use of filters and ensemble averaging of consecutive cardiac cycles to reduce this. The impact of a stenosis proximal to the measurement of wave intensity analysis on the single point method of calculation is not known; however, there is no known alternative to this. In the presence of single vessel coronary disease, the left ventricular changes incurred were due to regional ischaemia; however the manifestation of ischaemia affected the entire left ventricle. Total myocardial blood flow was not measured, thus the contributions of collateral flow to ischaemic regions and redistribution of blood flow were not measured.

4.6 CONCLUSIONS

This study delineates the changes occurring with demand ischaemia during dynamic exercise in humans, and the interaction of the heart with the systemic circulation. Importantly there is a biphasic response in patients with ischaemia, with low impact exercise exhibiting a beneficial effect on acute haemodynamics. Coronary wave

intensity analysis, accurately reflects the cardiac mechanical change occurring during exercise, thus has potential future application in the measurement of contractile function where invasive LV haemodynamics cannot be measured.

5 THE ROLE OF NITRATES IN ANGINA PECTORIS REVISITED

INTRODUCTION

Nitrates are the most effective drug for instant relief of acute ischaemia. A number of concepts have been used to describe how they work, including a reduction in myocardial oxygen consumption and beneficial effects on coronary blood flow. However, the precise and unique anti-ischaemic mechanism remains unclear. The importance of understanding these mechanisms, may facilitate the development of improved therapeutic agents without the setbacks of nitrate tolerance. The gold standard in-vivo measure of myocardial energy expenditure, cardiac performance and the interaction with the arterial system is by way of left ventricular (LV) pressure-volume (PV) loop analysis; the aim of this study was to examine the effect of nitrates on humans with the novel capability of measuring simultaneous LV pressure-volume relations and invasive measures of coronary blood flow, using a dual sensor pressure-flow coronary guide wire, in the cardiac catheter laboratory to perform real-time continuous assessment of the cardiovascular response to nitrates.

METHODS

Fifteen patients with significant coronary artery disease underwent cardiac catheterisation followed by intra-arterial administration of 1mg isosorbide dinitrate; continuous recording of invasive LV PV and coronary haemodynamic measurements were performed for the duration of administration and for 2 minutes after; changes induced by nitrates were compared to baseline; serial haemodynamic measurements were compared using one-way analysis of variance.

RESULTS

ISDN administration resulted in a reduction in preload and afterload, as evidenced by a reduction in end-diastolic pressure (13 ±5 versus 9±4mmHg; P<0.001) and arterial elastance (1.7±0.8 versus 2.2±1.1 mmHg/mL; *P* <0.05), with an overall decrease in total mechanical energy expenditure (1.2±0.4 versus 1.5±0.5 Joules; *P* <0.001) and therefore myocardial oxygen consumption. Consequently a leftward, downward shift of the pressure-volume loop was effected, increasing the efficiency of energy conversion to external work (68±10 versus 74±9%; *P* <0.05). Early coronary vasodilatation with a temporary increase in coronary blood flow velocity (20±11 versus 13±5 cm/sec; P<0.05) was followed by a reduction in the pressure gradient (4.8±3.7 versus 7.2±3.8 mmHg/cm/sec; P<0.05) and stenosis resistance (2.7±3.6 versus 4.4±3.3 mmHg/cm/sec; P<0.01) suggestive of stenosis dilatation. ISDN administration did not have a demonstrable effect on intrinsic myocardial properties, with no change in compliance or contractility seen.

CONCLUSIONS

The anti-anginal mechanism of nitrates in patients with ischaemic heart disease is mediated by its vasodilatory effects on the systemic vasculature and the coronary circulation; this drives both a reduction in demand and an increase in blood supply.

5.1 INTRODUCTION

Nitrates are the most effective drug for instant relief of acute myocardial ischaemia; they may also be administered as a preventative agent or in combination with other anti-anginals[221]. A number of concepts of how nitrates work at both a macroscopic and cellular level have been proposed, including clinically important anti-thrombotic activity; endothelin-derived relaxing factor activity enhancing endothelial dysfunction and positive remodelling following myocardial infarction.[159,222,223] Perhaps of most interest however, is how nitrates relieve acute ischaemia. The major action of nitrates is on vascular smooth muscle relaxation. The initial belief that the advantageous effect of nitrates was due to dilatation of the coronary circulation has since been discarded for two reasons: firstly, intracoronary vasodilators did not predictably relieve ischaemia and secondly, nitrates appear beneficial only in the presence of peripheral vasodilatation.[224,225] Thus the theory arose that the predominant action of nitrates was through a reduction in myocardial oxygen consumption by increasing peripheral vasodilatation and therefore reducing preload and afterload.[226-228] The preload reduction is demonstrated by decreased right heart pressure, chamber size and a decrease in cardiac output (although a modest increase in ejection fraction has been seen). This decline in systemic arterial pressure also triggers sympathetic nervous system activation with reflex increase in heart rate, thus driving a biphasic response: initial vasodilatation followed by reflex vasoconstriction.[229] Interestingly, nitrates improve ischaemia in areas receiving inadequate blood flow, although total myocardial blood flow may remain the same or decrease due to decreased oxygen consumption; it is presumed that decreased systolic wall tension redistributes myocardial blood flow.[230,231] Proposed coronary effects include stenosis dilatation (and therefore reduction in stenosis resistance),

enhanced collateral flow, and the reversal of coronary vasoconstriction. However, it is likely that a combination of myocardial, coronary and systemic effects contribute to the anti-anginal effect.[169,232] The precise and unique anti-ischaemic mechanism of action of nitrates remains much debated; importantly following repeated episodes of ischaemia, nitrate tolerance can develop and the effect is attenuated, with some suggestion of later harmful effects.[233] Thus by understanding the mechanism of nitrates, newer anti-anginal therapies could be developed. The gold standard for assessing cardiac performance and its interaction with the arterial system is pressure-volume (PV) analysis; simultaneous in-vivo pressure-volume measurements with a conductance catheter (CC) placed in the LV allow real-time assessment of the cardiac performance and its interaction with arterial load. [183] The combination of PV loop assessment and real-time invasive measures of coronary blood flow enables us to more precisely examine the cardiovascular changes that occur with nitrate administration.[38,195,234] Studies on the action of nitrates have examined the myocardial, systemic and coronary effects in isolation. Thus the aim of this study was to ascertain the cardiovascular response to nitrates by simultaneously assessing myocardial blood flow velocity, energetics and systemic vasculature changes in patients with known ischaemic heart disease.

5.2 METHODS

5.2.1 STUDY POPULATION

Patients were identified from routine waiting lists for coronary angiography ± proceed to angioplasty at St Thomas' Hospital, London, United Kingdom. Patients were selected for the study if they were symptomatic with Canadian Cardiovascular Society functional angina class II-III; angiographic criteria for inclusion was one or more epicardial coronary artery with > 50% diameter stenosis. Exclusion criteria were the presence of unstable angina, previous myocardial infarction, coronary artery bypass graft surgery, impaired left ventricular function, severe co-morbidities, valvular heart disease and atrial fibrillation. Patients with a left main stem stenosis, severe multi-vessel coronary disease or chronic total occlusions were also excluded. Oral nitrate preparations, calcium channel blockers and beta-blockers were stopped at least 48 hours before the procedure. All patients underwent written, informed consent prior to partaking in the study. This study received approval from the National Research Ethics Committee (09/H0802/39).

5.2.2 CATHETER LABORATORY INSTRUMENTATION AND PROTOCOL

Left heart catheterisation was performed via the right femoral artery using a standard 8Fr femoral sheath. Weight adjusted heparin was administered (70IU/kg) intra-arterially. Right and left coronary angiograms were then taken using standard diagnostic catheters. Intracoronary nitrates were not used. An 8Fr 80cm Launcher guide catheter (Medtronic Vascular, MN, USA) was introduced into the aortic root. A dual-sensor pressure velocity 0.014" coronary guide wire (ComboWire, Volcano Corp, San Diego, CA) was then connected to the ComboMap console (Volcano Corp) and was delivered

through the guide; auxiliary inputs were electronically routed to the Inca (CD Leycom) to enable for simultaneous acquisition, a further description is provided in section 2.3.2 and 3.2.1. The ComboWire pressure signal was normalised against the fluid filled catheter signal at the tip of the guide.[80,101] The guide catheter was then inserted into the coronary ostium and the ComboWire advanced distal to the stenosis in the target coronary artery (Figure 66). The guide catheter was then disengaged and left ventricular pressure and volume measurements were assessed with a 4Fr conductance catheter (CC) system (CD Leycom, The Netherlands). This flexible pigtail catheter has a solid-state pressure sensor and electrodes situated at regular intervals; continuous left ventricular volumes are calculated by measuring conductance; this technique has been previously validated and applied in the study of cardiac disease states.[184,185,193,194] The CC is connected to a signal processor (Inca, CD Leycom, Netherlands) and delivered to the ventricular cavity across the aortic valve via the guide. Correct positioning was confirmed by fluoroscopy and conductance signals, Figure 66. Volume calibration was performed by left ventricular (LV) volume measurements obtained from transthoracic three-dimensional echocardiography, further details regarding set-up and calibration can be found in section 2.2.3.2.[193] Optimisation of the coronary Doppler velocity traces and LV pressure-volume measurements was then performed.

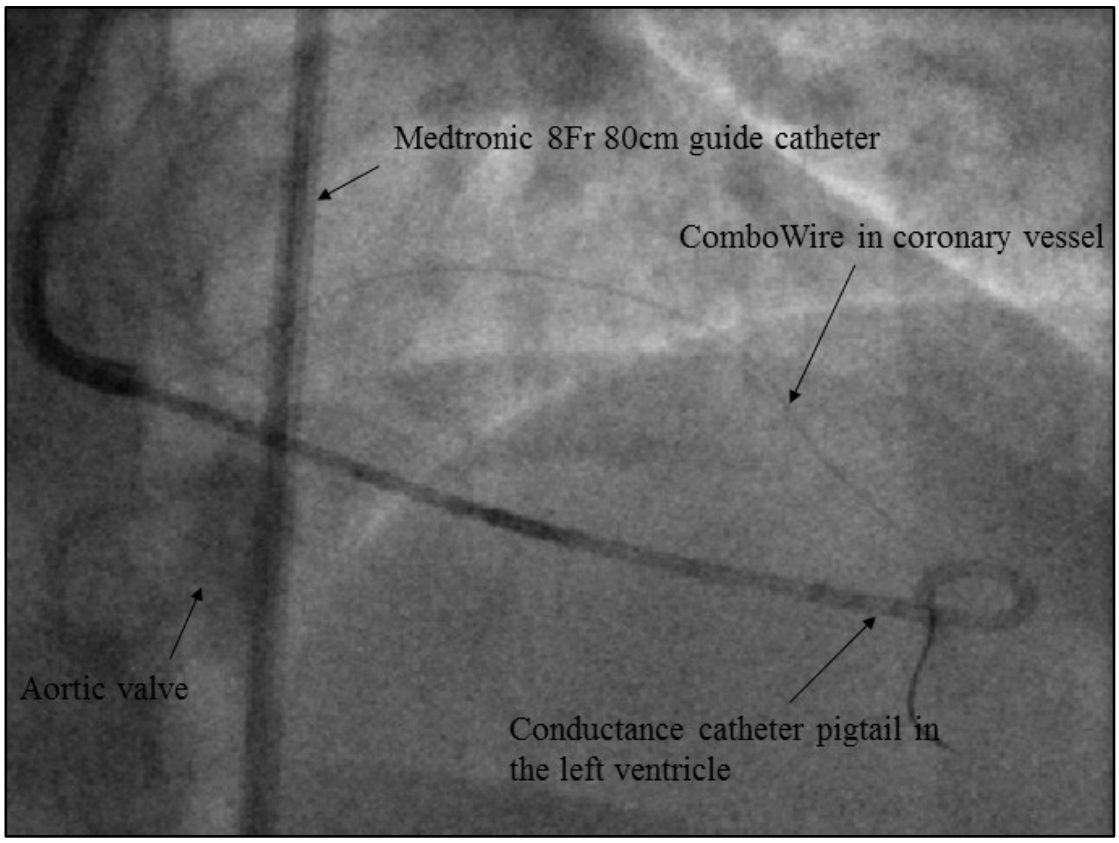


Figure 66. Instrumentation during ISDN (fluoroscopy).

Baseline measurements were taken before the patients received isosorbide dinitrate (ISDN). This was a standardised protocol: 2mL of sterile 0.1% ISDN solution was diluted 1:5 in 10ml 0.9% Saline, with a resulting drug concentration of 2mg/10mL. 1mg of ISDN was injected manually via the manifold over 5 seconds and deliver to the aortic root via the guide catheter. Continuous surface ECG recordings, left ventricular haemodynamic tracings, and coronary pressure and flow velocity signals were recorded throughout.

5.2.3 DATA ACQUISITION AND ANALYSIS

Coronary pressure and flow velocity signals were sampled at 200Hz and acquired online on the Combomap system (Volcano Corp); the coronary signals were electronically routed to the Inca (CD Leycom) to facilitate real-time simultaneous acquisition and visualisation of all (coronary and LV) haemodynamic variables. [198,199] CC measurements were acquired online using the dedicated data acquisition and analysis software (Conduct NT, version 3.18.1 CD Leycom); recording was continuous during the intervention. From the continuous recordings, at least three consecutive cardiac cycles were selected. For the purposes of analysis, the findings were separated into three stages: stage 1 at baseline, stage 2 following administration of ISDN at peak fall in LV systolic pressure (coinciding with peak fall in distal coronary pressure) and stage 3 the peak rise in LV pressure following the fall; these changes and the corresponding numbering are depicted graphically on a typical haemodynamic tracing in Figure 67. Coronary and LV data were imported into the in-house custom-made programme (King's College London, United Kingdom) for offline analysis, further details regarding the software programme and validation can be found in section 3.[198,199]

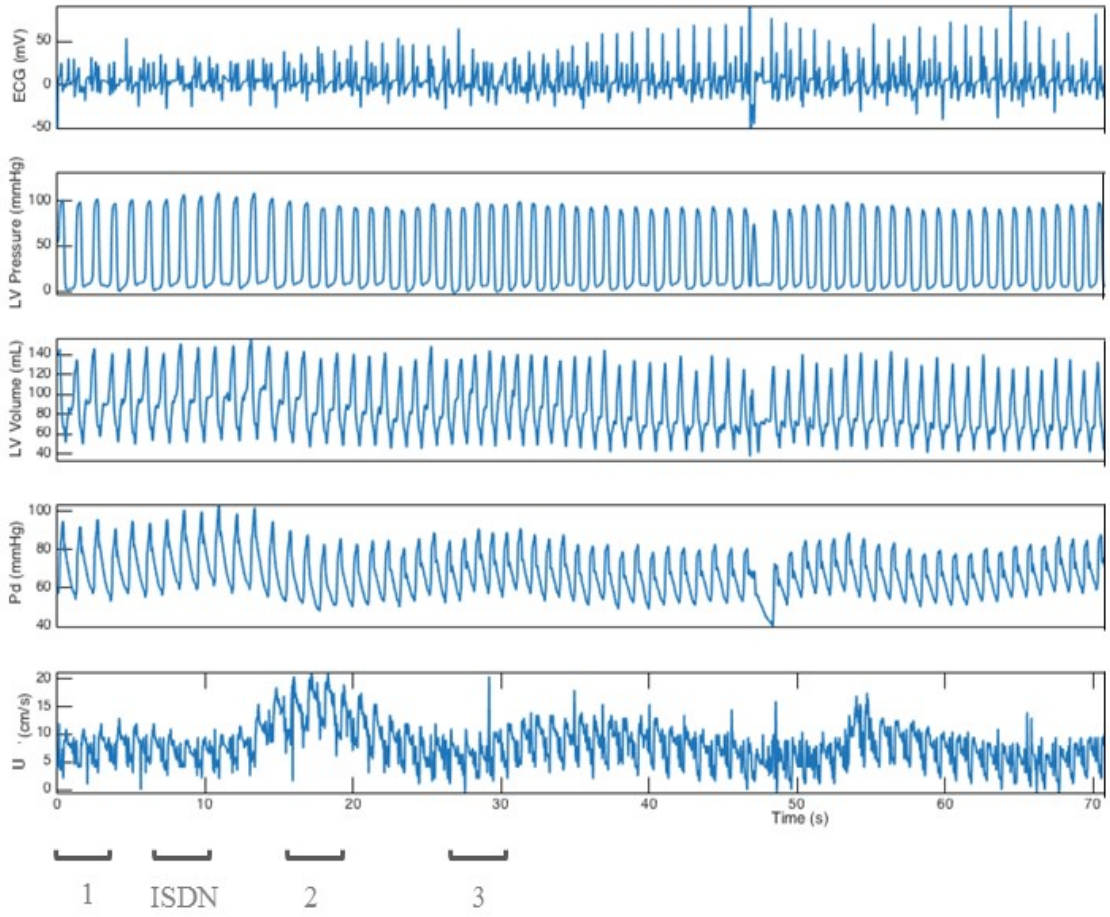


Figure 67 Simultaneous systemic and intracoronary recording.
From top to bottom panel: intra-cardiac electrocardiogram (ECG), left ventricular (LV) intra-cavity pressure, total left ventricular (LV) volume, distal coronary pressure (Pd), mean coronary blood flow velocity (U). Time points defined as baseline (1), following administration of ISDN, peak fall in LV systolic pressure (2) (coincides with peak fall in Pd) and the immediate rise in LV pressure following the fall (3).

Mean coronary blood flow velocity (U) and distal coronary pressure (Pd) were determined from the Doppler signal and high-fidelity pressure signal respectively, distal to the coronary stenosis. Pressure gradient (ΔP) across the stenosis was determined by:

Equation 21

$$\boldsymbol{Pressure\ gradient}\ \Delta \boldsymbol{P} = \frac{\boldsymbol{Pd}}{\boldsymbol{Pa}}$$

Where end-systolic pressure was used as a surrogate for mean aortic pressure.

Stenosis resistance was determined by:

Equation 22

$$\boldsymbol{Stenosis\ resistance}\ (\boldsymbol{SR}) = \frac{\boldsymbol{Pa - Pd}}{\boldsymbol{mean\ coronary\ blood\ flow}\ (\boldsymbol{U})}$$

Wave intensity analysis (WIA) explains phasic flow in terms of a series of wave fronts that underlie the changes in coronary pressure and flow velocity in the coronary arteries.[97] WIA enables separation of the local net waveform in the coronary artery into forward (arising proximally) and backward (arising distally) travelling components; thus WIA is a powerful tool for investigating cardiac-coronary interactions and has been used previously to interpret clinical data.[96,101,202] Adjustment for the non-physiological time-delay between the digitally archived signals (coronary pressure and velocity, 55ms; coronary and left ventricular pressure; 88ms) was performed[101,198] Time derivatives were obtained after smoothing the raw signals using an adaptive Savitzky-Golay filter; the adaptive filter algorithm has been shown to improve WIA robustness, thus providing an accurate standardised approach to coronary WIA.[192,196] Net wave intensity was performed and normalised to the sampling rate and separation into forward and backward components was performed using the single–point technique. [97,201] Administration of nitrates does not affect pulse wave velocity, thus baseline pulse

wave velocity measurements were implemented for WIA determination during ISDN administration to account for the limitations of the single-point technique used in determination of coronary WIA.[104]

CC measurement allows for acquisition of instantaneous LV volumes and pressure. Left ventricular conductance volumes (EDV, ESV) were calculated at the maximum rate of LV pressure rise (dP/dT_{max}) and pressure decay (dP/dT_{min}); stroke volume (SV) was calculated as the difference in these volumes, and cardiac output (CO) as the product of SV and heart rate. In addition to instantaneous LV volumes and pressure, the software calculates load-independent parameters of LV contractility.[217] The end-systolic PV relationship (ESPVR) represents the ratio of LV pressure to LV volume at the end of ventricular systole (uppermost left corner of the PV loop). The Starling contractile index (SCI) is calculated as the maximal rate of pressure change over time during isovolumetric contraction (dP/dT_{max}) normalised to end-diastolic volume (EDV). LV stroke work (SW) was calculated as the area of the PV loop; preload-recruitable stroke work (PRSW) was calculated by normalising the SW to EDV. LV stroke work was calculated as the product of peak LV peak systolic pressure and stroke volume.[193,218] Pressure volume are (PVA) a measure of total mechanical energy generated by ventricular contraction, was calculated as the sum of stroke work and elastic potential energy according to Equation 20. Systemic vascular resistance was calculated as the ratio between the pressure drop across the vascular bed and the cardiac output and decribed as Wood units (mmHg.min/L). End-diastolic pressure volume relations (EDPVR) were performed from single-beat estimations, previously validated in humans.[208] The slope of ESPVR was calculated using the single beat method (Ees),

shown to accurately reflect acute inotropic change, with minimal influence from loading conditions.[205] Arterial elastance (Ea) was calculated as the ratio of end-systolic pressure (ESP) to stroke volume (SV) to assess the impact of arterial load on the ventricle.[37] The efficiency of conversion of metabolic energy to mechanical energy was calculated as the ratio of stroke work to pressure-volume area and described as a percentage.[31]

5.2.4 STATISTICAL ANALYSIS

Statistical analysis was performed using GraphPad Prism v7.0 (GraphPad Software Inc., CA). Quantitative data are expressed as mean ± SD; categorical variables are described as proportions and percentages. Data were assessed for normality of (Gaussian) distribution both graphically and by use of the Shapiro-Wilk normality test. Statistical comparison of serial haemodynamic measurements (quantitative data) of normal distribution were performed using a repeated measures one-way analysis of variance with comparison to baseline and the previous step; repeated measures two-way analysis of variance was performed to assess for the interaction of functionally significant coronary disease within the serial haemodynamic measurements; adjustment for multiple comparisons were performed using the Bonferroni correction to generate adjusted P values. A P value < 0.05 was considered statistically significant for all tests. Results from different measurements of normal distribution were correlated using the Pearson correlation coefficient. [219]

5.3 RESULTS

Between December 2013 and April 2016, twenty patients were consented into the study. Figure 68 demonstrates the flow of patients in the study. Fifteen patients successfully completed the study protocol. Reasons for exclusion were as follows: no significant coronary disease (1), three-vessel coronary disease requiring coronary artery bypass graft surgery (1), coronary artery disease requiring rotational atherectomy (1), frailty (1); technical inability to perform pressure-volume measurements (1). Full background demographics and procedural details are shown in Table 8.

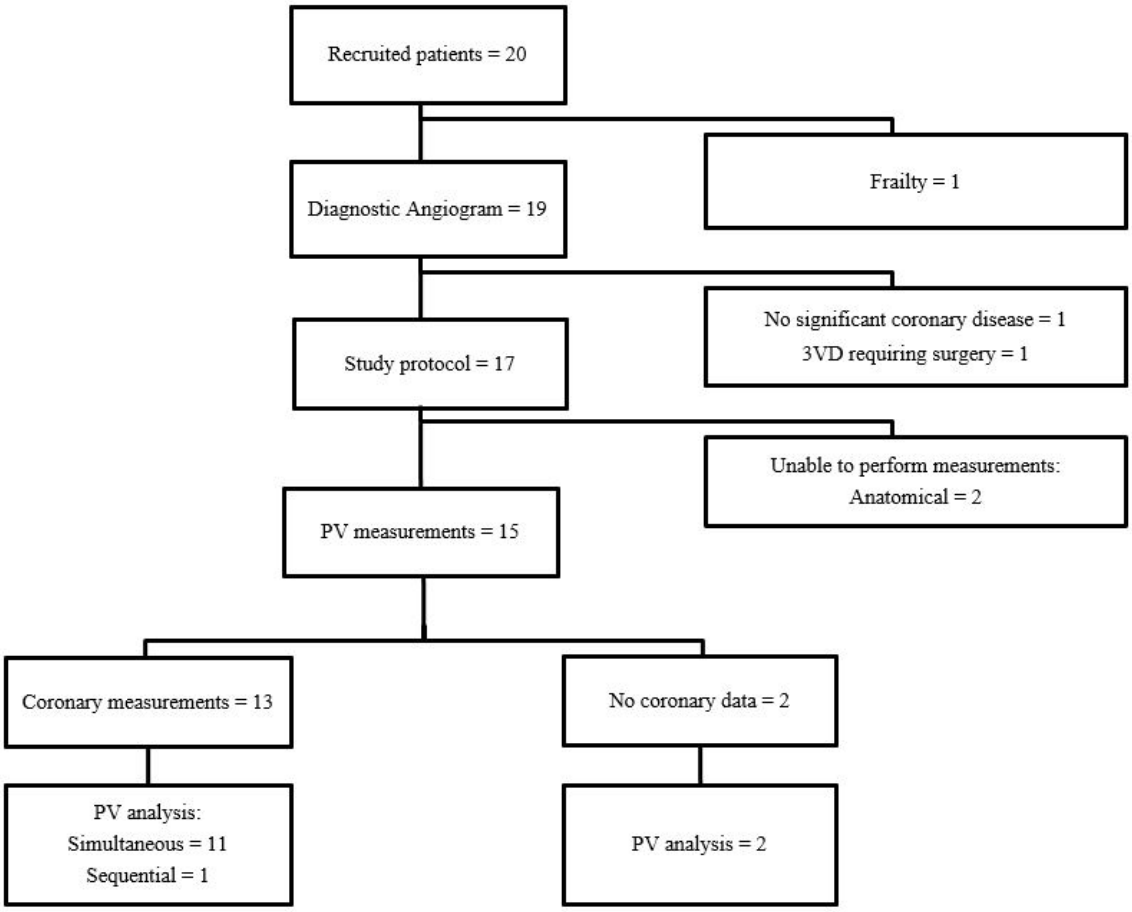


Figure 68 Patient flow diagram.
Abbreviations: 3VD three-vessel disease, PV pressure-volume loop.

Patient Demographics	Total (n=15)
Male sex	12/15 (80%)
Age, years	66±14
Height, cm	169.6±7.2
BMI kg/m^2	28.4±4.4
Previous PCI	9/15 (60%)
Previous MI	5/15 (33%)
LVEF, %	55±16
Diabetes mellitus	5/15 (33%)
Hypertension	10/15 (67%)
Dyslipidemia	5/15 (88%)
Family History	7/15 (47%)
Smoking history	2/15 (13%)
Current Medications	
Beta-blockers	10/15 (67%)
Nitrates	6/15 (40%)
Statins	12/15 (80%)
ACEi	10/15 (67%)
Aspirin	14/15 (93%)
Clopidogrel	14/15 (93%)
Procedural details	
Number of diseased vessels	1 (1 to 2)
> 50% stenosis of target lesion	15/15 (100%)
Target vessel (LAD/Cx/RCA)	13/1/2
FFR <0.8	12/15 (80%)
Duration of procedure (minutes)	76 (65 to 91)

Table 8 Baseline demographics and procedural details of study participants.
Categorical data are expressed as counts and percentages. Quantitative data that is normally distributed is described as mean +/- standard deviation; quantitative data that is not normally distributed is described as median and interquartile range (IQR). For List of Abbreviations see xvi.

Of fifteen patients, fourteen were administered intra-aortic isosorbide dinitrate and one patient received sublingual glyceryl trinitrate, therefore was not included in the final analysis. Invasive pressure-volume loop acquisition was performed in all patients; coronary physiology measurements were performed in thirteen patients (wave intensity analysis performed in eleven), simultaneous data were obtained in eleven patients; sequential coronary and LV physiological measurements were obtained in one patient.

Haemodynamic effects of Isosorbide Dinitrate

The haemodynamic effects of isosorbide dinitrate (ISDN) are summarised in Table 9. The functional significance of coronary artery disease was determined at the end of the study protocol following adenosine administration with an FFR<0.8; coronary artery disease with a resting Pd/Pa measurement of <0.8 and angiographically >70% stenosis was considered functionally significant and intravenous adenosine was not administered.[216] Of the fourteen patients who underwent final analysis, there were no significant differences in left ventricular, systemic or coronary response to nitrates between the patients who had functionally significant coronary artery disease (11) versus those who did not (3). Figure 67 shows a representative example of the signals recorded on ISDN administration. Following ISDN administration all pressures fell significantly (Figure 69). Compared to baseline (stage 1) at minimal left ventricular systolic pressure (stage 2), ISDN caused an early significant reduction in end-systolic pressure (ESP), end-diastolic and end-systolic volumes and dP/dt min ($P < 0.05$); there followed a late (stage 3) reduction in end-diastolic pressure (EDP), a sustained reduction in ESP, LV volumes, dP/dtmin and an increase in heart rate ($P < 0.05$). Overall stroke volume remained unchanged; however an early, marginal, but statistically significant, increase in cardiac output was seen compared to baseline

(4.5±1.7 versus 4.0±1.7 L/min; $P < 0.05$), predominantly driven by an increased heart rate (Figure 69). Systemic vascular resistance decreased at stage 2 compared to baseline (26±13 versus 39±22 mmHg.min/L; $P < 0.05$) and remained low. Arterial elastance, which is a component of lumped mean and pulsatile load on the left ventricle also decreased at stage 2 compared to baseline (1.7±0.8 versus 2.2±1.1 mmHg/mL; $P < 0.05$), Figure 70.

	ISDN administration (n=14)			P value		
	1	2	3	1vs2	1vs3	2vs3
HR bpm	63±11	69±14	68±11	0.14	<0.05*	>0.99
EDP mmHg	13±5	10±4	9±4	0.08	<0.001*	0.62
ESP mmHg	126±23	99±21	108±26	<0.001*	<0.05*	0.07
EDV mL	124±38	114±38	111±39	<0.05*	<0.05*	>0.99
ESV mL	56±24	46±22	49±24	<0.001*	<0.05*	0.66
EF %	55±12	59±14	55±12	0.08	>0.99	0.25
SV† mL	63±22	66±23	62±21	>0.99	0.37	0.31
CO† L/min	4.0±1.7	4.5±1.7	4.2±1.6	<0.05*	0.33	0.11
dP/dt_{max}	1282±240	1265±224	1333±228	>0.99	0.38	0.32
dP/dt_{min}	-1275±171	-1039±182	-1135±187	<0.001*	<0.05*	<0.05*
Load-independent markers of contractility						
SCI mmHg/mL/s	11±3	12±3	13±4	0.53	<0.05*	0.13
ESPVR mmHg/mL	2.6±1.2	2.5±1.1	2.5±0.9	>0.99	0.76	>0.99
PRSW mmHg	60±12	58±9	61±10	0.82	>0.99	0.35
Load independent markers of relaxation						
Tau ms	37±4	36±4	37±4	0.56	>0.99	>0.99
EDPVR Beta	5.9±0.2	5.9±0.2	5.8±0.2	>0.99	>0.99	0.06
EDPVR mmHg/mL	0.11±0.06	0.10±0.06	0.09±0.05	0.22	<0.05*	0.14
LV myocardial energetics						
SW mmHg.mL	7405±2567	6638±2491	6766±2464	<0.05*	<0.05*	>0.99
PVA (Joules)	1.5±0.5	1.2±0.4	1.3±0.5	<0.001*	<0.001*	0.26
SW: PVA %	68±10	74±9	72±10	<0.05*	<0.05*	0.43
Ventricular-arterial interaction						
SVR mmHg.min/L	39±22	26±13	31±20	<0.05*	<0.05*	0.12
Ea mmHg/mL	2.2±1.1	1.7±0.8	2.0±0.9	<0.05*	>0.99	0.13

Table 9 Haemodynamic variables following ISDN.
Data are expressed as mean±SD. List of Abbreviations see xvi. Stage 1 corresponds to baseline, stage 2 to peak LV pressure fall, stage 3 to peak LV pressure rise post fall. †Stroke volume and cardiac output calculated from the EDV at dP/dtmin and the ESV at dP/dtmax; *P<0.05 compared to baseline.

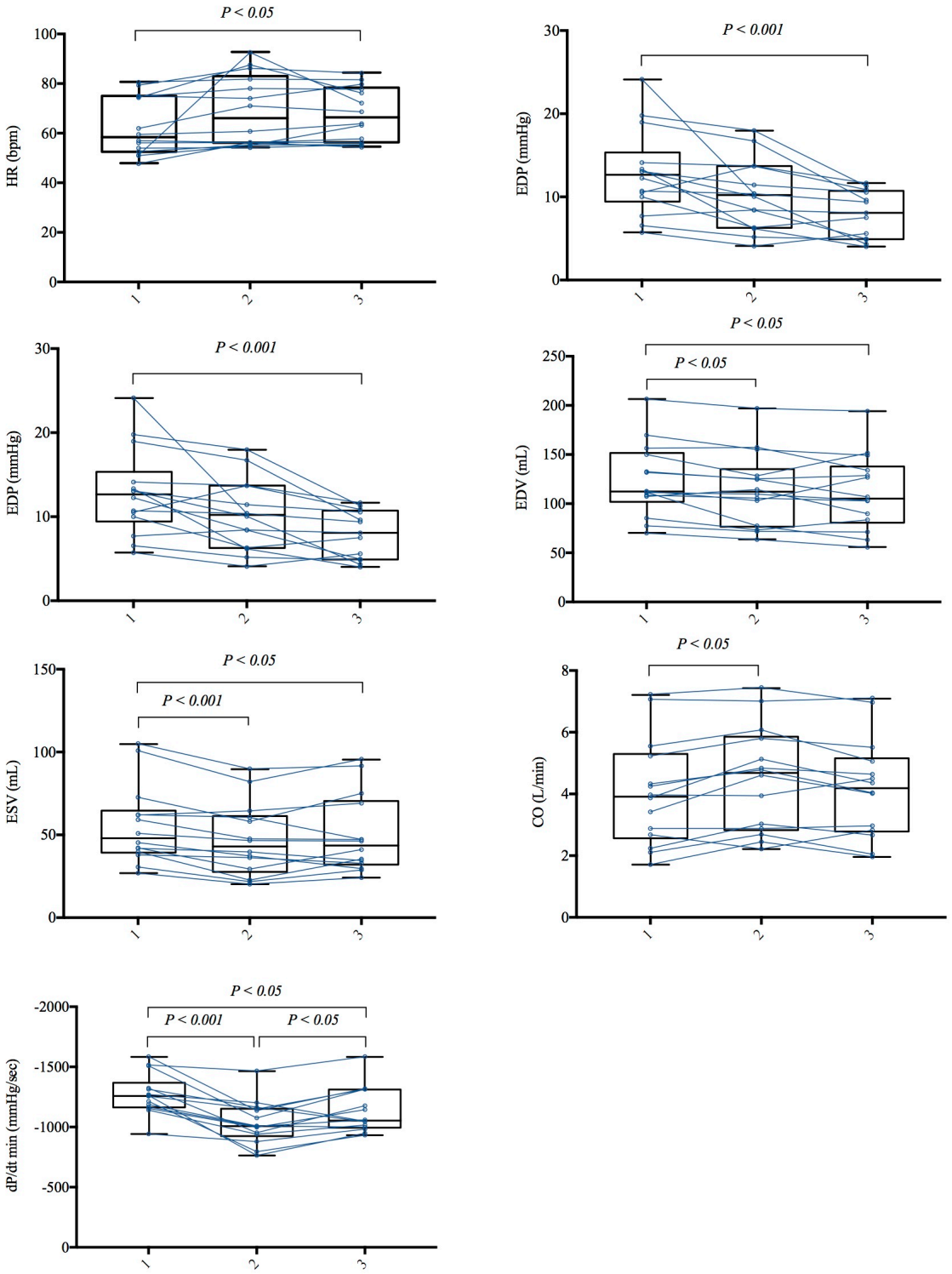


Figure 69 Graphical representation of haemodynamic change with ISDN
Heart rate (HR, beats per minute), end-diastolic pressure (EDP), end-systolic volume (ESV), the maximum rate of left ventricular pressure decay (dP/dtmin) and cardiac output (CO). Stage 1 corresponds to baseline, stage 2 to peak LV pressure fall, stage 3 to peak LV pressure rise post fall.

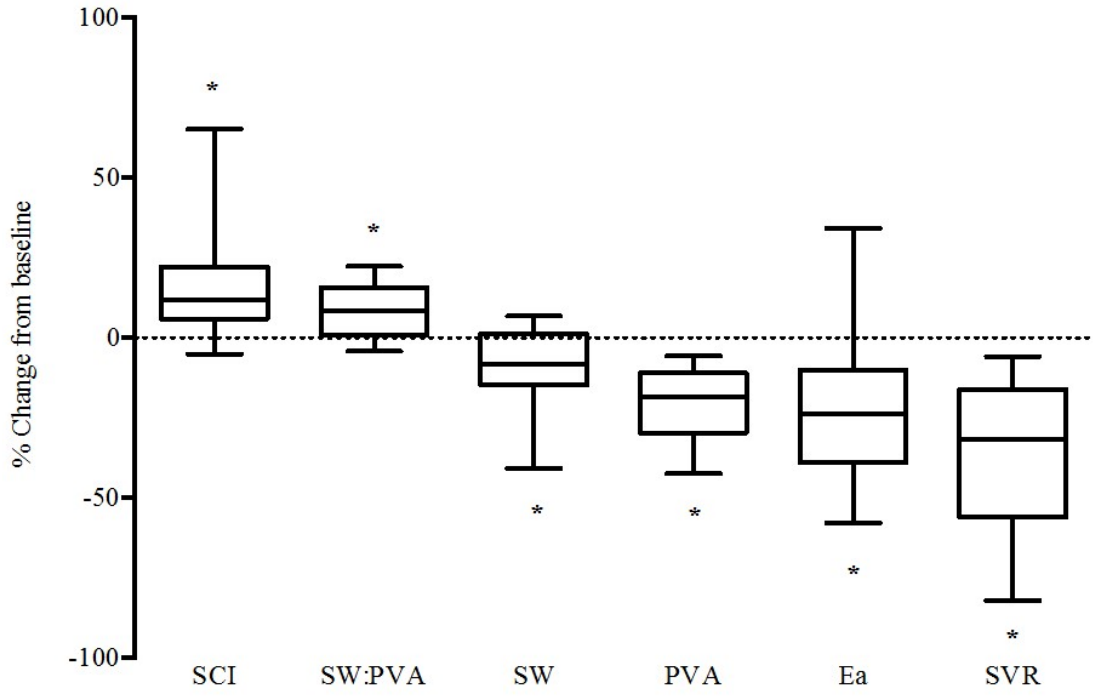


Figure 70. Percentage change from baseline following ISDN.
From left to right: Starling contractile index (SCI), stroke work: pressure volume area ratio (SW:PVA), stroke work (SW), pressure-volume area (PVA), arterial elastance (Ea), systemic vascular resistance (SVR)

Myocardial contractility, compliance and energetics

The starling contractile index (dP/dtmax normalised to end-diastolic volume), which is a load independent marker of contractility, increased at stage 3 compared to baseline (13±4 versus 11±3 mmHg/mL/s; P <0.05). However, other load independent markers of contractility (preload recruitable stroke work and ESPVR) did not. Compared to baseline, the external work performed by the heart (stroke work, SW) decreased (stages 1 and 2) (7405±2567 versus 6638±2491 mmHg.mL; P <0.05). The total mechanical energy expended by the heart (pressure volume area, PVA) also decreased compared to baseline (1.2±0.4 versus 1.5±0.5 Joules; P <0.001). Despite this, the efficiency of conversion of metabolic energy to mechanical energy (SW: PVA ratio) increased

following ISDN administration (68±10 versus 74±9 %; *P* <0.05), Figure 70. There were no significant changes in compliance (reflective of the late diastolic phase), a significant reduction in the end-diastolic pressure-volume relationship point was seen (0.11±0.06 versus 0.09±0.05 mmHg/mL; *P* <0.05); however, the slope of the EDPVR relationship remained unchanged. The changes in the pressure volume loop on administration of ISDN can be seen in Figure 71. A leftward, downward shift of the pressure-volume loop occurs, this is accompanied by a reduction in the total area of the pressure-volume loop.

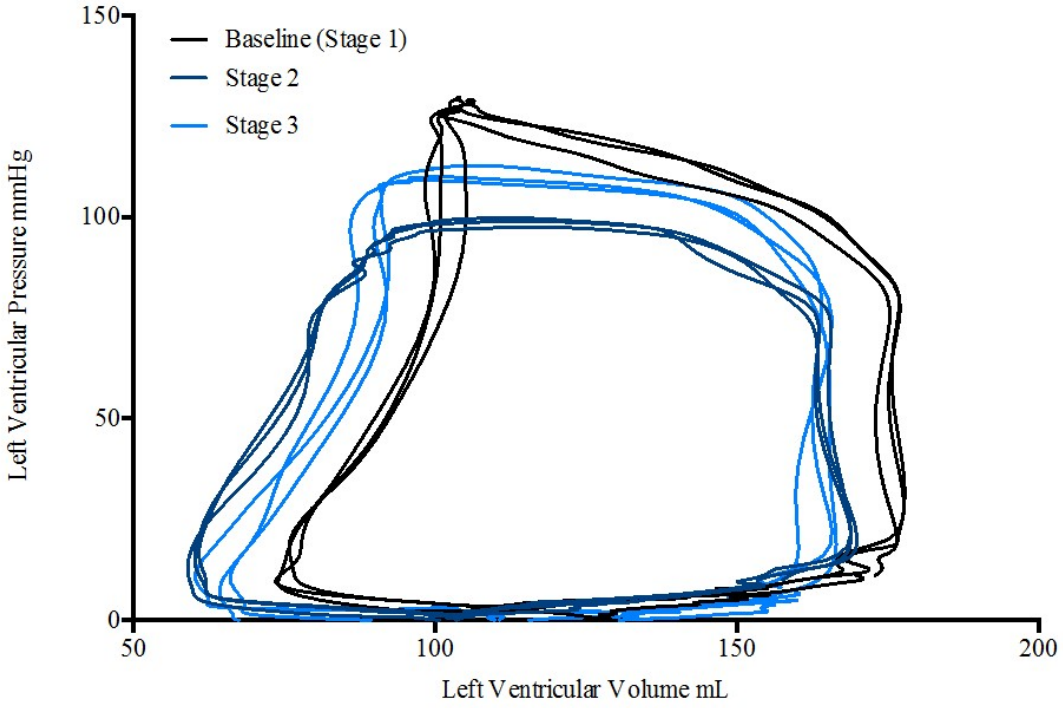


Figure 71 A representative example the pressure-volume loop following ISDN.
Stage 1 corresponds to baseline, stage 2 to peak LV pressure fall, stage 3 to peak LV pressure rise post fall.

The impact of ISDN on coronary artery disease and coronary wave energies

The coronary haemodynamic changes on administration of ISDN are summarised in Table 10. Typical examples of the haemodynamic signals obtained and the associated coronary wave intensity are depicted in Figure 72. Following administration of 1mg ISDN, an early increase in mean coronary blood velocity was seen compared to baseline (20±11 versus 13±5 cm/sec; P<0.05), this was accompanied by a decrease in mean distal coronary pressure (71±21 versus 83±21 mmHg; P<0.001); this resulted in an early decrease in microvascular resistance compared to baseline (35±29 versus 55±35 mmHg; P<0.01) with a reduction in pressure gradient across the stenosis (4.8±3.7 versus 7.2±3.8 mmHg/cm/sec; P<0.05) and stenosis resistance (2.7±3.6 versus 4.4±3.3 mmHg/cm/sec; P<0.01) (Figure 73). The increase in coronary blood velocity was not sustained, although the drop in pressure gradient and stenosis resistance persisted into stage 2. The main coronary wave energies are depicted in Figure 74 and summarised in. In all patients, the four main coronary wave energies were seen, which were in turn generated by the coronary pressure and velocity signals. At the onset of cardiac contraction, a backward compression wave or pushing wave was generated followed by a forward travelling compression or pushing wave in the coronary artery. At the onset of relaxation a forward travelling expansion wave can be seen, soon followed by a backward travelling expansion or suction wave. All the wave energies decreased following administration of ISDN (P<0.05). Interestingly, the energy of forward travelling compression wave, which is believed to be generated by left ventricular ejection, and is thought to accelerate flow, correlated with the ventricular-arterial interaction (r = -0.5; P<0.05), Figure 74.

	ISDN administration (n=14)			**P value**	**Multiple comparison**		
	1	2	3		1vs2	1vs3	2vs3
U cm/sec	13±5	20±11	18±15	0.1			
Pd mmHg	83±21	71±21	77±23	<0.05	<0.001*	0.10	0.13
ΔP mmHg	55±35	35±29	42±30	<0.05	<0.01*	<0.01*	0.07
SR mmHg/cm/sec	4.4±3.3	2.7±3.6	3.2±3.2	<0.05	<0.01*	<0.01*	0.20
MR mmHg/cm/sec	7.2±3.8	4.8±3.7	6.0±3.8	<0.001	<0.001*	<0.01*	0.06
DTF %	66±3	65±5	64±3	0.1			
Coronary Wave Energies†							
BCW $J/m^2/sec^2x10^3$	-6.0±3.6	-4.0±2.9	-4.5±3.3	0.08			
BEW $J/m^2/sec^2x10^3$	-8.3±5.1	-5.1±4.0	-4.0±2.4	<0.05	0.07	<0.05*	0.47
FCW $J/m^2/sec^2x10^3$	5.9±3.5	3.8±3.0	3.4±2.4	<0.05	<0.01*	<0.05*	>0.99
FEW $J/m^2/sec^2x10^3$	3.9±2.9	3.3±2.7	2.8±2.0	0.2			

Table 10 Coronary haemodynamics and wave energies
P values calculated by repeated measures ANOVA followed by bonferroni correction for multiple comparisons. *P<0.05 compared to baseline; †Total number of patients 11. Stage 1 corresponds to baseline, stage 2 to peak LV pressure fall, stage 3 to peak LV pressure rise post fall. For list of Abbreviations see xvi.

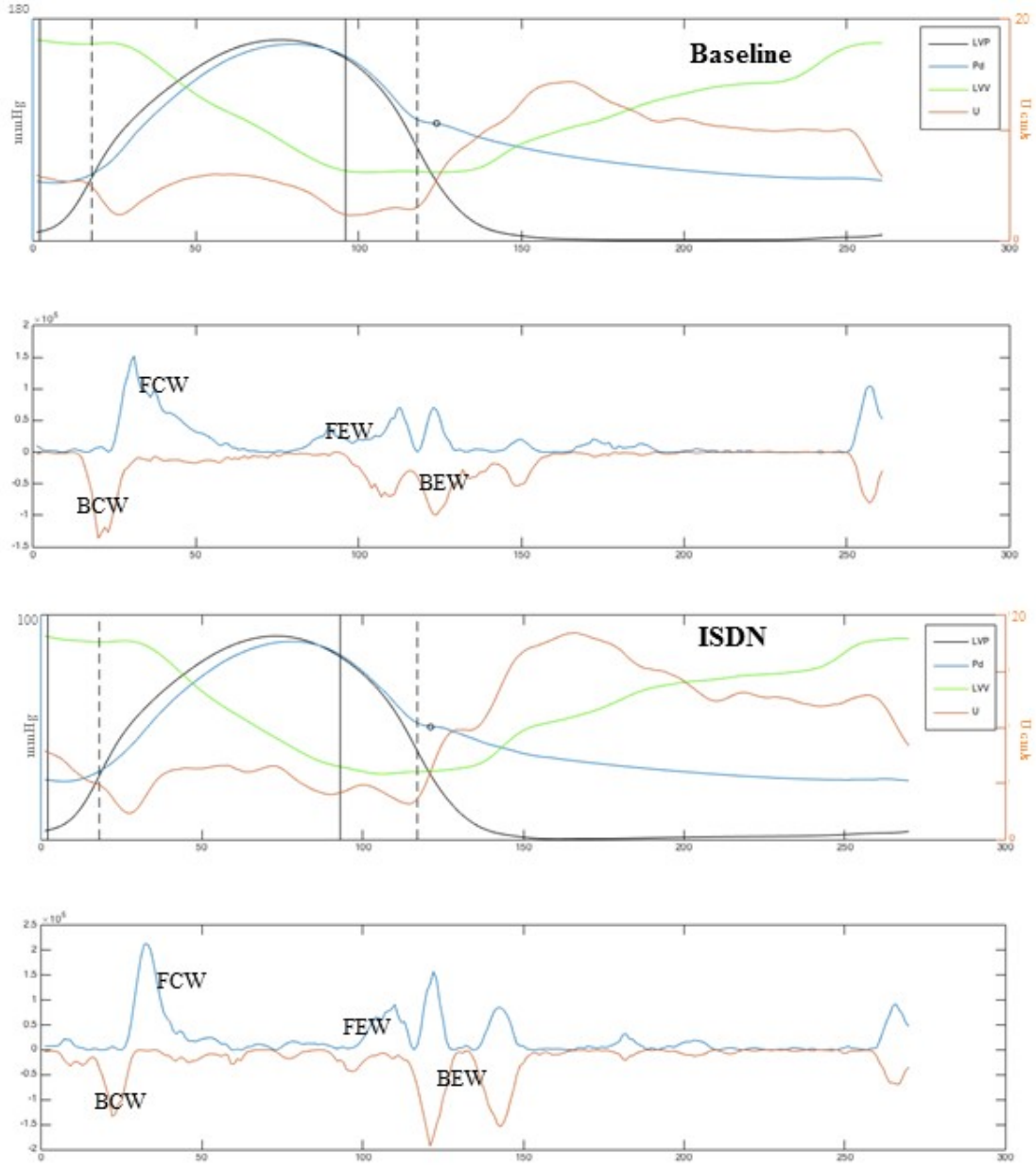


Figure 72 Typical haemodynamic tracings and wave intensity analysis.
Changes in coronary wave intensity at stage 2 of ISDN administration (lower frame) compared to baseline (upper frame). The cardiac cycles have been ensemble-averaged (above) and corresponding wave intensity generated ($Jm^{-2}s^{-2}x10^{5}$) (below).

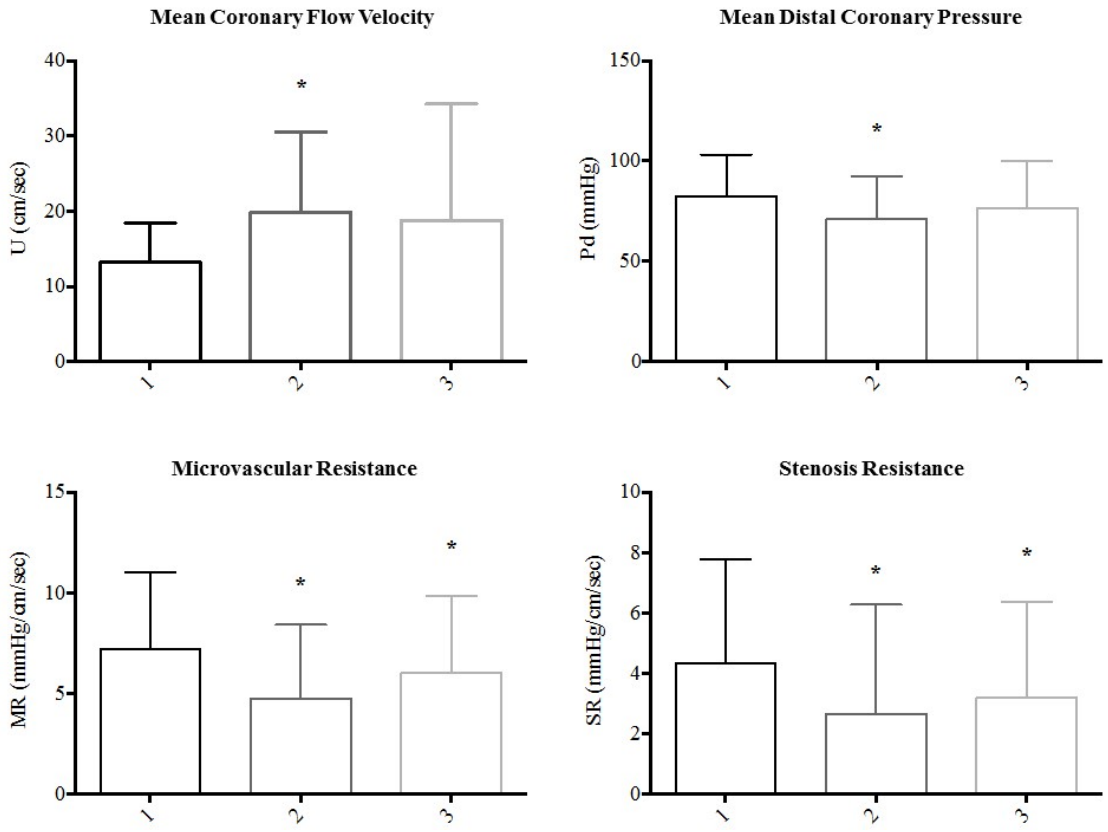


Figure 73 Changes in coronary haemodynamics.
Stage 1 corresponds to baseline, stage 2 to peak LV pressure fall, stage 3 to peak LV pressure rise post fall; mean coronary blood flow velocity (U; top left); distal coronary pressure (Pd; top right); microvascular resistance (MR; bottom left) and stenosis resistance (SR; bottom right); *P<0.05 compared to baseline.

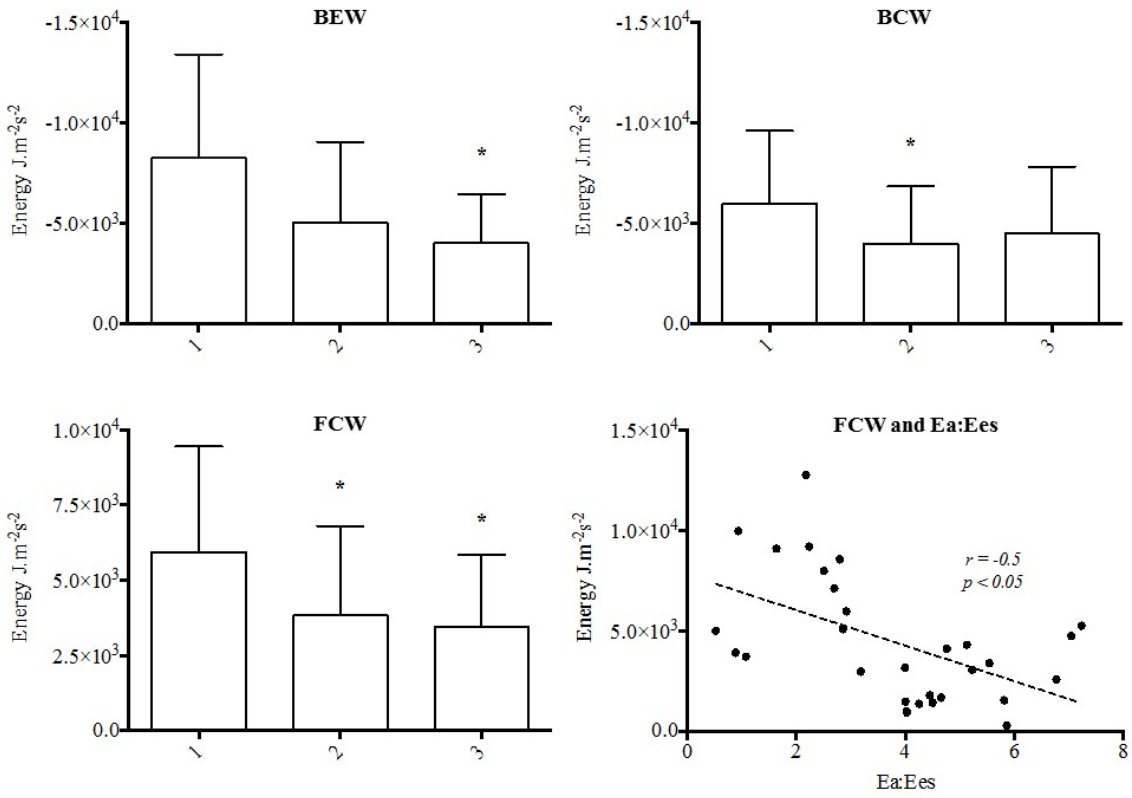


Figure 74 Changes in the coronary wave energies.
Stage 1 corresponds to baseline, stage 2 to peak LV pressure fall, stage 3 to peak LV pressure rise post fall; backward expansion wave (BEW, top left), backward compression wave (BCW, top right); forward compression wave (FCW, bottom left); *P<0.05 compared to baseline; Correlation of forward compression wave with cardiac mechanics: the ratio of arterial elastance (Ea) to contractile function (Ees) (bottom right).

5.4 DISCUSSION

This study shows that in patients with coronary artery disease, the beneficial effects of nitrates in preventing or reducing ischaemia is due to a complex interplay of cardiac, coronary and systemic changes. The main findings can be summarised as follows: 1) ISDN administration drives a reduction in preload and afterload, decreasing total mechanical energy expenditure and therefore myocardial oxygen consumption; 2) a leftward downward shift of the pressure-volume loop has favourable effects on left ventricular energetics, increasing the efficiency of energy conversion to external work 3) early coronary vasodilatation with a temporary increase in coronary blood flow velocity is followed by a reduction in the pressure gradient and stenosis resistance suggestive of stenosis dilatation. ISDN administration did not have a demonstrable effect on intrinsic myocardial properties, with no change in compliance or contractility seen.

LV preload, afterload and myocardial oxygen consumption

Isosorbide dintrate is known to be a potent vasodilator of smooth muscle; with differential effects on the venous and arterial circulation; Imhof et al demonstrated that at relatively low doses of nitroglycerin, venodilatation was maximal; however, higher doses were required to induce systemic arterial vasodilatation, the latter increasing progressively with increasing doses of nitroglycerin.[235,236] In this study, the administration of 1mg intra-arterial ISDN resulted in both a preload and afterload reduction; these findings are consistent with both venodilatation and arterial vasodilatation. Following ISDN administration all pressures fell significantly, as venodilatation has been shown to maximal at low doses of ISDN and not dose

dependent, it can be concluded that the preload reduction was a result of venous pooling.[235] We also demonstrated a significant reduction in invasive, accurate measures of afterload: an early and sustained decrease in systemic vascular resistance was demonstrated, and a measured reduction in arterial elastance. Acute reductions in LV loading conditions have been previously shown to reduce myocardial oxygen demand;[38] these findings are consistent with the changes in the pressure-volume loop demonstrated in this study: a decrease in total mechanical energy expenditure (or pressure-volume area, PVA) was effected by nitrates, and PVA is linearly related to myocardial oxygen consumption (MV02).[8] The intrinsic myocardial properties were not affected; although no change in myocardial compliance was demonstrated, the end-diastolic pressure to volume ratio decreased, this can be seen clearly consistent with a left shift of the pressure volume loop. These findings consistently support that one of the major mechanisms of nitrates, at this plasma concentration, is driven by both a preload and afterload reduction, reducing demand. Following the peak fall in LV pressure post-ISDN administration, an increase in heart rate and immediate increase in LV systolic pressure occurred. This may well be explained by ISDN-induced vasodilatation triggering baroreceptor activity in these patients, with a reflex sympathetic response. De Coster et al noted similar findings following administration of intracoronary ISDN.[225]

Coronary haemodynamic effects and wave intensity analysis

The results of this study demonstrate that the anti-ischaemic effects of nitrates are at least partially mediated by coronary vasodilatation. We directly measured coronary blood flow velocity and distal coronary pressure. The administration of ISDN was associated with an immediate sudden increase in coronary blood flow velocity, a

decrease in distal coronary pressure and therefore an overall reduction in microvascular resistance; this was not sustained, however, despite a reduction in aortic perfusion pressure, the pressure gradient across the coronary lesions decreased with an accompanied decrease in stenosis resistance, this reduction was in the region of 30 to 40%. These findings are consistent with earlier work performed by Brown et al. They measured luminal area in diseased and normal portions of coronary arteries using coronary angiographic data. They demonstrated a 38% reduction in stenosis resistance in severely diseased vessel, the greater the stenosis, the more marked the percentage gain in luminal area.[169] De Coster et al also concluded shat the anti-ischaemic effect of nitrates was due to stenosis dilatation and increased perfusion, although they did not measure coronary artery diameter or blood flow directly.[225] Interestingly, this study has demonstrated in cohort of patients with ischaemic heart disease a very similar pattern of systemic, cardiac and coronary effects, whereas previous studies have shown marked inter-patient variability. Furthermore, the beneficial coronary effects were demonstrated in the absence of exercise-induced angina, bringing into question the early theory that nitrates only exhibit a beneficial effect in the presence of peripheral vasodilatation.[169,224]

All the wave energies decreased following administration of ISDN, this was despite the observed decrease in microvascular and stenosis resistance. The reduction in wave energies mirrored the drop in left ventricular and systemic pressure. As shown in section 3.3.4, the forward travelling waves are more dependent on the ventricular-arterial interaction than initially thought; we have previously shown that these waves are delimited by diastolic blood pressure. Interestingly, and consistent with these findings, the energy of forward travelling compression wave that is believed to

accelerate flow correlated with ventricular-arterial coupling (Ea:Ees ratio). These findings would support the hypothesis generated in section 3.3.4.

5.5 LIMITATIONS

The coronary findings were suggestive of stenosis dilatation, which may not be angiographically detectable; total myocardial blood flow was not measured, therefore redistribution of myocardial blood flow and collateral blood flow was not assessed. The action of ISDN on coronary artery stenosis is not clear in the absence of vasoconstriction, and at the site of a severe stenosis there may be a degree of ischaemia at rest. However, the main advantage of this current body of work is the use of very accurate measures of coronary and left ventricular haemodynamics enabling definitive observations and description of the cardiovascular response as a whole.

5.6 CONCLUSION

In this study the anti-anginal mechanism of nitrates in patients with ischaemic heart disease has been shown to be mediated by its vasodilatory effects on the systemic vasculature and the coronary circulation; both a reduction in demand and an increase in blood supply were seen.

6 THREE-DIMENSIONAL MYOCARDIAL DEFORMATION IMAGING: A NOVEL NON-INVASIVE MEASURE OF CONTRACTILITY

INTRODUCTION

Subclinical systolic and diastolic left ventricular (LV) dysfunction have been shown to be independently related to atherosclerosis. 3D speckle tracking echocardiography (3DSTE) is a relatively new technique that provides a more comprehensive evaluation of LV mechanics than has previously been possible. Deformation imaging has been shown to detect subclinical myocardial dysfunction earlier than biomarkers or conventional echocardiographic indices. Identifying non-invasive parameters that closely reflect contractility and relaxation is of high importance (ideally during resting conditions); there is a need for validation of parameters of mechanical dyssynchrony with myocardial properties. The aim of this study was to correlate non-invasive parameters of strain obtained by 3DSTE with invasive load-independent measures of LV function.

METHODS

16 patients with ischaemic heart disease and preserved LV function underwent invasive simultaneous left ventricular pressure-volume loop assessment in the cardiac catheter laboratory under resting conditions followed by 3DSTE data acquisition. Global LV longitudinal (GLS), circumferential (GCS), and radial strain was compared with left ventricular haemodynamic assessment. Quantitative data were compared by use of Student t-test; ategorical data were compared by use of the Fisher exact test; results from different measurements were correlated with Pearson’s correlation coefficient;

receiver-operating characteristics (ROC) curves were generated for echocardiographic measures of LV function

RESULTS

GCS correlated with end-systolic pressure volume relationship (ESPVR: $r = -0.8$; $P < 0.001$), pre-load recruitable stroke work (PRSW: $r = -0.6$, $P = 0.002$) and the starling contractile index (SCI: $r = -0.7$; $P < 0.01$) more than GLS. However GLS generated the greatest area-under the curve for the ROC curves (AUC = 0.7, SE=0.1), compared to GCS (0.5, SE=0.1).

CONCLUSIONS

The use of 3DSTE for prediction of contractile function is feasible in a cohort of patients with ischaemic heart disease. Close correlation with PV loop analysis suggests that 3DSTE has the potential for use in prognostication and risk stratification.

6.1 INTRODUCTION

Among patients with suspected coronary artery disease (CAD), risk categorisation based on clinical characteristics is traditionally used to identify patients who would benefit from diagnostic testing.[237,238] Identification of left ventricular (LV) systolic or diastolic dysfunction significantly increases the likelihood of significant CAD and therefore need for further investigation.[239,240] In those without overt dysfunction, stress echocardiography has traditionally been used as a widely available low-cost approach to detection of ischaemia and contractile reserve; however, its assessment remains subjective requiring adequate training of the observer.[241] Importantly, the presence of subclinical LV dysfunction has also been suggested as a marker of CAD; both subclinical systolic and diastolic dysfunction have been shown to be independently related to CAD, providing incremental value over traditional risk stratification.[49,242] Several studies have demonstrated that progressive subclinical LV diastolic dysfunction is related to the degree of atherosclerosis; the effect of repeated subclinical ischaemia either leading to impaired relaxation or remodelling of the myocardium.[243,244] Myocardial deformation imaging enables frame-by-frame tracking of speckle patterns on grey-scale images to calculate the variation of the segment length from baseline.[245,246] 3D speckle tracking echocardiography (3DSTE) is a relatively new technique that provides a more comprehensive evaluation of left ventricular mechanics from 3D datasets than has previously been possible, with lower rates if inter- and intra-observer variability.[247] Detection of impaired myocardial mechanics by deformation imaging has been shown to detect subclinical myocardial dysfunction earlier than biomarkers or conventional echocardiographic indices of ventricular function; in

clinical studies of cardiotoxic agents and thyroid carcinomas, early left ventricular systolic and diastolic dysfunction demonstrated by impaired longitudinal and circumferential strain were seen relative to baseline.[248,249] Deformation imaging as an adjunct to stress echocardiocardiography has been shown to increase its predictive value.[51] Global measures of strain have been shown to have superior prognostic properties over left ventricular ejection fraction alone. The validity of which has been extensively studied in pre-clinical and clinical non-invasive studies.[245,250] The gold standard for assessing left ventricular chamber properties is using invasive LV pressure-volume analysis and invasive measures of coronary blood flow velocity and pressure respectively. Invasive LV haemodynamic assessment enables derivation of load-independent markers of both contractility and relaxation, accurately reflecting systolic and diastolic function respectively.[195] There is a need for a more specific validation of parameters of strain that correlate with contraction and relaxation.[53,251] Only one animal study and no human studies have investigated the relationship between strain and with invasive measures of systolic function, identifying non-invasive parameters that closely reflect contractility and relaxation is of high importance (ideally during resting conditions); serial assessment of systolic and diastolic dysfunction with non-invasive testing for prognostication and risk stratification purposes in patients with a known history of coronary artery disease could be an important issue for clinical investigation and may be a feasible alternative to stress echocardiography in certain cohorts of patients.[53] The aim of this study was to examine patients with preserved LV ejection fraction with a history of coronary artery disease but in the absence of significant atherosclerosis, to correlate non-invasive parameters of strain obtained by 3DSTE with invasive load-independent measures of LV function.

6.2 METHODS

6.2.1 STUDY POPULATION

Patients were considered suitable if they had a left ventricular ejection fraction (LVEF) >50% on two-dimensional echocardiography with non-obstructive coronary artery disease on coronary angiography. Patients were between 18 and 90 years of age. Patients were excluded from the study if it was not possible to obtain adequate 2D (parasternal or any of the 3 apical views) or 3D datasets for analysis (>2 segments not be visualised or visible translational artefacts). Patients were excluded if they had LV regional wall motional abnormalities, functionally significant coronary artery disease, a history of cardiomyopathy, the presence of significant valvular heart disease (moderate or severe), or had undergone previous coronary artery bypass grafting. The study was approved by the National Research Ethics Committee to be performed at St Thomas' Hospital, London, UK. All patients gave written informed consent prior to undertaking the study. All patients underwent LV PV measurements in the cardiac catheter laboratory followed by 3D echocardiography.

6.2.2 HAEMODYNAMIC MEASUREMENTS

Patients underwent cardiac catheterisation via the right femoral artery using a 6Fr femoral sheath (Terumo). Left and right coronary angiograms were performed as per standard protocol to assess for coronary artery disease. On identification of atheroma, a standard 6Fr guide catheter was used to engage the coronary ostium of the target vessel with introduction of dual-sensor pressure flow wire to the target vessel; intravenous

adenosine was administered to identify functionally significant coronary artery disease (FFR<0.8), patients underwent angioplasty if necessary.[92] Access via the right femoral arterial sheath was then used to perform baseline simultaneous LV pressure volume (PV) measurements, three sequential recordings of 30 seconds to 1 minute, with the patient in a supine position. This was performed using a 4Fr conductance catheter CD Leycom, Zoetermeer, Netherlands). The specifications of the conductance catheter (CC) are described in section 2.2.1, and the set-up and calibration techniques are described in section 2.2.3.2. In brief, this flexible pigtail catheter (no inner lumen) is introduced into the LV using guide catheter (commercially available 6 Fr 80cm Judkins Right 4.0 Launcher; Medtronic). The CC has 10 equally spaced electrodes with a solid-state pressure sensor and is connected to a PV signal processor (Inca, CD Leycom); continuous LV volume tracings are calculated by measuring parallel electric conductance between adjacent ventricular blood segments delineated by selected catheter electrodes; this technique has been shown to reflect LV segmental volumes in pre-clinical and clinical studies and has been utilised in the assessment of heart failure device therapies.[183,193,195] Accurate CC positioning is confirmed by fluoroscopy and on inspection of the segmental PV loop signals. Measurements were performed during steady-state conditions, avoiding excessive arrhythmia from premature beats. Recorded variables were averaged from 10 cardiac cycles to minimise inaccuracies from beat-to-beat variation and change in venous return from respiration; repeat baseline recordings ensured reproducibility of CC measurements.

6.2.3 2D ECHOCARDIOGRAPHY

2D echocardiography was performed by Dr Kapetenakis using a commercially available system: Sonos 7500 (Philips) with an S5-1 transducer. LV dimensions and fractional shortening were obtained with M-mode from the parasternal long axis view. Apical 2- and 4-chamber views were acquired for calculation of LVEF with biplane method of disks. Pulsed Doppler was used to calculate the myocardial performance index. Analyses were subsequently performed offline with EchoPac.

6.2.4 3D REAL-TIME TRANSTHORACIC ECHOCARDIOGRAPHY

3DRTE uses the X4 matrix array transducer to obtain pyramidal volume in real-time. This has previously been described, in summary, full volume acquisition (FVA) is necessary to visualise the entire LV, and thus 4 smaller real-time volumes are acquired from alternate cardiac cycles and are combined to provide a larger pyramidal volume (Figure 75). FVA is performed during breath hold and requires a relatively stable R-R interval to minimise translation artefacts between the 4 acquired sub-volumes. Apical FVAs of the LV were obtained in all patients. To optimise the frame rate of acquisition, depth was minimised to include mitral and aortic valves only, required for spatial orientation in subsequent analyses. The endocardial border was semi-automatically detected and traced with an LV cast created (Figure 75B) that provides LV time-volume data for one cardiac cycle. This is then subdivided into pyramidal sub-volumes to obtain time-volume data for each of the 16-myocardial segments. All acquisitions were digitally stored for offline analysis by TomTec software (TomTec Imaging Systems, Unterschleissheim, Germany). LVEF was determined as follows:

Equation 23

$$\boldsymbol{LVEF = \left[\frac{LVEDV - LVESV}{LVEDV}\right] x\ 100}$$

Total LVEF was automatically generated by the software volume changes during the cardiac cycle. The LV mass was calculated as:

Equation 24

$$\boldsymbol{(LV\ epicardial\ volume - LV\ endocardial\ volume) x\ 1.05 (g/mL)}$$

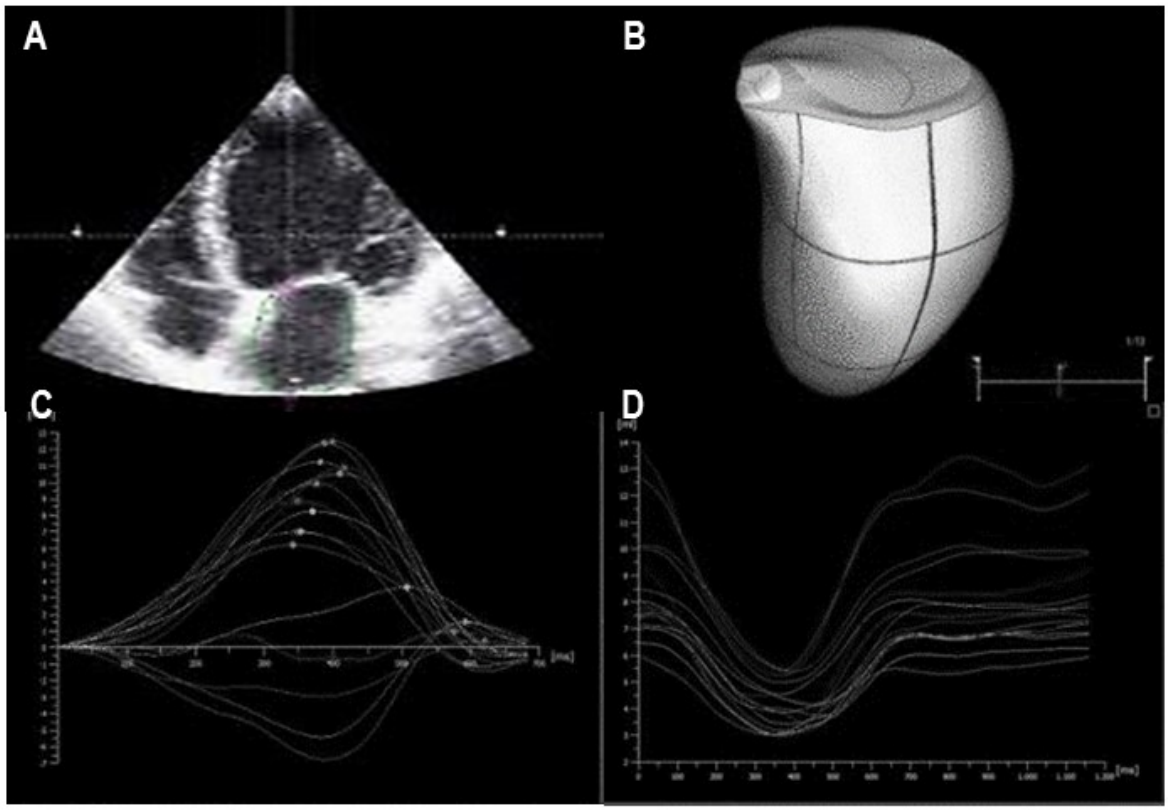


Figure 75 Full volume analysis
Full volume analysis (A); LV cast produced by quantitative analysis (B); regional volume curves in normal systolic function (C); global volume curves in normal systolic function (D)

6.2.5 SPECKLE-TRACKING ECHOCARDIOGRAPHY

As mentioned previously, relative deformation imaging enables characterisation of regional and global myocardial function. 3D strain describes the tangential deformation of the longitudinal and circumferential strain components. 3D strain measurements of the LV were performed using 3DSTE, following import of 3D full volume datasets analysed by a highly experienced investigator using vendor-independent 3D speckle tracking software (4D LV analysis, version 3.1.2. TomTec Imaging Systems). Automatic reconstruction of the 3D endocardial surface was performed on identification of the apex and mitral annular line within the largest LV long-axis dimensions, performed in both end-diastolic and end-systolic frames. Manual adjustment of the endocardial border was performed when necessary. For strain analysis, the LV was divided into 16 myocardial segments (described above); the software provided averaged longitudinal, circumferential, radial and 3D strain time curves from each segmental strain-time curve, from which peak global strain was determined. Systolic timing dispersion index (SDII), defined as the difference between the earliest (#1) and the most delayed (#2) peak systolic phase (%) among the 16 cardiac segments. Second was the systolic dyssynchrony index (SDI) described by Kapetanakis et al., defined as the systolic dyssynchrony of peak systolic phases in the 16 cardiac segments, which is a simple reproducible method of quantifying global LV dyssynchrony. [251,252]

6.2.6 DATA ANALYSIS

CC data analysis was performed with dedicated data acquisition and analysis software (Conduct NT, version 3.18.1, CD Leycom). Conductance volumes (EDV, ESV) were calculated at the maximum rate of LV pressure rise (dP/dt+) and pressure decay (dP/dt-),

stroke volume was calculated as the difference in these volumes. In addition to instantaneous LV volumes and pressure, this software calculates load-independent parameters of LV contractility.[217] The end-systolic PV relationship (ESPVR) represents the ratio of LV pressure to LV volume at the end of ventricular systole (uppermost left corner of the PV loop). The Starling contractile index (SCI) is calculated as the maximal rate of pressure change over time during isovolumetric contraction (dP/dT_{max}) normalised to end-diastolic volume (EDV). LV stroke work (SW) was calculated as the area of the PV loop; preload-recruitable stroke work (PRSW) was calculated by normalising the SW to EDV. LV stroke work was calculated as the product of peak LV peak systolic pressure and stroke volume.[193,218] Pressure volume area (PVA) was calculated as according to Equation 20.

6.2.7 STATISTICAL ANALYSIS

Statistical analysis was performed using GraphPad Prism v7.0 (GraphPad Software Inc., CA). Quantitative data are expressed as mean±SD, categorical variables are described as proportions and percentages. Data were assessed for normality of (Gaussian) distribution both graphically and by use of the Shapiro Wilk's test. Statistical comparison of categorical data was performed using paired student t-tests were performed. Statistical comparison of quantitative data not falling within a normal distribution was performed using the Friedman test. Categorical data were compared by use of the Fisher exact test. Results from different measurements were correlated with Pearson's correlation coefficient. A P value of <0.05 was considered statistically significant for all tests.

6.3 RESULTS

Between March 2014 and November 2015, 21 patients were recruited into the study. 16 patients successfully completed the protocol. Reasons for exclusion were as follows: inability to obtain adequate echocardiographic datasets (4) procedure related complication during angioplasty leading to type 2 myocardial infarction (1). Full background characteristics, cardiac risk factors and current anti-anginal therapy of the patient cohort are shown in Table 11. The patients' clinical characteristics were representative of a cohort of patients with ischaemic heart disease. Invasive left ventricular pressure volume loops assessment and myocardial deformation imaging was performed in all patients and the data are presented in Table 12; myocardial deformation imaging (strain analysis) and PV loop assessment were performed by two independent observers.

Demographic	**Total (n=17)**
Age (years)	65±12
Male sex	13/17 (76%)
Height (cm)	168±7
Body Mass Index (kg/m^2)	28.8±3.3
Cardiac Risk Factors	
Hypertension	14/17 (82%)
Diabetes Mellitus	9/17 (53%)
Hypercholesterolaemia	14/17 (82%)
Smoking History	11/17 (65%)
Previous Myocardial Infarction	3/17 (18%)
Previous Percutaneous Coronary Intervention	10/17 (59%)
Family History	8/17 (47%)
Medications	
Beta-Blocker	14/17 (82%)
Statin	2/17 (12%)
Nitrate	1/17 (6%)
ACEi/AIIRB	13/17 (76%)
Calcium Channel Antagonist	5/17 (29%)
Nicorandil	2/17 (12%)
Aspirin	15/17 (88%)
Clopidogrel	15/17 (88%)

Table 11 Baseline demographics.
The baseline characteristics, cardiovascular risk factors and current medications of study participants is described. Categorical data are expressed as counts and percentages. Quantitative data that is normally distributed is described as mean +/- standard deviation

3D Echocardiographic Parameters	
LV Mass, grams	137.4±10.2
Global Longitudinal Strain %	-16.7±9.3
Global Circumferential Strain %	-26.3±16.0
Twist degrees/sec	12.5±8.1
Torsion degrees/cm	1.5±1.0
Systolic Dyssynchrony Index %	5.2±1.9
Systolic Timing Dispersion Index %	9.3±5.3
Pressure-Volume Loop Assessment	
Markers of Contractility	
dP/dT max, mmHg/sec	1376±61
End-Systolic Pressure Volume Relationship, mmHg/mL	4.0±0.8
Starling Contractile Index, **mmHg/mL/s**	14±1
Preload Recruitable Stroke Work, mmHg	70±6
Markers of Relaxation	
dP/dT min, mmHg/sec	-1404±62
End-Diastolic Pressure Volume Relationship, mmHg/mL	0.16±0.07

Table 12 Echocardiographic parameters and LV PV loop assessment.
Categorical data are expressed as counts and percentages. Quantitative data that is normally distributed is described as mean +/- standard deviation.

Correlations between PV measurements and 3DSTE parameters

In the cohort of patients with ischaemic heart disease, myocardial deformation imaging accurately reflected left ventricular myocardial mechanical properties. As would be expected, left ventricular mass correlated with stroke work (the external work performed by the heart for contraction) (SW: r=0.6; $P < 0.05$) and the pressure volume area (total mechanical energy expenditure of the heart) (PVA: r= 0.8; $P < 0.01$). The measure of global circumferential strain (GCS) correlated with load-independent markers of contractility: the end-systolic pressure volume relationship (ESPVR: $r = -0.8$; $P < 0.001$), pre-load recruitable stroke work (stroke work normalised to end-diastolic volume) (PRSW: $r = -0.6$, $P = 0.002$) and the starling contractile index (dP/dt max normalised to end-diastolic volume) (SCI); GCS also correlated with the maximum rate of pressure increase in the left ventricle (dP/dt max: $r = -0.5$, $P = 0.02$), Figure 76. Global longitudinal strain was not shown to correlate with ESPVR, PRSW, SCI or dP/dt max. Interestingly, GCS also correlated with the maximum rate of pressure decay in the left ventricle (dP/dt min: $r = -0.7$; $P < 0.05$).

Comparison of echocardiographic techniques for prediction of contractility

Receiver-operating characteristics (ROC) curves were generated for both echocardiographic global measures of contractility. This was performed by dichotomising the variable for strain, to represent good LV function (GCS<-20, GLS<-15) or poor LV function. The greatest area-under the curve (AUC) for the ROC curves was generated by GLS (AUC = 0.678, SE=0.1112), this was greater than the AUC for GCS (0.500, SE=0.112). These were compared using GraphPad Prism using the following equation:

Equation 25

$$z = \frac{(Area\ 1 - Area\ 2)}{\sqrt{SE\ (Area\ 1)^2 + SE\ (Area\ 2)^2}}$$

These are demonstrated in Figure 77.

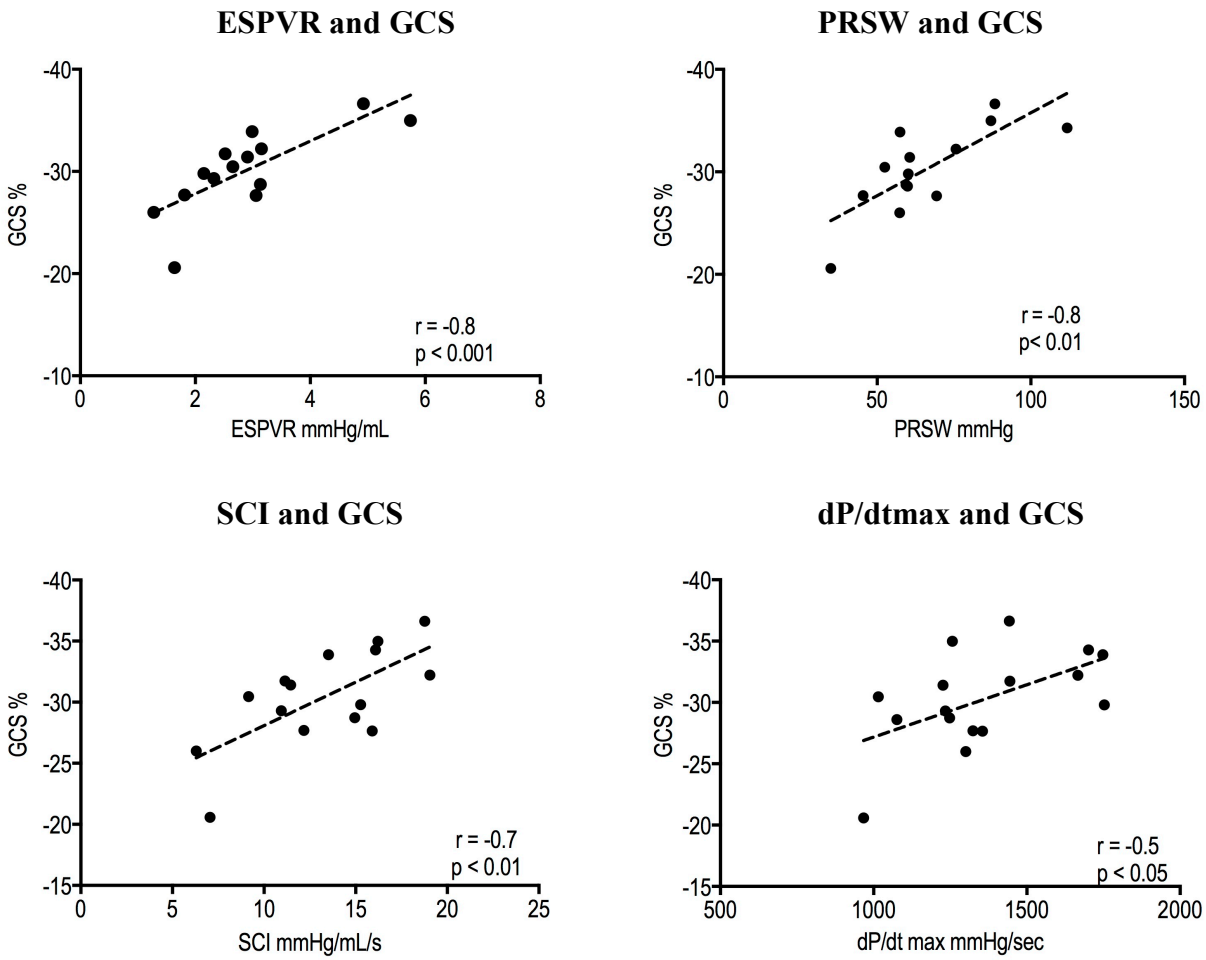


Figure 76 Correlation of global circumferential strain (GCS) with contractility
End-systolic pressure volume relationship (ESPVR, top left); pre-load recruitable stroke work (PRSW, top right); starling contractile index (SCI, bottom left); maximum rate of pressure increase in the left ventricle (dP/dt max, bottom right).

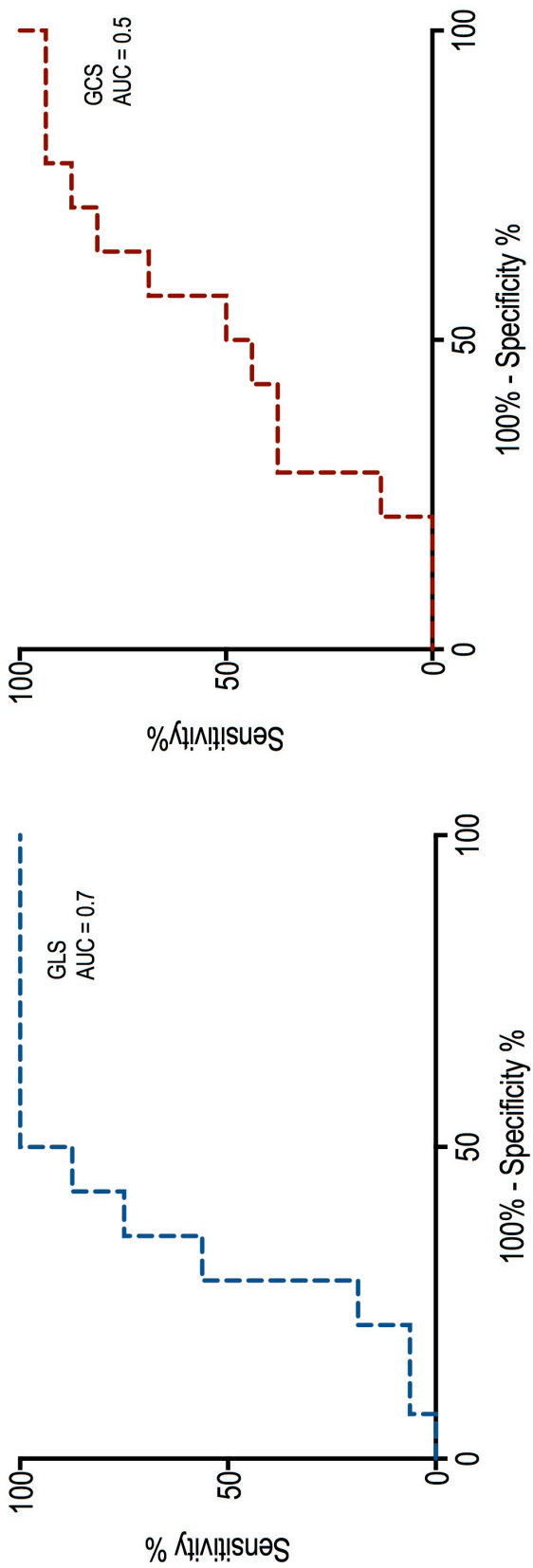


Figure 77 Receiver operating characteristics curves
These describe the sensitivity and 1-specifity (as percentages) of global longitudinal strain (GLS) and global circumferential strain (GCS) as predictors of contractile function (end-systolic pressure volume relationship, ESPVR); AUC area under the curve

6.4 DISCUSSION

The results of this study show that in cohort of patients with known ischaemic heart disease, myocardial deformation imaging: 1) correlates with load-independent contractility indices derived from invasive PV loop assessment, 2) is predictive of contractile function at rest. This is the first study of its kind to have been performed in humans correlating invasive with non-invasive measures of left ventricular function. The importance of these findings is that strain parameters are able to closely reflect invasive markers of contractility and therefore may enable us to estimate contractility non-invasively in a consecutive manner and even during resting conditions in humans. In agreement with a previous rat model, we demonstrated that GCS correlated with ESPVR, PRSW, SCI and dP/dt max.[53] We also demonstrated that GCS is a very poor predictor of contractility, this has implications in taking this measure forward. The additional value of myocardial deformation imaging in this cohort of patients with preserved left ventricular function on 2D echocardiography can be seen from the identification of patients with sub-clinical left ventricular dysfunction and the ability of GLS to predict contractile function. Although strain has previously been validated against gold-standard non-invasive techniques, to our knowledge, this has not been performed against the invasive gold-standard. The search for powerful non-invasive systolic parameters is important not only for research purposes, but also in the clinical arena. Superiority of speckle tracking derived parameters to predict subtle myocardial injury has been previously shown in pre-clinical and clinical data, moreover the reduced inter- and intra-observer variability provided by 3D echocardiographic techniques has made this an even better tool. We therefore propose myocardial deformation imaged

using 3DSTE may be a valuable tool in the determination of contractile function at rest.

6.5 LIMITATIONS

This study was performed in a cohort of patients with ischaemic heart disease, therefore the findings cannot be transferable to all patient cohorts without a wider validation study; however, they accurately reflect findings in animal studies previously performed in both normal and diseased hearts.

6.6 CONCLUSIONS

The use of 3DSTE for prediction of contractile function is feasible in a cohort of patients with ischaemic heart disease. Close correlation with PV loop analysis suggests that 3DSTE has the potential for use in prognostication and risk stratification.

7 PERCUTANEOUS VENTRICULAR RESTORATION USING THE PARACHUTE DEVICE: THE PARACHUTE III PRESSURE-VOLUME LOOP SUB-STUDY

INTRODUCTION

Left ventricular dilatation and remodelling following acute myocardial infarction increases wall stress, ventricular volumes and leads to heart failure (HF), which is associated with a high mortality. Percutaneous ventricular restoration (PVR) therapy reduces LV volumes leading to a more effective ejection without the increased morbidity and mortality associated with surgery. This study investigated the haemodynamic effects of LV volume reduction from PVR on LV performance and its interaction with the arterial system.

METHODS

Ten patients with symptomatic ischemic HF of New York Heart Association (NYHA) classes II to IV with LV antero-apical wall akinesia underwent Parachute implantation. Pressure-volume loops were recorded immediately pre- and post PVR implantation and at 6 month follow up.

RESULTS

PVR significantly reduced end-diastolic volume (228±76 versus 294±69; $P<0.05$), with a greater relative reduction (average 33% versus 21%) in end-systolic volume (139±74 versus 99±53; $P<0.05$) with overall 6% increase in ejection fraction (40±13 versus 46±14; $P<0.05$). Furthermore, a reduction in dyssynchrony was evident on the

segmental loops; this was found to be statistically significant as measured by a reduction in the dyssynchrony index by 5% (19±4 versus 15±5 %; $P < 0.05$) immediately post-procedure, sustained at 6-months. A marked improvement in ventricular-arterial coupling was seen (reduction in Ea:Ees ratio from 1.8±1.0 to 1.1±0.6; mean ±SD; $P<0.05$) and all load-independent indices of contractility: end-systolic pressure-volume relationship, starling contractile index,and preload recruitable stroke work ($P<0.54$)

CONCLUSION

This present study assessed both the immediate haemodynamic effects of LV volume reduction using the Parachute percutaneous ventricular restoration device. The Parachute device improved synchronous contraction, reduced wall stress and was associated with LV reverse remodelling.

7.1 INTRODUCTION

Left ventricular dilatation and remodelling following acute myocardial infarction (AMI) are most commonly associated with anterior AMI and have been well documented in both experimental and clinical investigations.[173-175] One third of patients enrolled in the GISSI-3 trial (n=13,679) demonstrated evidence of this progressive LV dilatation and remodelling following AMI.[163] Treatment advances have led to increased survival from AMI; however this may have led to a larger population at risk of congestive heart failure (CHF).[177] Despite huge advances in pharmacological and device therapies, the onset of CHF is associated with a 32% 1-year mortality.[177] LV remodelling following AMI leads to scar formation, distorted geometry, increased wall stress and eventual dilatation; thus LV volume assessment in CHF can be used as an independent predictor of clinical outcomes.[178] An important measure of therapeutic efficacy is the demonstrable improvement in LV volume and geometry. The aim of percutaneous ventricular restoration (PVR) therapy in this cohort of CHF patients is to reduce LV volumes and thus reduce wall stress; remodelling of the LV thus increasing synchronicity can lead to a more effective ejection without the increased morbidity and mortality associated with surgery.[179] PVR is a catheter-based approach to delivery of a compliant partitioning (PARACHUTE) device to the LV apex, thus partitioning the akinetic myocardium; the conical nitinol frame with ePTFE membrane enables device compression and therefore percutaneous implantation. Initial studies demonstrated safety and feasibility with improved NYHA functional status, LV end-systolic volume index (LVESVI), LV end-diastolic volume index (LVEDVi), ejection fraction (EF) and LV end-diastolic pressure (EDP); improved survival compared to historical cohorts was shown.[180,181] Device safety and feasibility has demonstrated to 3 years following the

first-in-human studies.[253] More recently, an observational registry of 100 subjects supports PVR safety and efficacy at 1-year follow up in a real-world setting.[254] However data on the haemodynamic consequences are lacking, importantly, the effect of the device on LV preload, afterload, dyssynchrony indices and contractility. Accurate assessment of cardiac performance is critical in CHF to gauge prognosis and assess therapeutic response. Although ejection fraction is the most commonly used measure of cardiac function, the gold standard for assessing cardiac performance and its interaction with the arterial system is pressure-volume (PV) analysis. In CHF ventricular-arterial uncoupling occurs, this can accurately be measured by PV analysis as the ratio of Ea:Ees where Ea is a measure of net arterial load and Ees is a load-independent measure of LV contractility. Optimal efficiency is achieved when the ratio of Ea:Ees=1, in failing hearts this has been shown to be elevated.[37,40,128] Simultaneous in-vivo pressure-volume measurements with a conductance catheter (CC) placed in the LV allow real-time assessment of the cardiac performance and its interaction with arterial load.[183] PVR provides a unique model for assessing both the immediate haemodynamic effects of LV volume reduction and geometrical restoration and reverse remodelling on LV performance and its interaction with the arterial system; this percutaneous technique eliminates the confounding effects of cardio-pulmonary bypass.

7.2 METHODS

7.2.1 STUDY DESIGN

The PARACHUTE III (PercutAneous Ventricular RestorAtion in Chronic Heart FailUre due to Ischaemic HearT DiseasE) PV Loop sub-study was a prospective, single arm study conducted in 2 centres in Europe. The study was designed to assess safety,

feasibility and efficacy of the PARACHUTE device through investigation of immediate changes in LV PV relationships during PVR using a CC and to relate these findings to acute haemodynamic changes and 6-month haemodynamic and clinical outcomes.

7.2.2 PATIENT SELECTION

Participants with symptomatic ischaemic HF of New York Heart Association (NYHA) classes II to IV were included in this study. Participants were between 18 and 79 years of age (inclusive) with LV antero-apical wall motion abnormality (akinesis or dyskinesis) secondary to myocardial infarction; LV ejection fraction between 15% and 40%, and managed with stable doses of standard HF medical therapy for at least 3 months, as determined by the site investigator. Subjects with myocardial ischaemia requiring revascularisation or cardiac resynchronisation therapy within 60 days, and those with significant valve disease were excluded from the study. All sites obtained approval from an institutional review board or ethics committee before study commencement, and written informed consent was obtained from all subjects at the appropriate time before involvement in the study.

7.2.3 STUDY DEVICE AND PROCEDURE

The Parachute system includes the Parachute device, the pre-shaped delivery catheter and dilator, and the balloon delivery system that facilitates expansion of the device, Figure 30.The Parachute device is composed of a self-expanding nitinol frame (16 struts; radio-opaque), an ePTFE impermeable membrane, and an atraumatic polymer foot available in 4 sizes (65, 75, 85 and 95mm) with two different “foot” heights. The tips of the struts anchor the device on the myocardium and the atraumatic foot provides contact between the LV apex and the device, orientating it toward the LV outflow tract.

As per protocol, subjects were enrolled based on the following criteria: 1) written, informed consent form; 2) baseline evaluation for anatomical suitability and device compatibility; performed using echocardiography, multi-slice computed tomography (CT) and cardiac magnetic resonance imaging (Figure 41); and 3) successful placement of a 14F or 16F sheath in the femoral artery and pulmonary artery catheter in the femoral vein. Multi-modality imaging was also used to provide accurate measurements and to exclude LV thrombus and severe calcification. The procedure is described in Figure 78 and was performed under conscious sedation in the catheterisation laboratory. [253,254] All subjects were required to receive 12 months of aspirin and anticoagulation with warfarin post–device implant.

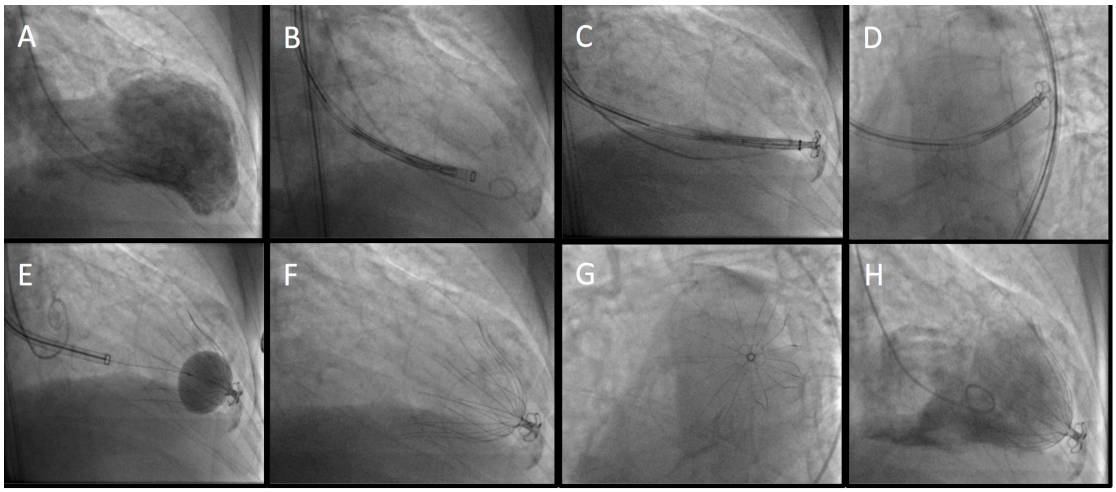


Figure 78 Parachute Study Procedure.
LV angiography is performed with a pigtail catheter in the LV (**A**), the delivery catheter is positioned in the apex (**B**), the Parachute foot is then exposed and contact is made with the antero-apical wall, confirmed in left anterior oblique, LAO (**C**) and right anterior oblique, RAO (**D**) views. Device delivery is facilitated by 20cc balloon expansion (**E**), retraction of the delivery system, followed by fluoroscopic confirmation of position in LAO (**F**) and RAO (**G**) views. LV angiogram confirms partitioning of akinetic myocardium (**H**).

7.2.4 INSTRUMENTATION

Simultaneous LV PV measurements were performed immediately prior to and following the Parachute implant and where possible at 6-months post implantation. Measurements were performed during steady-state conditions, avoiding excessive arrhythmia from premature beats. Recorded variables were averaged from 10 cardiac cycles to minimise inaccuracies from beat-to-beat variation and change in venous return from respiration; repeat baseline recordings ensured reproducibility of CC measurements. These were performed using a 7Fr CC (CD Leycom, Zoetermeer, the Netherlands); this flexible over-the-wire pigtail catheter is introduced into the LV using a super-stiff 0.025" J-wire. The catheter has 12 equally spaced electrodes with a central high fidelity, solid-state pressure sensor and is connected to a PV signal processor (Inca, CD Leycom), this device is described in more detail in section 2.2.1. The conductance method calculates continuous LV volume tracings by measuring parallel electric conductance between adjacent ventricular blood segments delineated by selected catheter electrodes; this technique has been shown to reflect LV segmental volumes in pre-clinical and clinical studies and has been utilised in the assessment of heart failure device therapies. [184,185,193] Accurate CC positioning is confirmed by fluoroscopy and on inspection of the segmental PV loop signals. LV Volume calibration was performed via right-heart catheterisation: a 6Fr single-lumen, balloon tipped Swan-Ganz catheter (Arrow International, USA) was positioned in the pulmonary artery to perform thermodilution and subtraction of calculated parallel conductance was performed by injection of 10mL boluses of 6% hypertonic saline through the distal port of the Swan-Ganz catheter, further detail with regard to invasive calibration methods can be found in section 2.2.3.4. [255]

7.2.5 DATA ANALYSIS

CC data analysis was performed with dedicated data acquisition and analysis software (Conduct NT, version 3.18.1, CD Leycom). Conductance volumes (EDV, ESV) were calculated at the maiximum rate of LV pressure rise (dP/dt+) and pressure decay (dP/dt), stroke volume was calculated as the difference in these volumes. In addition to instantaneous LV volumes and pressure, this software calculates load-independent parameters of LV contractility. [217] The end-systolic PV relationship (ESPVR) represents the ratio of LV pressure to LV volume at the end of ventricular systole (uppermost left corner of the PV loop). The Starling contractile index (SCI) is calculated as the maximal rate of pressure change over time during isovolumetric contraction (dP/dT_{max}) normalised to end-diastolic volume (EDV). LV stroke work (SW) was calculated as the area of the PV loop; preload-recruitable stroke work (PRSW) was calculated by normalising the SW to EDV. LV stroke work was calculated as the product of peak LV peak systolic pressure and stroke volume. [193,218] Cardiac output and cardiac index (CI) for volume calibration were calculated using the Fick method.[256] Participant follow up at 6-months was performed with elective admission for repeat invasive haemodynamic assessment, this included clinical follow up and assessment of functional status, transthoracic echocardiography and multi-slice CT. Clinical endpoints were: death, recurrent hospitalisation, emergency surgery, NYHA functional class and 6-minute walk test (6-MWT). The haemodynamic endpoints for the PV loop sub-study were a measurable change in LV volumes, assessment of LV contractility and mid-term improvement in ventricular-arterial coupling.

7.2.6 STATISTICAL ANALYSIS

Statistical analysis was performed using GraphPad Prism v7.0 (GraphPad Software Inc., CA). The study was not powered to show a significant difference in haemodynamic endpoints due to the absence of previous invasive haemodynamic data. Quantitative data are expressed as mean±SD, categorical variables are described as proportions and percentages. Data were assessed for normality of (Gaussian) distribution both graphically and by use of the D'Agostino-Pearson omnibus test. Statistical comparison of serial haemodynamic measurements (quantitative data) of normal distribution was performed using a repeated measures one-way ANOVA, adjustment for multiple comparisons was performed using the Bonferroni correction to explain significant differences; in the presence of only pre and post (absence of 6 month) data, paired t-tests were performed. Statistical comparison of quantitative data not falling within a normal distribution was performed using the Friedman test for repeated haemodynamic measurements and a 2-tailed Wilcoxon signed-rank test for paired samples. Categorical data were compared by use of the Fisher exact test. A two-sided alpha of 0.05 was considered statistically significant for all tests.

7.3 RESULTS

Procedural Outcomes

Between December 2013 and May 2015, eleven subjects were enrolled at 2 sites in Europe: Onze-Lieve-Vrouwziekenhuis, Aalst, Belgium and St Thomas' Hospital, London, UK. Of the eleven patients consented, no attempt to deliver the device was made in one subject because of anatomical reasons. Ten patients underwent successful Parachute implantation (baseline characteristics in Table 13) and haemodynamic data were obtained in all patients prior to implantation and nine patients post implantation: one patient had a major vascular complication requiring surgical repair, therefore the CC could not be reinserted immediately post procedure or at 6-month follow up. Immediate surgical explant (within 72 hours) was performed in two patients for non-optimal positioning of the device and therefore seven patients were discharged with device in-situ. There were no aortic valve complications. These seven patients underwent 6-month outpatient clinical follow-up, and a total of six patients underwent 6-month invasive repeat haemodynamic assessment with simultaneous LV PV loop analysis; one patient died from traumatic subdural haematoma during repeat admission prior to catheter laboratory measurements. Disposition of patients enrolled is described in Figure 79.

Baseline Characteristic	**Total**
Device Success	8/10 (80%)
Age, years	61.0±10.4
Gender, male	9/10 (90%)
Weight, kg	94.0±21.9
Height, cm	169.4±10.0
BMI kg/m^2	32.3±4.1
Ischaemic heart failure	10/10 (100%)
NYHA II	6/10 (60%)
NYHA III	4/10 (40%)
NYHA IV (ambulatory)	0/10 (0%)
6-MWT, metres	327±131*
Smoking history	8/10 (80%)
History of stroke	1/10 (10%)
History of hypertension	4/10 (40%)
History of diabetes mellitus	4/10 (40%)
History of dyslipidemia	8/10 (80%)
Prior ICD implantation	5/10 (50%)
Prior CRT device	4/10 (40%)
Previous PCI	10/10 (100%)
Previous CABG	1/10 (10%)

Table 13 Baseline characteristics

Data are presented as counts (n/N) and percentages (%) or as mean ± SD. * Data available in only nine patients. Abbreviations: BMI body mass index, NYHA New York Heart Association Functional Class, 6-MWT 6-minute walk test, ICD implantable cardioverter defibrillator, CRT (±D) cardiac resynchronisation therapy ± defibrillator, PCI percutaneous coronary intervention, CABG coronary artery bypass graft surgery, HF congestive heart failure

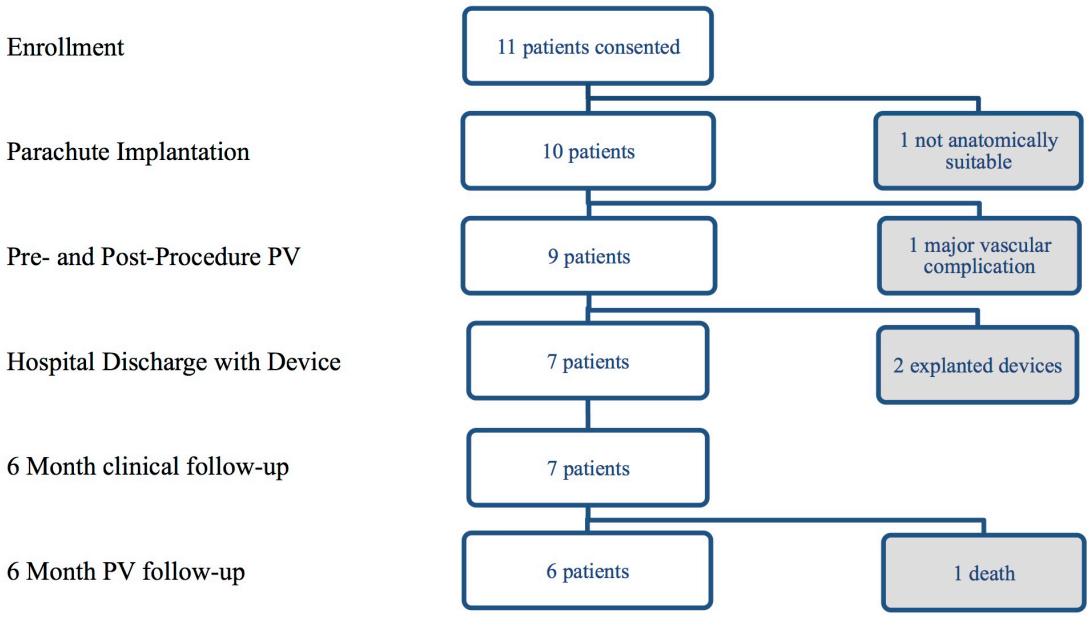


Figure 79 Disposition of patients enrolled.
LV PV (pressure-volume) measurements were performed in 9 patients pre- and post-procedure and in 6 patients pre-, post- and 6 months.

Haemodynamic, Functional Outcomes and Dyssynchrony Index

Figure 80 shows the New York Heart Association class distribution for 12 months post-procedure. Symptomatic improvements were evident in 50%, with no change in 37.5% and worsening in 12.5%, consistent with previous studies.[253,257] The median NHYA class, however, remained unchanged between baseline, 6 and 12 months (P= 0.5) due to the small sample size. All haemodynamic variables are summarised in, Table 14. Haemodynamic measurements were performed before and after Parachute implantation under conscious sedation. Haemodynamic measurements at 6-month follow up were performed under local anaesthetic. At 6-month haemodynamic follow-up, the parachute device significantly reduced both end-diastolic and end-systolic volumes by a mean of 44 (95% CI -69 to -20) and 40 ml (95% CI -63 to -16) respectively (Figure 81); there was an overall increase in ejection fraction by 5% [median 39% (IQR 27-51) to 44%

(IQR 35-59)] (Figure 82). A significant reduction in the measured dyssynchrony index [median 20% (IQR 14-22) to 14% (IQR 11-21); $P < 0.05$] was seen immediately post procedure and sustained to 6-months (Figure 83). End-systolic pressure increased significantly by mean 28mmHg (95% CI 12-45), end-diastolic pressure did not significantly change immediately post implantation, but was elevated at 6-month follow up. Percentage changes of major haemodynamic variables are summarised in (Figure 84).

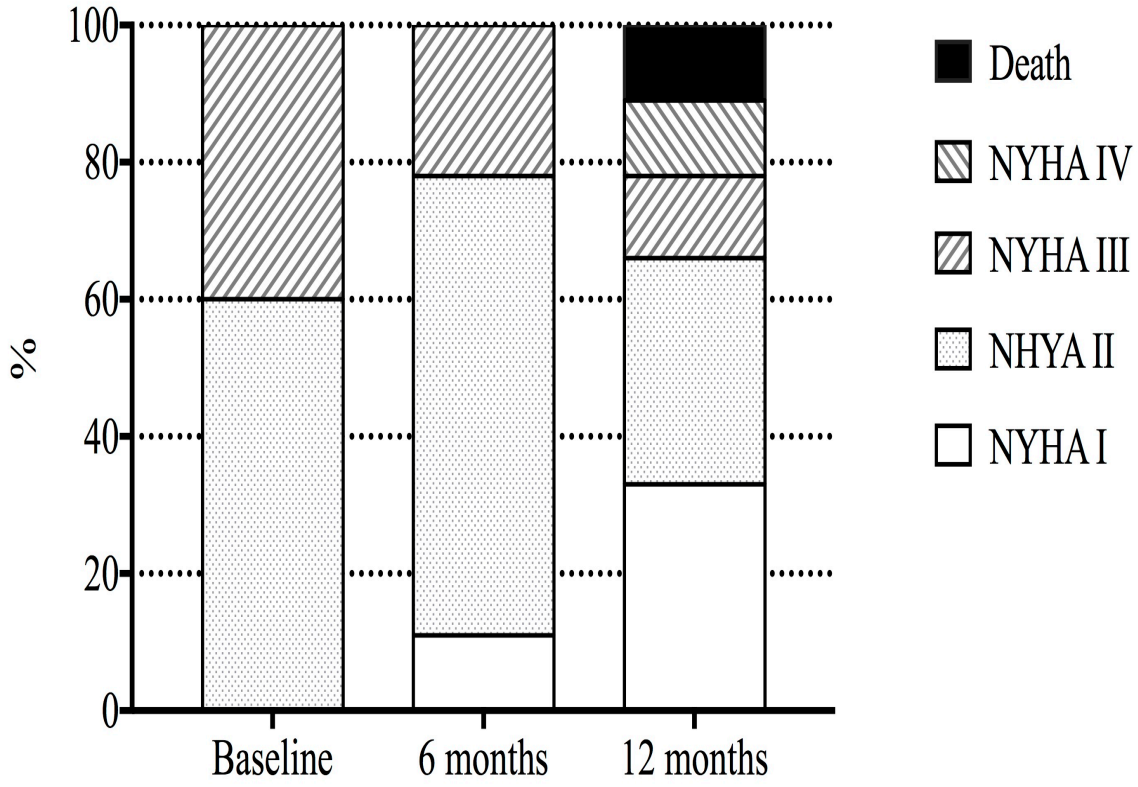


Figure 80 Clinical outcomes.
n=10, according to New York Heart Association classes I to IV.

	Baseline	Post Parachute	6 months Parachute	Baseline vs Post		Baseline vs 6months		Post vs 6months	
				Mean diff. 95% CI mean	P value	Mean diff. 95% CI mean	P value	Mean diff. 95% CI mean	p value
HR, bpm	79±12	76.5±14.3	74.7±12.5	-2.4 (-7.3 to 2.6)	0.3	-4.0(-18.1 to 10.2)	0.5	-3 (-18 to 13)	0.7
SV, mL	82.8±21.2	81.8±24.6	87.37±21.3	-1.0 (-8.4 to 6.4)	0.8	2.9 (-6.4 to 12.2)	0.5	2.9 (-6.4 to 12.3)	0.5
EF %	39.8±14.3	41.3±13.7	45.6±13.5	1.9 (-1.1 to 5.0)	0.2	5.8 (1.1 to 10.4)	0.02*	4.5 (-0.1 to 9.0)	0.05*
EDV, mL	228±76	210±82	194±69	-18 (-36 to 1)	0.03*	-45 (-69 to -21)	0.005*	-24 (-59 to11)	0.13
ESV, mL	139±74	123±74	99±53	-15 (-26 to-2)	0.03*	-40 (-63 to -16)	0.007*	-23 (-50 to 3)	0.07
EDP, mmHg	14±4	16±4	17±4	1.4 (-0.2 to 3)	0.07	3.3 (-0.1 to 6.6)	0.054	1.8 (-1.2 to 4.9)	0.2
MDP, mmHg	10±4	12±4	11±3	1.7 (0.5 to 3.0)	0.01*	1.1 (-0.7 to 3.0)	0.18	-0.7 (-2.6 to 1.2)	0.4
ESP, mmHg	79±18	84±24	108±12	4.7 (-3 to 12.5)	0.2	28.7(12 to 45)	0.007*	24.5 (5.3 to 41.6)	0.002*
SW, mmHg.mL	5905±1725	5559±1689	7266±1398	-194 (-775 to 387)	0.4	1361 (-329 to 3051)	0.09	1707 (311 to 3103)	0.02
dP/dt+ mmHg/s	766±205	758±261	983±209	225 (-32 to 482)	0.6	217 (-18 to 452)	0.06	225 (-32 to 482)	0.07
Tau ms	46.6±9.3	47.5±12.3	43.4±8.4	1.0 (-2.4 to 4.4)	0.5	-3.2 (-8.4 to 1.9)	0.2	-4 (-9.8 to 1.5)	0.1
Tau msT	46.6±9.3	47.5±12.3	43.4±8.4	-0.5 (median)	0.8	-4.7 (median)	0.3	-4.3 (median)	0.09
dP/dt- mmHg/s	-679±224	-722±250	-962±189	-31 (-100 to 38)	0.3	-284 (-520 to -47)	0.028*	-240 (-463 to -17)	0.039*
ESPVR mmHg/mLT	0.72±0.36	0.91±0.48	1.47±0.87	0.06 (median)	0.09	0.55 (median)	0.03*	0.29 (median)	0.03*
PRSW	27±10	29±13	42±16	3 (0 to 6)	0.07	15 (3 to 27)	0.02	13 (0 to 24)	0.04*
SCI	3.7±1.6	4.3±2.5	5.8±2.6	0.5 (-0.6 to 1.7)	0.3	2.1 (0.5 to 3.8)	0.02*	1.5 (-0.5 to 3.5)	0.1
DS2	19.0±4.3	15.3±4.9	16.1±4.9	-5.1 (-10.2 to 0)	0.04*	-3.0 (-7 to 1.4)	0.14	5.6 (-5.2 to 6.6)	0.8
DS3	28.7±4.8	28.2±6.1	26.9±2.3	-1.8 (-7.2 to 3.8)	0.5	-1.8 (-8 to 4.5)	0.5	-1.3 (-8.7 to 6.1)	0.7
PFR	851±276	749±368	616±160	-85 (-241 to 71)	0.2	-235 (-430 to 40)	0.03*	-132 (-455 to 190)	0.3
PER	-574±149	-509±156	-534±152	70 (8 to 132)	0.03*	39 (-65 to 143)	0.4	-26 (-147 to 95)	0.6
EaT	1.1±0.6	1.2±0.8	1.3±0.4	0.08 (median)	0.2	0.24 (median)	0.2	0.21 (median)	0.8
Ea:Ees	1.8±1.0	1.6±0.9	1.1±0.6	-0.2 (-0.4 to 0.1)	0.1	-0.6 (-1.1 to -0.1)	0.03*	-0.4 (-0.8 to -0.1)	0.03*
PVA	11334±3430	10395±2791	12324±1895	-722(-1865to 422)	0.2	991 (-1356to 3337)	0.3	1929 (128 to3730)	0.04*
SW: PVA %	54.7±14.9	54.8±14.5	59.8±13.7	0.9 (-3.2 to 4.9)	0.6	5.2 (0.5 to 9.8)	0.04*	4.9 (-0.1 to 10.1)	0.05*

Table 14 Haemodynamic variables, abbreviations see xvi

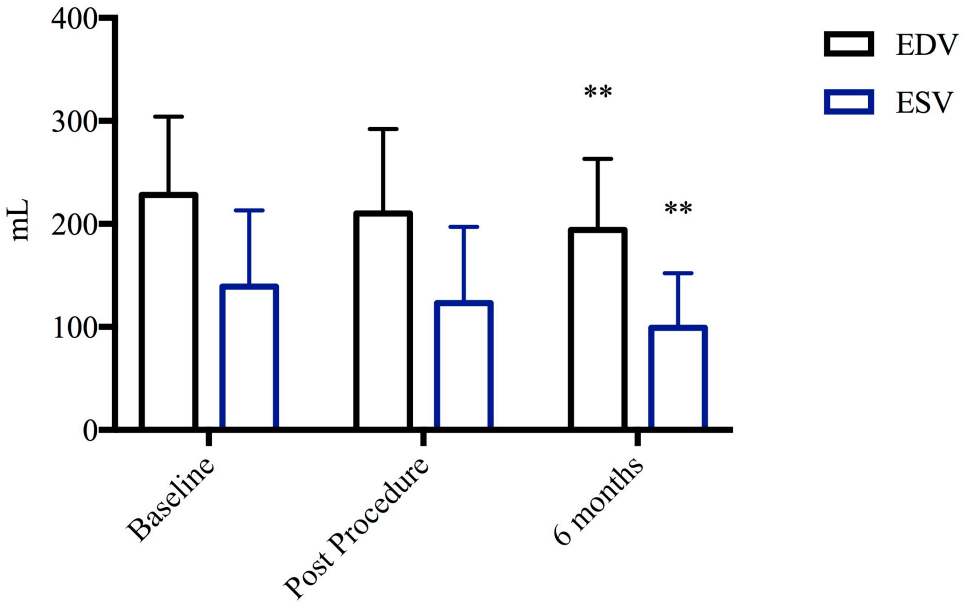


Figure 81 End-Diastolic Volume (EDV) and End-Systolic Volume (ESV).
Change in EDV and ESV from baseline. ** Indicates statistically significant difference baseline versus 6 months and post procedure versus 6 months.

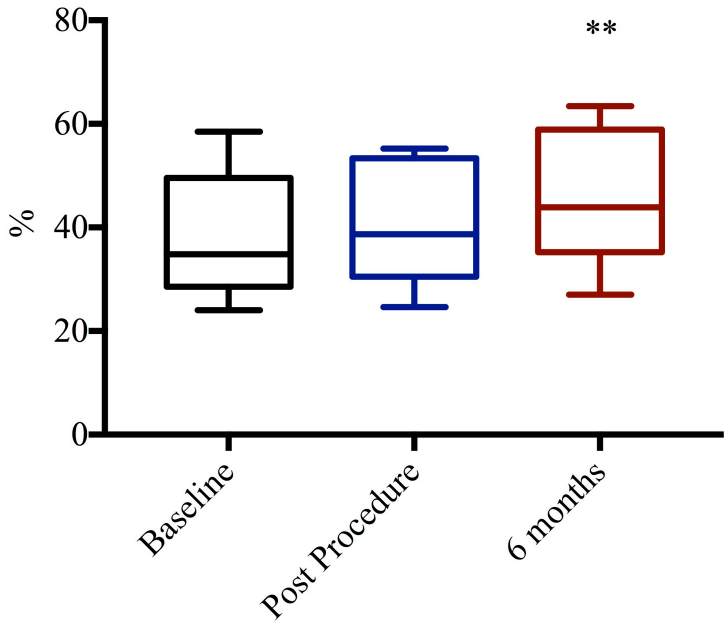


Figure 82 Ejection Fraction.
Change in ejection fraction from baseline. ** Indicates statistically significant difference baseline versus 6 months and post procedure versus 6 months.

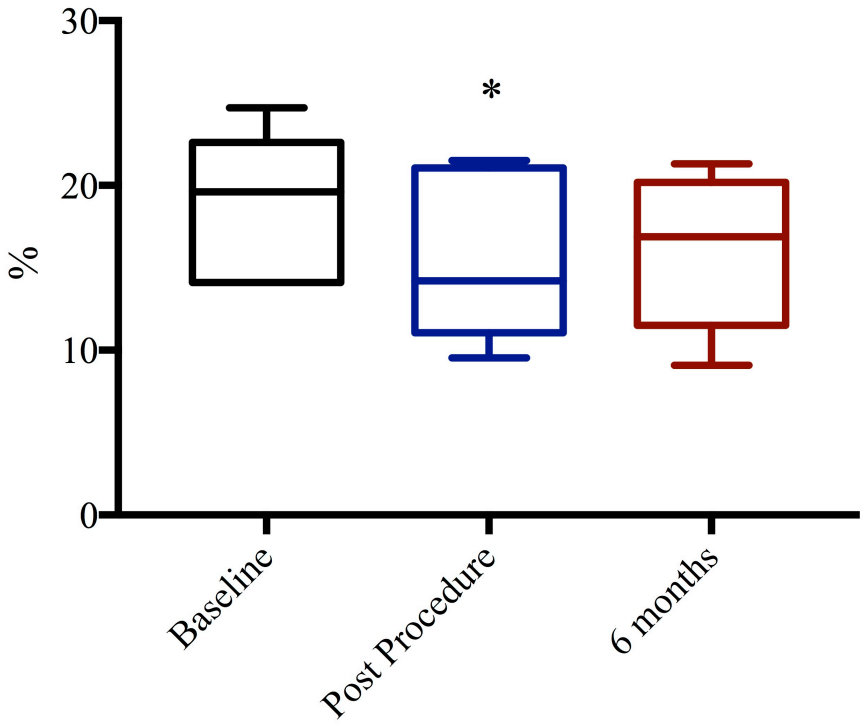


Figure 83 Dyssychrony Index.
Change in dyssynchrony from baseline. * Indicates statistically significant difference baseline versus post procedure.

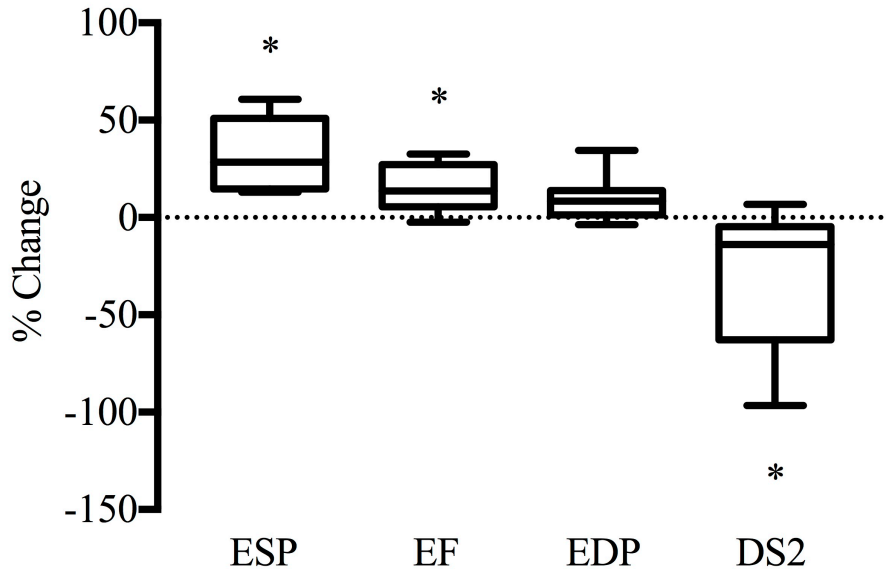


Figure 84 Percentage change in haemodynamic variables.
Baseline to 6 months post procedure; * indicates statistically significant change. Box and whisker plots demonstrate mean with maximum and minimum values. Abbreviations see xvi.

LV Contractility, Ventricular-Vascular Coupling and Myocardial Energetics

The reversal of LV dyssynchrony was accompanied by a leftward PV loop shift, and therefore leftward shift of the ESPVR curve and an increase in stroke work The maximum rate of LV pressure increase (dP/dt+), a load-dependent marker of LV contractility showed a trend toward increase (P=0.06). Load-independent markers of contractility: ESPVR (*P=0.03*), SCI (*P=0.02*) and PRSW (*P=0.04*) all significantly increased at 6 months post-procedure in line with the increase ejection fraction (described above) (Figure 86).

The interaction between the heart and the vascular loading system determines the external work and metabolic efficiency of the heart.[40] Therefore the elevation of end-systolic pressure (ESP) and relief of dyssynchrony in this cohort was associated with a significant increase in external stroke work. Despite the increase in ESP, the net arterial load, as measured by effective arterial elastance (Ea), remained unchanged. Furthermore, at 6-month follow up, a marked improvement in ventricular-arterial coupling was seen (reduction in Ea:Ees ratio from 1.8±1.0 to 1.1±0.6; mean ±SD; *P<0.05*) (Figure 87). Although total ventricular work increased, the ratio of external stroke work (SW) to total work (PVA), the efficiency of energy transfer, increased significantly, from 54.7% to 59.8% (*P<0.05*) (Figure 88).

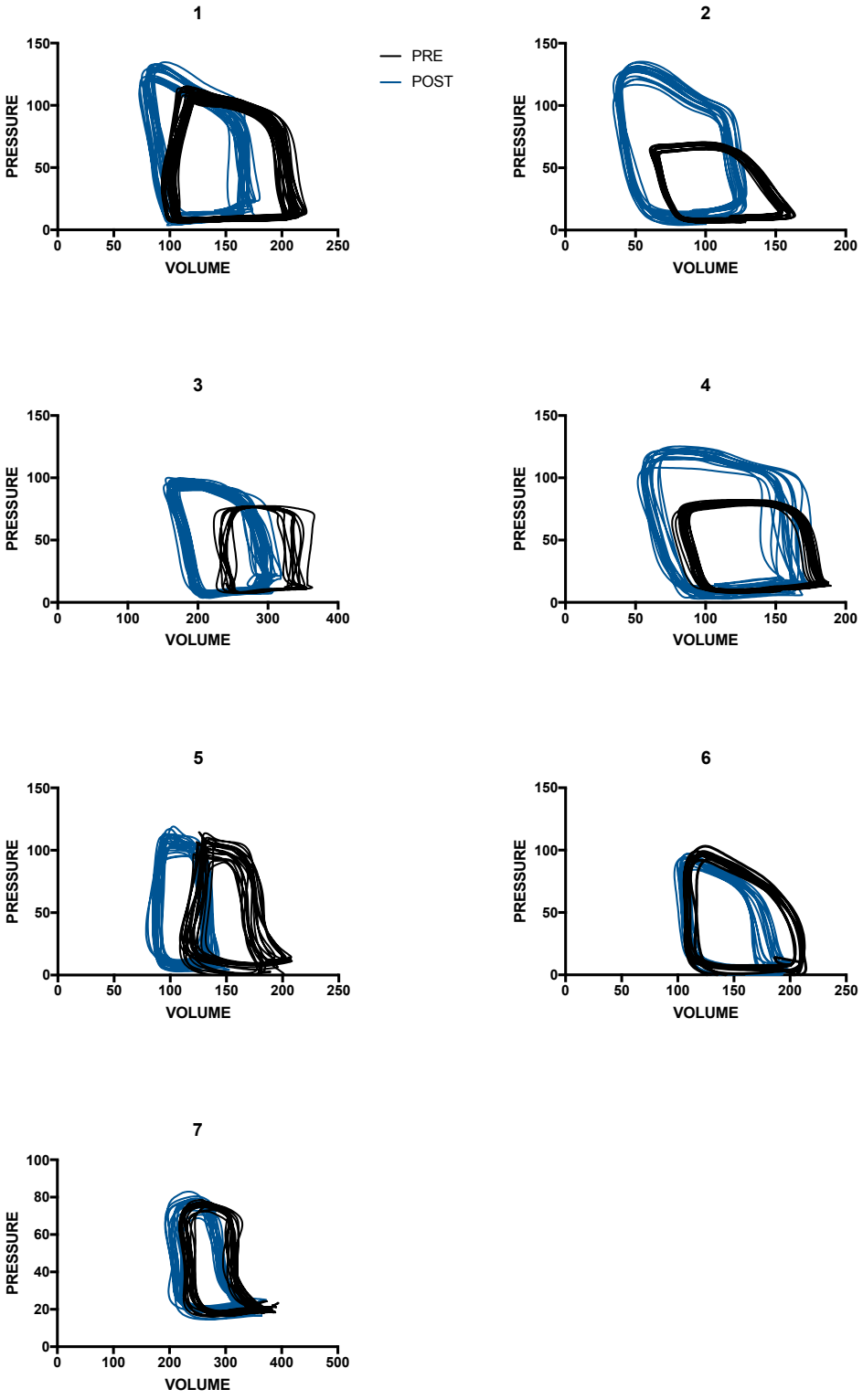


Figure 85 Pressure volume loops performed in 7 patients prior to implant (**black**) and post implant (**blue**). The total PV loop prior to implant demonstrates a leftward shift in response to a decrease in dyssynchrony.

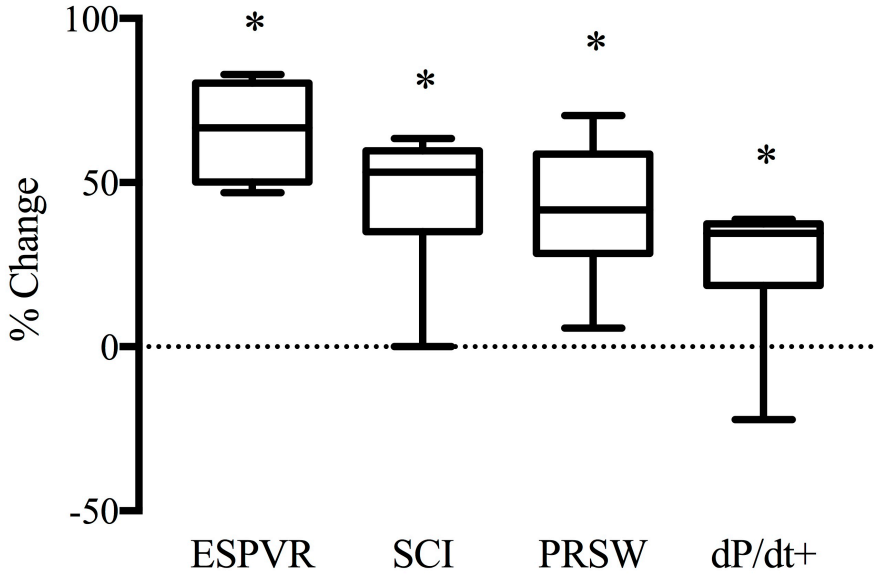


Figure 86 Percentage change in indices of contractility.
Baseline to 6 months post procedure. *Indicates statistically significant change. Box and whisker plots demonstrate mean, maximum and minimum value. Abbreviations see xvi.

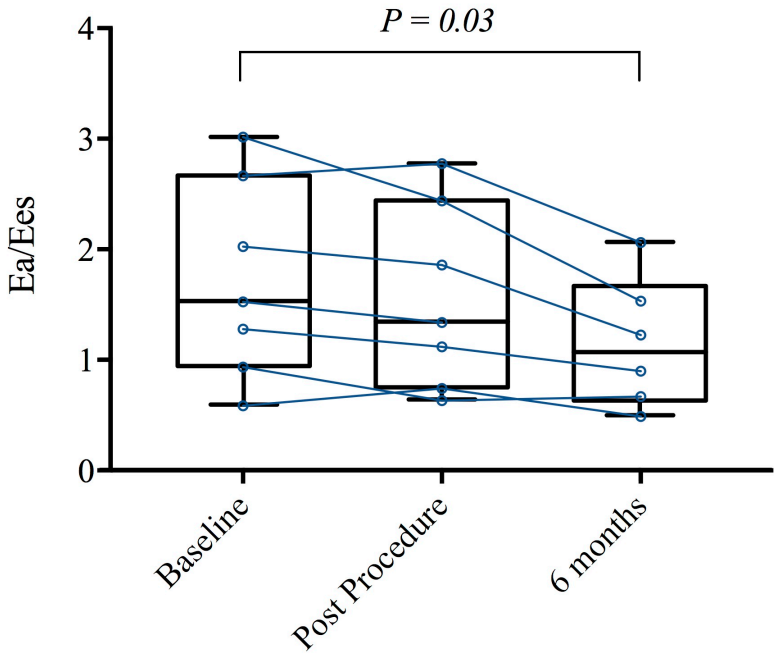


Figure 87 Ratio of Ea:Ees.
This demonstrates the interaction of the left ventricle with the arterial system at baseline compared to 6 months post procedure.

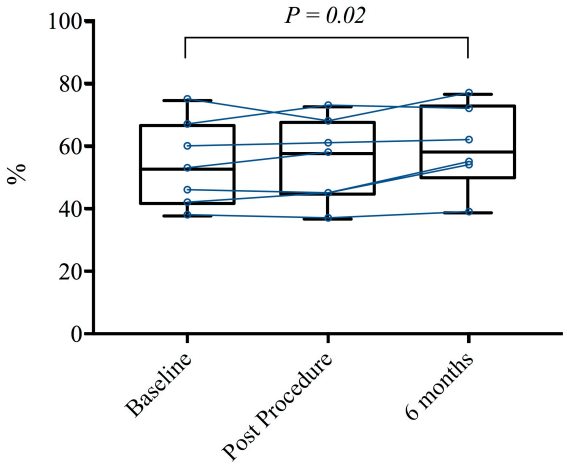


Figure 88 Ratio of SW:PVA expressed as a percentage.
This demonstrates the efficiency of conversion of metabolic energy to external stroke work at baseline compared to 6 months post procedure.

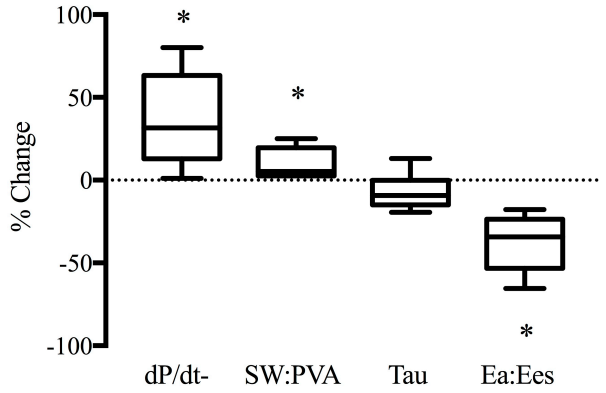


Figure 89 Percentage change in markers of LV relaxation and efficiency.
From baseline to 6 months post procedure. * Indicates statistically significant change. Box and whisker plots demonstrate mean with maximum and minimum values. Abbreviations: SW:PVA stroke work to pressure volume area ratio, Ea:Ees arterial elastance to end-systolic elastance ratio.

Indices of LV Relaxation

A significant improvement in active LV relaxation as measured by the maximum derivative of LV pressure decay (dP/dt-) (-679±244 to -962±189mmHg/s; *P<0.05*) was demonstrated with a trend toward reduction in Tau (*P=0.09*) ( ). An improvement in LV compliance as measured by LV end-diastolic pressure and EDPVR (End-Diastolic Pressure Volume Relationship) could not be demonstrated at 6-month follow up, this is likely due to the effect of heavy sedation on a reduction in diastolic stiffness in heart

failure patients during peri-procedural measurements that was absent on 6-month follow-up; the large volume reduction and the small patient cohort.[258]

7.4 DISCUSSION

The Parachute device partitions and isolates the apical region of the LV from the rest of the chamber. The goal is to exclude infarcted, dyskinetic regions of myocardium to optimize the use of contractile energy produced by remaining myocardium for generating forward cardiac output and blood pressure. Pressure-volume analysis showed that both immediately after and 6 months following implant, the Parachute device reduced chamber volume, and enhanced pressure generation with trends towards increased stroke volume in most of the patients studied. These were the result of leftward/upward shifts of the ESPVRs and EDPVRs. Along with these, we also saw increased SW/PVA ratio indicating a greater proportion of ventricular work expressed externally. Initial studies demonstrated safety and feasibility with improved NYHA functional status and improved survival compared to historical cohorts.[180,181] Device safety and feasibility has been demonstrated to 3 years following the first-in-human studies [253] and in over 100 subjects at 1-year follow up in a real-world setting.[254] However there were significant complications with this device implantation thus it was associated with significant (40%) morbidity. Left ventricular dilatation and remodelling following acute myocardial infarction (AMI) is most commonly associated with anterior AMI and has been well documented in both experimental and clinical investigations;[173-175] One third of patients demonstrate evidence of progressive LV dilatation and remodelling.[163] Treatment advances have led to increased survival from AMI; [177] however the onset of CHF is associated with a 32% 1-year mortality. [177] The assessment

of cardiac performance is critical in CHF to gauge prognosis and assess therapeutic response. This study examined the immediate and mid-term haemodynamic effects of percutaneous ventricular restoration (Parachute) device implantation on cardiac performance and ventricular-arterial interaction and their relationship to clinical outcomes in a cohort of patients with akinetic aneurysmal apices secondary to acute myocardial infarction. It was not able to demonstrate that every patient responded as intended haemodynamically, which would be consistent with the clinical response that is seen in approximately half of patients.

Left ventricular dyssynchrony is frequently observed in congestive heart failure, it leads to inefficient left ventricular contraction and decreased cardiac output. This places patients at increased risk of cardiac events and is an important predictor of outcome. [259] In congestive heart failure, LV function is disturbed by a combination of factors: reduced contractile function, abnormal loading conditions and dyssynchronous contraction. The conductance catheter method is an alternative and invasive measure of LV dyssynchrony, traditionally used to measure global systolic and diastolic volumes; the segmental conductance signals are able to describe temporal and spacial indices and have been previously described and validated.[260] Ventricular dyssynchrony is associated with a rightward shift of the PV loop (and therefore ESPVR) with a reduction in stroke work (PV loop area) and stroke volume, with an accompanied decline in dP/dt+. [259,261,262] In the patients that responded (4 out of 7) implantation of the Parachute device, through partitioning of the dyskinetic left ventricular apex, increased synchronicity of contraction, with observed increases in contractility and ventricular efficiency. Continuous assessment of instantaneous LV pressure and volume enabled real-time display of the reversal of dyssynchrony in this study through normalization of

segmental PV loops. This was further supported by a leftward shift in the total pressure-volume loop in the responders, a leftward shift of ESPVR and an increase in stroke work, accompanied by an improvement in load-independent markers of contractility. An improvement in dP/dt-, representative of the early diastolic phase, is likely to be related to preceding systole, thus reflecting enhanced contraction, rather than passive diastolic properties. The ability to measure EDV by the conductance method enables a direct measure of the preload imposed on the heart, partitioning of the ventricle lead to reduced end-systolic and diastolic volumes, thus reducing the abnormal excessive loading conditions that predominate in CHF. A reduction in wall stress and improved contractile function at 6 months is suggestive of LV reverse remodelling.

The dynamic interaction between the heart and the systemic vasculature is fundamental to the heart providing adequate cardiac output and the arterial pressures necessary for distal organ perfusion.[109,114] Ventriculo-arterial coupling correlates inversely to pump efficiency, this can accurately be measured by PV analysis as the ratio of Ea:Ees where Ea is a measure of net arterial load and Ees is a load-independent measure of LV contractility. Ea:Ees is an important parameter that measures the interaction between the left ventricle and the arterial system and is a determinant of net ventricular performance and cardiac energetics.[37,38] The heart is optimally efficient at a ratio of 0.7; in CHF ventricular-arterial uncoupling occurs and an Ea:Ees>1.0 is seen.[37,40,128]. Following Parachute implantation we observed enhanced ventricular-arterial coupling, this was seen to be mediated by the increase in contractility observed from the relief of dyssynchrony. We therefore conclude that the immediate beneficial effects of the Parachute device are predominantly mediated by its ability to reduce LV dyssynchrony, with long term reduction in wall stress and likely reverse remodelling. Although

medical therapy remains the mainstay of treatment in CHF, mortality remains significantly high in this cohort. [177,263,264] Other than CRT, there are no known percutaneous interventional therapies that aim to restore mechanical synchrony.[218] Several hypotheses underlie the failure of surgical ventricular restoration in the STITCH trial including the absence of dyskinetic wall motion in 50% of patients, with only a modest degree of volume reduction, depite immediate acute decrease in mechanical synchrony observed froollowing ventricular restoration.[255,265-267] Thus a percutaneous approach with the Parachute device may achieve a more reproducible volume reduction without the increased risk of surgery in appropriately selected patients, although it is not without risk, and as yet we are unable to determine which patients will respond haemodynamically and clinically to the device. Thus this is the first demonstration of the therapeutic efficacy of the parachute through restoration of mechanical synchrony, in a cohort of patients with apical dyskinesis.

7.5 LIMITATIONS

This study has limitations due to the small sample size and the unblinded single arm nature of the study. Absolute conclusions cannot be drawn in the absence of a control group to demonstrate efficacy and superiority of the device when compared to optimal HF therapies alone. Due to study design, bias cannot be ruled out in the adjudication process. This study was associated with 40% complication rate, thus it should be recommended that the device be used with caution in the appropriate patient group.

7.6 CONCLUSIONS

This present study assessed both the immediate haemodynamic effects of LV volume

reduction and geometrical restoration and reverse remodelling on LV performance and its interaction with the arterial system. Percutaneous ventricular restoration was associated with a reduction in end-diastolic and end-systolic volumes and LV reverse remodelling in the mid-term. The on-going large-scale Parachute IV study will establish the role of this novel therapeutic approach in ischaemic heart failure.[268]

Potential Impoact

The Parachute device provides a novel therapeutic approach for patients with systolic heart failure; this haemodynamic study validates and supports the previously observed favorable clinical outcomes thereby supporting the adoption of this device in a specific cohort of patients.

8 SYNTHESIS

Synthesis

In this chapter, the main findings of the thesis are discussed. The aim of this synthesis is to review the studies performed, the addition of knowledge to the existing literature, the implications of this work and future directions of study.

Origins and design

Fundamental to advancing our understanding of cardiovascular pathophysiology and therapeutics is the examination of the components of the cardiovascular system and the coordinated response to physiological and non-physiological changes. For the purposes of addressing the aims of this research, this can be separated into the ventricular-arterial (VA) interaction, how the pump interacts with the system and the cardiac-coronary interaction. Instinctively, we know this to be an artificial divide; however, the interactions within the system are likely to be far more complex than initially appreciated.

Coronary blood flow is known to be phasic in nature, increasing in systole and decreasing in diastole. The mechanism of coronary systolic flow impediment has generated great interest and extensive work in this area over the past 4 decades.[72,187,188] The close proximity of the coronary vasculature to the myocardium means a two-way interaction exists; and coronary blood flow morphology is not merely a function of aortic pressure. Recent work has centred around examining the product of simultaneous changes in the coronary pressure and flow velocity signals to describe these in terms of

successive wavefronts or wave intensity analysis. [96,97]As WIA can differentiate between proximally arising waves from the aorta and distally arising waves from the microcirculation, this has enabled a greater understanding of the aortic and myocardial components driving (and impeding) coronary blood flow. More recently it was proposed that WIA was more closely related to cardiac mechanics than initially understood; attempts to further delineate this focussed on independent measurement of left ventricular pressure and coronary pressure and flow velocity.

The instantaneous ventricular pressure-volume (PV) relationship is crucial to describing intrinsic myocardial properties; thus to understand cardiac mechanics, it is necessary to appreciate that PV relationships represent force-length relations at the ventricular level, thus is the most accurate means of measuring chamber geometry, compliance and contractile function in humans. Progression of technology and validation of the impedance method has enabled the accurate measurement of the PV relationship in humans.

Aims

The study of coronary physiology and left ventricular (LV) pump properties are two separate fields of work. The aim of this thesis was to bring together these research interests to enable a greater understanding of the interaction between the components of the cardiovascular system, which is poorly understood.

This was performed in 4 stages, which are described and summarised as main findings.

Chapter 3: The Development Of A Novel Analytical Software System

In this results chapter the development of a novel software system was described. The configuration of existing commercially available hardware enabled creation of a tool capable of simultaneous online assessment of LV properties, and therefore the VA interaction and coronary haemodynamics. An analytical software programme incorporating automated algorithms to measure the simultaneous tracings was validated and used to describe 1) the influence of cardiac mechanics on coronary waves and 2) the mechanical determinants of coronary blood flow. The following work has not been previously performed, and would not have been possible without the generation of this software. The origins of coronary wave energies are incompletely understood. Here we demonstrated that forward travelling wave arising from the aorta were the product of the ventricular-arterial interaction, the generation of these waves is dependent on peak LV pressure exceeding diastolic aortic pressure. This suggests that a complex interplay comprising, preload, afterload (lumped mean and pulsatile) and contractile force is involved in wave generation in the coronary artery. Furthermore backward travelling waves were found to mirror the ventricular pressure-volume relationship very closely, the backward travelling suction wave commences immediately after the ventricle has reached its state of maximal contraction and continues until cross-bridge uncoupling is complete. Coronary blood flow velocity was found to be uniquely linked to LV elastance on abolition of autoregulation, suggesting the unique morphology of coronary flow is as a result of a combination of transmural compressive forces and intra-vascular forces generated by the resistance vessels.

The development of the above tools facilitated examination of the cardiovascular response to exercise and the pathophysiological mechanism of exercise-induced ischaemia.

Chapter 4: Myocardial Systolic And Diastolic Function During Exercise-Induced Ischaemia

The cardiovascular response to exercise is the most important circulatory adjustment the body has to make; this is therefore the most important means of understanding how the components of the system interact. Survival of the Homo Sapien species was dependent on the procurement of food, hence gene selection in the Late Paleolithic era was influenced by physical activity. Convincing evidence shows that this genome has remained essentially unchanged over the past 10,000 years. The findings of this study demonstrate that in the presence of significant coronary artery disease, a biphasic LV response to exercise occurs. Although early diastolic abnormalities are demonstrated, in an attempt to increase circulating blood flow to exercising muscles, contractile function and cardiac output increase; a threshold is then reached, believed to be a certain duration and intensity of ischaemia (inability of supply to meet demand), beyond which impairment of contractile function and ventricular-arterial coupling occurs. Interestingly in an attempt to ameliorate these stressors, the system firstly maintains diastolic time fraction to maintain coronary blood flow and secondly, reduces external work. Variations in dP/dt closely correlated with generated wave energies suggesting that wave intensity analysis may well be a potential surrogate for changes cardiac

mechanics. This is the first time to our knowledge that these processes have been examined to this accuracy.

This study provided great insight into the adverse pathophysiological mechanisms surrounding exercise-induced angina, facilitating a new look at therapeutic agents and the anti-ischaemic mechanisms of nitrates.

Chapter 5: The Anti-Ischaemic Mechanism Of Nitrates

The importance of this work centred on delineating the precise mechanism of action of nitrates. Previous studies have examined coronary blood flow and LV haemodynamics in isolation, thus it was felt extremely important to examine the coordinated cardiovascular response. We demonstrated that the administration of nitrates had no measured effect on intrinsic myocardial properties (contractile function and compliance); however, the beneficial effects were found to be restoration of the imbalance between supply and demand. Stenosis dilatation and reduced myocardial oxygen consumption, were driven by the vasodilator effects of nitrate, specifically 3 mechanisms were demonstrated: 1) preload reduction through venodilatation 2) afterload reduction by systemic arterial vasodilation and therefore enhanced ventricular-arterial coupling 3) increased pump efficiency both in terms of the VA interaction and with regard to myocardial energy transfer.

Chapter 6: 3D Myocardial Deformation Imaging

Subclinical systolic and diastolic left ventricular (LV) dysfunction have been shown to be independently related to atherosclerosis, providing incremental value over traditional

risk stratification. This was the first validation of 3D speckle tracking echocardiographic indices of strain with invasive measures of contractility in humans; although further work is required with larger scale validation, 3D STE may be useful as a prognostic tool.

Chapter 7: Left Ventricular Partitioning Device

Ischaemic cardiomyopathy is the end stage of ischaemic heart disease; interventions are limited beyond pharmacological therapy. An important measure of therapeutic efficacy is the demonstrable improvement in LV volume and geometry. In this chapter the results of the haemodynamic effects of percutaneous ventricular restoration therapy (PVR) were presented. We demonstrated that PVR reduces LV volumes and dyssynchrony through geometrical restoration and induces reverse remodelling. The resulting effect on LV performance is improved contractility and ejection and enhanced VA coupling (interaction of the ventricle with the arterial system) without the associated morbidity and mortality of surgery.

Conclusions

A complex interaction exists between the myocardium, coronary arteries and systemic vasculature. By developing novel tools that enabled simultaneous analysis of these components of the system we were able to describe the impact of cardiac mechanics on coronary blood flow and the origins of wave energies in the coronary arteries. The pathophysiological response to exercise in a cohort of patients with ischaemic heart disease demonstrated a biphasic response to exercise. The mechanism of nitrates were shown to be a through a combination of coronary, cardiac and systemic effects that

restore the supply-demand imbalance by stenosis dilatation and increased cardiac efficiency. PVR was shown to be a feasible therapeutic option in end-stage heart failure by improving chamber geometry and inducing LV reverse remodelling.

Future Work

For true simultaneous online analysis to be possible the novel software system would need to be integrated into the commercially available hardware; this is the next stage in software development. The potential for this analytical tool is vast, the work produced in this thesis has already been fundamental to establishing other avenues of research including: 1) An enhanced understanding of biventricular pacing by way of simultaneous LV - aortic and right ventricular - pulmonary artery flow measurements. 2) The investigation of haemodynamic support devices during high-risk angioplasty to determine of the combined effects on LV function, afterload and coronary perfusion.

9 BIBLIOGRAPHY

1. Solaro, R. J. *Regulation of Cardiac Contractility*. (Morgan & Claypool Life Sciences, 2011).
2. Kobayashi, T. & Solaro, R. J. Calcium, thin filaments, and the integrative biology of cardiac contractility. *Annual review of physiology* **67,** 39–67 (2005).
3. Hinken, A. C. & Solaro, R. J. A dominant role of cardiac molecular motors in the intrinsic regulation of ventricular ejection and relaxation. *Physiology (Bethesda, Md.)* **22,** 73–80 (2007).
4. Klabunde, R. *Cardiovascular Physiology Concepts*. (Lippincott Williams & WIlkins, 2011).
5. Bers, D. M. Calcium cycling and signaling in cardiac myocytes. *Annual review of physiology* **70,** 23–49 (2008).
6. Greenstein, J. L. & Winslow, R. L. Integrative systems models of cardiac excitation-contraction coupling. *Circulation research* **108,** 70–84 (2011).
7. Bers, D. M. *Excitation-Contraction Coupling and Cardiac Contractile Force*. (Springer Science & Business Media, 2001).
8. Suga, H. Ventricular energetics. *Physiological reviews* **70,** 247–277 (1990).
9. Robison, G. *Cyclic AMP*. (Elsevier, 2012).
10. Koss, K. L. & Kranias, E. G. Phospholamban: A Prominent Regulator of Myocardial Contractility. *Circulation research* **79,** 1059–1063 (1996).
11. Burkhoff, D. MECHANICAL PROPERTIES OF THE HEART AND ITS iteraction with the CVS. 1–23 (2002).
12. Beer, E. L. *et al.* Effect of sarcomere length and filament lattice spacing on force development in skinned cardiac and skeletal muscle preparations from the rabbit. *Basic research in cardiology* **83,** 410–423 (1988).
13. Blix, M. Die Länge und die Spannung des Muskels 1. *Skandinavisches Archiv Für Physiologie* **5,** 150–173 (2012).
14. Gordon, A. M. & Pollack, G. H. Effects of calcium on the sarcomere length-tension relation in rat cardiac muscle. Implications for the Frank-Starling mechanism. *Circ Res* **47,** 610–619 (1980).
15. Keurs, Ter, H. E. D. J., Rijnsburger, W. H., Van Heuningen, R. & Nagelsmit, M. J. in *Cardiac Dynamics* **2,** 25–36 (Springer Netherlands, 1980).
16. Diamond, G. *et al.* Dlastolic Pressure-Volume Relationship in the Canine Left Ventricle. *Circulation research* **29,** 267–275 (1971).
17. Jacob, R. & Kissling, G. Ventricular pressure-volume relations as the primary basis for evaluation of cardiac mechanics. Return to Frank's diagram. *Basic research in cardiology* **84,** 227–246 (1989).
18. Laird, J. D. Asymptotic slope of log pressure vs log volume as an approximate index of the diastolic elastic properties of the myocardium in man. *Circulation* **53,** 443–449 (1976).
19. Levine, H. J. Compliance of the left ventricle. *Circulation* **46,** 423–426 (1972).
20. Braunwald, E. & ROSS, J. The ventricular end-diastolic pressure. Appraisal of its value in the recognition of ventricular failure in man. *Am J Med* **34,** 147–150 (1963).
21. Suga, H., Yamada, O., Goto, Y. & Igarashi, Y. Peak isovolumic pressure-volume relation of puppy left ventricle. *American journal of physiology. Heart*

and circulatory physiology **250,** H167–H172 (1986).
22. Fabiato, A. & Fabiato, F. Dependence of calcium release, tension generation and restoring forces on sarcomere length in skinned cardiac cells. *Eur J Cardiol* **4 Suppl,** 13–27 (1976).
23. Hibberd, M. G. & Jewell, B. R. Calcium-and length-dependent force production in rat ventricular muscle. *The Journal of physiology* **329,** 527–540 (1982).
24. Grossman, W., Braunwald, E., Mann, T., McLaurin, L. P. & Green, L. H. Contractile state of the left ventricle in man as evaluated from end-systolic pressure-volume relations. *Circulation* **56,** 845–852 (1977).
25. Suga, H. & Sagawa, K. Instantaneous pressure-volume relationships and their ratio in the excised, supported canine left ventricle. *Circ Res* **35,** 117–126 (1974).
26. Sagawa, K. & Relation, I. P.-V. V. Editorial: the end-systolic pressure-volume relation of the ventricle: definition, modifications and clinical use. *Circulation* **63,** 1223–1227 (1981).
27. Suga, H., Sagawa, K. & Shoukas, A. A. Load independence of the instantaneous pressure-volume ratio of the canine left ventricle and effects of epinephrine and heart rate on the ratio. *Circ Res* **32,** 314–322 (1973).
28. Nozawa, T. *et al.* Relation between oxygen consumption and pressure-volume area of in situ dog heart. *The American journal of physiology* **253,** H31–40 (1987).
29. Gibbs, C. L. Cardiac energetics. *Physiological reviews* **58,** 174–254 (1978).
30. Hasenfuss, G. *et al.* Energetic aspects of inotropic interventions in rat myocardium. *Basic research in cardiology* **82 Suppl 2,** 251–259 (1987).
31. Burkhoff, D. & Sagawa, K. Ventricular efficiency predicted by an analytical model. *The American journal of physiology* **250,** R1021–R1027 (1986).
32. Nozawa, T., Cheng, C. P., Noda, T. & Little, W. C. Effect of exercise on left ventricular mechanical efficiency in conscious dogs. *Circulation* **90,** 3047–3054 (1994).
33. Little, W. C. *et al.* Comparison of measures of left ventricular contractile performance derived from pressure-volume loops in conscious dogs. *Circulation* **80,** 1378–1387 (1989).
34. Kelly, R. P. *et al.* Effective arterial elastance as index of arterial vascular load in humans. *Circulation* **86,** 513–521 (1992).
35. Nichols, W. W. & Pepine, C. J. Left ventricular afterload and aortic input impedance: implications of pulsatile blood flow. *Progress in cardiovascular diseases* **24,** 293–306 (1982).
36. O'Rourke, M. F. Vascular impedance in studies of arterial and cardiac function. *Physiological reviews* **62,** 570–623 (1982).
37. Sunagawa, K., Maughan, W. L., Burkhoff, D. & Sagawa, K. Left ventricular interaction with arterial load studied in isolated canine ventricle. *The American journal of physiology* **245,** H773–80 (1983).
38. Kass, D. A. Ventricular arterial stiffening: integrating the pathophysiology. *Hypertension* **46,** 185–193 (2005).
39. Cingolani, O. H. & Kass, D. A. Pressure-volume relation analysis of mouse ventricular function. *American journal of physiology. Heart and circulatory physiology* **301,** H2198–206 (2011).
40. De Tombe, P. P., Jones, S., Burkhoff, D., Hunter, W. C. & Kass, D. A.

Ventricular stroke work and efficiency both remain nearly optimal despite altered vascular loading. *The American journal of physiology* **264,** H1817–24 (1993).
41. Smedsrud, M. K. *et al.* Echocardiographic assessment of myocardial strain. *Journal of the American College of Cardiology* **58,** 1401–1413 (2011).
42. Miyatake, K. *et al.* New method for evaluating left ventricular wall motion by color-coded tissue Doppler imaging: in vitro and in vivo studies. *J Am Coll Cardiol* **25,** 717–724 (1995).
43. Heimdal, A., Støylen, A., Torp, H. & Skjaerpe, T. Real-time strain rate imaging of the left ventricle by ultrasound. *Journal of the American Society of Echocardiography : official publication of the American Society of Echocardiography* **11,** 1013–1019 (1998).
44. Urheim, S., Edvardsen, T., Torp, H., Angelsen, B. & Smiseth, O. A. Myocardial strain by Doppler echocardiography. Validation of a new method to quantify regional myocardial function. *Circulation* **102,** 1158–1164 (2000).
45. D'hooge, J. *et al.* Regional strain and strain rate measurements by cardiac ultrasound: principles, implementation and limitations. *European journal of echocardiography : the journal of the Working Group on Echocardiography of the European Society of Cardiology* **1,** 154–170 (2000).
46. Yamada, E., Garcia, M., Thomas, J. D. & Marwick, T. H. Myocardial Doppler velocity imaging--a quantitative technique for interpretation of dobutamine echocardiography. *Am J Cardiol* **82,** 806–9, A9–10 (1998).
47. Notomi, Y. *et al.* Assessment of left ventricular torsional deformation by Doppler tissue imaging: validation study with tagged magnetic resonance imaging. *Circulation* **111,** 1141–1147 (2005).
48. Derumeaux, G. *et al.* Doppler tissue imaging quantitates regional wall motion during myocardial ischemia and reperfusion. *Circulation* **97,** 1970–1977 (1998).
49. Edvardsen, T. *et al.* Quantification of left ventricular systolic function by tissue Doppler echocardiography: added value of measuring pre- and postejection velocities in ischemic myocardium. *Circulation* **105,** 2071–2077 (2002).
50. Skulstad, H. *et al.* Postsystolic shortening in ischemic myocardium: active contraction or passive recoil? *Circulation* **106,** 718–724 (2002).
51. Hanekom, L. *et al.* Incremental value of strain rate analysis as an adjunct to wall-motion scoring for assessment of myocardial viability by dobutamine echocardiography: a follow-up study after revascularization. *Circulation* **112,** 3892–3900 (2005).
52. Becker, M. *et al.* Analysis of myocardial deformation based on ultrasonic pixel tracking to determine transmurality in chronic myocardial infarction. *European heart journal* **27,** 2560–2566 (2006).
53. Kovács, A. *et al.* Strain and strain rate by speckle-tracking echocardiography correlate with pressure-volume loop-derived contractility indices in a rat model of athlete's heart. *American journal of physiology. Heart and circulatory physiology* **308,** H743–8 (2015).
54. Borg, T. K. & Caulfield, J. B. The collagen matrix of the heart. *Federation proceedings* **40,** 2037–2041 (1981).
55. Gray, H. *VI. The Arteries. 1. Introduction. Gray, Henry. 1918. Anatomy of the Human Body.* (1918).

56. Chilian, W. M. Coronary microcirculation in health and disease. Summary of an NHLBI workshop. *Circulation* **95,** 522–528 (1997).
57. van den Wijngaard, J. P. H. M. *et al.* Porcine coronary collateral formation in the absence of a pressure gradient remote of the ischemic border zone. *Am J Physiol Heart Circ Physiol* **300,** H1930–7 (2011).
58. Chilian, W. M., Eastham, C. L. & Marcus, M. L. Microvascular distribution of coronary vascular resistance in beating left ventricle. *The American journal of physiology* **251,** H779–88 (1986).
59. Marcus, M. L. *et al.* Understanding the coronary circulation through studies at the microvascular level. *Circulation* **82,** 1–7 (1990).
60. Algranati, D., Kassab, G. S. & Lanir, Y. Why is the subendocardium more vulnerable to ischemia? A new paradigm. *American journal of physiology. Heart and circulatory physiology* **300,** H1090–100 (2011).
61. Tillmanns, H., Steinhausen, M., Leinberger, H., Thederan, H. & Kübler, W. Pressure measurements in the terminal vascular bed of the epimyocardium of rats and cats. *Circ Res* **49,** 1202–1211 (1981).
62. Hoffman, J. I., Baer, R. W., Hanley, F. L. & Messina, L. M. Regulation of transmural myocardial blood flow. *J Biomech Eng* **107,** 2–9 (1985).
63. Bruinsma, P., Arts, T., Dankelman, J. & Spaan, J. A. Model of the coronary circulation based on pressure dependence of coronary resistance and compliance. *Basic research in cardiology* **83,** 510–524 (2016).
64. Merkus, D. *et al.* Prolonged diastolic time fraction protects myocardial perfusion when coronary blood flow is reduced. *Circulation* **100,** 75–81 (1999).
65. Fokkema, D. S. *et al.* Diastolic time fraction as a determinant of subendocardial perfusion. *Am J Physiol Heart Circ Physiol* **288,** H2450–6 (2005).
66. Tune, J. D., Gorman, M. W. & Feigl, E. O. Matching coronary blood flow to myocardial oxygen consumption. *Journal of applied physiology* **97,** 404–415 (2004).
67. van de Hoef, T. P. *et al.* Coronary pressure-flow relations as basis for the understanding of coronary physiology. *Journal of molecular and cellular cardiology* **52,** 786–793 (2012).
68. Bassenge, E. & Heusch, G. Endothelial and neuro-humoral control of coronary blood flow in health and disease. *Reviews of physiology, biochemistry and pharmacology* **116,** 77–165 (1990).
69. Komaru, T., Kanatsuka, H. & Shirato, K. Coronary microcirculation: physiology and pharmacology. *Pharmacology & therapeutics* **86,** 217–261 (2000).
70. MOSHER, P., ROSS, J., MCFATE, P. A. & SHAW, R. F. Control of Coronary Blood Flow by an Autoregulatory Mechanism. *Circ Res* **14,** 250–259 (1964).
71. Chilian, W. M. & Layne, S. M. Coronary microvascular responses to reductions in perfusion pressure. Evidence for persistent arteriolar vasomotor tone during coronary hypoperfusion. *Circ Res* **66,** 1227–1238 (1990).
72. Westerhof, N., Boer, C., Lamberts, R. R. & Sipkema, P. Cross-talk between cardiac muscle and coronary vasculature. *Physiological reviews* **86,** 1263–1308 (2006).
73. Koller, A. & Bagi, Z. Nitric oxide and H2O2 contribute to reactive dilation of isolated coronary arterioles. *Am J Physiol Heart Circ Physiol* **287,** H2461–7 (2004).

74. Koller, A. & Kaley, G. Endothelial regulation of wall shear stress and blood flow in skeletal muscle microcirculation. *The American journal of physiology* **260,** H862–8 (1991).
75. Brown, B. G., Bolson, E., Frimer, M. & Dodge, H. T. Quantitative coronary arteriography: estimation of dimensions, hemodynamic resistance, and atheroma mass of coronary artery lesions using the arteriogram and digital computation. *Circulation* **55,** 329–337 (1977).
76. Young, D. F. & Tsai, F. Y. Flow characteristics in models of arterial stenosesII. Unsteady flow. *Journal of biomechanics* **6,** 547–559 (1973).
77. Kern, M. J. *et al.* Physiological assessment of coronary artery disease in the cardiac catheterization laboratory: a scientific statement from the American Heart Association Committee on Diagnostic and Interventional Cardiac Catheterization, Council on Clinical Cardiology. *Circulation* **114,** 1321–1341 (2006).
78. Gould, K. L. Pressure-flow characteristics of coronary stenoses in unsedated dogs at rest and during coronary vasodilation. *Circulation research* **43,** 242–253 (1978).
79. Gould, K. L. Quantification of coronary artery stenosis in vivo. *Circulation research* **57,** 341–353 (1985).
80. Siebes, M. *et al.* Single-wire pressure and flow velocity measurement to quantify coronary stenosis hemodynamics and effects of percutaneous interventions. *Circulation* **109,** 756–762 (2004).
81. Young, D. F., Cholvin, N. R., Kirkeeide, R. L. & Roth, A. C. Hemodynamics of arterial stenoses at elevated flow rates. *Circ Res* **41,** 99–107 (1977).
82. Gould, K. L. & Kelley, K. O. Physiological significance of coronary flow velocity and changing stenosis geometry during coronary vasodilation in awake dogs. *Circulation research* **50,** 695–704 (1982).
83. Gould, K. L., Lipscomb, K. & Hamilton, G. W. Physiologic basis for assessing critical coronary stenosis: instantaneous flow response and regional distribution during coronary hyperemia as measures of coronary flow reserve. *Am J Cardiol* **33,** 87–94 (1974).
84. Hoffman, J. I. Maximal coronary flow and the concept of coronary vascular reserve. *Circulation* **70,** 153–159 (1984).
85. Kern, M. J. *et al.* Variations in normal coronary vasodilatory reserve stratified by artery, gender, heart transplantation and coronary artery disease. *J Am Coll Cardiol* **28,** 1154–1160 (1996).
86. Baumgart, D. *et al.* Improved Assessment of Coronary Stenosis Severity Using the Relative Flow Velocity Reserve. *Circulation* **98,** 40–46 (1998).
87. Baumgart, D. *et al.* Current concepts of coronary flow reserve for clinical decision making during cardiac catheterization. *Am Heart J* **136,** 136–149 (1998).
88. McGinn, A. L., White, C. W. & Wilson, R. F. Interstudy variability of coronary flow reserve. Influence of heart rate, arterial pressure, and ventricular preload. *Circulation* **81,** 1319–1330 (1990).
89. Pijls, N. H., van Son, J. A., Kirkeeide, R. L., De Bruyne, B. & Gould, K. L. Experimental basis of determining maximum coronary, myocardial, and collateral blood flow by pressure measurements for assessing functional stenosis severity before and after percutaneous transluminal coronary

angioplasty. *Circulation* **87,** 1354–1367 (1993).
90. Pijls, N. H. *et al.* Fractional flow reserve. A useful index to evaluate the influence of an epicardial coronary stenosis on myocardial blood flow. *Circulation* **92,** 3183–3193 (1995).
91. De Bruyne, B., Bartunek, J., Sys, S. U. & Heyndrickx, G. R. Relation between myocardial fractional flow reserve calculated from coronary pressure measurements and exercise-induced myocardial ischemia. *Circulation* **92,** 39–46 (1995).
92. Pijls, N. H. J. *et al.* Measurement of fractional flow reserve to assess the functional severity of coronary-artery stenoses. *New England Journal of Medicine* **334,** 1703–1708 (1996).
93. Meuwissen, M. *et al.* Role of variability in microvascular resistance on fractional flow reserve and coronary blood flow velocity reserve in intermediate coronary lesions. *Circulation* **103,** 184–187 (2001).
94. Meuwissen, M. *et al.* Role of fractional and coronary flow reserve in clinical decision making in intermediate coronary lesions. *Interventional Cardiology* **1,** 237–255 (2009).
95. Parker, K. H. & Jones, C. J. Forward and backward running waves in the arteries: analysis using the method of characteristics. *J Biomech Eng* **112,** 322–326 (1990).
96. Davies, J. E. *et al.* Evidence of a dominant backward-propagating 'suction' wave responsible for diastolic coronary filling in humans, attenuated in left ventricular hypertrophy. *Circulation* **113,** 1768–1778 (2006).
97. Parker, K. H. An introduction to wave intensity analysis. *Med Biol Eng Comput* **47,** 175–188 (2009).
98. Smiseth, O. A. *et al.* The pulmonary venous systolic flow pulse—its origin and relationship to left atrial pressure. *Journal of the American College of Cardiology* **34,** 802–809 (1999).
99. Siebes, M., Kolyva, C., Verhoeff, B.-J. J., Piek, J. J. & Spaan, J. A. Potential and limitations of wave intensity analysis in coronary arteries. *Med Biol Eng Comput* **47,** 233–239 (2009).
100. Rolandi, M. C. *et al.* Coronary wave intensity during the Valsalva manoeuvre in humans reflects altered intramural vessel compression responsible for extravascular resistance. *The Journal of physiology* **590,** 4623–4635 (2012).
101. Lockie, T. P. E. *et al.* Synergistic adaptations to exercise in the systemic and coronary circulations that underlie the warm-up angina phenomenon. *Circulation* **126,** 2565–2574 (2012).
102. Bramwell JC. Hill, A. V. The velocity of the pulse wave in man. *Proc R Soc Lond B* 298–306 (1922).
103. Hamilton, W. F. & Dow, P. An experimental study of the standing waves in the pulse propagated through the aorta. *American Heart Journal* **18,** 121–122 (1939).
104. Rolandi, M. C. *et al.* Wave speed in human coronary arteries is not influenced by microvascular vasodilation: implications for wave intensity analysis. *Basic research in cardiology* **109,** 405–11 (2014).
105. Green, H. D., Gregg, D. D. & Wiggers, C. J. The phasic changes in coronary flow established by differential pressure curves. *American Journal of Physiology--Legacy Content* **112,** 627–639 (1935).

106. Gregg, D. E. & Eckstein, R. W. Measurements of intramyocardial pressure. *American Journal of Physiology--Legacy Content* **132,** 781–790 (1941).
107. Sun, Y.-H., Anderson, T. J., Parker, K. I. M. H., Tyberg, J. V. & Parker, K. H. cutting-edge report. **1,** 1636–1644 (2000).
108. Williamson, J. W. & Friedman, D. B. 913 HEART RATE AND BLOOD PRESSURE RESPONSES AT THE ONSET OF DYNAMIC EXERCISE. *Medicine and science in sports and exercise* **26,** S163 (1994).
109. Buckwalter, J. B., Mueller, P. J. & Clifford, P. S. Sympathetic vasoconstriction in active skeletal muscles during dynamic exercise. *Journal of applied physiology (Bethesda, Md. : 1985)* **83,** 1575–1580 (1997).
110. Laughlin, M. H. Cardiovascular response to exercise. *The American journal of physiology* **277,** S244–59 (1999).
111. LIND, A. R. Cardiovascular Responses to Static Exercise (Isometrics, Anyone?). *Circulation* **41,** 173–176 (1970).
112. Laird, W. P., Fixler, D. E. & Huffines, F. D. Cardiovascular response to isometric exercise in normal adolescents. *Circulation* **59,** 651–654 (1979).
113. Muller, J. M., Myers, P. R. & Laughlin, M. H. Vasodilator responses of coronary resistance arteries of exercise-trained pigs. *Circulation* **89,** 2308–2314 (1994).
114. Laughlin, M. H. Skeletal muscle blood flow capacity: role of muscle pump in exercise hyperemia. *The American journal of physiology* **253,** H993–1004 (1987).
115. Hautala, A. J., Kiviniemi, A. M. & Tulppo, M. P. Individual responses to aerobic exercise: the role of the autonomic nervous system. *Neurosci Biobehav Rev* **33,** 107–115 (2009).
116. Davidson, N. S., Goldner, S. & McCloskey, D. I. Respiratory modulation of barareceptor and chemoreceptor reflexes affecting heart rate and cardiac vagal efferent nerve activity. *The Journal of physiology* **259,** 523–530 (1976).
117. Akselrod, S. *et al.* Power spectrum analysis of heart rate fluctuation: a quantitative probe of beat-to-beat cardiovascular control. *Science* **213,** 220–222 (1981).
118. Goldstein, D. S. Differential responses of components of the autonomic nervous system. *Handb Clin Neurol* **117,** 13–22 (2013).
119. Joyner, M. J. & Casey, D. P. Regulation of Increased Blood Flow (Hyperemia) to Muscles During Exercise: A Hierarchy of Competing Physiological Needs. *Physiological reviews* **95,** 549–601 (2015).
120. Kitamura, K., Jorgensen, C. R., Gobel, F. L., Taylor, H. L. & Wang, Y. Hemodynamic correlates of myocardial oxygen consumption during upright exercise. *Journal of applied physiology* **32,** 516–522 (1972).
121. Duncker, D. J. & Bache, R. J. Regulation of coronary blood flow during exercise. *Physiological reviews* **88,** 1009–1086 (2008).
122. Holmberg, S., Serzysko, W. & Varnauskas, E. Coronary circulation during heavy exercise in control subjects and patients with coronary heart disease. *Acta medica Scandinavica* **190,** 465–480 (1971).
123. Tune, J. D., Richmond, K. N., Gorman, M. W. & Feigl, E. O. Control of coronary blood flow during exercise. *Experimental biology and medicine (Maywood, N.J.)* **227,** 238–250 (2002).
124. Gorlin, R., Cohen, L. S., Elliott, W. C., Klein, M. D. & Lane, F. J. Effect of

supine exercise on left ventricular volume and oxygen consumption in man. *Circulation* **32,** 361–371 (1965).
125. Paulus, W. J. *et al.* Different effects of two types of ischemia on myocardial systolic and diastolic function. *The American journal of physiology* **248,** H719–28 (1985).
126. Fedor, J. M., Rembert, J. C., McIntosh, D. M. & Greenfield, J. C. Effects of exercise- and pacing-induced tachycardia on coronary collateral flow in the awake dog. *Circ Res* **46,** 214–220 (1980).
127. Asanoi, H., Kameyama, T., Ishizaka, S., Miyagi, K. & Sasayama, S. Ventriculoarterial coupling during exercise in normal human subjects. *International journal of cardiology* **36,** 177–186 (1992).
128. Chantler, P. D., Lakatta, E. G. & Najjar, S. S. Arterial-ventricular coupling: mechanistic insights into cardiovascular performance at rest and during exercise. *Journal of applied physiology (Bethesda, Md. : 1985)* **105,** 1342–1351 (2008).
129. Asanoi, H., Sasayama, S. & Kameyama, T. Ventriculoarterial coupling in normal and failing heart in humans. *Circ Res* **65,** 483–493 (1989).
130. Graham, I. *et al.* European guidelines on cardiovascular disease prevention in clinical practice: executive summary Fourth Joint Task Force of the European Society of Cardiology and Other Societies on Cardiovascular Disease Prevention in Clinical Practice (Constituted by re. *European heart journal* **28,** 2375–2414 (2007).
131. Allender, S., Scarborough, P. & Peto, V. European cardiovascular disease statistics 2012. *European Heart* (2012).
132. Jorgensen, T. *et al.* Population-level changes to promote cardiovascular health. *European journal of preventive cardiology* **20,** 409–421 (2013).
133. COLLINS, P. Pathophysiology of angina. *The Lancet* **335,** 94–96 (1990).
134. Silverman, M. E. William Heberden and Some Account of a Disorder of the Breast. *Clinical cardiology* **10,** 211–213 (1987).
135. Thadani, U. Medical therapy of stable angina pectoris. *Cardiology clinics* **9,** 73–87 (1991).
136. Maseri, A. *et al.* Mechanisms and significance of cardiac ischemic pain. *Progress in cardiovascular diseases* **35,** 1–18 (1992).
137. Colbeck, E. H. ANGINA PECTORIS: A CRITICISM AND A HYPOTHESIS. *The Lancet* **161,** 793–795 (1903).
138. Crea, F. & Gaspardone, A. New look to an old symptom: angina pectoris. *Circulation* **96,** 3766–3773 (1997).
139. Crea, F. *et al.* Role of adenosine in pathogenesis of anginal pain. *Circulation* **81,** 164–172 (1990).
140. van Calker, D., Müller, M. & Hamprecht, B. Adenosine regulates via two different types of receptors, the accumulation of cyclic AMP in cultured brain cells. *J Neurochem* **33,** 999–1005 (1979).
141. SYLVÉN, C. Mechanisms of pain in angina pectoris--a critical review of the adenosine hypothesis. *Cardiovascular drugs and therapy / sponsored by the International Society of Cardiovascular Pharmacotherapy* **7,** 745–759 (1993).
142. Malliani, A., Lombardi, F. & Pagani, M. Sensory innervation of the heart. *Progress in brain research* **67,** 39–48 (1986).
143. Davies, G. J. *et al.* Sequence and magnitude of ventricular volume changes in

painful and painless myocardial ischemia. *Circulation* **78,** 310–319 (1988).
144. Tomai, F. *et al.* Mechanisms of cardiac pain during coronary angioplasty. *J Am Coll Cardiol* **22,** 1892–1896 (1993).
145. Grossman, W., Serizawa, T. & Carabello, B. A. Studies on the mechanism of altered left ventricular diastolic pressure-volume relations during ischaemia. *European heart journal* **1,** 141–147 (1980).
146. Carroll, J. D., Hess, O. M., Hirzel, H. O. & Krayenbuehl, H. P. Exercise-induced ischemia: the influence of altered relaxation on early diastolic pressures. *Circulation* **67,** 521–528 (1983).
147. Sunagawa, K. *et al.* Effects of coronary arterial pressure on left ventricular end-systolic pressure-volume relation of isolated canine heart. *Circ Res* **50,** 727–734 (1982).
148. Remmelink, M. *et al.* The effect of repeated ischaemic periods on left ventricular dynamics during percutaneous coronary intervention. *EuroIntervention : journal of EuroPCR in collaboration with the Working Group on Interventional Cardiology of the European Society of Cardiology* **6,** 623–629 (2010).
149. Kass, D. A., Midei, M., Brinker, J. & Maughan, W. L. Influence of coronary occlusion during PTCA on end-systolic and end- diastolic pressure-volume relations in humans. *Circulation* **81,** 447–460 (1990).
150. Remmelink, M. *et al.* Acute left ventricular dynamic effects of primary percutaneous coronary intervention from occlusion to reperfusion. *Journal of the American College of Cardiology* **53,** 1498–1502 (2009).
151. Remmelink, M. *et al.* Coronary microcirculatory dysfunction is associated with left ventricular dysfunction during follow-up after STEMI. *Netherlands heart journal : monthly journal of the Netherlands Society of Cardiology and the Netherlands Heart Foundation* **21,** 238–244 (2013).
152. Dawson, J. R. & Gibson, D. G. Left ventricular filling and early diastolic function at rest and during angina in patients with coronary artery disease. *British heart journal* **61,** 248–257 (1989).
153. Momomura, S. *et al.* The relationships of high energy phosphates, tissue pH, and regional blood flow to diastolic distensibility in the ischemic dog myocardium. *Circ Res* **57,** 822–835 (1985).
154. Bronzwaer, J. G., De Bruyne, B., Ascoop, C. A. & Paulus, W. J. Comparative effects of pacing-induced and balloon coronary occlusion ischemia on left ventricular diastolic function in man. *Circulation* **84,** 211–222 (1991).
155. Takano, H. & Glantz, S. A. Left ventricular contractility predicts how the end-diastolic pressure-volume relation shifts during pacing-induced ischemia in dogs. *Circulation* **91,** 2423–2434 (1995).
156. Steendijk, P., Baan, J. & Velde, der, E. T. Effects of critical coronary stenosis on global systolic left ventricular function quantified by pressure-volume relations during dobutamine stress in the canine heart. *J Am Coll Cardiol* **32,** 816–826 (1998).
157. Parker, J. D. & Parker, J. O. Nitrate therapy for stable angina pectoris. *The New England journal of medicine* **338,** 520–531 (1998).
158. Fung, H. L., Chung, S. J., Bauer, J. A., Chong, S. & Kowaluk, E. A. Biochemical mechanism of organic nitrate action. *Am J Cardiol* **70,** 4B–10B (1992).

159. Ignarro, L. J. Endothelium-derived nitric oxide: pharmacology and relationship to the actions of organic nitrate esters. *Pharm. Res.* **6,** 651–659 (1989).
160. Fung, H. L. *et al.* Cellular mechanisms of nitrate action. *Z Kardiol* **78 Suppl 2,** 14–7– discussion 64–7 (1989).
161. Quyyumi, A. A. *et al.* Contribution of nitric oxide to metabolic coronary vasodilation in the human heart. *Circulation* **92,** 320–326 (1995).
162. Conti, C. R. *et al.* Effect of glyceryl trinitrate on coronary and systemic hemodynamics in man. *Am J Med* **74,** 28–32 (1983).
163. de Kam, P. J. *et al.* Prediction of 6 months left ventricular dilatation after myocardial infarction in relation to cardiac morbidity and mortality. Application of a new dilatation model to GISSI-3 data. *European heart journal* **23,** 536–542 (2002).
164. Haber, H. L. *et al.* Bolus intravenous nitroglycerin predominantly reduces afterload in patients with excessive arterial elastance. *J Am Coll Cardiol* **22,** 251–257 (1993).
165. Ludbrook, P. A., Byrne, J. D., Kurnik, P. B. & McKnight, R. C. Influence of reduction of preload and afterload by nitroglycerin on left ventricular diastolic pressure-volume relations and relaxation in man. *Circulation* **56,** 937–943 (1977).
166. Ludbrook, P. A., Byrne, J. D. & McKnight, R. C. Influence of right ventricular hemodynamics on left ventricular diastolic pressure-volume relations in man. *Circulation* **59,** 21–31 (1979).
167. Fung, H. L. Do nitrates differ? *Br J Clin Pharmacol* **34 Suppl 1,** 5S–9S (1992).
168. Fujita, M., Yamanishi, K., Inoko, M. & Miwa, K. Preferential dilation of recipient coronary arteries of the collateral circulation by intracoronary administration of nitroglycerin. *J Am Coll Cardiol* **24,** 631–635 (1994).
169. Brown, B. G., Bolson, E., Petersen, R. B., Pierce, C. D. & Dodge, H. T. The mechanisms of nitroglycerin action: stenosis vasodilatation as a major component of the drug response. *Circulation* **64,** 1089–1097 (1981).
170. Hess, O. M. *et al.* Diltiazem alone and combined with nitroglycerin: effect on normal and diseased human coronary arteries. *European heart journal* **10 Suppl F,** 142–146 (1989).
171. Hess, W., Klein, W., Mueller-Busch, C. & Tarnow, J. Haemodynamic effects of dopamine and dopamine combined with nitroglycerin in patients subjected to coronary bypass surgery. *British journal of anaesthesia* **51,** 1063–1069 (1979).
172. Kingma, I. *et al.* A mechanism for the nitroglycerin-induced downward shift of the left ventricular diastolic pressure-diameter relation. *Am J Cardiol* **57,** 673–677 (1986).
173. Pfeffer, M. A. & Braunwald, E. Ventricular remodeling after myocardial infarction. Experimental observations and clinical implications. *Circulation* **81,** 1161–1172 (1990).
174. Gaudron, P., Eilles, C., Kugler, I. & Ertl, G. Progressive left ventricular dysfunction and remodeling after myocardial infarction. Potential mechanisms and early predictors. *Circulation* **87,** 755–763 (1993).
175. Stone, P. H. *et al.* Prognostic significance of location and type of myocardial infarction: Independent adverse outcome associated with anterior location. *Journal of the American College of Cardiology* **11,** 453–463 (1988).
176. Singh, R. B. GISSI-Prevenzione trial. *Lancet* **354,** 1556–1557 (1999).

177. Chen, J., Normand, S.-L. T., Wang, Y. & Krumholz, H. M. National and Regional Trends in Heart Failure Hospitalization and Mortality Rates for Medicare Beneficiaries, 1998-2008. *JAMA* **306,** 1669–1678 (2011).
178. Konstam, M. A., Kramer, D. G., Patel, A. R., Maron, M. S. & Udelson, J. E. Left ventricular remodeling in heart failure: current concepts in clinical significance and assessment. *JACC. Cardiovascular imaging* **4,** 98–108 (2011).
179. Oliveira, G. H., Al-Kindi, S. G., Bezerra, H. G. & Costa, M. A. Left ventricular restoration devices. *J Cardiovasc Transl Res* **7,** 282–291 (2014).
180. Mazzaferri, E. L. *et al.* Percutaneous left ventricular partitioning in patients with chronic heart failure and a prior anterior myocardial infarction: Results of the PercutAneous Ventricular RestorAtion in Chronic Heart failUre PaTiEnts Trial. *Am Heart J* **163,** 812–820 (2012).
181. Sagic, D. *et al.* Percutaneous implantation of the left ventricular partitioning device for chronic heart failure: a pilot study with 1-year follow-up. *European journal of heart failure* **12,** 600–606 (2010).
182. Cilingiroglu, M., Rollefson, W. A. & Mego, D. Percutaneous implantation of a parachute device for treatment of ischemic heart failure. *Cardiovascular Revascularization Medicine* **14,** 236–240 (2013).
183. Baan, J. *et al.* Continuous measurement of left ventricular volume in animals and humans by conductance catheter. *Circulation* **70,** 812–823 (1984).
184. Burkhoff, D. *et al.* Accuracy of volume measurement by conductance catheter in isolated, ejecting canine hearts. *Circulation* **72,** 440–447 (1985).
185. van der Velde, E. T. *et al.* Left ventricular segmental volume by conductance catheter and Cine-CT. *European heart journal* **13 Suppl E,** 15–21 (1992).
186. Mirsky, I. Assessment of diastolic function: suggested methods and future considerations. *Circulation* **69,** 836–841 (1984).
187. Hoffman, J. I. & Spaan, J. A. Pressure-flow relations in coronary circulation. *Physiological reviews* **70,** 331–390 (1990).
188. Krams, R., van Haelst, A. C., Sipkema, P. & Westerhof, N. Can coronary systolic-diastolic flow differences be predicted by left ventricular pressure or time-varying intramyocardial elastance? *Basic research in cardiology* **84,** 149–159 (1989).
189. Downey, J. M. & Kirk, E. S. Inhibition of coronary blood flow by a vascular waterfall mechanism. *Circulation research* **36,** 753–760 (1975).
190. Mulligan, L. J., Escobedo, D. & Freeman, G. L. Mechanical determinants of coronary blood flow during dynamic alterations in myocardial contractility. *The American journal of physiology* **265,** H1112–8 (1993).
191. Sun, Y.-H. H., Anderson, T. J., Parker, K. H. & Tyberg, J. V. Effects of left ventricular contractility and coronary vascular resistance on coronary dynamics. *Am J Physiol Heart Circ Physiol* **286,** H1590–5 (2004).
192. Rivolo, S., Nagel, E., Smith, N. P. & Lee, J. Automatic selection of optimal Savitzky-Golay filter parameters for Coronary Wave Intensity Analysis. *Conference proceedings : ... Annual International Conference of the IEEE Engineering in Medicine and Biology Society. IEEE Engineering in Medicine and Biology Society. Annual Conference* **2014,** 5056–5059 (2014).
193. Gaemperli, O. *et al.* Real-time left ventricular pressure-volume loops during percutaneous mitral valve repair with the MitraClip system. *Circulation* **127,** 1018–1027 (2013).

194. Kapur, N. K. *et al.* Mechanically unloading the left ventricle before coronary reperfusion reduces left ventricular wall stress and myocardial infarct size. *Circulation* **128,** 328–336 (2013).
195. Burkhoff, D., Mirsky, I. & Suga, H. Assessment of systolic and diastolic ventricular properties via pressure-volume analysis: a guide for clinical, translational, and basic researchers. *Am J Physiol Heart Circ Physiol* **289,** H501–12 (2005).
196. Rivolo, S. *et al.* Enhancing coronary Wave Intensity Analysis robustness by high order central finite differences. *Artery research* **8,** 98–109 (2014).
197. Rivolo, S. *et al.* Accurate and Standardised Coronary Wave Intensity Analysis. *IEEE transactions on bio-medical engineering* 1–1 (2016). doi:10.1109/TBME.2016.2593518
198. Patterson, T. *et al.* NOVEL INSIGHTS INTO THE PHYSIOLOGY OF CARDIAC-CORONARY INTERACTION: A FIRST-IN-HUMAN STUDY UTILISING INVASIVE REAL-TIME SIMULTANEOUS MEASURES OF CORONARY AND LEFT VENTRICULAR HEMODYNAMICS. *Journal of the American College of Cardiology* **67,** 376 (2016).
199. Patterson, T. *et al.* 94 Flow-Contraction Matching in The Human Heart: A Novel Invasive Study of The Complex Cardiac-Coronary Interaction in Ischaemic Heart Disease. *Heart* **102,** A66.3–A67 (2016).
200. De Vecchi, A. *et al.* Catheter-induced errors in pressure measurements in vessels: An in-vitro and numerical study. *IEEE Transactions on Biomedical Engineering* **61,** 1844–1850 (2014).
201. Davies, J. E. *et al.* Use of simultaneous pressure and velocity measurements to estimate arterial wave speed at a single site in humans. *Am J Physiol Heart Circ Physiol* **290,** H878–85 (2006).
202. De Silva, K. *et al.* Coronary and microvascular physiology during intra-aortic balloonudotcounterpulsation. *JACC Cardiovasc Interv* **7,** 631–640 (2014).
203. Savitzky, A. & Golay, M. J. E. Smoothing and Differentiation of Data by Simplified Least Squares Procedures. *Analytical Chemistry* **36,** 1627–1639 (1964).
204. Krishnan, S. R. & Seelamantula, C. S. On the Selection of Optimum Savitzky-Golay Filters. *IEEE Transactions on Signal Processing* **61,** 380–391 (2013).
205. Senzaki, H., Chen, C. H. & Kass, D. A. Single-beat estimation of end-systolic pressure-volume relation in humans. A new method with the potential for noninvasive application. *Circulation* **94,** 2497–2506 (1996).
206. Shishido, T. *et al.* Single-beat estimation of end-systolic elastance using bilinearly approximated time-varying elastance curve. *Circulation* **102,** 1983–1989 (2000).
207. Chen, C.-H. H. *et al.* Noninvasive single-beat determination of left ventricular end-systolic elastance in humans. *J Am Coll Cardiol* **38,** 2028–2034 (2001).
208. Klotz, S. *et al.* Single-beat estimation of end-diastolic pressure-volume relationship: a novel method with potential for noninvasive application. *Am J Physiol Heart Circ Physiol* **291,** H403–12 (2006).
209. Mirsky, I. Assessment of passive elastic stiffness of cardiac muscle: mathematical concepts, physiologic and clinical considerations, directions of future research. *Progress in cardiovascular diseases* **18,** 277–308 (1976).
210. Bache, R. J. & Cobb, F. R. Effect of maximal coronary vasodilation on

transmural myocardial perfusion during tachycardia in the awake dog. *Circulation research* **41,** 648–653 (1977).
211. Nesto, R. W. & Kowalchuk, G. J. The ischemic cascade: temporal sequence of hemodynamic, electrocardiographic and symptomatic expressions of ischemia. *Am J Cardiol* **59,** 23C–30C (1987).
212. Mann, T., Goldberg, S., Mudge, G. H. & Grossman, W. Factors contributing to altered left ventricular diastolic properties during angina pectoris. *Circulation* **59,** 14–20 (1979).
213. Aroesty, J. M. *et al.* Simultaneous assessment of left ventricular systolic and diastolic dysfunction during pacing-induced ischemia. *Circulation* **71,** 889–900 (1985).
214. Fujibayashi, Y. *et al.* Comparative echocardiographic study of recovery of diastolic versus systolic function after brief periods of coronary occlusion: differential effects of intravenous nifedipine administered before and during occlusion. *Journal of the American College of Cardiology* **6,** 1289–1298 (1985).
215. Paulus, W. J. Upward shift and outward bulge. Divergent myocardial effects of pacing angina and brief coronary occlusion. *Circulation* **81,** 1436–1439 (1990).
216. De Bruyne, B. *et al.* Fractional flow reserve-guided PCI versus medical therapy in stable coronary disease. *The New England journal of medicine* **367,** 991–1001 (2012).
217. Kass, D. A. Clinical evaluation of left heart function by conductance catheter technique. *European heart journal* **13 Suppl E,** 57–64 (1992).
218. Steendijk, P. *et al.* Hemodynamic effects of long-term cardiac resynchronization therapy: analysis by pressure-volume loops. *Circulation* **113,** 1295–1304 (2006).
219. Bland, J. M. & Altman, D. G. Statistical methods for assessing agreement between two methods of clinical measurement. *Lancet* **1,** 307–310 (1986).
220. Redwood, S. R., Ferrari, R. & Marber, M. S. Myocardial hibernation and stunning: from physiological principles to clinical practice. *Heart* **80,** 218–222 (1998).
221. Wijns, W. *et al.* Guidelines on myocardial revascularization. *European heart journal* **31,** 2501–2555 (2010).
222. Hirsh, P. D., Hillis, L. D., Campbell, W. B., Firth, B. G. & Willerson, J. T. Release of Prostaglandins and Thromboxane into the Coronary Circulation in Patients with Ischemic Heart Disease. *New England Journal of Medicine* **304,** 685–691 (1981).
223. Jane Scott, M. A randomized prospective trial of intravenous nitroglycerin in patients with acute myocardial infarction. *The Journal of emergency medicine* **2,** 65–66 (1984).
224. GANZ, W. & MARCUS, H. S. Failure of Intracoronary Nitroglycerin to Alleviate Pacing-Induced Angina. *Circulation* **46,** 880–889 (1972).
225. De Coster, P. M. *et al.* Combined effects of nitrates on the coronary and peripheral circulation in exercise-induced ischemia. *Circulation* **81,** 1881–1886 (1990).
226. Abrams, J. Hemodynamic effects of nitroglycerin and long-acting nitrates. *Am Heart J* **110,** 217–224 (1985).
227. Manyari, D. E. *et al.* Isosorbide dinitrate and glyceryl trinitrate: Demonstration

of cross tolerance in the capacitance vessels. *The American journal of cardiology* **55,** 927–931 (1985).
228. *Nitric Oxide*. **143,** (Springer Berlin Heidelberg, 2000).
229. De Coster, P. M. *et al.* Combined effects of nitrates on the coronary and peripheral circulation in exercise-induced ischemia. *Circulation* **81,** 1881–1886 (1990).
230. Gorman, M. W. & Sparks, H. V. Nitroglycerin causes vasodilatation within ischaemic myocardium. *Cardiovascular research* **14,** 515–521 (1980).
231. Moir, T. W. Subendocardial Distribution of Coronary Blood Flow and the Effect of Antianginal Drugs. *Circ Res* **30,** 621–627 (1972).
232. Gage, J. E. *et al.* Vasoconstriction of stenotic coronary arteries during dynamic exercise in patients with classic angina pectoris: reversibility by nitroglycerin. *Circulation* **73,** 865–876 (1986).
233. Mikhed, Y. *et al.* Nitroglycerin induces DNA damage and vascular cell death in the setting of nitrate tolerance. **111,** (2016).
234. Kass, D. A. & Maughan, W. L. From 'Emax' to pressure-volume relations: a broader view. *Circulation* **77,** 1203–1212 (1988).
235. Imhof, P. R., Ott, B., Frankhauser, P., Chu, L. C. & Hodler, J. Difference in nitroglycerin dose-response in the venous and arterial beds. *European Journal of Clinical Pharmacology* **18,** 455–460 (1980).
236. Imhof, P. R., Ott, B., Weiss, A., Chu, L. C. & Chasseaud, L. F. in *Nitrates III* 66–74 (Springer Berlin Heidelberg, 1981). doi:10.1007/978-3-642-68085-4_10
237. Diamond, G. A. & Forrester, J. S. Analysis of Probability as an Aid in the Clinical Diagnosis of Coronary-Artery Disease. *New England Journal of Medicine* **300,** 1350–1358 (1979).
238. Pryor, D. B., Harrell, F. E., Lee, K. L., Califf, R. M. & Rosati, R. A. Estimating the likelihood of significant coronary artery disease. *Am J Med* **75,** 771–780 (1983).
239. Cheitlin, M. D. *et al.* ACC/AHA/ASE 2003 guideline update for the clinical application of echocardiography: summary article: a report of the American College of Cardiology/American Heart Association Task Force on Practice Guidelines (ACC/AHA/ASE Committee to Update the 1997 Guidelines for the Clinical Application of Echocardiography). *Circulation* **108,** 1146–1162 (2003).
240. YUDA, S. Association of severe coronary stenosis with subclinical left ventricular dysfunction in the absence of infarction. *Journal of the American Society of Echocardiography* **16,** 1163–1170 (2003).
241. Hoffman, R., Marwick, T. H., Poldermans, D. & Lethen, H. *Refinements in stress echocardiographic techniques improves interinstitutional agreement in interpretation of dobutamine stress echocardiograms*. (Eur Heart J, 2002).
242. Nucifora, G. *et al.* Incremental value of subclinical left ventricular systolic dysfunction for the identification of patients with obstructive coronary artery disease. *Am Heart J* **159,** 148–157 (2010).
243. Bonow, R. O. *et al.* Improved left ventricular diastolic filling in patients with coronary artery disease after percutaneous transluminal coronary angioplasty. *Circulation* **66,** 1159–1167 (1982).
244. Tanaka, H. *et al.* Improved regional myocardial diastolic function assessed by strain rate imaging in patients with coronary artery disease undergoing

percutaneous coronary intervention. *Journal of the American Society of Echocardiography : official publication of the American Society of Echocardiography* **19,** 756–762 (2006).
245. Amundsen, B. H. *et al.* Noninvasive myocardial strain measurement by speckle tracking echocardiography: validation against sonomicrometry and tagged magnetic resonance imaging. *Journal of the American College of Cardiology* **47,** 789–793 (2006).
246. Amundsen, B. H. *et al.* Regional myocardial long-axis strain and strain rate measured by different tissue Doppler and speckle tracking echocardiography methods: a comparison with tagged magnetic resonance imaging. *European journal of echocardiography : the journal of the Working Group on Echocardiography of the European Society of Cardiology* **10,** 229–237 (2009).
247. Tanaka, H., Hara, H., Saba, S. & Gorcsan, J., III. Usefulness of Three-Dimensional Speckle Tracking Strain to Quantify Dyssynchrony and the Site of Latest Mechanical Activation. *The American journal of cardiology* **105,** 235–242 (2010).
248. Abdulrahman, R. M. *et al.* Abnormal cardiac contractility in long-term exogenous subclinical hyperthyroid patients as demonstrated by two-dimensional echocardiography speckle tracking imaging. *Eur J Endocrinol* **163,** 435–441 (2010).
249. Kalogeropoulos, A. P., Georgiopoulou, V. V., Gheorghiade, M. & Butler, J. Echocardiographic evaluation of left ventricular structure and function: New modalities and potential applications in clinical trials. *Journal of cardiac failure* **18,** 159–172 (2012).
250. Helle-Valle, T., Edvardsen, T. & Crosby, J. *New non-invasive method for assessment of LV rotation-Speckle tracking echocardiography*. (…, 2004).
251. Kapetanakis, S. *et al.* Real-time three-dimensional echocardiography: a novel technique to quantify global left ventricular mechanical dyssynchrony. *Circulation* **112,** 992–1000 (2005).
252. Kapetanakis, S. *et al.* Real-time 3D echo in patient selection for cardiac resynchronization therapy. *JACC. Cardiovascular imaging* **4,** 16–26 (2011).
253. Costa, M. A., Mazzaferri, E. L., Sievert, H. & Abraham, W. T. Percutaneous ventricular restoration using the parachute device in patients with ischemic heart failure: three-year outcomes of the PARACHUTE first-in-human study. *Circ Heart Fail* **7,** 752–758 (2014).
254. Thomas, M. *et al.* Percutaneous ventricular restoration (PVR) therapy using the Parachute device in 100 subjects with ischaemic dilated heart failure: one-year primary endpoint results of PARACHUTE III, a European trial. *EuroIntervention* **11,** 710–717 (2015).
255. Schreuder, J. J. *et al.* Acute decrease of left ventricular mechanical dyssynchrony and improvement of contractile state and energy efficiency after left ventricular restoration. *The Journal of Thoracic and Cardiovascular Surgery* **129,** 138–145 (2005).
256. SELZER, A. & SUDRANN, R. B. Reliability of the determination of cardiac output in man by means of the Fick principle. *Circ Res* **6,** 485–490 (1958).
257. Mazzaferri, E. L., Jr. *et al.* Percutaneous left ventricular partitioning in patients with chronic heart failure and a prior anterior myocardial infarction: Results of the PercutAneous Ventricular RestorAtion in Chronic Heart failUre PaTiEnts

Trial. *American Heart Journal* **163,** 812–820.e1 (2012).
258. Brinke, ten, E. A. *et al.* Haemodynamics and left ventricular function in heart failure patients: comparison of awake versus intra-operative conditions. *European journal of heart failure* **10,** 467–474 (2008).
259. Bader, H. *et al.* Intra-left ventricular electromechanical asynchrony. A new independent predictor of severe cardiac events in heart failure patients. *Journal of the American College of Cardiology* **43,** 248–256 (2004).
260. Steendijk, P. *et al.* Quantification of left ventricular mechanical dyssynchrony by conductance catheter in heart failure patients. *AJP: Heart and Circulatory Physiology* **286,** H723–30 (2004).
261. Chakir, K. *et al.* Mechanisms of enhanced beta-adrenergic reserve from cardiac resynchronization therapy. *Circulation* **119,** 1231–1240 (2009).
262. Park, R. C., Little, W. C. & O'Rourke, R. A. Effect of alteration of left ventricular activation sequence on the left ventricular end-systolic pressure-volume relation in closed-chest dogs. *Circ Res* **57,** 706–717 (1985).
263. Kramer, D. G. *et al.* Quantitative evaluation of drug or device effects on ventricular remodeling as predictors of therapeutic effects on mortality in patients with heart failure and reduced ejection fraction: a meta-analytic approach. *Journal of the American College of Cardiology* **56,** 392–406 (2010).
264. Packer, M. Long-term strategies in the management of heart failure: looking beyond ventricular function and symptoms. *Am J Cardiol* **69,** 150G–154G (1992).
265. Castelvecchio, S., Menicanti, L. & Donato, M. D. Surgical ventricular restoration to reverse left ventricular remodeling. *Curr Cardiol Rev* **6,** 15–23 (2010).
266. Jones, R. H. *et al.* Coronary Bypass Surgery with or without Surgical Ventricular Reconstruction. *The New England journal of medicine* **360,** 1705–1717 (2009).
267. Witkowski, T. G. *et al.* Surgical ventricular restoration for patients with ischemic heart failure: determinants of two-year survival. *Ann Thorac Surg* **91,** 491–498 (2011).
268. Costa, M. A. *et al.* The PARACHUTE IV trial design and rationale: percutaneous ventricular restoration using the parachute device in patients with ischemic heart failure and dilated left ventricles. *Am Heart J* **165,** 531–536 (2013).

10 APPENDIX

10.1 PATIENT INFORMATION SHEET. VERSION 4.

21/12/2015 LREC Study Number: 09/H0802/39

Title of project: The Role of Nitrates in Angina Pectoris

You are being invited to take part in a research study. Before you decide it is important for you to understand why the research is being done and what it will involve. Please read the following information carefully. Ask us if there is anything that is not clear or if you would like more information. You may withdraw from the study at any stage.

1. What is the purpose of the study? Patients who have narrowings in their heart arteries may suffer with chest pains known as angina. Glyceryl trinitrate (GTN) has been shown to alleviate the symptoms of angina, and is usually given to patients in the form of a spray under the tongue. GTN has also been shown to prevent angina when it is given before a period of exertion; for example exercise. However, although GTN has been used successfully in the treatment of angina for many years, the exact mechanism via which it works remains unclear. If we can observe one particular mechanism via which GTN works, then this would prove very useful as this mechanism could then be specifically targeted by future research studies. The latest techniques in cardiac magnetic resonance imaging (CMR) will be used to investigate this occurrence, in addition to the use of a special catheter to measure pressure inside the heart and a special wire that measures blood flow in the heart arteries.

2. Why have I been chosen? You qualify for this study, because you are have narrowings in your heart arteries and suffer from angina. You have been shown not to experience "warm-up angina" on a recent exercise test.

3. What will happen to me if I take part? There is a flowchart at the end of this document summarising the steps involved.

Standard procedure:

Continue with anti-anginal tablets. You will remain on the waiting list for an angiogram with possible subsequent angioplasty or heart bypass operation (if applicable).

Study procedure:

Any medical or surgical treatment planned for you will not be delayed because of the study. As a screening procedure to see if you are suitable for the study you will undergo one further exercise test using the same specially adapted bicycle. On this occasion just before the test we will give you 2 puffs of a GTN spray to see how this affects your performance. If it does improve things then you be invited to continue with the study. If it makes no difference then we shall not need you to participate further in this study. We may ask you to stop some of your usual anti-anginal medications prior to the exercise test as they can interfere with the results. It is possible that you will experience some discomfort during the exercise procedure, but this does not increase the risk of having a heart attack. The next stage of the study involves a cardiac MRI (CMR) scan, which will require an additional visit by you to our new purpose-built research centre at St. Thomas' hospital. During the scan you will be asked to carry out 2 periods of exercise similar to that performed previously on the exercise bike. This is so that we can see what is happening to your heart during these episodes. You may be asked to stop some of your anti-anginal medications as before. The scan will last about

1 hour in total and will involve an agent needed to provide contrast for the CMR scan. The agent contains gadolinium, a substance widely used for such scans in medicine. This injection will require the insertion of a small cannula, or "drip" onto your arm. Before the second period of exercise, we will administer 2 sprays of GTN under your tongue 5 minutes before the start of the exercise. We will scan your heart with the MRI scanner after both sets of exercise, and will then compare the differences between the 1st and the 2nd periods of exercise. Following the CMR scan you will return to St Thomas' for your planned angiogram and/or angioplasty procedure. The procedure will be carried out via the main blood vessel in your wrists or groin which is the standard approach in many cases. During this procedure a special catheter (1.3 mm tube) will be placed inside the heart through one tube and is very similar to a catheter that is normally used during angiography to assess heart function but this can measure pressure too; in addition a special wire, very similar in structure to the standard wire that is used for the angioplasty procedure through another tube will be passed into the coronary blood vessel that contains the narrowing. This wire is designed to measure blood flow and it will take careful measurements while you undertake a further 2 periods of exercise using a specially adapted supine exercise bike. A second wire will be passed via the same artery, and will be used to take additional flow measurements from the main artery; called the aorta. As before, you may be asked to stop some of your anti-anginal medications. Slightly different to the CMR study, you will be given 2 sprays of GTN during the first period of exercise. You will then have your stenting procedure as normal. The total time for both the treatment and the research procedures will be no longer than 2 hours. The standard procedure normally takes about 1 hour. You will be

invited to complete a feedback survey in the form of a questionnaire at the end of the study.

4. What are the side effects of the procedure received when taking part? There are no serious risks from stopping the anti-anginal medications that we have authorised, whatever the length of time you are off them. You may experience a worsening of your angina symptoms, but this does not increase the risk of a heart attack. Supervised treadmill tests are safe. However, they do carry a small risk (1 in 10,000) of a significant complication such as a serious heart rhythm abnormality, heart attack, or death. Exercise tests are widely used, however, and it is likely that you will need to undergo one anyway as part of your routine clinical work-up. You will undergo a total of 6 exercise tests over the course of the entire study. GTN given in the form of 2 sprays under the tongue, is used routinely by many patients who have angina to successfully alleviate this symptom. In this study we are expecting any anginal symptoms which may be experienced with the treadmill tests, to be reduced with GTN. Side effects from GTN may include flushing, headache, dizziness; however the standard dose of GTN will be used once in each study only, and therefore side effects should be no more likely than from one routine use in a different environment. The CMR scan is very safe and does not involve any exposure to X-rays. The scanner is quite enclosed and some people may feel uncomfortable (claustrophobic) but this is very unusual. There will be a buzzer for you to press if you feel unwell or uncomfortable and would like to stop the scan. The scanning time is about 1 hour in total. For the exercise part of the scanning procedure you will be taken out of the scanner, and undertake similar exercise tests as before. When you reach a certain point during the exercise you will be returned to the

scanner, but only for a very short period of time, approximately 1 minute. You will then come out of the scanner again and have a chance to recover from the exercise. Although generally very safe, there are some risks associated with the gadolinium-based contrast agent, which will be given by injection during the scan. Mild headache, nausea and a local burning sensation can occur. Rarely (less than 1in100), low blood pressure and light headedness occurs. This can be treated immediately with fluid given through a vein. Very rarely (less than 1 in 1000), patients are allergic to the contrast agent. The use of the special flow wire is safe and this device is used in routine clinical practice. For this study, it will be inserted through a small artery in your wrist instead of at the top of your leg, as is more usual in clinical practice. It can sometimes take a few minutes longer to position the wire correctly and this may involve a very small additional dose of x-ray radiation. In addition, it will take a further couple of minutes to position the additional flow wire that will also be inserted through the same cut in the wrist, and will be positioned in the aorta (the main blood vessel leaving the heart carrying oxygen-rich blood to the rest of the body. The additional dose of x-ray radiation has been assessed by the radiation safety team who suggest a 1 in 5,600 chance of it being associated with any excess risk of cancer. The total radiation dose for both the clinical and research aspects of the study is estimated to be 12.5 millisieverts (mSv). The additional radiation dose is 3.1 mSv, which is equivalent to 14 months' exposure to background radiation. If the procedure is performed using both wrists, you will have wrist band applied to both sides, thus there is a small risk of bleeding from either wrist (less than 5% risk of vascular complications). The exercise cycle protocol in the MRI scanner and in the catheterisation lab is not a routine research tool. However, we do not anticipate any additional risk from it. You will be monitored very carefully

throughout. Should you want to withdraw from the study at any point you will be entirely free to do so, and this will not affect your treatment in any way.

5. What are the possible benefits of taking part? There is no direct benefit to study participants. The information we will get might help improve the treatment of other people with angina.

6. Will my taking part in the study be kept confidential? Yes. All the information about your participation in this study will be kept confidential.

7. Expenses and payments: Travel expenses will be reimbursed for the extra hospital visits required by this study. Otherwise there is no payment for taking part.

8. What if there is a problem? Any complaint about the way you have been dealt with during the study or any possible harm you might suffer will be addressed.

Thank you for reading this information sheet and considering taking part in this study.

Contact address:

Dr Tiffany Patterson

Department of Cardiology

6th Floor East Wing

St Thomas' Hospital, London SE1 7EH

Tel: 07894054817 (24 hours)

Email tiffany.patterson@gstt.nhs.uk

The Mechanisms of Exercise Induced Angina

Abstract

Although well described, the mechanisms behind the clinically observed phenomenon of exercise-induced angina are poorly understood. Complex haemodynamic changes occur during exercise that may in fact protect the heart from the deleterious effects of ischaemia on subsequent bouts of exercise. Potential causes include an increase in coronary blood flow, a reduction in cardiac work, or an adaptation of the heart muscle to make it more resistant to ischaemia. We intend to investigate these phenomena as part of a series of studies using a serial exercise protocol under a range of haemodynamic conditions, utilising both perfusion MRI and invasive coronary flow studies. We will determine changes in coronary blood flow, myocardial perfusion distribution and indices of cardiac work with exercise, and hope to use this data to improve our understanding of this clinically important phenomenon. Such work has not been previously performed and it will utilise our local expertise in each of these areas.

Background

The variable relation between exercise and angina has been recognised for more than 200 years[1]. The terms “first effort”, “warm up”, or “first-hole” angina, have been used to describe the ability of some patients to exercise to angina, rest, and then continue exertion with reduced symptoms or none at all. In the experimental setting, the salient observation is that at the accumulated work (exercise duration) causing max ST-segment depression on first exercise, on second exercise there is less ST depression, chest pain and dysrhythmia[2]. The traditional view is that angina is the result of an imbalance between the supply and demand of the myocardium for blood[3, 4]. However,

the mechanisms underlying the warm-up phenomenon are still poorly known and somewhat controversial. Potential causes of the warm-up phenomenon include: (1) an improvement of blood flow, which, in turn, may be caused by stenosis dilation, collateral recruitment or myocardial perfusion redistribution[5-7]; (2) an adaptation of the myocardium to ischaemia, such as that caused by ischaemic preconditioning[3, 8-10]; and (3) peripheral effects causing a slower increase of cardiac workload, such as seen during training[11] or changes in central blood pressure. Initial results from our own department suggest that changes in collateral flow have little influence[2]. Not all patients, however, seem to benefit from warm-up angina with it being clinically detectable in only about 50 percent of patients. In those that do not demonstrate warm-up it has been postulated that the haemodynamic changes induced by commonly used cardiac medications such as nitrates, beta-blockers or calcium channel antagonists simulate many of the changes that underlie this phenomenon. Demonstrating these changes may greatly enhance our understanding of the mechanisms of angina and its relation to exercise.

Okazaki et al[9] suggested that the benefits observed during serial exercise were due to changes in regional myocardial oxygen consumption rather than increases in blood flow. The investigators, however, relied on great cardiac vein catheterisation to assess flow through thermodilution which has been shown to be inaccurate and highly dependent on the position of the catheter[12]. In addition, because it only assesses global flow this method cannot determine the changes that may occur in a particular vessel or the redistribution of flow between the different myocardial layers which may have a very important role[13]. Williams et al[8] performed a similar protocol but relied on rapid right ventricular pacing, a non-physiological surrogate for exercise, to induce tachycardia stress in a small group of stable coronary disease patients with exertional

symptoms but not necessarily warm-up angina. They also relied on great cardiac vein sampling to determine global coronary flow and similarly concluded to the Okazaki group that warm-up angina could not be explained by an increase in coronary flow alone.

The transmural distribution of myocardial blood flow from endocardium to epicardium is critical during exercise as the contractile forces within the heart have a disproportionate effect on the subendocardial layer which renders it much more sensitive to ischaemia[23]. When coronary blood flow control mechanisms are intact, the flow distribution across the myocardium is relatively uniform through local autoregulation with vasodilatation of the myocardial resistance vessels[24]. When this vasodilatory capacity is exhausted (such as during exercise), subendocardial conductance becomes inversely dependent on heart rate and is decreased as the diastolic time fraction (DTF) shortens. Subepicardial perfusion, in contrast, is generally unaffected by these changes[25]. DTF is the relative duration of diastole with respect to the duration of the heart cycle and decreases with increasing heart rate. In the presence of a coronary stenosis, the autoregulatory mechanisms regulating myocardial blood flow are exhausted at an earlier stage during exercise (or even at rest) rendering the subendocardial layer even more critically dependent on the DTF[26]. Interestingly, at this point DTF has been shown to be dependent on distal perfusion pressure rather that the heart rate with no correlation found between DTF and heart rate at the ischaemic threshold[27,28]. Changes in DTF were also found to reduce microvascular resistance and hence improve perfusion[25]. It has been suggested that an increase in diastolic duration during ischaemia may therefore be an important mechanism for matching coronary supply and demand of oxygen by simultaneously decreasing demand and increasing

supply. It is possible that such changes contribute to the protective effects of serial exercise observed during warm-up angina.

Ischaemic preconditioning (IPC), is the term used to describe the increased myocardial resistance to ischaemia that follows a brief episode of ischaemia. In animal models it protects against infarct size and arrhythmias[16] and has shown to have a similar beneficial effect in human studies[2, 17]. Patients with coronary artery disease have been observed to exercise longer before developing angina and may develop less angina and ischemia during a second exercise test compared with a first test when these tests are separated by a brief rest period[9, 18]. It has been suggested that the clinical observation of the warm-up phenomenon may represent one aspect of IPC in humans[10]. IPC, like warm-up angina is also unexplained by a down-regulation of contractile function or an increase in collateral myocardial perfusion induced by initial exercise[19, 20]. Warm-up angina, however, does not seem to be mediated by adenosine or by cardiac adenosine triphosphate-sensitive potassium channels[21, 22] suggesting that it is mechanistically distinct from classic ischemic preconditioning.

The mechanisms by which nitrates exert anti-anginal effects are widespread. In the first instance there is a reduction in myocardial oxygen demand, through a reduction in preload[29-38], a reduction in afterload[31,35,36,38] and a reduction in arterial pressure augmentation[38-39]. There is also an improvement in myocardial perfusion, through vasodilatation of epicardial coronary arteries[40-45], enhanced collateral recruitment[43,46], coronary stenosis enlargement[41,43,47], improved endothelial function[48], and preferential redistribution of blood to the subendocardium from the subepicardium[49-55].

It is postulated that the protective effects of nitrates are mechanistically similar to those induced by the warm-up effect on second exercise. Nitroglycerin (NTG) is rapidly

converted to nitric oxide (NO) at or near the plasma membrane of vascular smooth muscle cells. NO activate guanylate cyclise which catalyzes the formation of cyclic guanosine monophosphate (cGMP); this induces a fall in intracellular calcium and subsequent vasodilation. Thus it may be that an increase in cGMP is central to the protective effects induced by nitrates and warm-up angina.

Phosphodiesterase type 5 selective inhibitors block the degradative action of phosphodiesterase type 5 (PDE-5) on cGMP in vascular smooth muscle cells, and therefore also produce an increase in cGMP which provokes vasodilatation. PDE-5 is expressed in a variety of tissues including the coronary and pulmonary vasculature, as well as high concentrations in the corpora cavernosa. Sildenafil (a PDE-5 inhibitor) has been postulated to induce cardioprotection via pharmacological preconditioning; most probably through an increase in nitric oxide generated from endothelial and/or inducible nitric oxide synthases, and opening of mitochondrial ATP-sensitive potassium channels[56,57]. Cardioprotective effects observed include a reduction in myocardial infarction, anti-arrhythmic effects, and an improvement in ventricular functional recovery[58]. Furthermore, in a recent study PDE-5 inhibitors were shown to augment haemodynamic effects of calcium channel inhibitors in NO deficient rats, highlighting the pivotal role of the NO-cGMP pathway[59].

The current proposal aims to investigate the relationship between serial exercise and angina by assessing the relative influences of changes in blood flow, myocardial workload or intrinsic adaptation using a combination of cardiac magnetic resonance imaging (CMR) and invasive coronary physiological measurements, during a serial exercise protocol. We will then investigate the effect of a pharmacologically manipulated increase in cGMP on the above parameters. To induce such a reproducible

and reliable increase in cGMP, the two most plausible methods would be to use a PDE-5 inhibitor or a nitrate. Glyceryl trinitrate (GTN) provides the safest and easiest method in which to achieve such conditions. It is available for use as a sub-lingual spray, and produces well described haemodynamic effects with a rapid onset of action, whilst maintaining a good safety profile. Furthermore, as an established anti-anginal agent, patients with angina are familiar with its use and side effects.

Therefore the typical haemodynamic effects induced by sublingual GTN spray will be examined in the second period of exercise. Patients who demonstrate the "warm-up" effect will be specifically excluded as they will be enrolled in a very closely related study (08/H0802/136 The assessment of coronary blood flow in patients with warm-up angina: Increased flow or reduced need?). As well as producing important data in its own right this study will also validate the novel methods used in the protocol to show that detectable differences in cardiac work and flow can be made on serial exercise. Subsequent studies are expected to examine further haemodynamic conditions using other agents that influence myocardial ischaemia on exercise including beta-blockers, I_f channel blockers and calcium channel antagonists.

Hypotheses

The NO-cGMP axis is central to the processes of warm-up angina and also triggers the related phenomenon of ischaemic preconditioning. Currently is unclear how this axis influences these processes. In patients with coronary artery disease and angina there are 3 possibilities

The typical systemic haemodynamic changes following activation of the NO-cGMP axis reduce cardiac work

The typical local coronary haemodynamic changes following activation of the NO-cGMP axis result in improved perfusion of the subendocardium

The activation of the NO-cGMP axis results in direct cardiac protection that manifests as an anti-anginal action in the absence of 1 or 2.

Within this application we will activate the NO-cGMP axis with sublingual GTN in the first instance since this method is better established and likely better tolerated than inhibition of PDE5.

Rationale for the chosen methods

There has been very limited experimental data examining the mechanism of angina during serial exercise. The few studies published have either used outmoded or inaccurate means to determine cardiac work or coronary flow[8, 9]. Other more contemporary studies have examined changes in blood flow in patients with coronary disease under a range of haemodynamic conditions using adenosine[60], dobutamine[61], nitroprusside[62] or rapid right ventricular pacing[62] but, importantly, all of these fail to recreate the physiological conditions actually experienced during exercise. The artificial milieu induced by pharmacological vasodilatation augments the "steal" of perfusion from the subendocardial layer but does not provoke the simultaneous increase in oxygen demand required during exercise and the important consequent effects this has on cardiac work, heart rate, DTF and consequently perfusion[13]. Actual balloon occlusion of the coronary artery to stimulate repetitive ischaemia has been used by our own department to examine coronary collateral flow during these conditions[2] but once again this falls short of recreating the physiological conditions of exercise necessary to examine the phenomenon of warm-up angina. With its experience and expertise in the

measurement of invasive coronary indices, the latest high-resolution cardiac MRI perfusion techniques and an established basic sciences research programme into the mechanisms underlying warm-up angina and cardiac protection the host department is uniquely positioned to carry out such an important, albeit ambitious, research proposal. GTN spray has been chosen to alter the haemodynamic conditions of second exercise for the reasons outlined previously.

Method

Patients will be recruited from routine waiting lists for percutaneous coronary intervention (PCI) for single vessel coronary disease, or awaiting a routine treadmill−exercise test as part of the investigations for stable angina pectoris.

Inclusion criteria: Stable, single vessel PCI (for coronary disease)

Exclusion criteria: Unstable symptoms, severe left ventricular impairment (ejection fraction <30%), severe renal impairment, pacemaker (or other reason patient cannot undertake an MRI scan), severe co−morbidities.

Patients will undergo a screening sequential supine exercise test to exclude those with significant "warm-up". Warm up will be defined as clear ST segment depression at peak exercise on first effort and definitely less marked ST depression on second effort at the equivalent time-point. At this time-point on first and on second effort patients will undergo CMR and coronary physiological assessment.

CMR protocol

This will be carried out on a 3T Philips MR scanner. The study will include localisers, cine images and rest and exercise-stress perfusion imaging. 3 perfusion scans will be

carried out following each episode of exercise stress, with 0.6mg sublingual GTN given 5 minutes before the 3rd period of exercise. A 15 minute rest period will occur after each exercise stress. Exercise will be carried out on an MR compatible supine ergometer which is mounted securely onto the MR table. Following peak exercise stress, subjects will be repositioned inside the MR scanner. Immediate contrast-enhanced perfusion imaging will be performed using a double bolus intravenous injection of non-ionic gadolinium (0.05-0.1mmol/kg bodyweight), and signal intensity and time to contrast wash in will be measured. From this data, subendocardial to subepicardial perfusion ratios and full perfusion quantification (ml/kg/min) will be calculated. DTF will be deduced from the R wave on the ECG and closure of the aortic valve.

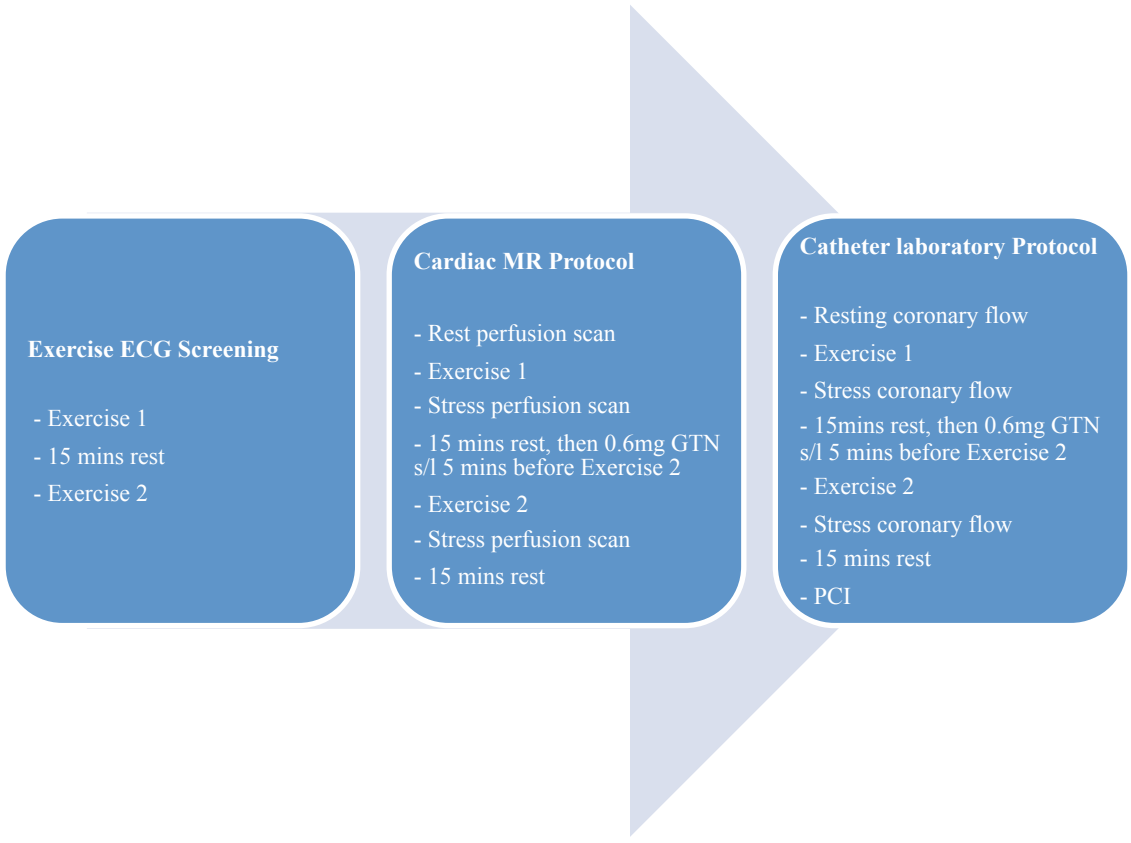
PCI procedure

Patients will be catheterised via the right and left radial artery and a pressure−flow dual sensor wire (ComboWire®, Volcano therapeutics) passed into the target coronary vessel and a pressure-volume catheter (Inca®, CD Leycom, Netherlands) will be placed in the left ventricle. Baseline measurements will be taken before the patient undergoes 2 periods of exercise, with sublingual GTN given 5 minutes before the 2nd period of exercise. Coronary flow and LV pressure measurements alongside ECG and central aortic pressure traces will be monitored continuously throughout the study. Additional monitoring will be performed by means of a central venous line in the pulmonary artery. The velocity time integral (VTI) will be measured from the peak Doppler trace obtained at a similar point of the coronary artery. DTF will be determined from the R-R interval and the dicronotic notch in the central aortic pressure trace as previously described[24]. Microvascular resistance will be defined as the ratio of mean distal coronary pressure to

distal velocity time integral (VTI). Rate pressure product (RPP), calculated as the product of heart rate and systolic pressure, will be used as an estimate of myocardial oxygen consumption (MvO_2). The patient will then undergo PCI as planned using the same wire.

GTN

GTN will be administered by 2 puffs of sublingually, with a total dose of 600 micrograms. This is the standard dose used for angina pectoris. The time to peak concentration occurs after 2 – 3 minutes, and the half life 4 – 5 minutes; therefore exercise will be performed 5 minutes following administration. Common side effects of GTN include flushing, headache and dizziness. Rarer side effects can include vomiting, diarrhoea and syncope.



Principal endpoints will be obtained at peak of first effort and the equivalent time of second effort and will include measures of myocardial blood flow: VTI, central aortic pressure (*during cath*), and, transmural contrast wash-in (*during CMR*), and measures of myocardial work: left ventricle pressure-volume relations – end systolic (ESPVR) and end diastolic (EDPVR) and Pressure-Volume loops (*during cath*), and regional wall motion (*during CMR*).

Secondary endpoints will include an index of relative microvascular function (P_d/V), coronary flow reserve (CFR) and DTF (*during cath*) and other measures of MR perfusion and cardiac efficiency.

Sample Size Calculation

There will be differences in coronary blood flow sought between the serial exercise protocols as well as being compared to blood flow following PCI. The student's t−test will be used to compare means and seek to assess the difference between the groups.

The main outcome will be coronary flow reserve (CFR) as measured by a Doppler probe in the coronary artery. From previous studies, in similar patients to whom we will be studying a value of 1.7 ±0.25 was recorded for the CFR (mean ± SD). As it is the first time that this type of intervention is suggested for CFR there is no available data for the equivalent post-treatment values for mean and SD. The proposed study will form a pilot for this novel approach and thus there is no need for formal power and sample size calculations.

We aim to show a difference of 25% by measuring the CFR in the same vessel before and after exercise i.e. we will be using same patient as a control. A basic sample size calculation has been carried out to determine the minimum required number of patients

to be as small as possible but at the same adequately numbered to provide the baseline information needed for extending our study following this pilot.

The difference of 25% is deemed significant from other experimental scenarios and we ideally would like to detect that difference with a minimum of 80% power, with the significance set at the 95% level. Based on the available baseline data above (before intervention, 1.7+- 0.25) we estimated the sd of the difference after intervention as 0.7.

This background information (diff:0.25, baseline mean =1.7, sd(diff)=0.7, power=90%, P-value<0.05) the desired sample size would be 29 patients. If the power were to be lowered to 80% the required sample size fall s to 22, hence we would be happy to settle for 22 pilot patients. (sample size calculations were carried out using openepi.com).

As this calculation is based on an sd(diff) estimate we propose to adjust the figures after the first 10 patients have been recorded. We expect that the final number of patients would not exceed 58.

29 patients were required for the initial investigation into the role of nitrates in Angina Pectoris (which has completed recruitement) and a further 29 patients will be required for this further project to perform the additional pressure-volume measurements based on the above sample size calculations.